Integrating single-cell transcriptomics with orthogonal experimental approaches and datasets to enhance characterization of the maternal-fetal interface

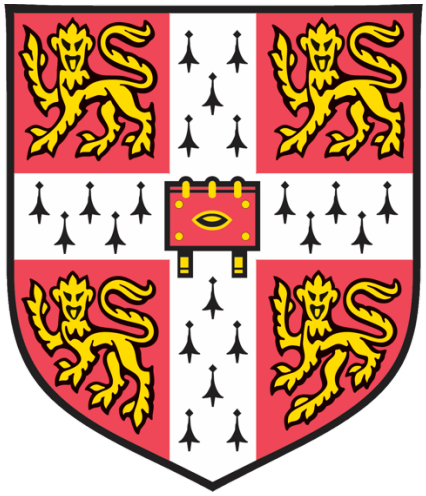

Angela Elizabeth Zou

Wellcome Trust Sanger Institute
Churchill College
University of Cambridge

This dissertation is submitted for the degree of Master of Philosophy.
20 April 2018

Abstract

During early pregnancy, the maternal immune system shapes the uterine environment to facilitate the implantation and development of an antigenically foreign fetus. Critical to orchestrating this process are unique cell populations within the uterine lining (maternal decidua) and the fetal placenta, which together comprise the maternal-fetal interface. In this study, we sought to comprehensively profile specific cell types and their respective functions at the maternal-fetal interface at single-cell resolution, through analytical approaches combining single-cell RNA-sequencing (scRNA-seq) with other experimental datasets.

scRNA-seq data derived from early pregnancy (6-13 weeks) decidua, placenta, and maternal peripheral blood were analyzed in tandem with other sequencing data, flow cytometric data, and publicly available gene signature and gene expression datasets. We first employed cutting-edge methods to determine via scRNA-seq the maternal or fetal origin of cell populations in the decidua and placenta, both with and without incorporation of genotype data. We then evaluated the utility of bulk RNA-sequencing as quality control for scRNA-seq by analyzing the expression of scRNA-seq-upregulated genes associated with dissociation-induced effects in decidual bulk RNA-sequencing data. Our analysis identified a small number of heat shock protein genes (HSPs) as scRNA-seq-associated technical artifacts. Next, through paired analyses of scRNA-seq with FACS index sorting and mass cytometry data, we further characterized novel subpopulations of decidual NK cells, T cells, and mononuclear phagocytes at both the transcriptome and protein level. Additional comparison of marker genes distinguishing the maternal mononuclear phagocyte populations with known macrophage gene signatures and with tissue-level gene expression data from the Human Protein Atlas showed that these cell subsets do not strictly exhibit classical M1/M2 polarization and express placenta- and endometrium-enriched genes, suggesting their heavily tissue-specific function. Finally, we curated genes with established links to pregnancy complications and fertility and used scRNA-seq to study their cell-type specific expression patterns at the maternal-fetal interface. Our results highlight, among other insights, the specialized role of decidual stromal cell subsets in mediating insulin-like growth factor (IGF) signaling, an important regulator of fetal growth. Cumulatively, these analyses have enhanced the potential of scRNA-seq to robustly unravel novel biology at the maternal-fetal interface.

Declaration of originality

This dissertation is the result of my own work and includes nothing which is the outcome of work done in collaboration except as declared in the Preface and specified in the text. It is not substantially the same as any that I have submitted, or, is being concurrently submitted for a degree or diploma or other qualification at the University of Cambridge or any other University or similar institution. I further state that no part of my dissertation has already been submitted, or, is being concurrently submitted for any such degree, diploma or other qualification at the University of Cambridge or any other University or similar institution. Finally, my dissertation does not exceed the word limit prescribed by the Degree Committee for the Faculty of Biology (it is 19,921 words in length, excluding abstract, figures, tables, references, and appendices).

Preface

The work presented in this dissertation was part of a study conceived by Sarah Teichmann and Roser Vento-Tormo. Tissue dissection and processing, fluorescence-activated cell sorting (FACS), droplet- and plate-based single-cell RNA-sequencing, and mass cytometry (CyTOF) experiments were carried out by Roser Vento-Tormo with help from Margherita Turco, Rachel Botting, Jongeun Park, and Rebecca Payne. DNA/RNA library preparation, whole genome sequencing, and bulk RNA-sequencing were carried out by the Sanger Institute sequencing facility. Mirjana Efremova and Roser Vento-Tormo performed the initial quality control, analysis, interpretation, and annotation of cell populations in the single-cell RNA-sequencing data. I performed the single-cell genotyping analyses, bulk RNA-sequencing evaluation of heat shock proteins, CyTOF data analysis, public gene signature-based analysis and functional annotation of maternal mononuclear phagocyte populations, and cell type-level analysis of genes associated with complications of pregnancy and fertility-related conditions, which are presented in this thesis. Davis McCarthy, Raghd Rostom, and Krzysztof Polanski provided helpful advice and scripts facilitating our approach for genotyping single cells without whole genome sequencing data.

Acknowledgements

First and foremost, I wish to thank my supervisor, Sarah Teichmann, for opening her lab to me over this past year and providing invaluable mentorship and direction for my MPhil research. Sarah's continuous support and thoughtful insights have greatly shaped the development of my work and of this thesis. I am also tremendously grateful to Roser Vento-Tormo and Mirjana Efremova, for their immeasurable help and guidance over the course of this project. Apart from giving me the chance to play around with some truly fascinating, one-of-a-kind datasets, Roser and Mirjana have taught me so much about maternal-fetal biology and single-cell data analysis, and they have provided endless doses of feedback and encouragement during my research and the writing of this thesis.

I am also very indebted to the members of my thesis committee, Jacqui Shields and Martin Hemberg, for taking the time to offer constructive advice about my work throughout this year. A big thank you as well to Davis McCarthy, Raghd Rostom, and Krzysztof Polanski, for the discussions and pieces of code they shared in helping me set up a pipeline to genotype single cells based on single-cell RNA-seq variant calling. And I wish to thank the entire Teichmann group for hosting my stay and for all of the conversations – both enlightening and entertaining – that we have shared at group meetings, in Murray's, or around the water cooler.

I am very lucky to have had my year in Cambridge supported by a Churchill Scholarship from the Winston Churchill Foundation of the United States. Churchill College and the Wellcome Trust Sanger Institute have been a wonderful home for me this year, and my friends on both sides of the Atlantic, both new and old, have been the best source of strength, inspiration, and laughter that I could have asked for. Finally, I want to thank my parents and boyfriend for their unwavering love, and for believing in me, supporting me, and cheering me on through thick and thin.

Table of Contents

Chapter 1 - Introduction

The establishment and maintenance of pregnancy relies on successful fetal implantation and placental development in a receptive uterine environment. At the epicenter of these processes is the maternal-fetal interface, where cells comprising the maternal uterine lining, or decidua, encounter and interact with invading fetal extravillous trophoblast cells (EVT)[1]. The invasion of EVT is crucial in forming the placenta and facilitating proper nutrient and gas exchange between the fetus and the mother. Additionally, maternal immune cells residing in the decidua must adapt to tolerate the semi-allogeneic fetal cells, which express paternal antigens, and support their growth and coexistence over the duration of pregnancy[2]. In this chapter, I will first describe the biology and immunology of the maternal-fetal interface during early pregnancy, providing an overview of the characterized cell types and functions. Next, I will describe existing questions with regard to the maternal-fetal interface and how these motivate the aims and design of the study described in this thesis.

1.1 Formation of the maternal-fetal interface during early pregnancy

1.1.1 Decidualization is critical to establishing a favorable uterine environment for pregnancy

The human endometrium, or inner epithelial layer of the uterus, progresses through extensive growth, remodeling, shedding, and regeneration with each menstrual cycle[3]. During the postovulatory (secretory) phase of the cycle, rising levels of uterine progesterone and elevation of intracellular cyclic adenosine monophosphate (cAMP)[4,5] activate signaling pathways targeting HOXA10, FOXO1, HAND2, and other transcription factors to initiate the process of decidualization[6,7]. Decidualization is marked by an extensive series of structural and functional changes to the endometrium, including the differentiation of endometrial stromal cells (ESCs) from a fibroblastic to epithelial morphology. These epithelioid, decidualized ESCs secrete an extensive repertoire of hormones, cytokines, and growth factors, including prolactin (PRL)[8], IL-15[9], and IGFBP-1[10]; extracellular matrix proteins, such as fibronectin and collagen[11]; and angiogenic regulators, such as vascular endothelial growth factor (VEGF)[12]. Meanwhile, uterine glands embedded throughout the endometrium also exhibit increased secretory activity[13], and specialized immune cells, primarily tissue-resident decidual NK cells and macrophages[14,15], begin to increasingly infiltrate the endometrium. These radical changes collectively transform the endometrium into a dense, vascularized tissue known as the decidua, which in the event of a pregnancy is capable

of mediating embryo homing and attachment to the uterus[16], undergoing extensive vascular and tissue remodeling[17,18], regulating placental growth and nourishing the embryo during placenta formation[13,19], and modulating local immune responses to the fetus and placenta[14,15], among other functions. Ultimately, the decidua is uniquely primed to receive an implanting embryo, facilitate the successful establishment of a pregnancy, and undergo further adaptations to support a pregnancy.

1.1.2 Fetal implantation and placentation

After fertilization, the zygote develops into a blastocyst consisting of an inner cell mass, which evolves into the embryo, and a trophectoderm, which gives rise to the placenta and other extraembryonic tissues[20]. Following initial contact and stable adhesion of the blastocyst to the endometrium, various trophoblast lineages emerge to guide embryo implantation and placentation. In the villous pathway, cytotrophoblasts fuse into multinucleated syncytiotrophoblast cells (SCT), which make up the outermost layer of the trophectoderm[21]. SCT ultimately come into contact with the maternal blood, enabling the maternal-fetal exchange of gases and nutrients which is essential to the growth and development of the fetus[20].

As the blastocyst is anchored in the uterus, cytotrophoblasts continue proliferating, forming cell columns that penetrate past the syncytiotrophoblast and eventually give rise to the chorionic villi of the placenta[22]. Cytotrophoblasts within these extensions differentiate along the extravillious pathway into interstitial and endovascular EVT, which play complementary roles in vascular remodeling and immunomodulation[1,21]. The interstitial EVT invade further into the decidualized endometrium and the myometrium, promoting the recruitment of uterine arterioles and ultimately fusing into multinucleated placental giant bed cells at the end of their migration[21]. In the process, they come into direct contact with maternal immune cells and decidual stromal cells, and are therefore involved in modulating immune responses at the maternal-fetal interface[23]. Meanwhile, endovascular EVT invade directly into the uterine vasculature, replacing vascular endothelial and smooth muscle cells lining the maternal spiral arteries[22]. This transforms the arteries into dilated, low resistance vessels that circulate maternal blood into the trophoblast-lined intervillous space of the placenta[21]. In the intervillous space, maternal blood bathes the placental chorionic villi and establishes direct contact with the SCT to permit nutrient and gas exchange.

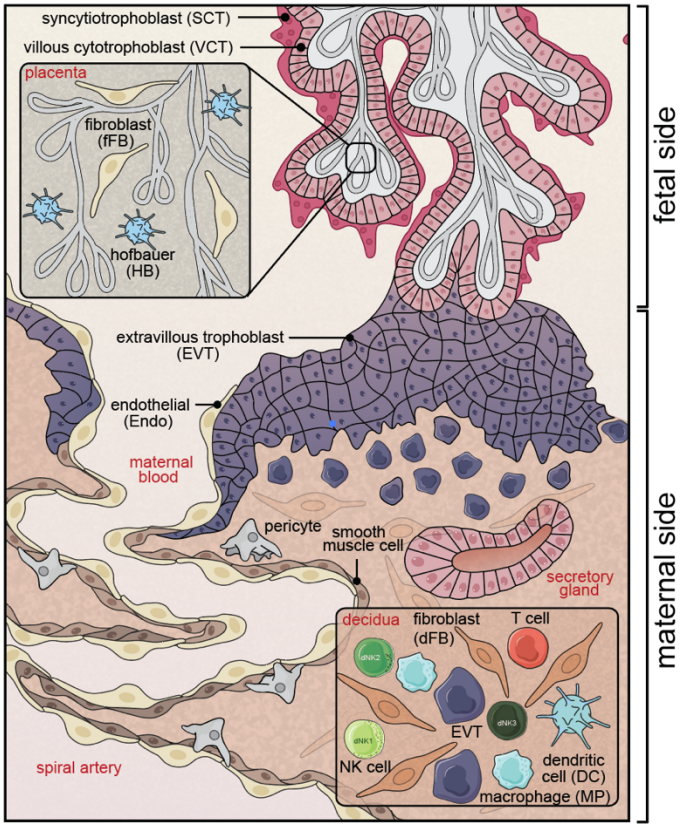

Figure 1. Diagram of the structure and primary cell populations of the maternal-fetal interface. (from Vento-Tormo R, Efremova M, et al., under submission)

Precise control of trophoblast invasion and differentiation is crucial for pregnancy success, and a multitude of factors govern this process. The coordinated production of matrix metalloproteinases and tissue inhibitors of metalloproteinases by both trophoblast cells and decidual cells is critical to fine-tuning the timing and extent to which trophoblasts degrade the uterine extracellular matrix and migrate through the endometrium[24]. Additionally, as trophoblasts in the oxygen-poor decidual milieu invade towards the maternal spiral arteries and encounter an increasingly oxygen-rich environment, they shift from a proliferative to differentiating state[25]. Meanwhile, exposure to various cytokines, growth factors, and other molecules of the decidual secretome prompts trophoblast cells to undergo integrin switching and to upregulate expression of angiogenic factors, such as VEGF and VEGFR[26,27], and cell adhesion ligands, such as vascular cell adhesion molecule 1 (VCAM-1) and platelet endothelial cell adhesion molecule (PECAM-1; CD31)[26,28]. In addition to further modulating trophoblast invasiveness, these mechanisms also alter the adhesive properties of trophoblasts to resemble those of endothelial cells, thus enhancing their capacity to localize to and integrate into the maternal spiral arteries[26,29].

Overall, successful establishment of the maternal-fetal interface relies on the spatiotemporal synchronization of numerous molecular and cellular interactions between the decidual and fetal cells[20,22]. This complex interplay is highly consequential in configuring the maternal and fetal vascular systems to facilitate proper gas exchange, nutrient and waste transfer, and adequate delivery of immunoglobulins and other molecules critical to embryonic development throughout the duration of pregnancy[30]. Impairments in many processes involved in placentation, such as defective trophoblast invasion or incomplete remodeling of the maternal spiral arteries, have been shown to be strongly predisposing factors for preeclampsia[20,25,31], fetal growth restriction[22,28,32], and other serious complications of pregnancy.

Additionally, over the course of placentation and pregnancy, fetal trophoblasts come into direct contact with the immune cell-rich uterine tissues and the maternal blood[21,33]. While this hemochorial placenta is highly efficient, it also poses an immunological challenge in which maternal leukocytes must continuously encounter invading, semi-allogeneic fetal cells. Given the considerable levels of maternal immune cell recruitment to the maternal-fetal interface and the radical morphological changes and functional adaptations that maternal and fetal tissues undergo during early pregnancy[2,20], the maternal immune system must develop tailored responses at the maternal-fetal interface that at once facilitate local tissue disruption and repair, tolerate maternal-fetal coexistence, and promote successful fetal growth and development.

The trophoblasts appear to be equipped with their own mechanisms of escaping immune elimination. Most notably, they do not express the classical MHC I molecules HLA-A and HLA-B, which are the primary targets of traditional T cell-mediated allogeneic responses, instead preferentially expressing HLA-G as well as HLA-E and HLA-C[20,34,35]. This unique surface repertoire enables them to regulate immune responses at the maternal-fetal interface by binding receptors expressed by decidual NK and myeloid cells[22,23,35].

1.2 Immune cell constituents of the maternal-fetal interface

1.2.1 Decidual natural killer cells

Decidual NK cells (dNK) begin to accumulate in the secretory endometrium prior to blastocyst implantation and comprise around 70% of the immune cell population at the maternal-fetal interface during early pregnancy[36]. In contrast to their peripheral blood counterparts, they exhibit a $CD56^{+}CD16^{-}$

$CD9^+$ surface phenotype[37] and produce a distinct set of cytokines, growth factors, and chemokines[38,39]. These characteristics impart unique properties to dNK, including their ability to regulate EVT migration into the decidua[39]. While conventional NK cells tend to release cytolytic granzyme- and perforin-containing granules to destruct target cells, dNK demonstrate poor killing upon activation, a mechanism potentially contributing to maternal immune tolerance towards semi-allogeneic fetal cells[2,31].

NK cell function is generally regulated by the interaction of various NK receptors with MHC class I molecules on target cells. The functional outcome of NK receptor-MHC engagement depends on whether the receptor is inhibitory or activating, leading to either dampening or stimulation of NK cell response[40]. In particular, the family of killer cell immunoglobulin-like receptors (KIRs) expressed by NK cells consists of both inhibitory and activating receptors that are often variably or stochastically expressed between one NK cell and another[41].

HLA-G, which is expressed by EVT, binds to NK cell receptor LIR-1, impairing dNK cytotoxicity and possibly inducing the secretion of cytokines and angiogenic factors to further promote endometrial vascularization[42]. HLA-E binds the NK inhibitory receptor NKG2A and also engages the activating receptor NKG2C at lower affinity[35,43]. Meanwhile, HLA-C molecules are capable of binding both inhibitory and activating KIRs, with relative affinity to specific KIRs dictated by HLA-C allotype[44]. The *HLA-C* gene is highly polymorphic, with more than 2000 documented variant alleles[45], which broadly give rise to either HLA-C1-type or HLA-C2-type molecules. The genes encoding KIRs are multiallelic as well and can be inherited in variable copy number between generations in addition to being expressed in varied combinations on individual NK cells[41]. Because the genetic diversity of KIR and HLA genes is germline-encoded, KIR and HLA genes on different chromosomes are inherited independently[41,45]. As a result, KIRs on maternal NK cells may be able to bind fetal HLA-C allotypes that the mother herself does not possess (i.e. paternal in origin), and similarly, fetal HLA-C molecules may be ligands to maternal KIRs that the fetus does not possess. Thus, different KIR/HLA-C interactions can conceivably produce different degrees of NK activation and inhibition, and in turn, alter the extent to which dNKs and trophoblasts collectively promote tolerogenicity and inflammation at the maternal-fetal interface[46]. Indeed, particular maternal KIR and fetal HLA-C pairings have been shown to influence risk of developing pregnancy complications. Combinations of fetal HLA-C2 allotypes with maternal KIR haplotypes containing inhibitory NK receptor KIR2DL1 are associated with poor placentation and greater incidence of preeclampsia[44] and fetal growth restriction[47]. On the other hand, combinations of

fetal HLA-C2 with maternal haplotypes containing activating NK receptor KIR2DS1 are associated with fetal overgrowth[48]. NK receptor-mediated crosstalk therefore appears to substantially regulate dNK function and heavily influence the successful establishment and progression of pregnancy. The range of cell types and mechanisms by which occurs and their respective consequences have not been fully elucidated yet will be critical to understanding the balance between remodeling, immunity, and tolerance maintained by dNK cells.

1.2.2 Decidual macrophages

Mononuclear phagocytes, including macrophages, account for ~20-25% of decidual leukocytes[2,49] and collectively appear to assume multifaceted roles during early pregnancy. As the second most abundant immune cell population in the decidua, they serve as the predominant antigen processing and presenting cells at the maternal-fetal interface and are hypothesized to help promote maternal immune tolerance through moderation of local NK and T cell responses. Among other mechanisms, decidual macrophages have been shown to produce high levels of the immunosuppressive cytokine IL-10[50]; dampen T cell activation and cytokine production through signaling via inhibitory PD-1 and B7-family molecules[51]; express low levels of B7-1 and B7-2, which are activating ligands for the CD28 co-receptor on T cells[50]; induce regulatory T cells via IDO and TGF-β production[52]; and reduce cytolytic activity in dNK cells through TGF-β[53].

At the same time, during blastocyst implantation, parturition, uterine infection, and other events in pregnancy characterized by a proinflammatory state, macrophages have been observed to significantly accumulate at the maternal-fetal interface[2,49]. Indeed, decidual macrophages exhibit high expression of pattern recognition receptors, including CD163, CD206 (mannose receptor), and CD209 (DC-SIGN)[54,55], and facilitate self-recruitment through the production of monocyte chemoattractants and mitogens[2,56], indicating their ability to detect pathogens and damaged cells and to initiate inflammatory responses. Furthermore, upon stimulation by LPS, decidual macrophages have been shown to secrete the inflammatory cytokines IL-1β and TNF; however, other classical proinflammatory cytokines, such as IL-12, are not produced, and IL-10 production is still constitutively elevated[56,57]. This suggests that macrophages are capable of orchestrating a state of controlled inflammation at the maternal-fetal interface in which pathogen clearance and response to damaged tissue are balanced with the maintenance of a tolerogenic environment.

Additionally, macrophages have been directly linked to vascular and tissue remodeling and trophoblast differentiation, as they localize to the decidual arteries alongside dNK cells prior to the replacement of vascular endothelial and smooth muscle cells by extravillous trophoblasts[2,58]. They express elevated levels of the extracellular matrix proteins fibronectin and collagen[54], matrix metalloproteinases MMP7 and MMP9[54,58], complement protein C1q[54], and angiogenic factor VEGF and its receptor VEGFR-1/FLT-1[56,59]. Fibronectin and C1q may specifically be involved in enhancing macrophage phagocytosis of apoptotic vascular cells before their persistence in the decidua triggers acute inflammation[60,61]. In addition, decidual macrophages have been shown to produce IL-33, which stimulates cytotrophoblast proliferation and extravillous trophoblast migration[62]. Reciprocally, the activation of decidual macrophages has been linked to trophoblast and potentially endometrial stromal cell-mediated production of M-CSF, GM-CSF, and IL-10[57,63].

Existing knowledge of decidual macrophages has primarily been described in relation to the M1/M2 model of macrophage polarization, developed to parallel the concept of Th1/Th2 differentiation in T helper cells[64]. M1 macrophages are associated with Th1 response and are referred to as “classically activated” macrophages[65]. They express pattern recognition receptors and upon stimulation by factors such as IFN-γ, TNF, LPS, or GM-CSF, secrete pro-inflammatory cytokines, upregulate antigen-presenting MHC class II molecules, antigen-processing peptidases, and costimulatory molecules, and initiate other responses congruent with Type 1 inflammation and pathogen elimination[66]. Meanwhile, stimuli of M2 macrophages include “alternative activation” by IL-4/IL-13, immune complexes in combination with TLR engagement, and IL-10 and glucocorticoids[65,67]. Overall, M2 macrophages exhibit an umbrella of phenotypes including wound healing and tissue remodeling, resolution of inflammation, and Th2-type immune responses[68]. Specifically, IL-4 induces macrophage fusion and decreases phagocytosis, and IL-10/glucocorticoid-stimulated macrophages exhibit induction of complement (C1Q), IL-10, CD163, and mannose receptor (MRC1), among other molecules[69].

There are varying hypotheses for how macrophages polarize within the decidua. One model posits that decidual macrophages are M2 at baseline and induced towards M1 upon pathogen stimulation or during the implantation and parturition stages of pregnancy[49]. Another proposes the existence of two distinct decidual macrophage subsets which are distinguished primarily by high and low expression of the integrin adhesion receptor CD11C but do not fall completely along the M1/M2 polarization axis in terms of their phenotypes or their cytokine profiles[70,71].

An emerging consensus, however, is that the M1/M2 model should be revised[72–74], as it is overly rigid and fails to account for the phenotypic plasticity and functional diversity of macrophages. In particular, tissue-resident macrophages tend to exhibit adaptations heavily tailored to their local environments and the unique functional demands of their tissues[73], with notable examples being splenic red pulp and liver macrophages, which are specialized for heme group processing[75,76], and osteoclasts, which are critical for bone remodeling[77]. Such observations are inadequately accounted for by the general M1/M2 macrophage model. Thus, further characterization of decidual macrophages may prove insightful in further understanding the potential spectrum of functions performed by tissue-resident macrophages as well as further clarify the overall biology of the maternal-fetal interface.

1.2.3 Decidual dendritic cells

Dendritic cells (DCs) are present in low proportions at the maternal-fetal interface, comprising less than 2% of the immune compartment[78]. Various surface phenotypes have been described for decidual DCs, with mature cells expressing CD83[79] and subsets distinguishable by $BDCA1^+$ and $BDCA3^+$ expression[80] or by $HLADR^+$ and $HLADR^-$ expression[78].

In general, DCs either reside in the lymphoid organs or are situated within nonlymphoid peripheral tissues. Although both classes of DCs engage in antigen uptake and presentation, nonlymphoid tissue-resident DCs have shown to be the main mediators of T cell priming and response to peripheral tissue antigens, as upon activation, they are able to migrate through the lymphatic vessels to the draining lymph nodes[81,82]. However, the antigen-presenting potential of decidua-resident DCs must be reconciled with the observation that during pregnancy, the fetus is tolerated and there is no apparent fetal allorecognition and rejection. Studies in mice, for example, have shown that fetal antigens are still presented to T cells in draining lymph nodes and other secondary lymphoid organs, but there is no resulting accumulation of T cells at embryo implantation sites, suggesting that decidual DCs and other maternal antigen-presenting cells fail to initiate allogeneic T-cell responses to fetal and placental antigens[2,82].

In mice, decidual DC densities have been found to steadily decrease during early pregnancy, and in humans, decidual stromal cells have been demonstrated to inhibit DC differentiation and T cell activation via prostaglandin E2 and IDO production[83]. Moreover, even upon LPS stimulation, activated and mature murine decidual DCs are unable to migrate to regional draining lymph nodes[84]. This

phenomenon, termed DC entrapment, appears to be due in part to the absence of lymphatic vessels near the decidual spiral arterioles, thus preventing trophoblast-activated DCs from homing to uterine lymph nodes[84]. Rather, the only lymphatic vessels in the mouse uterus expressing CCL21, the chemokine ligand directing DC homing[85], are restricted to the myometrium[82]. In humans, similar mechanical and biochemical barriers may apply to limit DC activation, migration, and recruitment of peripheral T cells[83].

On the other hand, complete absence of decidual DCs also appears to be detrimental to pregnancy, as DC-depleted mice exhibited impaired spiral artery remodeling[86]. This points to a potential role for DCs in ensuring vascular restructuring and interacting with other cell populations localized to the uterine vasculature[87,88]. Moreover, mature $CD83^+$ DCs appear to still be capable of stimulating Th2 responses in T cells, although their ability to initiate Th1 responses may be impaired[89]. Thus, decidual DCs, despite being functionally suppressed as a potential threat to the fetoplacental unit, may still serve as potential antigen-presenting cells to decidual T cells, perhaps to direct contained, localized immune responses to pathogens.

1.2.4 Decidual T cells

T cells represent around 10-20% of the decidual leukocyte population during early pregnancy[90], consisting of roughly similar proportions of $CD4^+$ and $CD8^+$ T cells, along with small numbers of gamma-delta T cells[91] and $CD4^-CD8^-$ T cells[90]. Among $CD4^+$ T cells in first trimester human decidua, around 5% are Tregs[92], and overall, most T cells are antigen-experienced rather than naive ($CD45RO^+/CD45RA^-$)[93]. However, the precise proportions of these subsets and their enrichment in decidua relative to peripheral blood remain unclear, as some populations were analyzed in non-perfused decidua samples and therefore may in fact be intravascular[90]. The proportion of decidual T cells actually exhibiting specificity towards fetal antigens remains unknown as well[2]. Many T cells, including regulatory T cells, may traffic through peripheral tissues even in the absence of local inflammation or infection, and thus their presence in a tissue does not imply antigen-specific homing. Additionally, many T cells may have populated the decidua before or at the time of blastocyst implantation[90].

Most existing studies view effector T cells as antagonistic towards fetal tolerance and pregnancy success. Indeed, effector T cell accumulation at the maternal-fetal interface is associated with

complications such as chronic deciduitis[94], villitis of unknown etiology[95], and chronic chorioamnionitis[94,96], although the antigen specificities of these T cells are unknown. There is also no apparent path of direct antigen presentation to T cells residing in the secondary lymphoid organs via migrating DCs, which are trapped in the decidua[84]. Instead, fetal antigens reaching the lymph nodes appear to be disseminated systemically through the blood in a cell-free manner. Rather than promoting massive effector T cell activation and expansion, this less acute mode of antigen exposure results in the deletion of many responding T cells or their conversion into regulatory T cells (Tregs)[23]. Meanwhile, based on mice studies, even in the event of peripheral T cell expansion into activated Th1 and CTLs, their ability to actually extravasate into the decidua appears to be impaired due to epigenetic silencing of the genes producing Th1 and cytotoxic T cell chemokines CXCL9, CXCL10, CXCL11, and CCL5 in decidual stromal cells[97]. Given the low proportion of naive T cells in the decidua, however, it is possible that rather than initially encountering antigens at the maternal-fetal interface, the T cells first encountered antigen elsewhere before migrating to the uterus, where local antigen presentation by decidual DCs may further reinforce their activation[90]. One possible role for the persistence of effector T cells in the decidua and the potential for intradecidual DC antigen presentation may be to retain the ability to combat decidual infections and pathogens yet avoid compromising the overall tolerogenicity of the maternal-fetal interface[78,90].

A similar concept may apply to decidua-resident Treg subsets. In mice, Tregs were induced in lymph nodes upon DC presentation of seminal fluid antigens and exposure to TGF-β, and shown to home to the endometrium during the peri-implantation period[90,98]. Following blastocyst implantation and throughout the progression of early pregnancy, decidual Tregs may further expand upon local, possibly DC-mediated[78], exposure to fetal antigens, in order to dampen the activity of effector T cells at the maternal-fetal interface, or to counter general decidual inflammation through antigen nonspecific mechanisms such as secretion of IL-10 and TGF-β[90].

1.3 Recapitulating questions regarding the maternal-fetal interface

Cellular functions at the maternal-fetal interface appear to center around balancing immunological tolerance to the antigenically foreign fetus, immunity towards pathogens and generation of controlled inflammatory responses, and important nonimmune processes such as placentation and tissue remodeling. However, complete knowledge of the biology of the human maternal-fetal interface remains

limited by several factors. First, much existing knowledge of the initial events in embryonic development and the biology of implantation and placentation have been inferred from animal models of pregnancy[2,99]. While these share some key parallels with human pregnancy[99], they also differ in important aspects. For example, mice possess a dissimilar placental anatomy and exhibit significantly more superficial trophoblast invasion into the decidua[2]. This means that many findings in animal models may be species-specific and of limited relevance to humans. Meanwhile, due to ethical restrictions and limited availability, human fetal and decidual samples from the initial stages of pregnancy or during early pregnancy are unable to be widely obtained and studied[20]. Furthermore, many previous studies of the immunological state of human pregnancy have treated maternal-fetal coexistence as analogous to host-graft interactions, in which a constant state of immunosuppression is necessary to promote the growth of the fetus or maintenance of the transplant[23,100,101]. However, this model has since been challenged by accumulating evidence of the many dynamic adaptations exhibited by the maternal immune system during the establishment and early stages of pregnancy[23,102,103]. As a result, knowledge of the biology of early pregnancy in the human context remains largely incomplete. While many targeted studies of specific decidual and placental cell populations have proven insightful, the full range of cell types at the maternal-fetal interface and their potential functions and interactions remain uncharacterized.

Additionally, it is clear from existing studies that decidual and placental biology, and fetal implantation and development, reciprocally shape each other while heavily influencing pregnancy outcomes and the pathological mechanisms underlying infertility, preeclampsia, recurrent miscarriage, aberrant fetal growth, premature birth, and other reproductive and developmental disorders[2]. A more complete understanding of the maternal-fetal interface would therefore also advance efforts to better identify the cellular basis for these conditions. Moreover, the *in utero* environment has been increasingly linked to long-term health impacts[104], suggesting that the biology of the maternal-fetal interface may become consequential for general human health as well.

1.4 Introduction to the project

1.4.1 Studying the maternal-fetal interface at single-cell resolution

In this project, single cell RNA-sequencing (scRNA-seq) was applied to study cell types and cell functions in the human maternal-fetal interface during early pregnancy. Since the first assay to sequence all mRNAs in an unbiased fashion from single cells[105], a number of technological advances,

including improvements in single-cell isolation, cell capture, and methods for sample multiplexing (combining and parallel processing of samples), have facilitated both the large-scale generation and sensitive profiling of single cell transcriptomes[106–108]. These developments have made it possible to leverage scRNA-seq to analyze whole tissues, such as the decidua and placenta, at single-cell resolution. Meanwhile, advances in computation and in methods to meaningfully analyze single-cell data have enabled scRNA-seq to resolve distinct cell types and cell states on the basis of gene expression differences, as well as capture processes such as cellular differentiation and cell-cell communication[107], both of which would greatly contribute to dissecting the maternal-fetal interface. Thus, utilizing scRNA-seq to comprehensively identify and characterize cell populations comprising the decidua and placenta represents a promising avenue for furthering our understanding of the biology of early human pregnancy and of the maternal-fetal interface.

However, there are still remaining challenges in analyzing and interpreting scRNA-seq data. One challenge is confidently distinguishing cells in samples where the constituent cells may be derived from genetically distinct donors or from multiple sources (e.g. unwanted contamination). In the context of the maternal-fetal interface, this is particularly relevant as the decidual and placental tissues contain both cells from the mother and cells from the fetus. Robustly determining the genetic origin of each will be critical for annotating cellular functions and studying maternal-fetal crosstalk. Additionally, because scRNA-seq experiments are still accompanied by many practical limitations and potential sources of technical artifacts[106], such as the confounding influence of cellular dissociation protocols on gene expression[109], these must be detected and corrected for in the single-cell data of the maternal-fetal interface. Finally, a necessary task of every single-cell transcriptome-based study is placing findings in the context of existing knowledge of the cell types or tissues under study. Thus, consideration of existing gene expression data of the healthy and diseased decidua and placenta, as well as assays of gene expression at the protein level, would serve as important enhancements for an scRNA-seq-based analysis of the maternal-fetal interface.

1.4.2 Project aims

We sought to obtain a comprehensive overview of the maternal-fetal interface at the single-cell level through analyses integrating single cell transcriptomics of the decidua and placenta with orthogonal experimental approaches and datasets. First, we aimed to robustly annotate all cell populations

comprising the maternal-fetal interface by combining scRNA-seq gene expression analysis with inference of the maternal or fetal genetic origin of each cell, and by identifying and excluding cells exhibiting scRNA-seq-induced perturbations in observed gene expression. Next, we aimed to further study the local adaptation of the maternal immune system during early pregnancy by performing protein-level validation of marker genes distinguishing novel maternal immune populations, and by identifying potential functions assumed by these cells that are tailored to the unique functional demands of maternal-fetal interface. Finally, we aimed to better understand the cellular basis for various complications of pregnancy and other fertility-related traits, by mapping genes previously implicated in these conditions to specific cell types at the maternal-fetal interface.

1.4.3 Project design

Four maternal decidua samples, two fetal placenta samples, and matched maternal peripheral blood samples from early pregnancies were sequenced via droplet-based scRNA-seq (10x Chromium)[110]. An additional five decidua and two peripheral blood samples, enriching for specific cell subsets of interest, were also sorted via FACS and sequenced using the plate-based scRNA-seq protocol Smart-seq2[111]. Both sets of single-cell transcriptomic data were used to identify preliminary cell types and cell states at the maternal-fetal interface.

In order to better annotate cell populations, we sought to determine the fetal or maternal origin of all decidual and placental cells with the use of corresponding maternal and fetal whole genome sequencing data. We also aimed to ensure the robustness of our scRNA-seq-based analyses by identifying and excluding putative cell subpopulations exhibiting aberrantly high levels of tissue dissociation-induced genes[109].

For selected cell populations at the maternal-fetal interface, we sought to improve their functional annotation by leveraging Gene Ontology and Reactome term enrichment analysis, gene expression signatures of known cell types, and public placental and endometrial gene expression datasets. We also used FACS and CyTOF to validate the characterization of these cell populations at the protein level. Finally, in order to examine all identified cell populations in terms of their relevance to diseases and conditions affecting the maternal-fetal interface, we examined the cell type-level expression patterns of genes previously linked with complications of pregnancy or fertility-related conditions via genome-wide association studies (GWAS) or functional genomics studies.

1.4.4 Overview of thesis

This thesis is divided into six chapters. Following this introduction (Chapter 1), Chapter 2 provides a description of the experiments and data analyses performed in this study. In Chapter 3, I present the results of combining scRNA-seq with whole genome sequencing to infer the maternal or fetal genetic identity of each cell, and of utilizing bulk RNA-sequencing to determine the presence of potential technical artifacts in scRNA-seq data. Next, in Chapter 4, I discuss our protein-level validation of novel immune cell subsets at the maternal-fetal interface, along with our additional functional characterization of maternal mononuclear phagocyte populations in the context of established gene signatures and tissue-level gene expression data. Chapter 5 describes our single cell transcriptomics-level analyses of genes previously linked to complications of pregnancy or fertility-related conditions, and our insights into the relevance of specific cell types to these diseases or conditions. Finally, in Chapter 6, I summarize the overall conclusions from this study and potential future work to be undertaken.

Chapter 2 - Materials and Methods

Experimental procedures

Experiments associated with the data presented in this thesis were performed by Roser Vento-Tormo with help from Margherita Turco, Rachel Botting, Jongeun Park, and Rebecca Payne, and are described in Appendix 1.

Data analysis

I performed all analyses described in the following sections with the exception of the work described under "Single-cell RNA-sequencing data analysis," which was performed by Mirjana Efremova.

Single-cell RNA-sequencing data analysis

Droplet-based scRNA-seq data was aligned and quantified using the Cell Ranger Single-Cell Software Suite (v.2.0)[110] against the GRCh38 human reference genome. Cells with fewer than 500 detected genes or more than 20% mitochondrial gene content were removed. Genes expressed in fewer than 3 cells were also removed. SmartSeq2 sequencing data was aligned with HISAT2[112] using the same genome reference and annotation as the droplet-based data. Gene-specific read counts were calculated using HTSeq-count[113]. Cells with fewer than 1,000 detected genes or more than 20% mitochondrial gene content were removed. Genes expressed in fewer than 3 cells were also removed. Downstream analyses such as gene expression log-normalization, k-nearest neighbor graph clustering, differential expression analyses (Wilcoxon rank-sum test), and visualization using the t-SNE algorithm[114] were performed using the R package Seurat v.2.1.0[115]. t-SNE analyses were performed using a perplexity of 30. Clusters were annotated based on expression of canonical cell type markers listed in Appendix 2. We further removed cells we did not gate for (most likely maternal blood B cells and fetal brain tissue), clusters for which the top markers were genes associated with dissociation-induced effects[116], or mitochondrial genes, and a fibroblast cluster with high expression of hemoglobin genes due to background contamination of cell-free RNA.

Maternal-fetal single-cell genotyping

Whole-genome sequencing alignment and variant calling:

Maternal and fetal whole-genome sequencing data were mapped to the GRCh37.p13 reference genome using BWA-MEM v.0.7.15[117]. The SAMtools[118] fixmate utility v.1.5 was used to update read pairing information and mate-related flags. Reads near known indels from the Mills[119] and 1000G[120] gold standard reference set for GRCh37/hg19 were locally realigned using GATK IndelRealigner v.3.7[121] (*-model* KNOWNS_ONLY *-LOD* 0.4). Base calling assessment and base quality scores were adjusted with GATK BaseRecalibrator and PrintReads v.3.7[121]. PCR duplicates were identified and removed using Picard MarkDuplicates v.2.14.1[121,122]. Finally, bcftools mpileup and call v.1.6[123] were used to produce genotype likelihoods and output called variants at all known biallelic SNP sites overlapping protein-coding genes, compiled from NCBI dbSNP build 138 (GRCh37/hg19)[124]. For each sample, variants called with phred-scale quality score (QUAL) ≥ 200, at least 20 supporting reads (DP ≥ 20), and mapping quality (MQ) ≥ 60 were retained as high-quality variants.

Inferring maternal/fetal genetic origin of single cells from droplet-based scRNA-seq using whole-genome sequencing variant calls:

To match the processing of the whole-genome sequencing datasets, droplet-based sequencing data from decidua and placenta samples were realigned and quantified against the GRCh37 human reference genome using the Cell Ranger Single-Cell Software Suite (v.2.0)[110]. The fetal or maternal origin of each barcoded cell was then determined using the tool demuxlet[125]. Briefly, demuxlet can be used to deconvolute droplet-based scRNA-seq experiments in which cells are pooled from multiple, genetically distinct individuals. Given a set of genotypes corresponding to these individuals, demuxlet infers the most likely genetic identity of each droplet by evaluating scRNA-seq reads from the droplet which overlap known SNPs. Demuxlet inferred the identities of cells in this study by analyzing each Cell Ranger-aligned BAM file from decidua or placenta in conjunction with a VCF containing the high-quality variant calls from the corresponding WGS of maternal and fetal DNA (*--field* GT). Each droplet was assigned to be maternal, fetal, or unknown in origin (ambiguous or potential doublet), and these identities were then linked with the transcriptome-based cell clustering data to confirm the maternal and fetal identity of each annotated cell type.

Inferring maternal/fetal genetic origin of single cells from droplet-based scRNA-seq read data alone:

10x Chromium droplet-based sequencing data from decidua and placenta samples were realigned and quantified against the GRCh37 human reference genome using STAR v.2.2.1[126] with the following parameters: *--alignSJoverhangMin* 8, *--alignSJDBoverhangMin* 1, *--alignIntronMin* 20 *--alignIntronMax*

1000000, *--alignMatesGapMax* 1000000, *--sjdbScore* 2, *--outFilterType* BySJout, *--outFilterMultimapNmax* 20, *--outFilterMismatchNmax* 999, *--outFilterMismatchNoverLmax* 0.04, *--outFilterScoreMinOverLread* 0.33, *--outFilterMatchNminOverLread* 0.33, *--outSAMstrandField* intronMotif, *--outFilterIntronMotifs* RemoveNoncanonical, *--outSAMattributes* NH HI NM MD AS XS, *--outSAMunmapped* Within, *--twopassMode* Basic.

Reads near known indels from the Mills[119] and 1000G[120] gold standard reference set for GRCh37/hg19 were locally realigned using GATK IndelRealigner v.3.7[121] (*-model* KNOWNS_ONLY *-LOD* 0.4). Base calling assessment and base quality scores were adjusted with GATK BaseRecalibrator and PrintReads v.3.7[121]. Next, reads in each sample BAM file were split by Chromium cellular barcode to produce a separate BAM file for each single cell from the sample. For each single-cell BAM file, PCR duplicates were identified and removed using Picard MarkDuplicates v.2.14.1[121,122]. Finally, GATK HaplotypeCaller v.3.7[121] was used to produce genotype likelihoods and output called variants for each cell based on reads containing known biallelic SNP sites from NCBI dbSNP build 138 (GRCh37/hg19)[124] overlapping the top 1000 genes most highly expressed in placental and endometrium RNA-seq data deposited in the Human Protein Atlas[127,128].

The vcf files from decidual and placental single cells were merged and the R/Bioconductor package vcfR v.1.6.0[129] was used to import the merged vcf into R as a sparse matrix. We performed filtering on the SNPs so that only SNPs called in more than one cell and with non-zero variance were retained for downstream analysis. Next, using the R/Bioconductor package pcaMethods v.1.68.0[130], we performed a probabilistic PCA ("ppca") on the SNP data with unit variance scaling ("uv") on two principal components and visualized the resulting projections using ggplot2, colored by tissue of origin or previously inferred cell identities.

Decidua bulk RNA-sequencing processing and heat shock protein expression analysis

Reads from five decidua bulk RNA-seq samples were mapped and quantified against the GRCh38 (release 88) human reference transcriptome using the lightweight-alignment (SMEM-based) mode in Salmon v.0.8.1[131]. The R/Bioconductor package tximport v.1.4.0[132] was used to aggregate the transcript-level abundances into gene-level expression estimates (TPM) with Ensembl gene IDs (GRCh38) as the primary identifier. Ensembl IDs were then mapped to HGNC gene symbols using R/Bioconductor package biomaRt v.2.32.1[133]. We specifically examined the expression of heat shock

protein-related genes *HSPA6, DNAJB1, HSPH1, DNAJA4, HSP90AA1, HSPA1A, HSPA1B, HSPD1, DNAJA1, HSPA8,* and *HSPB1* in the bulk RNA-seq datasets. These were among the most highly upregulated genes in the T3 T cell cluster identified from analysis of the decidua plate-based scRNA-seq data. *HSPB1, HSPA1A,* and *HSPA1B* were also among the genes previously found to be induced by single-cell dissociation protocols[109].

FACS and SmartSeq2 data analysis

FACS data were gated and compensated in FlowJo and exported as FCS files. Gating identities coupled with plate locations from index sorting were then imported into R using the Bioconductor package flowCore v.1.42.3[134] and linked to the metadata for each corresponding cell generated from Seurat analyses of decidua and peripheral blood SmartSeq2 data (as performed in "Single-cell RNA-sequencing data analysis"). This facilitated superimposition of the gated identities of cells onto the t-SNE projections defined by single-cell transcriptomes. Differential expression analysis between the dMP1 and dMP2 subsets was performed using the Seurat *FindMarkers* function (Wilcoxon rank-sum, among genes expressed in at least 10% of cells).

CyTOF data analysis

Populations of interest were manually gated in FlowJo and exported as FCS files. Subsequent analyses were conducted with the Bioconductor package cytofkit v.1.8.4[135]. First, signal intensities for each marker were transformed using the negative value pruned inverse hyperbolic sine transformation (cytofAsinh). To obtain two-dimensional visualizations of the CyTOF data, the t-SNE algorithm[114] was applied to 10,000 randomly selected cells from each dataset and plotted using the R package ggplot2. Marker expression was visualized on the t-SNE plots, with maximum intensity designated as marker expression intensities in the 99th percentile or higher.

Gene Ontology and Reactome term enrichment analysis

Genes significantly upregulated ($\log_2$(fold-change) ≥ 0.5, adjusted $p < 0.05$, Wilcoxon rank-sum) in each of the mononuclear phagocyte populations relative to other cell types at the maternal-fetal interface were functionally annotated using gene ontology (GO)[136] and Reactome[137] pathway terms. We used the R/Bioconductor package gProfileR v.0.6.4[138] to map gene lists ordered by decreasing $\log_2$(fold-

change) (*ordered_query* = T) to biological pathway (BP) and molecular function (MF) GO terms and Reactome pathway annotations. Through gProfileR we then performed statistical enrichment analysis to identify and output overrepresented terms with strong hierarchical filtering (*hier_filtering* = "strong"). All *p*-values were corrected for multiple testing using the gProfileR gSCS algorithm[138].

Intersection of M1/M2 gene signatures with maternal mononuclear phagocyte subset markers

We obtained a list of canonical M1 macrophage and M2 macrophage marker genes[139] and used biomaRt v.2.32.1[133] to map the gene symbols to corresponding Ensembl gene IDs. We then intersected this gene list with our lists of upregulated genes (adjusted $p < 0.05$, Wilcoxon rank-sum) from each of the mononuclear phagocyte populations relative to other decidual and placental cell types. Heatmaps showing single cell-level expression of the M1/M2 genes were plotted using the *DoHeatmap* function in Seurat, with genes presented in decreasing $\log_2$(fold-change), grouped by the mononuclear phagocyte population in which they were significantly upregulated. If a gene was upregulated in multiple mononuclear phagocyte subsets, it was grouped with the subset in which it exhibited the highest $\log_2$(fold-change) relative to other cell types.

Identification of placenta- and endometrium-specific genes and intersection with maternal resident immune cell population markers

Tissue-level RNA-seq data were downloaded from the Human Protein Atlas (www.proteinatlas.org)[127,128]. We obtained gene expression data (in tpm) for 37 human tissues sourced from 122 individuals; the associated experiment accession for this dataset in the ArrayExpress database is E-MTAB-2836.

To identify genes specifically enriched in the placenta and endometrium relative to other tissues, we employed the tissue specificity metric Tau[140], which was determined to be among the most robust methods for determining tissue-specific gene expression patterns in a recent comparative analysis[141] with other approaches, including expression enrichment (EE)[142], Hg (Shannon entropy)[143], tissue-specificity index (TSI)[144], and z-score[145]. For each gene, we calculated Tau using the following formula:

$$\tau = \frac{\sum_{i=1}^{n}\left(1-\widehat{x_i}\right)}{n-1}; \ \widehat{x_i} = \frac{x_i}{\max\limits_{1\le i\le n}(x_i)}.$$

where x_i is the expression of gene in tissue i and n is the total number of tissues. Genes with Tau ≥ 0.8[141] and tissue of highest level of expression being placenta or endometrium were determined to be significantly enriched in these tissues. A list of the 410 placenta- and endometrium-enriched genes is located in Appendix 5.

We then intersected this gene list with our lists of upregulated genes (adjusted $p < 0.05$, Wilcoxon rank-sum) from each of the maternal resident immune cell populations (T cells, NK cells, mononuclear phagocytes) relative to other decidual and placental cell types. Heatmaps showing single cell-level expression of the placenta- and endometrium-enriched genes were plotted using the *DoHeatmap* function in Seurat v.2.1.0, with genes presented in decreasing $\log_2$(fold-change), grouped by the maternal resident immune cell type in which they were significantly upregulated. If a gene was determined to be upregulated in maternal resident immune cell subsets, it was grouped with the population in which it exhibited the highest $\log_2$(fold-change) relative to other cell types.

Curation of genes associated with fertility or complications of pregnancy and analysis of cell-type specific expression at the maternal-fetal interface

Genes associated with abnormal birth weight or fetal growth, endometriosis/ovarian disease, gestational trophoblastic disorder/hydatidiform mole, preeclampsia, age of menopause or menstrual onset, preterm birth, recurrent miscarriage, placental abruption, and placenta accreta were curated from studies deposited in the NHGRI/EBI GWAS Catalog[146], OMIM database[147], and from literature searches. All genes selected from literature were linked with increased mutation or with alterations in expression or epigenetic regulation in studies of a particular condition in humans or human tissues. A full table of compiled genes, along with their associated conditions and their literature or database sources, is provided in Appendix 6.

We first intersected our curated gene list with our lists of upregulated genes (adjusted $p < 0.05$, Wilcoxon rank-sum) from each of the cell populations at the maternal-fetal interface relative to other decidual and placental cell types. Heatmaps showing cell type-averaged expression of the disease- or fertility-associated genes were plotted using the *heatmap* function in R, with genes presented in decreasing $\log_2$(fold-change), grouped with the cell type in which they were significantly upregulated. If a gene was determined to be upregulated in multiple cell types, it was grouped with the cell type in which it exhibited the highest $\log_2$(fold-change) relative to other cell populations. For our maternal- and fetal-specific

analyses, we first determined which genes were significantly upregulated (adjusted $p < 0.05$) in each maternal cell type relative to other maternal cell types, or in each fetal cell type relative to other fetal cell types, using the Seurat *FindMarkers* function (Wilcoxon rank-sum, among genes expressed in at least 10% of cells). We then intersected our curated gene lists with these maternal- and fetal-specific upregulated gene lists and plotted cell type-averaged gene expression using the *heatmap* function in R as previously described.

Chapter 3 - Combining single-cell transcriptomics with whole genome sequencing and bulk RNA-sequencing to improve cell-type annotations

3.1 Overview

A primary goal of this study is to generate a single-cell atlas of the maternal-fetal interface by comprehensively and robustly profiling the identities and potential functions of its constituent cell types and cell states. Beyond annotating cells by their gene expression patterns as detected by scRNA-seq, additional analyses utilizing other sequencing approaches are important for validating and further describing the identified cell populations. In this chapter, I first present our approaches for inferring the maternal or fetal genetic origin of single cells from decidua and placenta scRNA-seq data. I then discuss our use of bulk RNA-sequencing data to assess whether the detected gene expression signature of a specific cell population from scRNA-seq is a potential artifact attributable to single-cell sequencing protocols rather than a reflection of true biological variability.

3.2 Maternal-fetal single-cell genotyping

3.2.1 Droplet-based scRNA-seq and whole genome sequencing data

Previously, 37239 cells derived from four decidual and two placental samples were sequenced using droplet-based scRNA-seq (10x Genomics Chromium[110]) (sample information in **Table 1**). Unsupervised graph-based clustering was applied to the data, and marker genes from Appendix 2 were used to annotate clusters as specific cell populations (**Figure 1**). Overall, 28 cell states were predicted by this approach, including populations of decidual fibroblasts, glandular epithelial cells, endothelial cells, dNK cells, decidual myeloid cells, and decidual T cells, as well as subsets of trophoblasts, fetal fibroblasts, and Hofbauer cells (fetal macrophages).

Table 1. Droplet-based scRNA-seq and whole genome sequencing (WGS) sample information.

Donor	Post-conceptional weeks	Pregnancy	10x Chromium - Decidua	10x Chromium - Placenta	WGS - Tissues	Fetus sex
D1	9 to 11	2nd	6514 cells		Fetal placenta / Maternal blood	female
D2	6 to 8	1st	6546 cells		Fetal placenta / Maternal blood	female
D3	5 to 7	6th	8070 cells	5510 cells	Fetal placenta / Maternal decidua	male
D4	9 to 11	3rd	8860 cells	2029 cells	Fetal placenta / Maternal decidua	male

For each of the decidual and placental samples, genomic DNA from the corresponding mother and fetus were sequenced at 30x coverage (see Methods). Information about the genomic DNA samples

and fetus sex, as determined by filtered SNP calls on the sex chromosomes, are also described in **Table 1**.

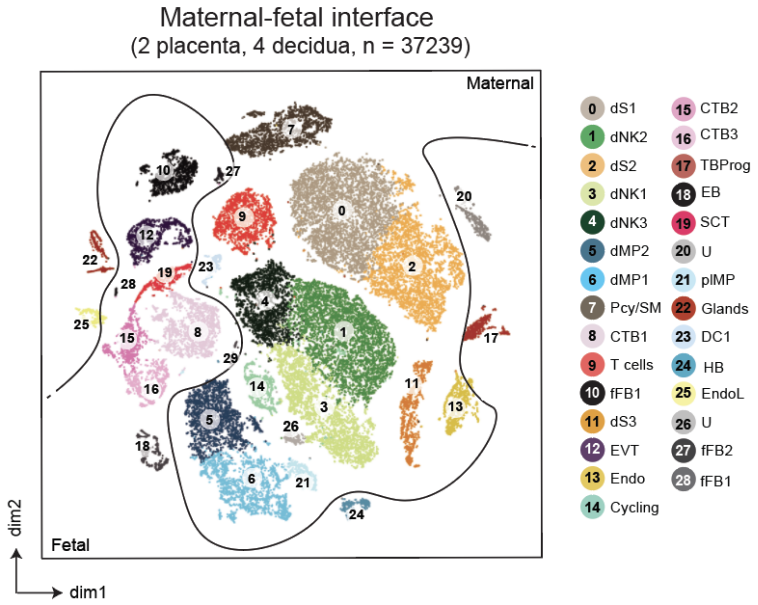

Figure 1. t-SNE visualization of cell populations at the maternal-fetal interface. Cells are colored by predicted cell type or cell state, as inferred by unbiased clustering of decidua and placenta droplet-based scRNA-seq data and annotation based on known markers (from Vento-Tormo R, Efremova M et al., under submission). Legend for cell population abbreviations: CTB = cytotrophoblast cells; EVT = extravillous trophoblast cells; SCT = syncytiotrophoblast cells; TBProg = trophoblast progenitor cells; dS = decidual stromal cells; DC = dendritic cells; dMP = decidual mononuclear phagocytes; plMP = placental mononuclear phagocytes; EndoL = lymphatic endothelial cells; Endo = endothelial cells; Tcell = T cells; dNK = decidual NK cells; ILC = innate lymphoid cells; fFB = fetal fibroblast cells; Glands = decidual glandular cells; HB = Hofbauer cells; Pcy/SM = pericytes/vascular smooth muscle cells.

3.2.1 Limitations in unbiased assignment of maternal/fetal origin to cells without genotype data

In order to evaluate the distribution of maternal and fetal cell populations in the decidua and placenta, we sought to independently determine the maternal or fetal genetic origin of all cells sequenced from these tissues. We first assessed whether it was possible to distinguish maternal-derived and fetal-derived cells based solely on variant calling from decidual and placental scRNA-seq data. Due to runtime constraints, we only called known SNPs from the reads in each barcoded cell that were mapped to the 1000 most highly expressed genes in placenta and endometrium, as determined from Human Protein Atlas[127,128] tissue-level gene expression data (see Methods). We then performed a probabilistic PCA (PPCA) on the called SNPs among all decidual and placental cells to assess whether cells originating from the mother would be distinguishable from cells originating from the fetus. While PPCA yielded separation between a fraction of the decidual cells, which are generally maternal in origin, and

the placental cells, which are generally fetal in origin, it failed to separate a majority of the remaining cells by tissue or expected individual of origin (**Figure 2a**).

We reasoned that the inherent sparsity of scRNA-seq data[148,149], the limited sequence information extractable from 3' end sequencing protocols such as the 10x Chromium droplet-based scRNA-seq[110], and the intuition that different cell types often exhibit divergent sets of expressed genes, all impede the ability to call a sufficient number of SNPs that are both consistently detectable across many analyzed cells and informative for genetically differentiating mother from fetus. Indeed, we observed that a significantly higher proportion of the genes sampled for variant calling were expressed in decidual non-immune cells and placental cells relative to decidual immune cells ($p < 2 \times 10^{-16}$) (**Figure 2b**). This suggests that fewer informative SNPs were callable in decidual immune cells, thus hindering the ability to distinguish maternal or fetal genotypes in these cells. We therefore then performed PPCA on a subset of non-immune cells which were previously inferred by single-cell transcriptome-based analyses to be maternal stromal cells, fetal trophoblast cells, and an unknown cell population (cluster 21) found in both decidua and placenta (**Figure 2c**). The PPCA reveals apparent separation between the maternal and fetal cells and places the unknown population closer to the fetal trophoblast population, suggesting that this approach is able to detect interindividual genetic heterogeneity among single cells belonging to specific cell types. However, we show that if the PPCA is repeated using a decidual immune cell population, such as the maternal macrophages, in place of maternal stromal cells, the qualitative separation between maternal and fetal cells is no longer apparent (**Figure 2d**). Overall, our implementation of an scRNA-seq-only variant calling and single-cell genotyping pipeline appears to be able to qualitatively distinguish certain cell types at the maternal-fetal interface by individual of origin but requires further development to be able to fully resolve maternal and fetal identities among all decidual and placental cells in an unbiased, cell type-independent manner.

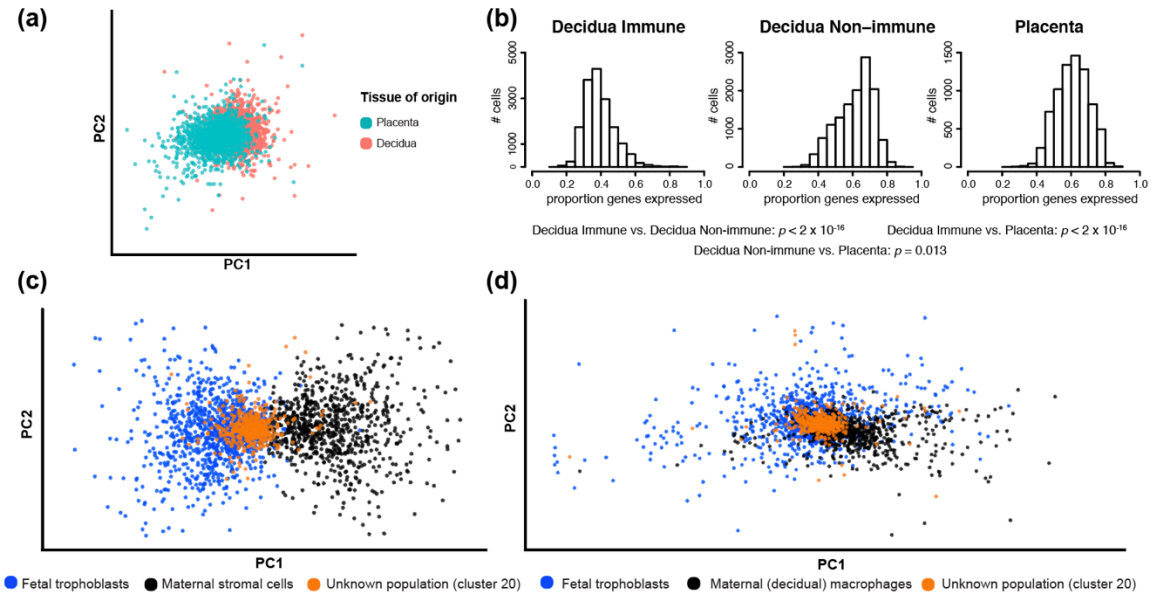

Figure 2. Variant calling from scRNA-seq data alone shows limitations in inferring the maternal or fetal genetic origin of cells from the decidua and placenta. (a) Probabilistic PCA (PPCA) on 19343 SNPs called in cells from Donor 4 yielded substantial overlap between maternal decidua-derived cells and fetal placenta-derived cells, suggesting limited ability to discriminate cells by tissue/individual of origin. **(b)** The 1000 most abundant genes in placenta and endometrium, which contain the SNP sites analyzed by the variant calling pipeline, are expressed in significantly different proportions between decidual immune cells, decidual non-immune cells, and placental cells (pairwise Student's t-test, Benjamini-Hochberg adjusted *p*-values). **(c)** PPCA of SNP calls in cells from three non-immune ($CD45^-$) subsets yields separation between maternal stromal and fetal trophoblast cells and suggests that the unknown cell population is fetal in origin. **(d)** PPCA of SNP calls in cells from both immune and non-immune populations is unable to qualitatively separate fetal trophoblast cells, maternal macrophages, or the unknown cells.

3.2.2 Comprehensive and unbiased assignment of single-cell genetic origin, leveraging demuxlet algorithm and WGS of maternal and fetal genomic DNA

Next, we assessed whether the incorporation of maternal and fetal WGS data would enable us to determine the genetic identity of each cell from the scRNA-seq data in an unbiased fashion. We used the recently published demuxlet tool[125], which leverages inter-individual genetic variation, as determined from provided genotype data, to infer the most likely origin of each cell in scRNA-seq experiments containing cells derived from distinct individuals. First, we performed alignment and variant calling on maternal and fetal WGS datasets corresponding to the decidua and placenta droplet-based scRNA-seq samples (see Methods; **Table 1**). We then used demuxlet to analyze the scRNA-seq data in conjunction with the maternal and fetal genotypes, in order to correlate detectable SNPs overlapping reads from decidual and placental cells with SNPs from maternal and fetal genomic DNA and probabilistically assign each cell as being maternal or fetal in origin. To visualize the results, we overlaid the maternal/fetal assignments from demuxlet onto a t-SNE representation of the decidual and placental

single-cell transcriptome data, facilitating direct comparison between annotated cell populations (**Figure 3a**), tissue of origin (**Figure 3b**), and demuxlet-inferred genetic origin (**Figure 3c**). Demuxlet assignments for each cluster or cell type are largely consistent with the known biology of these cells. For example, dNK cell populations (clusters 1, 3, 4), which are known to make up the largest maternal immune population at the maternal-fetal interface[2], were inferred to be maternal cells, and the trophoblast cells (clusters 8, 12, 15-17, 19), which comprise the growing placenta, were identified to be fetal cells. Additionally, as expected, cells originating from the decidua were largely determined to be of maternal origin, and cells from the placenta of fetal origin. One notable exception is the small fraction of decidua-derived EVT (cluster 12) identified to be fetal cells, which aligns with the observation that they invade the pregnant endometrium[150]. Meanwhile, the unknown cell population found in both decidual and placental samples (cluster 20) was determined to be fetally derived, consistent with what was qualitatively suggested by our DNA-free genotyping pipeline results (**Figure 2c**). Interestingly, a myeloid subset found exclusively in both placenta samples (cluster 21) and initially hypothesized to be a fetal macrophage population was inferred by demuxlet to be maternal in origin. These cells potentially correspond to patrolling maternal monocytes attached to the placental villi as previously described[151].

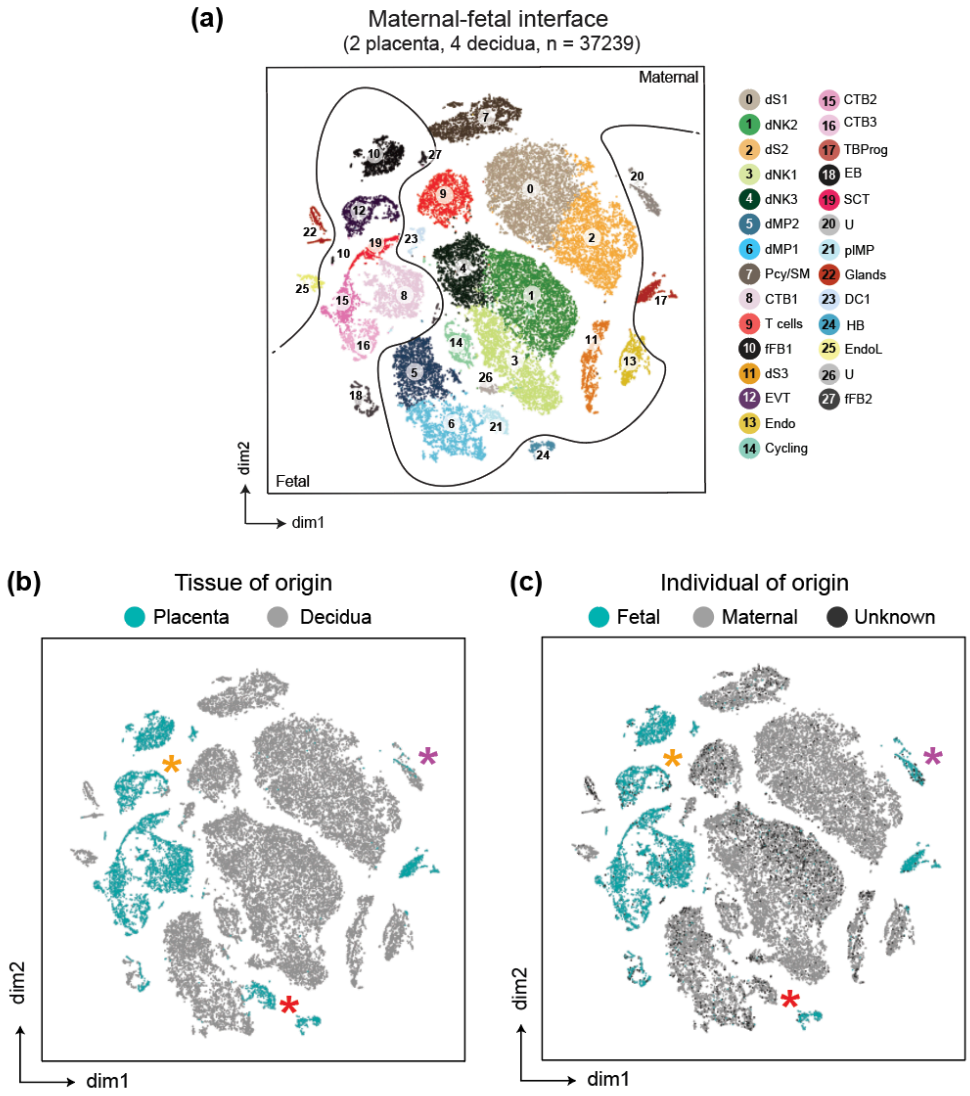

Figure 3. t-SNE visualizations juxtaposing cell type annotations, tissue of origin, and assignment of maternal and fetal identity. (a) Figure 1 reproduced for reference; cells colored by marker-based annotation. **(b)** Cells colored by tissue of origin (decidua or placenta). **(c)** Cells colored by demuxlet inference of origin (maternal, fetal, or unassigned). The orange star labels EVT found in the decidua that were determined to be of fetal origin. The purple star labels the unannotated cell population found in both decidua and placenta determined to be of fetal origin. The red star labels the mononuclear phagocytes derived from the placenta determined to be of maternal origin.

Demuxlet uses a maximum likelihood approach to infer the best-matching genotype and sample identity of each cell[125]. Thus, we further assessed the likelihood differences between assignment to fetal origin and assignment to maternal origin for all analyzed cells (**Figure 4a**). Although likelihood differences vary between individual cells, the 92.8% of cells with conclusively inferred maternal or fetal identity are on average highly confidently assigned. However, we observed that many of the cells with a larger number of quality control (QC)-passed scRNA-seq reads were called with lower confidence than their

counterparts with fewer QC-passed reads. The placental macrophages identified to be maternal in origin were among the cells with fewer QC-passed reads (**Figure 4b**), and we confirmed that confidence in their assignment did not significantly differ from that of other assigned maternal cells (p = 0.2638, Student's t-test).

Next, we evaluated the relative proportions of assigned fetal, maternal, and unknown cells in each of the annotated cell types (**Figure 4c**). Although the percentages of cells with unknown identity varied between cell types, a sufficient number of cells were conclusively identified within each cell type to infer a consensus fetal or maternal origin for each population. The sole exception is the cluster corresponding to erythrocytes and erythroblasts (EB), which contains significant proportions of both maternal and fetal cells, suggesting the presence of both maternal and fetal blood in the tissue samples. As all other documented cell types in the decidua and placenta are known to be exclusively maternal or fetal in origin, our results thus corroborate the single-cell transcriptome-based clustering and cell type annotations at the genetic level. Overall, our results suggest that demuxlet can be applied to confidently infer the genetic identities of individual cells in scRNA-seq samples of mixed maternal and fetal origin. Furthermore, we show that the single-cell genotyping results may in themselves reveal additional biological insights not immediately apparent from purely transcriptome-based analyses.

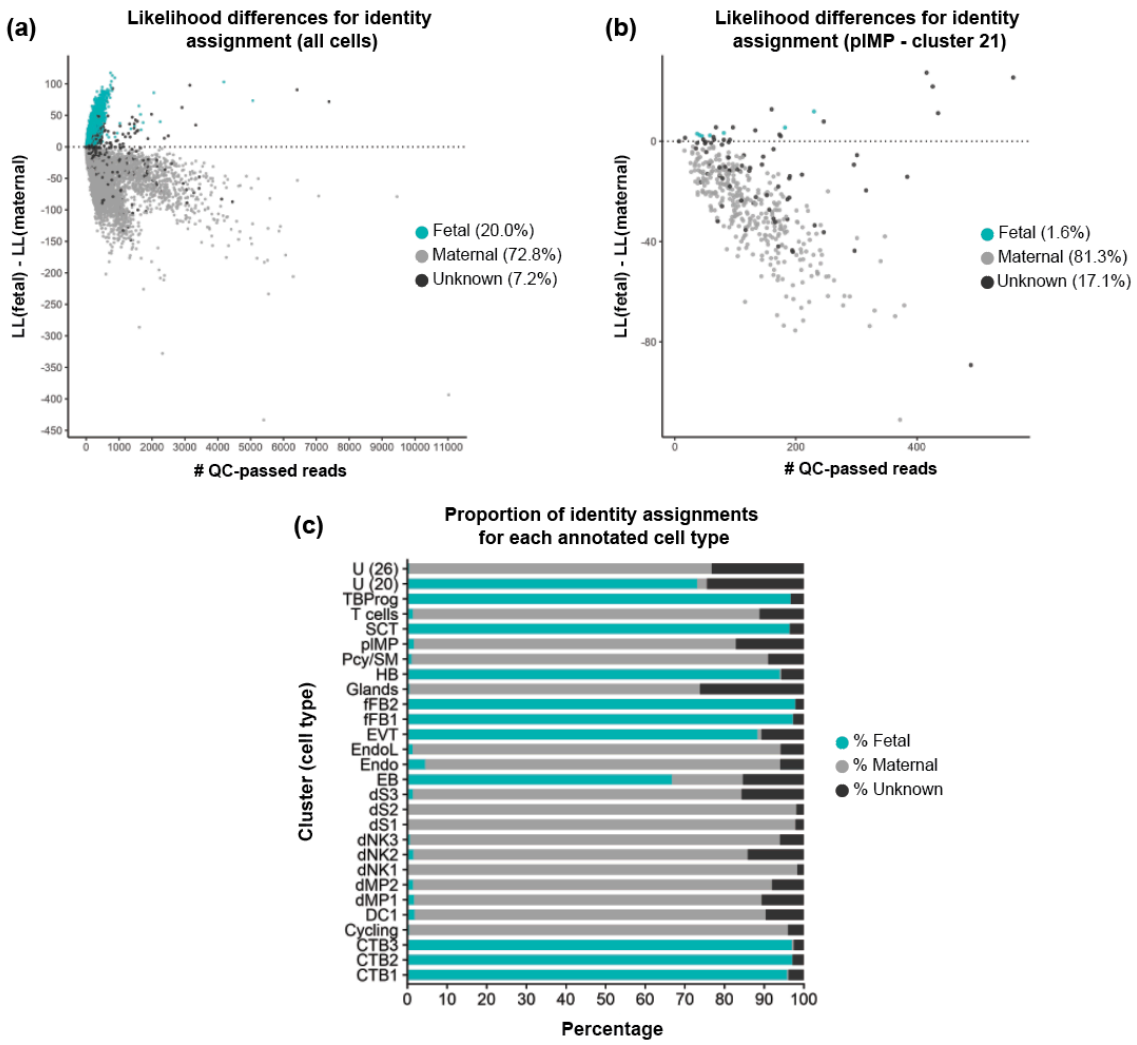

Figure 4. Assessment of demuxlet performance in genotyping all cell populations at the maternal-fetal interface. (a) Log-likelihood differences between assignment to fetal origin or assignment to maternal origin for all cells based on demuxlet SNP calling from the droplet-based scRNA-seq data. Cells are colored by their final origins as determined by demuxlet. **(b)** Log-likelihood differences between assignment to fetal or maternal origin for the maternal mononuclear phagocytes (pIMP) from the placenta. pIMP likelihood differences do not significantly differ from the likelihood differences associated with all other demuxlet-assigned maternal cells (p = 0.2638, Student's t-test). **(c)** Percentages of cells inferred to be of fetal, maternal, or unassigned origin for each annotated cell population.

3.3 Bulk RNA-sequencing evaluation of putative dissociation protocol-associated genes

Initial clustering and annotation of all plate-based scRNA-seq of maternal decidua cells identified a putative decidual T cell population (T3) with many of the most highly upregulated genes belonging to various heat shock protein (HSP) families[152] (**Figure 5a-b**, **Table 2**).

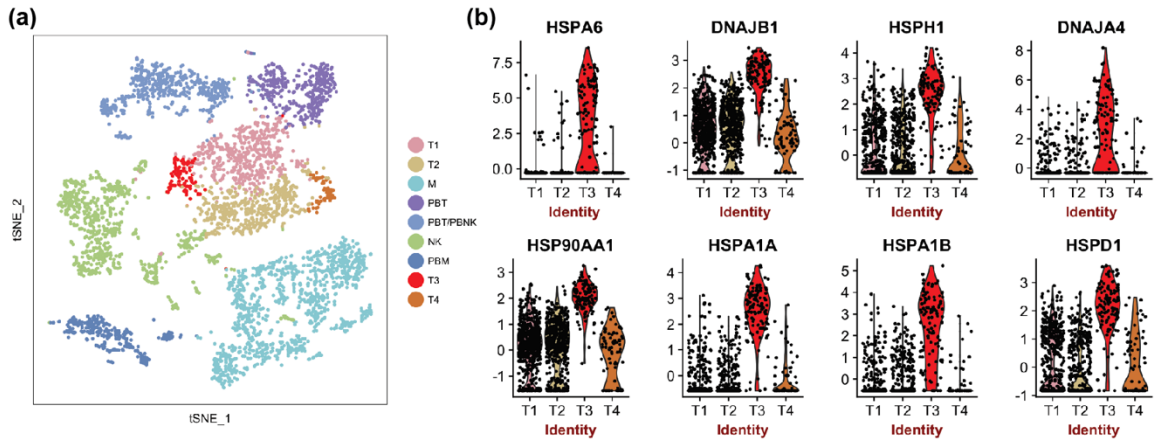

Figure 5. Identification of T cell subpopulation exhibiting significant upregulation of heat shock protein (HSP) genes from decidua plate-based scRNA-seq data. (a) t-SNE mapping of decidual cell populations as inferred from unbiased clustering, with the T cell subpopulation of interest (T3) in red. **(b)** Violin plot comparing the expression of the HSP genes comprising the top 10 most upregulated genes in T3 across all T cell subpopulations.

Table 2. Gene identifiers, fold changes, and *p*-values for the HSP genes of interest in T3. (Genes in blue were previously shown to be induced following tissue dissociation[109].)

Gene name	Ensembl gene ID	p value	ave $\log_2$(FC)	adjusted p value
HSPA6	ENSG00000173110	2.70E-69	3.043	8.17E-65
DNAJB1	ENSG00000132002	6.34E-68	2.910	1.92E-63
HSPH1	ENSG00000120694	1.17E-70	2.377	3.53E-66
DNAJA4	ENSG00000140403	1.08E-56	2.359	3.27E-52
HSP90AA1	ENSG00000080824	3.63E-67	2.286	1.10E-62
HSPA1A	ENSG00000204389	2.39E-78	2.213	7.23E-74
HSPA1B	ENSG00000204388	3.75E-68	2.160	1.14E-63
HSPD1	ENSG00000144381	1.32E-61	2.137	4.00E-57
DNAJA1	ENSG00000086061	6.91E-50	2.051	2.09E-45
HSPA8	ENSG00000109971	2.79E-55	1.991	8.46E-51
HSPB1	ENSG00000106211	1.17E-62	1.108	3.54E-58

A recent study demonstrated that HSPs are among the stress-induced genes in certain subpopulations of cells as a consequence of the tissue dissociation protocols used to extract cells for scRNA-seq[109]. In light of these findings, we evaluated the expression of the upregulated HSP genes in T3 cells in a set of bulk RNA-sequencing data generated on the same decidua samples. As single-cell tissue dissociation is not a necessary component of bulk RNA-sequencing experiments, we reasoned that comparing detectable genes between scRNA-seq and corresponding bulk RNA-seq datasets would enable us to account for the potential effects of these protocols. Upon performing alignment and gene quantification in the decidua bulk RNA-seq samples (see Methods), we specifically examined the expression levels of the HSP genes below, which were either highly upregulated in the T3 subpopulation or implicated in the single-cell dissociation protocol study (**Table 3**).

Table 3. Expression levels of the HSP genes from Table 2 in bulk decidua RNA-seq data (tpm).

Gene name	Ensembl gene ID	Donor 5	Donor 6	Donor 7	Donor 8	Donor 9
HSPA6	ENSG00000173110	0.51	1.43	1.95	1.81	1.04
DNAJB1	ENSG00000132002	13.64	17.67	12.01	15.77	14.66
HSPH1	ENSG00000120694	6.52	6.20	9.23	8.39	6.80
DNAJA4	ENSG00000140403	0.61	1.39	2.32	1.64	2.04
HSP90AA1	ENSG00000080824	39.55	31.69	40.28	49.02	38.08
HSPA1A	ENSG00000204389	0.00	2.32	0.90	3.92	10.80
HSPA1B	ENSG00000204388	0.00	0.00	0.00	0.00	0.04
HSPD1	ENSG00000144381	14.52	13.26	17.50	20.31	16.57
DNAJA1	ENSG00000086061	15.45	9.00	19.87	20.63	18.02
HSPA8	ENSG00000109971	282.95	134.65	289.29	305.98	228.79
HSPB1	ENSG00000106211	118.41	110.06	128.27	155.58	131.52

Overall, the HSP genes are also detectable in the bulk RNA-seq samples, although many are expressed at low levels. Because T cells comprise a small proportion of decidual cells[90], it is conceivable that these genes could be attributed to a particular T cell subpopulation in the decidua. However, we observed that *HSPA1B*, the 7th most highly upregulated gene in T3 decidual T cells, is not significantly expressed in any of the bulk decidua samples, suggesting that the genes found to be most significantly enriched in T3 are likely to be influenced by single-cell dissociation protocols rather than reflect a functionally distinct T cell subpopulation. Thus, we excluded the T3 cells from subsequent single cell-level annotations and analyses. These results suggest that evaluating the expression of a gene of interest in both scRNA-seq and corresponding bulk RNA-seq can serve as a rough heuristic for determining whether it is a potential dissociation protocol-related artifact.

3.4 Discussion

In this chapter, I evaluated different approaches for genetically distinguishing maternal and fetal cells in the decidua and placenta in an unbiased manner. I first presented our approach for inferring the maternal or fetal origin of cells based on variant calling on the scRNA-seq reads alone. This method presented limitations in the unbiased determination of fetal and maternal cells that I overcame by applying an established algorithm, demuxlet[125], on the scRNA-seq data in combination with maternal and fetal genotypes obtained from WGS.

Our results suggest that further optimizations are required to confidently perform maternal and fetal cell assignment based on allele calling from scRNA-seq data alone. One initial barrier to considering a larger pool of callable variants or performing *de novo* variant calling was that the runtime of variant calling using GATK HaplotypeCaller was found to be prohibitive. We therefore limited our analysis to

SNPs overlapping the 1000 genes most highly expressed in placenta and endometrium (see Methods). This approach yielded separation between a fraction of fetal and maternal cells, but failed to distinguish the identities of the remaining majority (**Figure 2a**). To evaluate whether the results are influenced by the cell types analyzed, we repeated the analysis on specific subsets of cells established with high confidence to be maternal and fetal in origin. For example, probabilistic PCA on a combination of maternal stromal cells, fetal trophoblast cells, and cells of unknown origin (cluster 20) from Donor 4 produced qualitative separation between the trophoblast and stromal cells and clustering of the unknown cells with the trophoblasts (**Figure 2c**). This was corroborated by the subsequent demuxlet output and was consistent with our previous knowledge regarding the identities of these cells. However, the same analysis performed on a combination of maternal mononuclear phagocytes, fetal trophoblast cells, and the unknown cells was unable to separate these populations (**Figure 2d**). This suggests that DNA-free single-cell genotyping is limited at least in part by cell type-dependent differences in expressed genes, and in turn, the sites of callable SNPs or other genetic variants. Two cells originating from the same individual may exhibit disparate gene expression profiles if they belong to different cell types, and as a result, they may not share a sufficient number of identifiable SNPs in common to both confidently relate them to each other and differentiate them from cells originating from another individual. This is further supported by the observation that a similar application of this pipeline to calling variants overlapping the 1000 most highly expressed genes in iPSCs performs well at distinguishing iPSCs derived from different human donors that were pooled and profiled by droplet-based scRNA-seq (Teichmann group, unpublished data). In contrast to our study, in which the cells have originated from tissues composed of heterogeneous cell types, the iPSCs were all derived from skin fibroblast cell cultures generated by the Human Induced Pluripotent Stem Cell Initiative (HipSci) resource. Future attempts to improve this pipeline for maternal/fetal identification may evaluate whether increasing the number of called SNPs improves its ability to separate genetically distinct cells, and whether alternative variant callers improve the runtime of this approach. Additionally, best practices for variant calling from RNA-seq data, not to mention scRNA-seq data, are still in development[153]. For example, the filtering parameters applied to called variant alleles and homozygous reference alleles may also merit optimizing.

I next presented our results using the demuxlet algorithm to perform unbiased maternal/fetal assignment of all cells sequenced via droplet encapsulation from the decidua and placenta (**Figure 3**).

I show that demuxlet confidently inferred the identities of ~93% of these cells, and that the assignments were largely consistent with our expectations of the maternal or fetal origins of these cells, given their derivation from either the decidua or placenta or their annotated cell types as determined by unbiased clustering and examination of marker genes from the known literature. For example, demuxlet successfully resolved the small number of invading EVT of fetal origin which were derived from the decidua samples. Demuxlet was also able to clarify or revise our understanding of other cell populations. One such population is cluster 21, corresponding to a mononuclear phagocyte subset localized to the placenta in both of the sequenced samples (**Figure 3b**), which was inferred by demuxlet to be maternal in origin (**Figure 3c**). This represents a particularly interesting finding as previous literature largely reports that the placental myeloid cells are primarily fetal Hofbauer cells[154,155]. A previous study, however, observed the recruitment and attachment of maternal mononuclear phagocytes to placental trophoblast cells[151]. In particular, these cells accumulate on the syncytial surface of the placenta, at sites where the placental layer has withstood damage. This mechanism must be precisely regulated, as increased placental accumulation of macrophages is observed in cases of villitis or other inflammatory conditions[156,157]. These findings suggest that the presence of maternal myeloid cells in the placenta is not a misassignment of single-cell genetic identities or attributable to sample contamination, but rather a bona fide reflection of maternal macrophage biology. Additionally, for cluster 20, a population observed in both the decidua and placenta which was unable to be classified as any known cell type based on transcriptome analysis, demuxlet identified a large majority of these cells to be fetal in origin (**Figure 3c**), which may be useful in guiding further attempts to annotate these cells or determine whether they may represent potential contamination from non-placental fetal tissues. Considering the demuxlet assignments and their likelihoods in aggregate, we noticed that some cells with more QC-passed reads were assigned maternal/fetal identities with lower confidence and that in some cell types, the proportions of cells with unknown identities were much higher than in others (**Figure 4a**). We believe this may be attributed to the fact that in these cells, fewer scRNA-seq reads overlap the variants which are most informative for genetically distinguishing mother and fetus. Since the callable variants in each cell are dependent on which genes the cell expresses and are detectable in the scRNA-seq data, this could result in some cell types being systematically genotyped with lower confidence than others, rather than a more stochastic distribution of confidence levels and unknown assignments across all cell types. Indeed, we observed that the vast majority of cells with high QC-

passed reads and lower confidence of assignment originated from sequencing runs consisting of immune cells isolated from two of the maternal decidua samples. Nevertheless, it was still possible to assign origins for these cells with a certain degree of confidence, given that demuxlet infers single cell identities by using genotypes as an independent, "ground truth" genetic reference. Thus, while the primary envisioned application of demuxlet may be to facilitate the demultiplexing of scRNA-seq experiments deliberately pooling cells from genetically different donors[125], our analysis in the context of the maternal-fetal interface demonstrates that this algorithm can also prove useful in scenarios in which cells from distinct genetic origins biologically coexist in a tissue in different, potentially variable quantities and collectively encompass distinct cell types, and in which the proportions of cells derived from each individual are not known *a priori* and the individuals of origin may themselves be genetically related.

In summary, unbiased genetic inference of the maternal or fetal origin of single cells in the decidua and placenta is associated with several challenges: i) cells exhibiting different transcriptomic profiles must be analyzed in tandem; ii) the mother and fetus share at least 50% identical genetic material; and iii) the cells originating from one individual may be present in very small proportions in a given tissue (e.g. EVT in the decidua). Overall, with the availability of maternal and fetal genotype data, algorithms such as demuxlet remain the most robust means of overcoming these challenges and genetically identifying cells based on single-cell transcriptomes. Ultimately, however, a means of performing accurate, unbiased genetic identification without the necessity of additional genotype or genomic information would be desirable, particularly as the number of samples and tissues to be profiled through scRNA-seq continues to grow.

Lastly, I used bulk RNA-seq to identify potential dissociation protocol-induced artifacts in the scRNA-seq data and prevent the misinterpretation of detected genes in certain cell populations. In this case, we showed how *HSPA1B*, a highly upregulated gene identified by plate-based SmartSeq2 in a T cell population (**Figure 5b**; **Table 2**), was absent in the bulk RNA-seq data from the same samples (**Table 3**), suggesting that the significantly upregulated markers in these cells may be attributable to technical rather than biological noise. At the same time, we still observed expression of other HSP-related genes in the bulk RNA-seq data (**Table 3**), suggesting that bulk RNA-seq sample processing is also capable of imposing stress on cells and that RNA-seq protocols in general are capable of introducing biases in observed gene expression[158]. Nevertheless, comparative analyses between scRNA-seq and matched bulk RNA-seq data still represent a valid strategy to correct for gene expression perturbations

specifically attributable to single-cell tissue dissociation protocols. One approach for detecting scRNA-seq-associated transcriptome alterations in a more comprehensive manner might be to perform a linear regression on the detected gene signatures from the single-cell data to determine which weights best fit the composite, population-level gene expression signals observed in the bulk RNA-seq data, and then determine which genes either from the scRNA-seq data account for the residual or distance in gene expression between these two datasets. Repeating this for different samples and across different tissues might be a potential way to generate a consensus list of genes specifically susceptible to perturbation in scRNA-seq protocols. However, due to the differential enrichment of cell types during tissue processing (e.g. depletion of B cells and epithelial cells from the decidua), a limitation of this approach is that the altered proportions of captured cells in scRNA-seq datasets relative to bulk RNA-seq datasets represents a confounding factor that would make detected residuals more difficult to interpret in an unbiased fashion. Moreover, many of the genes associated through this method with single-cell dissociation might harbor relevant biological functions that would be masked if their upregulation in cells were discounted or fully attributed to protocol-related effects. For example, HSP-family proteins including hsp70 (*HSPA1A/B*) and gp96 are involved in chaperoning peptide complexes for uptake, processing, and presentation by antigen-presenting cells[159]. In addition, HSPs themselves have been shown to modulate T cell responses in chronic inflammatory disease[160].

Conversely, another approach could involve applying computational deconvolution methods to the bulk RNA-seq data to obtain estimates of cell-type specific gene expression profiles, which would be compared in turn with the scRNA-seq datasets. However, several limitations exist here as well. Many existing deconvolution algorithms, including CIBERSORT[161], TIMER[162], and MCP-counter[163], were specifically developed to infer proportions of infiltrating immune cell subsets in tumors. Many currently available methods are also tailored towards deconvolution of microarray data rather than next-generation sequencing data[161,164], or are limited to estimating the enrichment or proportions of cell types in tissue of interest, but not actual cell type-specific gene expression patterns[165,166]. Moreover, these methods may often produce biases in deconvolving mixtures of similar cell types harboring correlated gene expression profiles (e.g. naive vs. activated T cells)[162,166]. For these reasons, these methods were not applied to our decidual and placental bulk RNA-seq data but could nevertheless be evaluated and represent a potential new avenue of study and development.

Chapter 4 - Integrating scRNA-seq with single cell-level protein-level data and established gene signatures to characterize maternal resident immune cell populations

4.1 Overview

Following the identification of several novel maternal immune subsets from scRNA-seq, we sought to examine markers distinguishing these populations at the protein level as well as begin defining their potential functions at the maternal-fetal interface. In this chapter, I first describe how protein abundance data from FACS coupled with plate-based scRNA-seq data, along with high-dimensional protein expression data derived from CyTOF, were used to validate identified decidual immune cell populations. Next, I present our further analysis of the maternal resident mononuclear phagocyte populations, in which we utilized established macrophage gene signatures and public tissue-level gene expression data of the placenta and endometrium to functionally annotate these cell types.

4.2 FACS and CyTOF validation of maternal resident immune cell subpopulations

Overlapping gating during FACS index sorting allowed us to enrich for the main immune subsets in the decidua using a 14-antibody panel selected based on previous knowledge of decidual immune cell surface markers (see Methods). The proportions of immune cells that were captured and sorted for sequencing therefore do not represent the true proportions observed *in vivo*, but are rather a consequence of our enrichment strategy. Following full-length scRNA-seq and unbiased transcriptome-based clustering of the sorted immune cells from five maternal decidua and two matched peripheral blood samples (sample information in **Table 1**), novel subsets of dNK cells, myeloid cells, $CD4^+$ and $CD8^+$ T cells, and Treg cells were defined as the main decidual immune populations, with their separation from the subsets containing peripheral blood-derived cells on t-SNE suggesting that these populations are tissue-resident cells rather than intravascular or circulating immune cells (**Figure 1a**). Next, FACS index sorting metadata was overlaid on the t-SNE mapping to link the gated identities of the cells with their transcriptome-defined identities (**Figure 1b**).

Table 1. Plate-based scRNA-seq sample information.

Donor	Post-conceptional weeks	Pregnancy	SmartSeq2 - Decidua	SmartSeq2 - Peripheral Blood	Fetus sex
D5	7 to 9	3rd	879 cells		male
D6	11 to 13	3rd	630 cells		female
D7	8 to 10	6th	1295 cells		female
D8	11 to 13	1st	1021 cells	539 cells	male
D9	8 to 10	1st	493 cells	724 cells	female

Overall, FACS gating was well-correlated with the transcriptome-based cell annotations. CD9 is a unique marker of dNK cells[37], and as expected, the $CD9^+$ NK cells are predominantly located among dNK cell clusters and absent among peripheral blood NK cells. In both decidua and blood, T cell clusters are definable by $CD4^+$ and $CD8^+$ identities. Interestingly, the two decidual mononuclear phagocyte populations (dMP1 and dMP2) are distinguishable by $CD14^+$HLA-DR^+ (Myeloid+) and $CD14^{++}$HLA-DR^{++} (Myeloid++) gating, suggesting that their transcriptome-level differences are paralleled by distinct surface protein expression profiles. A previous study of decidual macrophages identified two subsets defined by high and low expression of the integrin protein CD11C (ITGAX)[70]. Differential expression analysis between the two identified decidual mononuclear monocyte subsets confirmed *CD11C* as one of genes upregulated in dMP1 (Myeloid+ cells) relative to dMP2 (Myeloid++ cells) (**Figure 1c**).

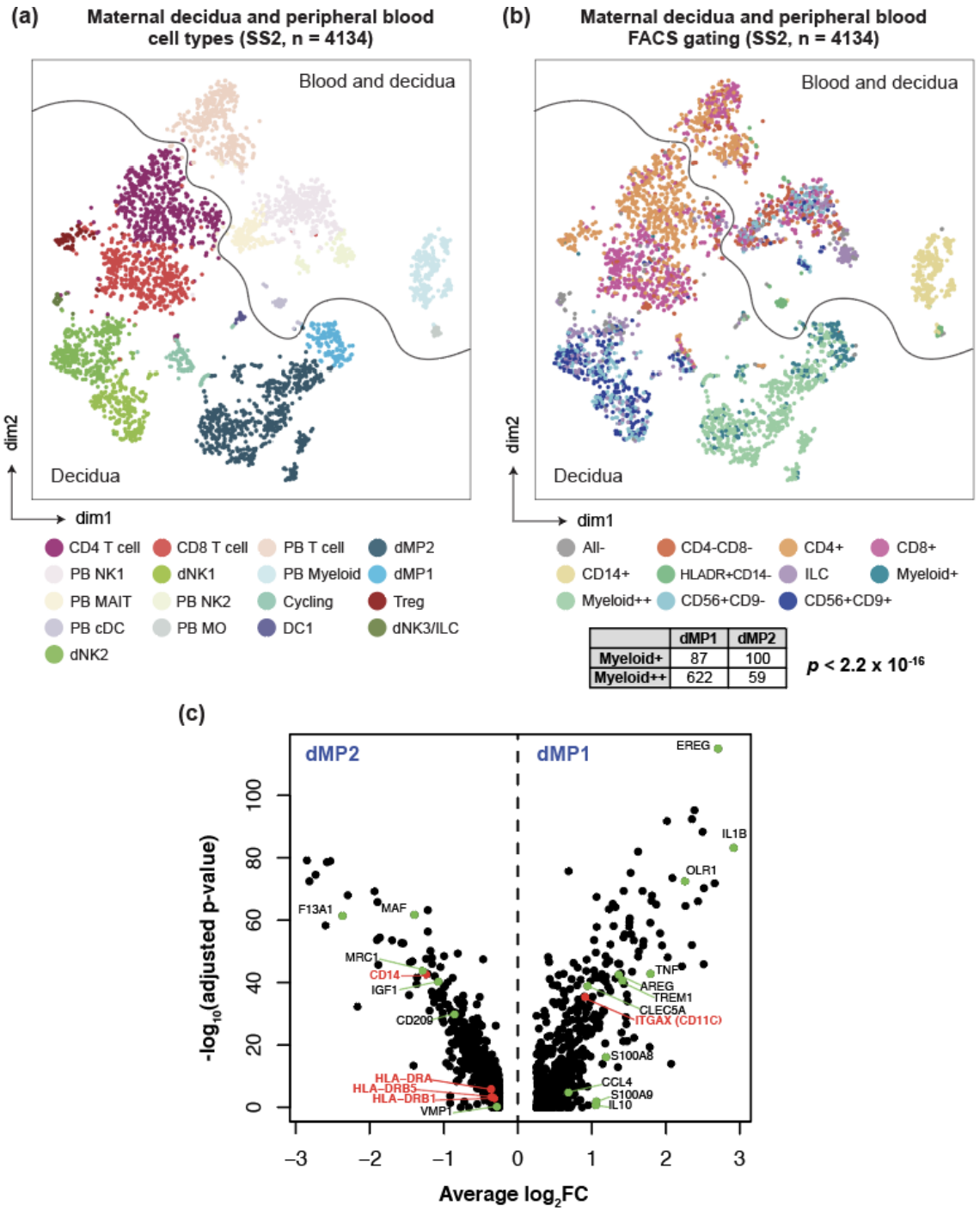

Figure 1. t-SNE visualizations juxtaposing cell type annotations and FACS gating distinguish two decidual mononuclear phagocyte populations. (a) Cells colored by predicted cell type or cell state as inferred by unbiased clustering on decidua SmartSeq2 scRNA-seq data and marker-based annotation (from Vento-Tormo R, Efremova E, et al., unpublished). **(b)** Cells colored by gates from FACS index sorting. Student's t-test shows significant enrichment of Myeloid++ cells in the dMP1 subset and Myeloid+ cells in the dMP2 subset ($p < 2.2 \times 10^{-16}$). **(c)** Volcano plot of differentially expressed genes between dMP1 and dMP2 showing upregulation of *CD14* and *HLA-DR* mRNA in dMP2, as well as upregulation of *CD11C* in dMP1 and differential expression of additional genes (in green) highlighted in a previous study of decidual macrophages[70].

We next performed CyTOF on the decidual samples in order to independently validate identified subpopulations and their transcriptome-defined markers at the protein level. CyTOF facilitated the

simultaneous quantification of 39 protein markers of interest (Appendix 3) at single-cell resolution by leveraging metal isotope-labeled antibodies coupled with mass spectrometry[167]. Analysis of the CyTOF data from $CD14^+$ immune cells in three maternal decidua confirms that there are indeed two distinct decidual mononuclear phagocyte populations, defined by high and low expression of CD11C. Additionally, we detected the presence of two dendritic cell subsets: DC1, which expresses high levels of the dendritic cell marker CLEC9A, and DC2, which expresses high levels of the dendritic cell marker CD1C (**Figure 2**).

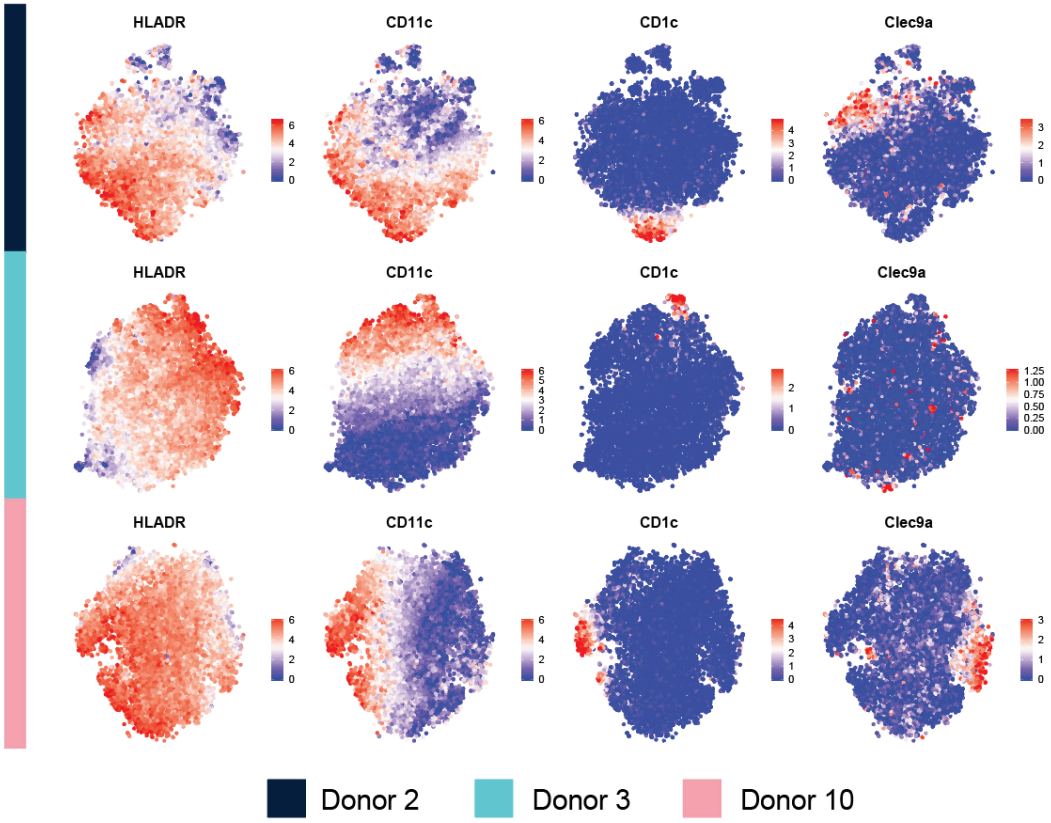

Figure 2. CyTOF validation of decidual myeloid cell subsets. t-SNE plots show protein expression of CD11C, CD1C, and CLEC9A on live cells gated on $CD45^+CD14^+$ events from three maternal decidua (Donors 2, 3, and 10).

Both droplet encapsulation and plate-based scRNA-seq approaches identified three main NK subsets in the decidua (Vento-Tormo R, Efremova M et al., under submission): dNK1, which exhibits high levels of cytotoxic granule (*GNLY, GZMA, GZMB*) and HLA-C-binding KIR genes (*KIR2DL1/DL2/DL3* and *KIR2DS1/DS4*); dNK2, which exhibits lower expression of both classes of genes; and dNK3/ILC1, which does not significantly express classical granzymes or HLA-C-binding KIRs, but rather expresses genes encoding the ILC1 markers *CD160*, *CD161* (*KLRB1*), and *CD103* (*ITGAE*), as well as *CD49d* (*ITGA4*),

a marker expressed by ILCs migrating into tissues[168]. Through CyTOF on $CD56^+$ immune cells from three maternal decidua, we confirmed that these dNK populations are also distinguishable by a subset of these markers at the protein level (**Figure 3a**, Appendix 7). The dNK3/ILC1 population expresses CD103, CD161 and CD49d while exhibiting low expression of GZMB. The dNK1 population highly expresses both KIR2DL1/DL3 and GZMB, while the population expressing GZMB but lower levels of the inhibitory KIRs likely corresponds to dNK2.

Finally, transcriptome-based clustering resolved populations of decidual $CD4^+$ T cells, $CD8^+$ T cells and $FOXP3^+$ Treg cells, which we were also able to identify through CyTOF analyses of $CD3^+$ T cells from three maternal decidua (**Figure 3b**, Appendix 7). While we observed a population of naive ($CD45RA^+$) $CD8^+$ T cells by CyTOF, most decidual T cells appear to be memory ($CD45RO^+$) T cells. A subset of the memory $CD8^+$ T cells additionally expressed the tissue residency marker CD103. Interestingly, the $CD8^+$ T cells exhibit low or absent expression of CD127 (IL-7R), a major mediator of homeostatic regulation and survival in most T cell populations[169]. Finally, we also detected small populations of $CD8^+$ gamma-delta T cells.

Overall, these results demonstrate that pairing of plate-based scRNA-seq data with FACS index sorting metadata enables us to generally validate transcriptome-level cell annotations at the protein level. At the same time, it allows us to reciprocally define certain cell types, such as the two decidual mononuclear phagocyte populations, on the basis of distinct surface protein expression. Meanwhile, CyTOF facilitates independent validation of identified cell subsets and their distinguishing markers. Its high-parameter capacity also allows for the simultaneous profiling of additional protein markers of interest that may prove useful in further describing these populations.

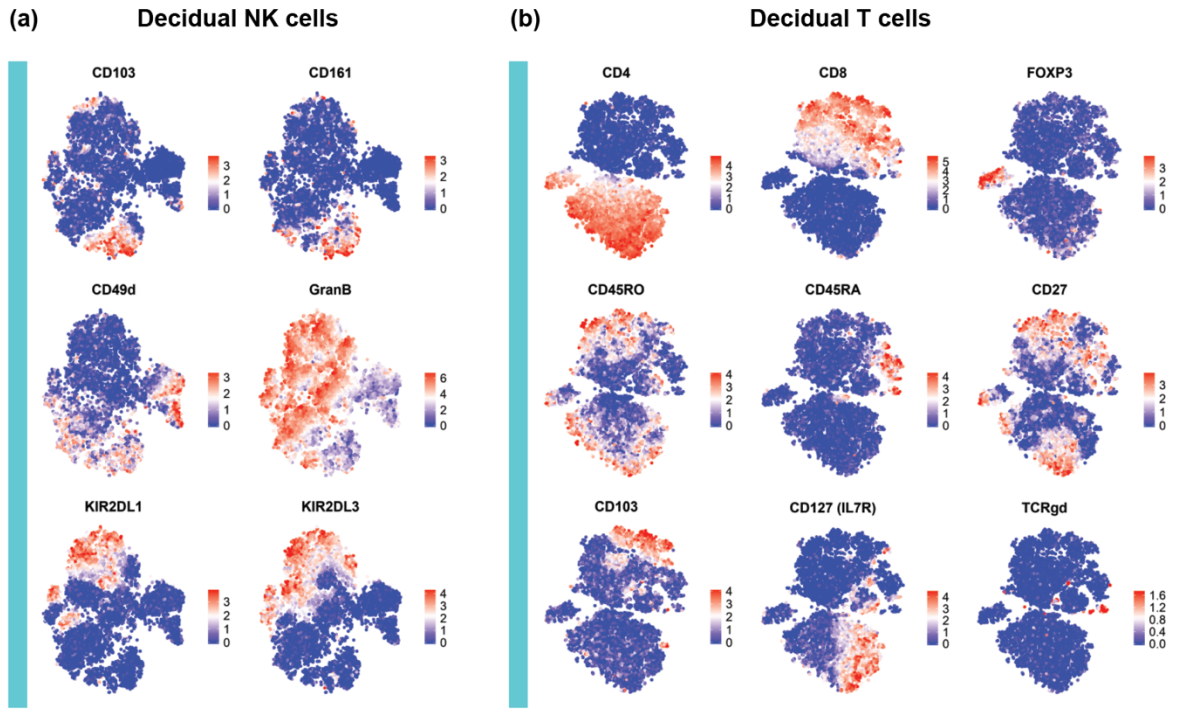

Figure 3. CyTOF validation of dNK and decidual T cell subsets. (a) t-SNE plots showing protein expression of dNK and ILC markers on live cells gated on $CD45^{+}CD56^{+}CD14^{-}HLA\text{-}DR^{-}CD3^{-}$ events from Donor 3 maternal decidua. **(b)** t-SNE plots showing protein expression of T cell markers on live cells gated on $CD45^{+}CD3^{+}CD14^{-}HLA\text{-}DR^{-}CD56^{-}$ events from Donor 3 maternal decidua. (CyTOF data from Donors 2 and 10 shown in Appendix 7.)

4.3 Further characterization of maternal mononuclear phagocyte populations

Given the evidence for three maternal mononuclear phagocyte populations from the droplet-based scRNA-seq data ($CD11c^{hi}$ dMP1, $CD11C^{lo}$ dMP2, and plMP, the placenta-localized maternal mononuclear phagocytes) (**Chapter 3**), we sought to further profile these cell populations based on their respective gene signatures and relate their characteristics to existing knowledge about macrophages and genes enriched in the placenta and endometrium.

Using the droplet-based scRNA-seq data, we first visualized the most highly upregulated genes in each subset relative to all other cell types at the maternal-fetal interface (**Figure 4**, additional upregulated genes in Appendix 8). We also performed differential gene expression analyses specifically between the three mononuclear phagocyte populations (Appendix 9). The $CD11c^{hi}$ dMP1 population exhibits high expression of monocyte genes (e.g. *S100A8* and *S100A9*) along with macrophage markers (e.g. *CD68*), suggesting a monocyte-derived macrophage phenotype. Meanwhile, the $CD11C^{lo}$ dMP2 population exhibits high expression of tissue-resident macrophage markers *CD209* (*DC-SIGN*), *CD206* (*MRC1*), and *MAF*, indicating a more differentiated macrophage phenotype. The expression of monocyte markers is also evident in plMP, suggesting its monocyte-derived origin. In addition, the plMP

population expresses *GCHFR*, a regulator of nitric oxide production, and high levels of *APOC1* and *APOE*, genes involved in lipoprotein synthesis.

Next, in order to functionally annotate the mononuclear phagocyte populations, we performed gene ontology (GO) and Reactome enrichment analysis on all genes significantly upregulated (log_2(fold-change) ≥ 0.5, adjusted $p < 0.05$) in each subset relative to other decidual and placental cell populations (**Figures 5-7**). We then examined the overrepresented Reactome pathways and GO terms from the biological process (BP) and molecular function (MF) categories. The results from our enrichment analyses suggest that the mononuclear phagocytes collectively play important roles in balancing immunity, inflammation, tolerogenicity, and tissue remodeling. Overrepresented terms describe processes related to phagocytosis and to pathogen response and debris clearance (e.g. dMP1: endopeptidase activity, pattern recognition receptor activity; dMP2: endopeptidase activity, antigen processing-cross presentation; plMP: intracellular pH reduction, scavenging by class A receptors), regulation of inflammatory and immunosuppressive responses (e.g. dMP1: arachidonic acid binding, chemokine receptors bind chemokines; dMP2: icosanoid biosynthetic process, myeloid leukocyte cytokine production; plMP: neutrophil aggregation, regulation of IL-10 secretion), and modulation of cell adhesion and tissue remodeling (e.g. dMP1: smooth muscle adaptation; dMP2: VEGFR signaling pathway; plMP: blood vessel morphogenesis, collagen degradation). Additionally, dMP1 and plMP specifically exhibit overrepresentation of terms associated with ROS production and detoxification (e.g. dMP1: respiratory burst, cellular oxidant detoxification; plMP: ROS biosynthetic process, detoxification of ROS), as well as lipid metabolism and transport (e.g. dMP1: fat cell differentiation, LDL receptor activity; plMP: positive regulation of cholesterol storage, lipid binding).

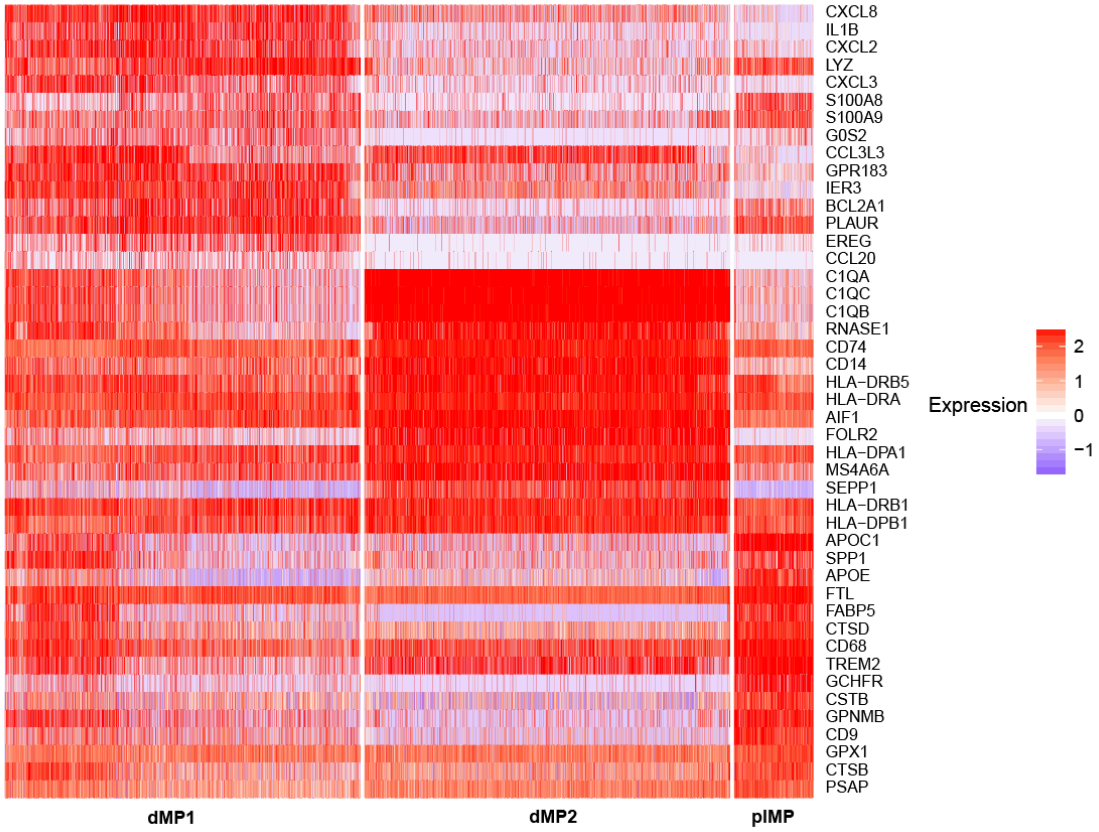

Figure 4. Heatmap of marker genes for the three identified maternal mononuclear phagocyte populations. The 15 most highly upregulated genes distinguishing each mononuclear phagocyte subset from all other cell types at the maternal-fetal interface are plotted in order of decreasing $\log_2$(fold-change). Genes which are significantly upregulated in multiple mononuclear phagocyte subsets are plotted with the subset in which they exhibit the greatest $\log_2$(fold-change). In particular, dMP1 and pIMP express high levels of the monocyte markers *S100A8* and *S100A9*, suggesting a monocyte-derived origin.

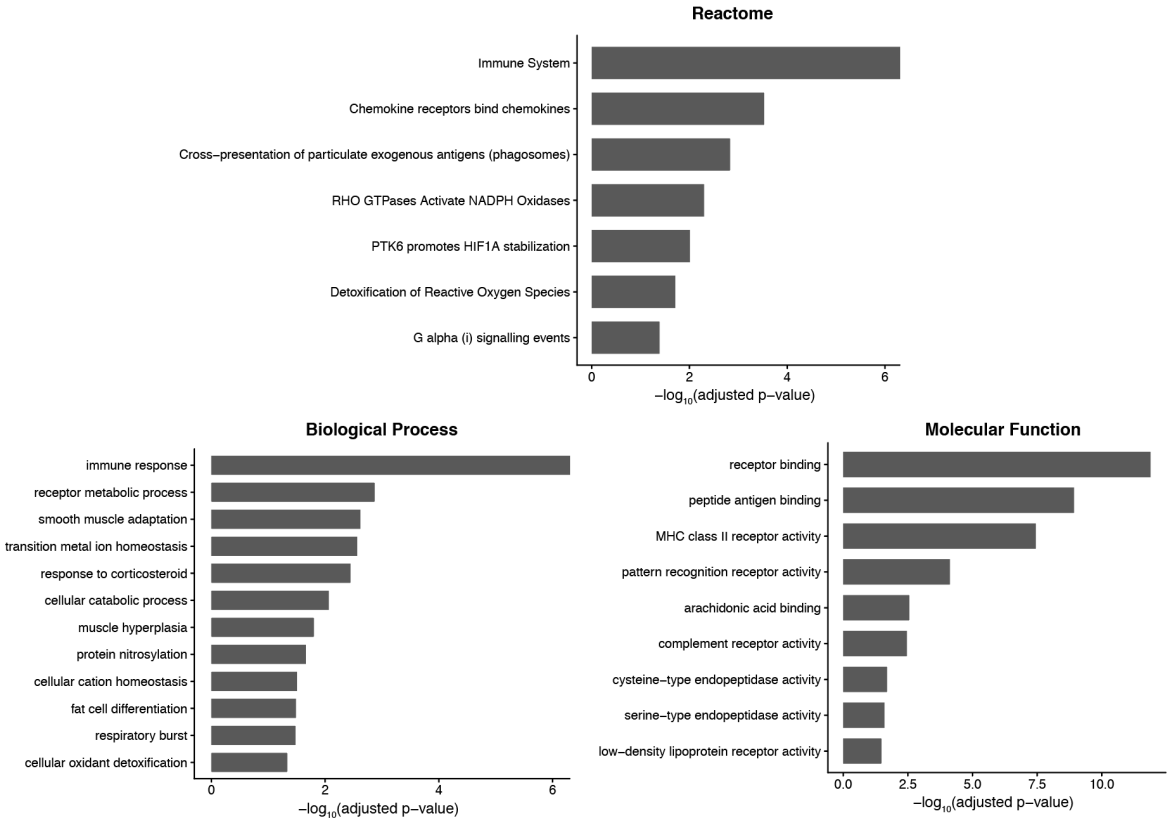

Figure 5. Genes involved in phagocytic activity and immune response, arachidonic acid signaling, ROS detoxification, tissue remodeling, and lipid metabolism are overexpressed in dMP1. GO and Reactome term enrichment analysis was performed on the genes upregulated by $\log_2$(fold-change) ≥ 0.5 in dMP1 relative to all other cell types at the maternal-fetal interface. Enriched terms are ordered by adjusted *p*-value.

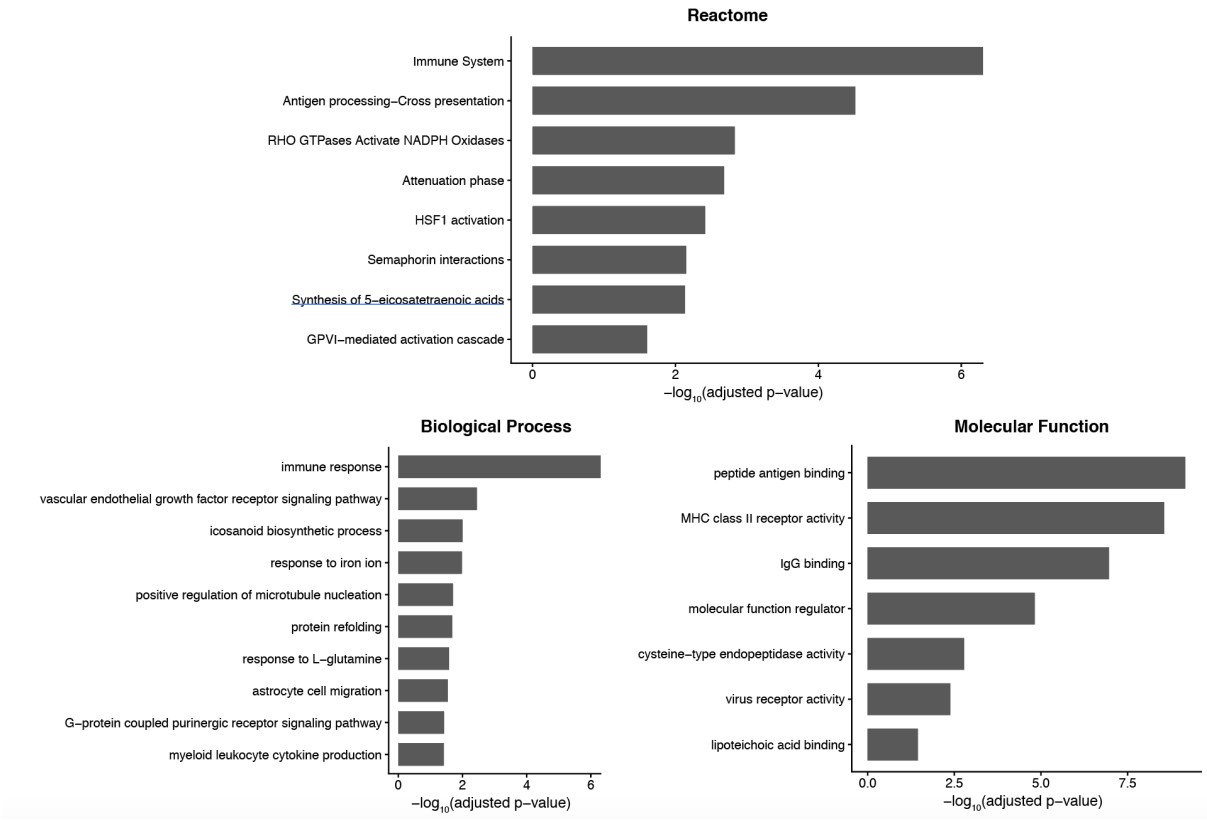

Figure 6. Genes involved in phagocytic activity and immune response, arachidonic acid signaling, and tissue remodeling are overexpressed in dMP2. GO and Reactome term enrichment analysis was performed on the genes upregulated by $\log_2$(fold-change) ≥ 0.5 in dMP2 relative to all other cell types at the maternal-fetal interface. Enriched terms are ordered by adjusted *p*-value.

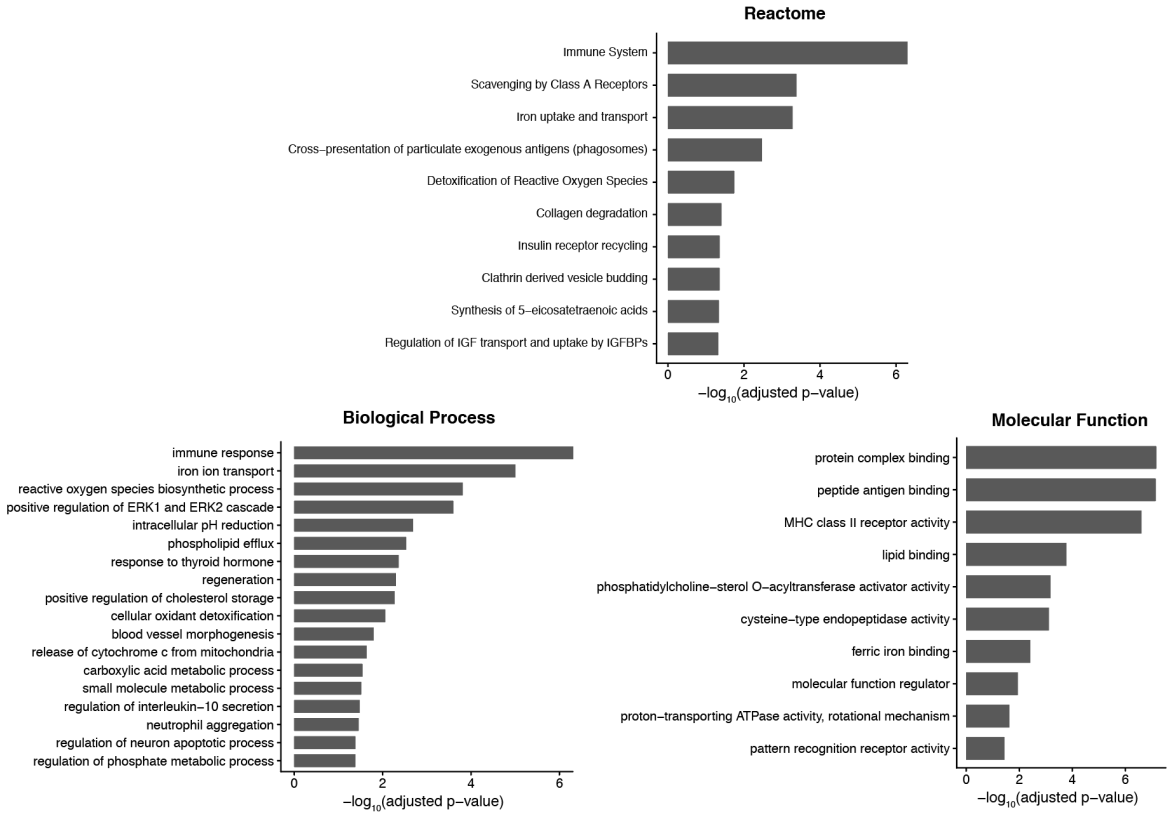

Figure 7. Genes involved in phagocytic activity and immune response, arachidonic acid signaling, ROS detoxification, tissue remodeling, and lipid metabolism are overexpressed in plMP. GO and Reactome term enrichment analysis was performed on the genes upregulated by $\log_2$(fold-change) ≥ 0.5 in plMP relative to all other cell types at the maternal-fetal interface. Enriched terms are ordered by adjusted *p*-value.

To further characterize the three mononuclear phagocyte subsets, we next examined their gene expression patterns in relation to the classical model of macrophage polarization into M1 (inflammatory) and M2 (non-inflammatory) populations[64]. We intersected a list of canonical M1 macrophage and M2 macrophage marker genes[139] with the upregulated gene sets associated with each of our three populations (**Figure 8**, Appendix 10). CD11c^{hi} dMP1 expressed significantly elevated levels of several classical M1 genes, including the inflammatory cytokines *CCL20* and *TNF*, while also expressing M2 genes such as *CXCR4* and *IL-10*, which have been implicated in resolving inflammation and tissue remodeling. CD11C^{lo} dMP2 exhibited enriched expression of several M2 genes, including *TGF-β*, the scavenger receptor *MSR1* and mannose receptor *MRC1*, and insulin-like growth factor *IGF2*, but also highly expressed the M1-associated interleukin receptor *IL2RA*. Finally, plMP showed upregulation of *SLC31A2*, associated with copper ion-mediated antimicrobial responses in M1 macrophages, along with M2 macrophage-linked *LIPA* (lysosomal lipase), scavenger receptor *CD36*, and *FN1* (fibronectin). Collectively, these results suggest that decidual and placental maternal mononuclear phagocytes appear to exhibit a mixture of conventional M1-like and M2-like characteristics, although dMP1 appears

to express more pro-inflammatory cytokines and dMP2 more genes involved in tissue clearance. Overall, however, these subsets cannot be fully distinguished along the classical M1/M2 polarization axis (p = 0.3806, Fisher's exact test).

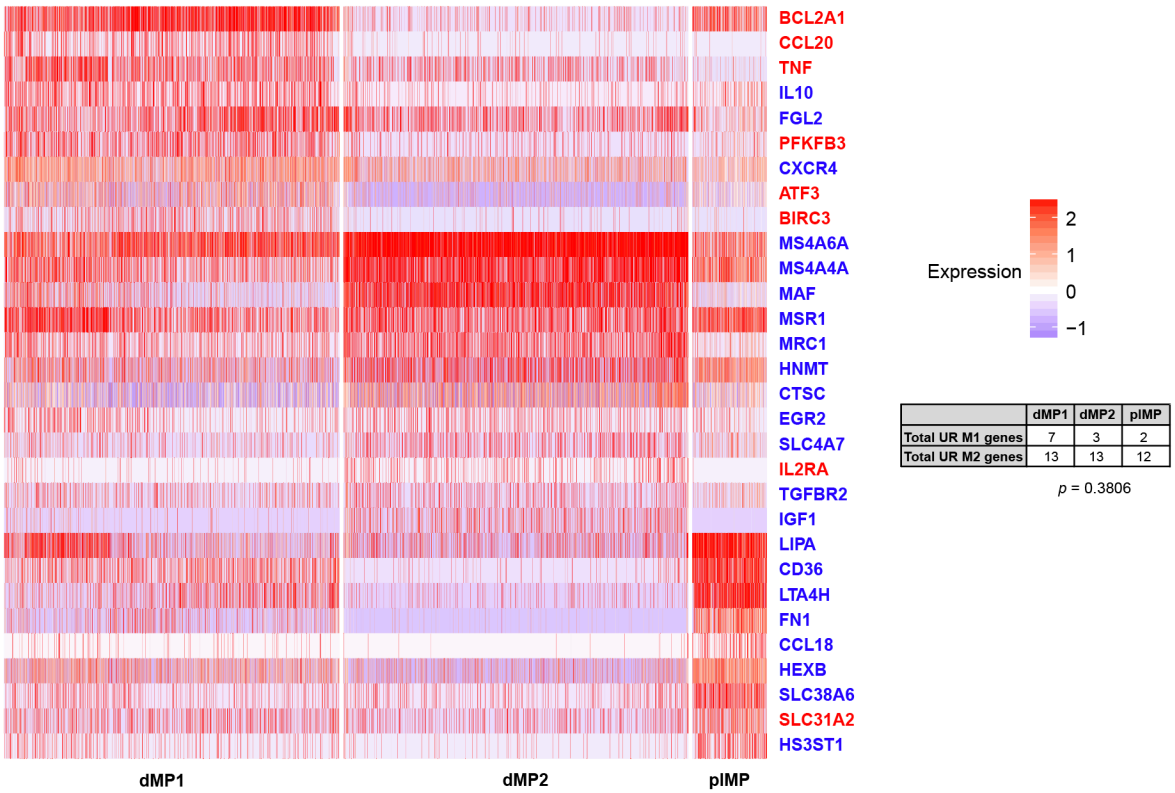

Figure 8. Each of the maternal mononuclear phagocyte populations exhibits upregulation of both canonical M1 and M2 macrophage genes. Heatmap plotting in order of decreasing $\log_2$(fold-change) genes that distinguish M1 macrophages (red) and M2 macrophages (blue)[64] and that are significantly upregulated in each mononuclear phagocyte population (full results in Appendix 10). Genes which are significantly upregulated in multiple mononuclear phagocyte subsets are plotted with the subset in which they exhibit the greatest $\log_2$(fold-change). The subsets express a mixture of pro-inflammatory and anti-inflammatory genes, suggesting they do not significantly align with the conventional M1/M2 transcriptional and functional polarization of macrophages (p = 0.3806, Fisher's exact test).

An emerging paradigm is that macrophages, in addition to their conventional phagocytic capacity and roles in regulating host immunity to infections, assume an array of specialized functions tailored to their tissue of residence, as reflected by distinct transcriptional and epigenetic programs[74]. For example, the specific roles of osteoclasts in regulating bone resorption and synthesis are mediated by their expression and activation of genes in the RANK signaling pathway[77]. Additionally, existing knowledge about the extensive tissue adaptation of populations such as the dNK cells suggests that this degree of specialization exists in other components of the immune cell compartment as well. We therefore sought to further profile the potential functions of our identified resident immune cell subsets from a tissue-

centered perspective, hypothesizing that these populations might upregulate certain genes which are enriched in the placenta and endometrium that would be indicative of their tissue-specific functions.

To compile a list of placenta- and endometrium-enriched genes to study in our resident immune cell subsets, we used tissue-level gene expression data deposited in the Human Protein Atlas[127,128], which was collectively generated from bulk RNA-seq of 37 different human tissues from 122 individuals. For each gene, we calculated a tissue-specificity index, Tau[140], and determined the tissue(s) in which the gene was most highly expressed, ultimately identifying 410 genes with Tau ≥ 0.8 (Appendix 5) to be significantly enriched in the placenta and/or endometrium relative to other tissues (see Methods). We then visualized the overlap between these tissue-enriched genes and the significantly upregulated genes among each of the maternal resident immune populations (**Figure 9**).

Overall, we observed that the mononuclear phagocyte populations express a large proportion of the immune cell marker genes which are enriched in placenta and endometrium, suggesting their high degree of tissue adaptation relative to even other resident immune cell populations. The upregulated placenta- and endometrium-enriched genes which characterize mononuclear phagocytes collectively span a number of potential tissue-specialized functions. Among these are lipid uptake and metabolism, as suggested by upregulation of genes encoding LDL receptor *OLR1* in dMP1, and *PLTP* and *ENPP2*, which modulate phospholipid transfer and lipid signaling, in dMP2. The mononuclear phagocytes additionally express a number of genes involved in cell adhesion and tissue or vascular remodeling, including *PECAM1* in dMP1; *PDGFB* (platelet-derived growth factor) in dMP2; and *SPP1* (osteopontin), *FN1* (fibronectin), and *CTSL* (cathespin L1, a collagen proteinase) in plMP. Furthermore, they appear to regulate inflammation and immunity through multiple mechanisms, including via immunoglobulin gamma Fc receptors *FCGR2A/B* in dMP2/1 and folate (*FOLR2*) or prostaglandin synthesis (*HPGDS*) and signaling in dMP2.

We also examined the tissue-resident profiles of other decidual immune populations. DCs exhibit upregulation of *IDO1*, an immunomodulatory molecule which dampens T cell function, and the peptidase inhibitor *SERPINB9*. dNK cells exhibit upregulation of genes including hypoxia-induced *EPAS1*, the NK receptor *KIR2DL1*, and *AREG*, which regulates gland development. Interestingly, these are all molecules defining the dNK1 subset (Vento-Tormo R, Efremova M et al., under submission), suggesting that this dNK population exhibits the strongest tissue-resident phenotype. Overall, intersection of the placenta- and endometrium-enriched gene set with the maternal resident immune

cell marker genes underscores the tissue specialization of all maternal immune cell populations, and in particular that of the decidual and placental mononuclear phagocytes.

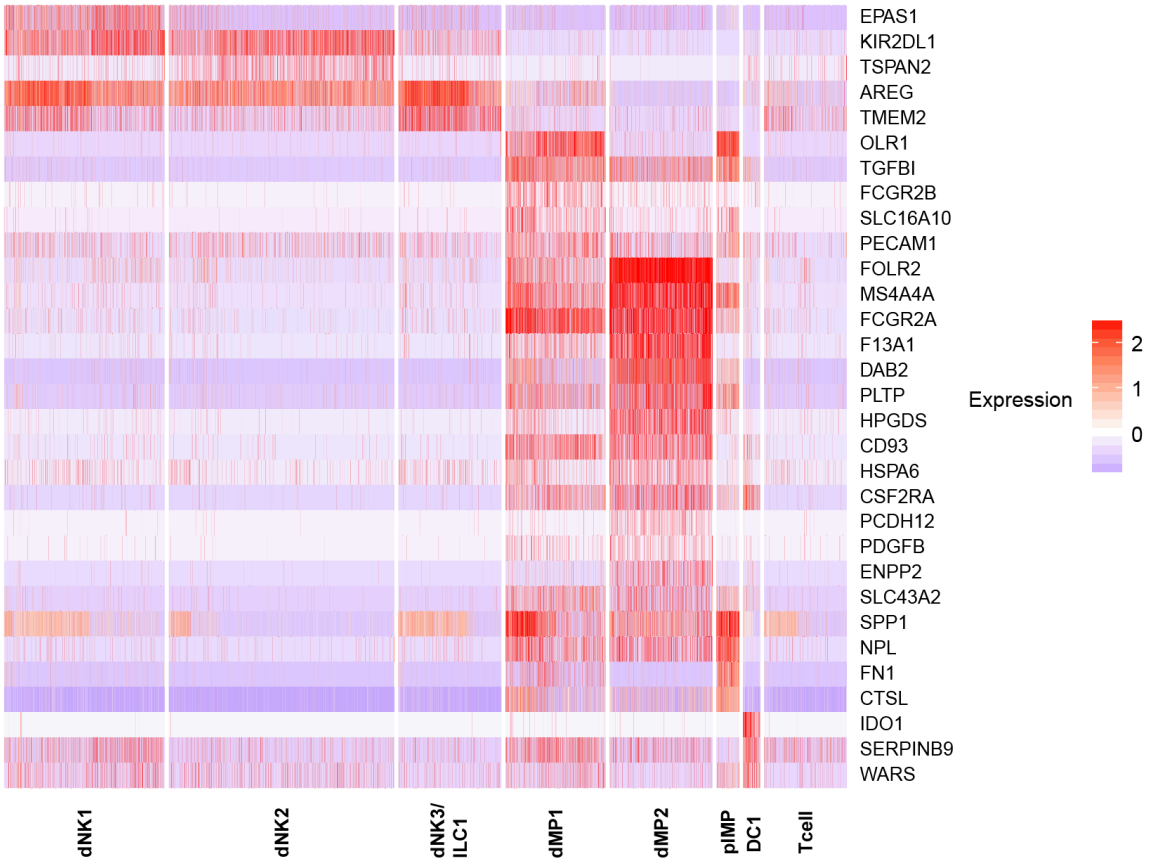

Figure 9. Maternal resident immune cell subsets exhibit upregulation of placenta- and endometrium-enriched genes. Heatmap plotting in order of decreasing $\log_2$(fold-change) the genes that are enriched in the placenta and endometrium and that are significantly upregulated in each maternal resident immune cell population. Genes which are significantly upregulated in multiple subsets are plotted with the subset in which they exhibit the greatest $\log_2$(fold-change). The maternal mononuclear phagocyte populations exhibit upregulation of a large number of the tissue-enriched genes relative to other immune subsets.

4.4 Discussion

In this chapter, I have integrated single cell-level protein and transcriptomic data to study the decidual immune cell populations in depth. I first presented results demonstrating the utility of FACS and CyTOF in validating the distinct immune subsets identified from transcriptome-based clustering and annotation. I then utilized gene ontology (GO) and Reactome enrichment analysis, M1/M2 macrophage signatures, and data from the Human Protein Atlas to functionally characterize the maternal mononuclear phagocyte subsets and dissect the tissue-resident transcriptional profiles of the decidual immune cell populations.

FACS gating revealed two myeloid cell populations distinguishable by $CD14^{+}HLADR^{+}$ and $CD14^{++}HLADR^{++}$ surface phenotypes that corresponded to the $CD11c^{hi}$ and $CD11C^{lo}$ decidual mononuclear phagocyte subsets defined by analysis of single-cell transcriptomes (**Figure 1**). Through CyTOF, we further confirmed the presence of $CD11c^{hi}$ and $CD11C^{lo}$ mononuclear phagocytes at the protein level, while also detecting two DC subsets, $CLEC9A^{+}$ DC1 and $CD1C^{+}$ DC2, in the decidua (**Figure 2**). CyTOF also validated the presence of $CD8^{+}$ and $CD4^{+}$ T cells and $FOXP3^{+}$ Treg cells in the maternal decidua, and identified a small population of gamma-delta T cells (**Figure 3b**). We show that most decidual T cells are antigen-experienced ($CD45RO^{+)}$, consistent with previous studies of T cell surface markers in early pregnancy decidua[170], and that a proportion of $CD8^{+}$ T cells express CD103, a marker of tissue residency. Interestingly, the CyTOF data confirms the absence of CD127 (IL-7R) among $CD8^{+}$ T cells. In most naive and mature T cell populations, IL-7/IL-7R signaling supports T cell survival and homeostasis through regulation of pro- and anti-apoptotic genes[169], induction of the JAK/STAT pathway, which mediates cell survival and proliferation[171], and modulation of glucose metabolism[172]. The lack of IL-7R in decidual $CD8^{+}$ T cells suggests that these populations are maintained and regulated through differential, perhaps decidua-specific, signaling mechanisms. Lastly, our CyTOF analysis also validated the three novel dNK subsets initially identified by scRNA-seq, confirming the presence of a dNK1 population expressing high levels of inhibitory KIR molecules and Granzyme B, dNK2 cells expressing Granzyme B but lower levels of KIR molecules, and a dNK3/ILC1 population with low Granzyme B expression but high expression of ILC1 markers CD161 and CD103 (**Figure 3a**). Overall, CyTOF independently validated the scRNA-seq-driven annotations of immune cell types by demonstrating that the distinctions between these cell subsets exist at the protein level as well as at the transcriptomic level. This has particular implications for defining the functional roles assumed by each identified cell population. For example, as evidenced by studies reporting the influence of maternal KIR molecules on susceptibility to preeclampsia[150] and other adverse pregnancy outcomes[44,47,48], the KIR repertoire expressed by dNK cells strongly shapes regulation of their activation and function. Thus, our demonstration through CyTOF that KIRs are variably expressed between dNK subsets underscores the potential that these populations can engage in differing interactions with other cell types at the maternal-fetal interface, and that the functional outcomes of these cell-cell interactions differ. In contrast to previous studies that consider dNK as a homogeneous population[39,150], we have

identified and validated the presence of dNK subsets that likely assume distinct functions at the maternal-fetal interface which reflect their respective transcriptional and phenotypic profiles.

Although decidual mononuclear phagocyte populations have been characterized previously through sorting based on CD11C and microarray gene expression profiling[70], scRNA-seq enabled unbiased, high-resolution dissection of the transcriptomes and potential functions corresponding to these subsets. Moreover, demuxlet analysis uncovered the presence of an additional maternal mononuclear phagocyte population in the placenta (plMP) that we further analyzed and compared with the two decidual mononuclear phagocyte subsets (CD11c^{hi} dMP1 and CD11C^{lo} dMP2). We first evaluated the most highly upregulated markers in each of the subsets relative to other cell populations at the maternal-fetal interface (**Figure 4**; **Appendix 8**). Consistent with previous literature reporting the upregulation of angiogenic factor VEGF[56], scavenger receptor CD163[55], complement protein C1q[54], and matrix metalloproteinases MMP7 and MMP9 in decidual macrophages[54,58], *VEGF* was specifically overexpressed in dMP1, *CD163* and *C1q* genes in dMP2, *MMP7* and *MMP9* in plMP. However, despite previous observations of elevated expression of *PDCD1* (*PD-1*) and B7-family molecules[51], *IDO*[52], and *VEGFR/FLT-1*[59] in decidual macrophages, we did not find them to be significantly overexpressed in any of the mononuclear phagocyte subsets relative to other decidual cell populations in our study.

Next, we performed differential expression analyses between each of the three mononuclear phagocyte populations using the droplet-based scRNA-seq data (Appendix 9). Consistent with the Houser et al. study describing two decidual CD11c$^{hi/lo}$ macrophage subsets[70], we observed upregulation of the pattern recognition receptor *CLEC5A*; growth factors *AREG*, *EREG*, and *IGF1*; lipoprotein receptor *OLR1*, and inflammatory mediator *TREM1* among CD11c^{hi} dMP1 mononuclear phagocytes. Similar to the CD11C^{lo} population described by Houser et al.[70], CD11C^{lo} dMP2 significantly upregulates *CD209* (*DC-SIGN*), *CD206* (*MRC1*), and *SEPP1*, a secreted glycoprotein associated with antioxidant activity[173]. We also found vacuole membrane protein 1 (*VMP1*) to be significantly overexpressed in CD11C^{lo} dMP2, consistent with observations that the CD11C^{lo} population is more highly vacuolated[70]. Finally, we observed that dMP1 exhibits upregulation of the genes encoding *CCL4* (*MIP-1β*), *IL-10*, *TNF-α*, and *IL1-β*, which were also among the cytokines found to be secreted preferentially by CD11c^{hi} relative to CD11C^{lo} macrophages[70]. Meanwhile, in contrast to Houser et al., *CD1C*, *UNC5B*, *DMD*, *HRH1*, *WNT5B*, and *STON2*, additional genes reported to be differentially expressed between CD11c^{hi} and CD11C^{lo} macrophages[70], were not found to be significantly differentially expressed in any of our three

mononuclear phagocyte subsets. The new plMP population we have identified does not express significantly high or low levels of CD11C, but exhibits elevated expression of *PPAR-γ*, lipoprotein receptor *OLR1*, and lipoprotein lipase (*LPL*), all previously associated with CD11c^{hi} macrophages, and upregulation of the insulin-like growth factor *IGF2* and IGF-binding protein *IGFBP3*. plMP also expresses significantly lower levels of *IL1-β*, *TNF-α*, and *CCL4* than the two decidual mononuclear phagocyte populations, which were among the cytokines reported to be highly secreted by CD11c^{hi} macrophages. Thus, taken together, the transcriptional profiles of dMP1 and dMP2 largely align with a previous study of CD11c^{hi} and CD11C^{lo} macrophages in the decidua, while the expression patterns of these same genes in plMP appear to distinguish this subset as a distinct population.

I subsequently performed gene ontology (GO) and Reactome enrichment analysis on the genes significantly overexpressed by $\log_2$(fold-change) ≥ 0.5 in each of the mononuclear phagocyte subsets relative to other cell types at the maternal-fetal interface (**Figure 5-7**). Overall, GO terms and Reactome pathways overrepresented among each of the subsets reflected many of the general functions known to be associated with decidual mononuclear phagocytes, including pattern recognition, scavenger, and chemokine receptor activity (dMP1/2, plMP); antigen processing and cross-presentation (dMP1/2, plMP); regulation by hormones (dMP1 and plMP); and pH reduction, GTPase activity, and catabolic functions indicative of phagosome maturation (dMP1/2, plMP). Moreover, consistent with the functional capabilities proposed by Houser et al. for CD11c^{hi} macrophages[70], dMP1 are associated with proinflammatory response (pattern recognition receptor and complement receptor activity) mediated by hormones (response to corticosteroids), and lipid metabolism functions including fat cell differentiation and LDL receptor activity. Meanwhile, dMP2 are linked to extracellular communication (semaphorin interactions, receptor binding), tissue and vascular remodeling (VEGFR signaling pathway), and cell growth (microtubule nucleation; enriched expression of multiple IGFBPs), as previously described in CD11C^{lo} macrophages[70]. At the same time, our GO analysis suggested that some of these functions are in fact shared across subsets rather than restricted to one population. For example, apart from dMP2, both dMP1 and plMP also appear to be enriched in genes regulating various aspects of tissue and vascular remodeling, as evidenced by the association of dMP1 with smooth muscle adaptation and of plMP with blood vessel morphogenesis and collagen degradation. Intriguingly, the GO and Reactome annotations also highlighted functions not previously well-described among macrophages at the

maternal-fetal interface, including arachidonic acid signaling, lipid transport and metabolism, and ROS generation and detoxification.

Meanwhile, our comparison of upregulated maternal mononuclear phagocyte genes to established M1 and M2 macrophage gene signatures reveals that none of the three subsets exhibited gene expression profiles aligning with this classical macrophage polarization scheme (**Figure 8**). These findings parallel previous observations that resident macrophages in many other tissues tend to exhibit phenotypic plasticity and characteristics which are uniquely specialized to their tissue of origin rather than fully describable by the M1/M2 binary classification[74]. Moreover, these results further reinforce the notion that in the decidual and placental milieu, where processes such as initiation and resolution of inflammation and tissue growth, disruption, and remodeling must be carefully fine-tuned over the duration of pregnancy, cell populations tend to exhibit mixed phenotypes rather than stark polarization in their functions.

The maternal mononuclear phagocytes, notably dMP2, appear to be among the most highly tissue-specialized immune cell populations, based on the number of placenta- and endometrium-enriched genes which are upregulated in these cells relative to other immune cell types (**Figure 9**). However, our analyses suggest that many of the maternal immune populations exhibit some degree of tissue adaptation. For example, the dNK express highest levels of KIR2DL1, an inhibitory receptor known to specifically engage HLA-C-expressing cells such as trophoblasts and a marker gene defined for our newly identified dNK1 population (**Figure 9**). Other dNK-upregulated genes include hypoxia-inducible factor EPAS1 and epithelial growth factor-related ligand AREG, reflecting the specialized roles of dNKs in regulating placentation and underscoring how the particular tissue microenvironment of early pregnancy (e.g. oxygen tension[1]) in turn shapes dNK phenotype and function. One limitation of our tissue-enriched gene analysis, however, is that the Human Protein Atlas gene expression data for placenta and endometrium includes both term placenta and decidua samples as well as samples from the non-pregnant endometrium[128,174], in contrast to our tissues exclusively derived from early pregnancy. Given the profound cellular and molecular changes known to occur at the maternal-fetal interface between the different reproductive stages, the placenta and endometrium gene list produced by our analysis may not completely reflect the genes that are actually expressed in a tissue-enriched manner during early pregnancy.

Taken collectively, our GO, Reactome, and placenta and endometrium gene enrichment analyses suggest some notably interesting new findings about the maternal mononuclear phagocytes in particular. First, it appears that all three of the identified subsets, and not just the CD11C^{lo} dMP2-like macrophages as previously reported[70], appear to be capable of participating in tissue remodeling activities at the maternal-fetal interface, as we found angiogenic factors such as VEGF, matrix metalloproteinases such as MMP7 and MMP9, and ECM-related proteins such as fibronectin and cathespin to also be highly expressed among the dMP1 and plMP populations (**Figure 4**; **Appendix 8**), and processes such as smooth muscle adaptation, blood vessel morphogenesis, and collagen degradation to be overrepresented in these subsets (**Figure 5-7**). Building on previous studies, we show that all maternal mononuclear phagocyte populations, in addition to modulating inflammation through secreting mixtures of proinflammatory and anti-inflammatory cytokines, regulate synthesis and signaling via arachidonic acid, an omega-6 fatty acid, and its metabolites, including prostaglandins and leukotrienes[175]. Arachidonic acid metabolism has previously been described in activated human alveolar macrophages[176] and resident mouse peritoneal macrophages[177,178], and its apparent regulation by the mononuclear phagocytes potentially serves to further modulate inflammatory processes at the maternal-fetal interface.

In addition to arachidonic acid signaling, GO analyses suggest that dMP1 and plMP also appear to be particularly specialized for general lipid processing and metabolism (**Figure 4-7**). While most mononuclear phagocytes are capable of metabolizing lipids obtained via phagocytosis, there is accumulating evidence that macrophages residing in certain tissues are particularly specialized in this function[179]. For instance, relative to other macrophage populations, liver Kupffer cells and alveolar macrophages are both enriched in core lipid metabolism genes, such as PPAR-γ, which modulates lipid uptake and cholesterol efflux[180,181], or liver X receptors (LXRs), which regulate cholesterol sensing and transport[182]. Alveolar macrophages deficient in PPAR-γ exhibit widespread alterations in gene expression[181] and impaired catabolism of pulmonary surfactant, a lipoprotein complex produced by alveolar epithelial cells to facilitate gas exchange in the lung[183]. This results in excess surfactant buildup in the macrophages and alveoli, inducing a state of low-grade inflammation and driving the development of pulmonary alveolar proteinosis[181]. Meanwhile, in atherosclerosis, the aggregation of pro-inflammatory lipoprotein-containing plaques on arterial walls promotes the recruitment of monocyte-derived macrophages[184]. Excess lipoprotein uptake and metabolism converts the macrophages into

cholesterol-laden foam cells, which exacerbate atherosclerotic plaque progression through the production of proinflammatory cytokines, proteases, and other factors[185]. Given the importance of macrophage-mediated lipid processing in other tissues, it is conceivable that macrophages are also central to maintaining lipid homeostasis at the maternal-fetal interface, particularly as apoptotic cell clearance and placental transfer of cholesterol and lipid metabolites are among the important processes occurring in this environment. Notably, pregnancies complicated by maternal obesity are associated with elevated placental triglyceride storage, altered lipid transport[186,187], and a persistent inflammatory state which has been shown to promote the increased recruitment of macrophages to the placenta[188]. Although the fetal or maternal origin of these macrophages was not conclusively determined, these data parallel the observation of increased maternal leukocyte accumulation and infiltration of the placenta in chronic noninfectious villitis, another complication of pregnancy which is positively correlated with increased maternal BMI[189]. Thus, lipid metabolism by the maternal mononuclear phagocytes may represent yet another means by which they promote or resolve inflammation at the maternal-fetal interface.

Additionally, we show that dMP1 and plMac upregulate genes involved in the production and detoxification of reactive oxygen species (ROS) (**Figure 4-7**). Although ubiquitously generated by cells as a byproduct of mitochondrial respiration, ROS are also specifically released by macrophages to mediate intracellular killing of pathogens[190], and have been shown to contribute to regulating macrophage differentiation and polarization[191]. At the maternal-fetal interface, ROS has also been found to assume important roles in facilitating endometrial changes, blastocyst implantation, and placentation, among other processes[192]. Notably, oxidative burst, or the rapid cellular release of ROS, has been shown to induce trophoblast invasion by triggering their switch from a proliferative to invasive state[193], to regulate the ability of trophoblasts to fuse into the syncytiotrophoblast layer of the placenta[194], and to modulate trophoblast autophagy and apoptosis[195]. Additionally ROS promotes increased production of VEGF, HIF-1[196], and other angiogenesis-promoting transcriptional factors[197], while also oxidizing phospholipids, which can independently promote vascular growth factor production by activating TLR2 signaling in endothelial cells[198]. On the other hand, excessive oxidative stress, either through elevated ROS generation or deficient antioxidant activity, has been linked with the onset of preeclampsia, intrauterine growth restriction, and other placenta-associated conditions[192]. Thus, the potential roles that dMP1 and plMP play in modulating the balance of ROS in decidual and placental tissues may have

direct implications for pregnancy success while representing yet another potential dimension through which they contribute to the fine-tuning of tissue homeostasis at the maternal-fetal interface.

As a whole, our analyses of the maternal mononuclear phagocyte compartment at the maternal-fetal interface have enabled us to characterize the transcriptional profiles and potential functional roles assumed by each of the three subpopulations. These annotations collectively highlight the tissue-specific nature of these cells rather than their adherence to the classical M1/M2 model of macrophage polarization.

Chapter 5 - Cell type-level analysis of genes implicated in pregnancy complications and fertility-related conditions

5.1 Overview

A number of studies have associated specific genes with increased incidence of pregnancy complications or other factors influencing fertility and reproductive success. However, the molecular and cellular mechanisms by which these genes contribute to the development of these conditions remain largely unknown. scRNA-seq data represents one means of furthering studies of candidate genes, as it facilitates identifying which specific cell types at the maternal-fetal interface preferentially express each implicated gene. Reciprocally, collective examination of the cell type-level expression patterns of all genes linked to a specific disease or condition enables us to map identified cell types to disease-specific or clinically relevant contexts. In this chapter, I describe our single-cell transcriptomics-level profiling of database- and literature-curated genes associated with fertility-related conditions or pregnancy outcome, and present the insights obtainable from these analyses with focus on genes linked to preeclampsia and abnormal fetal growth.

5.2 Curation of genes associated with pregnancy complications and fertility and intersection with genes upregulated in individual cell types at the maternal-fetal interface

We first curated a list of 306 genes previously associated with complications of pregnancy or fertility-related conditions from the NHGRI/EBI GWAS Catalog[146], OMIM database[147], and literature searches. A general summary of the conditions and genes studied is provided in **Table 1** and individual genes are described in Appendix 6.

Table 1. Number of genes and curation sources associated with each pregnancy complication or fertility-related condition of interest.

Disease or phenotype	# curated genes (total)	# maternally expressed	# fetally expressed	Sources
Abnormal birth weight/fetal growth	60	14	57	NHGRI/EBI, literature
Endometriosis/ovarian disease	53	53	2	NHGRI/EBI, literature
Gestational trophoblastic disorder/ hydatidiform mole	7	2	5	OMIM, literature
Age of menopause/menstrual onset	47	47	0	NHGRI/EBI, literature
Recurrent miscarriage	19	19	5	OMIM, literature
Placenta accreta	3	2	3	Literature
Placental abruption	21	17	9	OMIM, literature
Preterm birth	41	37	6	NHGRI/EBI, literature
Preeclampsia	95	57	50	NHGRI/EBI, OMIM, literature

We then intersected this gene list with the genes determined by droplet-based scRNA-seq to be significantly upregulated (adjusted $p < 0.05$) in each cell type relative to other populations at the

maternal-fetal interface. Finally, we visualized the cell type-averaged expression levels of all disease- and fertility-linked genes found to be significantly enriched in one or more of the cell populations (**Figure 1**). Collectively, each of the annotated cell types at the maternal-fetal interface exhibits upregulation of a subset of genes from our curated gene set. This underscores how the various cell populations in the decidua and placenta individually contribute to the proper functioning of the maternal-fetal microenvironment, or conversely, can be implicated in the processes leading to its dysregulation.

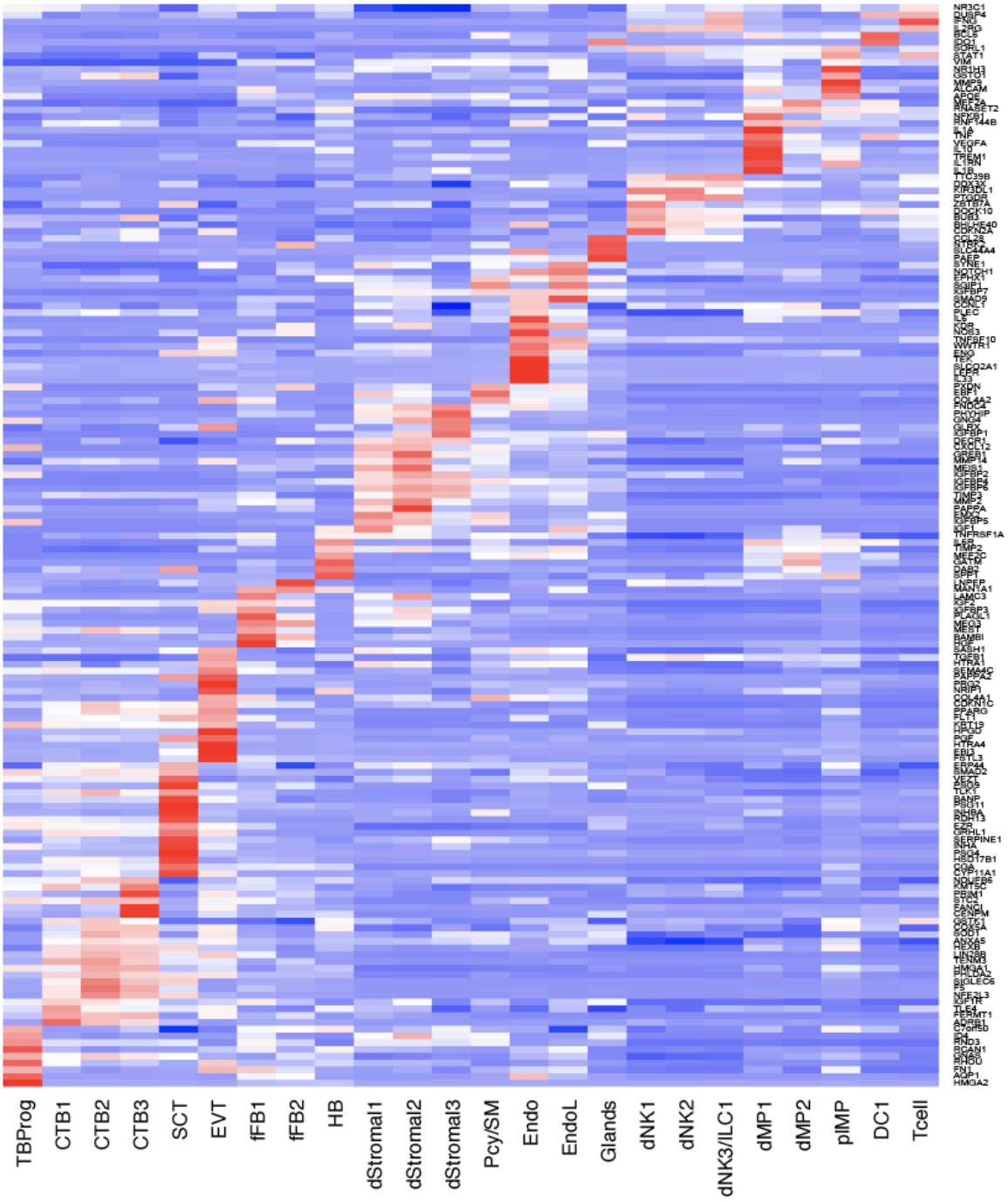

Figure 1. Genes associated with pregnancy complications or fertility are upregulated within all annotated cell types at the maternal-fetal interface. Heatmap plotting the disease- and fertility-linked genes which are

preferentially expressed in a particular cell type relative to all other populations identified at the maternal-fetal interface.

Many of the disease- and fertility-associated genes have been previously linked to maternal- or fetal-specific expression and function. After annotating each gene as being maternally and/or fetally associated based on literature curation efforts (Appendix 6), we sought to specifically intersect maternally expressed genes with the marker genes distinguishing maternal cell types, and fetally expressed genes with the marker genes distinguishing fetal cell types, in order to obtain a more functionally relevant understanding of the genes in their proper maternal or fetal context (**Figure 2a-b**). Results among maternal cells show that many maternally-associated genes are most highly expressed in the stromal cell and mononuclear phagocyte subsets, as well as in vascular smooth muscle and endothelial cells. Among the stromal cells and mononuclear phagocytes, relatively large numbers of genes are enriched in dStromal2, dMP1, and plMP (**Figure 2a**). Meanwhile, a majority of fetally-associated genes are specifically overexpressed among trophoblast cells, particularly in the differentiated SCT and invading EVT, although fibroblasts and Hofbauer cells were observed to upregulate a number of genes as well (**Figure 2b**).

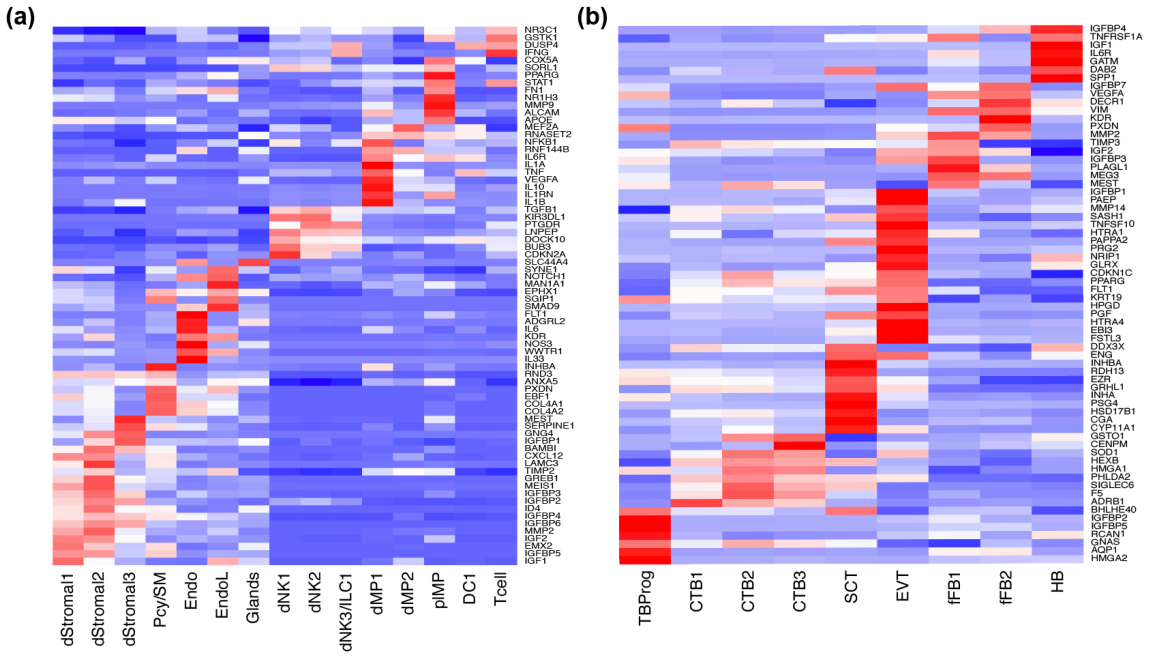

Figure 2. Specific maternal and fetal cell populations upregulate a number of the maternally-expressed and fetally-expressed genes associated with pregnancy complications and fertility. (a) Heatmap plotting the maternally expressed genes upregulated in identified maternal cell types; decidual stromal cells (dStromal1-3), vascular smooth muscle (Pcy/SM) and endothelial cells (Endo), and mononuclear phagocytes (dMP1/2 and plMP) exhibit upregulation of many of these genes. **(b)** Heatmap plotting the fetally expressed genes upregulated in

identified fetal cell types; the trophoblast cell subsets (TBProg, CTB1-3, SCT, and EVT), exhibit upregulation of many of these genes.

5.3 Analyses of maternally and fetally expressed genes implicated in preeclampsia and aberrant fetal growth

Next, we focused on individual pregnancy complications or fertility-related conditions, visualizing the cell type-level expression patterns of maternally and fetally expressed genes specifically associated with these conditions. We sought to gain a preliminary understanding of the relevance of each cell type to disease pathology, and reciprocally, determine in which cell type or types the gene set linked with each disease is most highly enriched. In addition to the results discussed below, heatmaps for other diseases and conditions in which relevant genes are highly expressed by specific cell populations are shown in Appendix 11.

Examining the genes associated with preeclampsia, a disorder characterized by hypertension and poor placentation, one notable observation is that trophoblast cells collectively express the largest proportion of fetal preeclampsia-linked genes (**Figure 3a**). Among these are genes involved in regulating cell growth and differentiation or apoptosis, such as *SOD1*, *HTRA1*, and *INHBA*; angiogenic factors including *Flt1*; and genes such as *PAPPA2* and *PRG2*, which are involved in regulating the insulin-like growth factor (IGF) pathway. This aligns with our previous understanding that precise coordination of trophoblast cell dynamics, including proliferation, differentiation, timing and extent of decidual invasion, is critical for ensuring sufficient arterial remodeling and placentation. Indeed, alterations in these mechanisms are known to be predisposing factors for preeclampsia and other placenta-associated pathologies[20,22].

Meanwhile, a number of maternal genes associated with preeclampsia are most highly expressed in the smooth muscle and endothelial cells encircling and lining the vessel walls in the maternal decidua (**Figure 3b**). This includes genes contributing to ECM formation, such as collagen IV subunit-encoding *COL4A1* and *COL4A2*, and *PXDN* (peroxidasin); genes regulating cell proliferation and growth, such as *INHBA* and *WWTR1* (*TAZ*); the inflammatory cytokine *IL-6*; endothelial nitric oxide synthase *NOS3*; and *Flt-1/sFlt-1*, which modulate angiogenesis. The selective enrichment of these genes in cells of the decidua vasculature reinforces our understanding that a number of vascular smooth muscle and endothelial cell functions are critical for ensuring proper maternal vascular adaptation in early pregnancy[199]. The dysregulation of processes such as tissue remodeling and vascular homeostasis in

these maternal cells represents another set of mechanisms potentially contributing to the pathogenesis of preeclampsia.

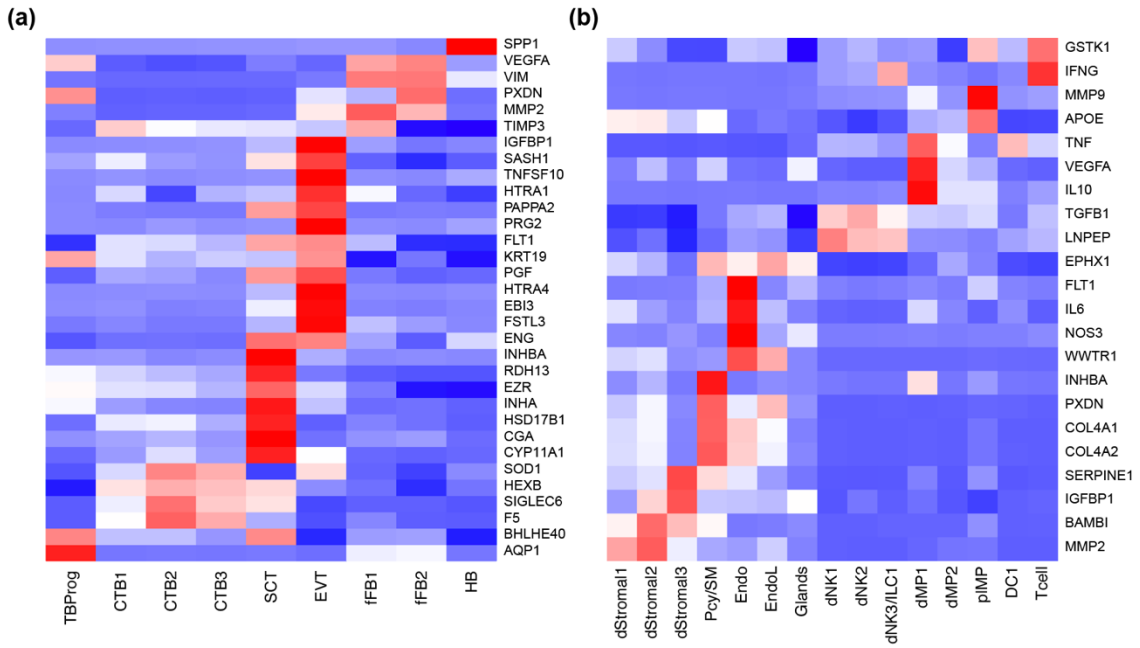

Figure 3. Preeclampsia-associated genes are preferentially expressed by fetal trophoblasts and by maternal endothelial and vascular smooth muscle cells. (a) Heatmap plotting the preeclampsia-linked genes that are known to be fetally expressed and that are significantly upregulated in specific fetal cell populations. Trophoblasts, particularly SCT and EVT, are shown to upregulate a number of these genes. **(b)** Heatmap plotting the preeclampsia-linked genes that are known to be maternally expressed and that are significantly upregulated in specific maternal cell populations. Vascular smooth muscle cells and endothelial cells exhibit enriched expression of a number of these genes.

Meanwhile, examining the genes implicated in aberrant fetal growth and birth weight, we observed that interestingly, decidual stromal cell populations exhibit upregulation of a particularly large proportion of the maternally expressed genes which are implicated in fetal growth (**Figure 4a**). Most of these genes are members of the IGF signaling pathway, with dStromal1 expressing enriched levels of the insulin-like growth factors *IGF1* and *IGF2*, and dStromal2/3 expressing high levels of the genes encoding IGF binding proteins *IGFBP1-6*. Fetally expressed genes in the IGF pathway have also been linked to fetal growth and birth weight, and we observed that elevated expression of the fetal IGFs and their binding proteins is distributed across several placental cell populations (**Figure 4b**), with EVT and trophoblast progenitors expressing high levels of *IGFBP1, 2, 5, 7*; fetal fibroblasts exhibiting upregulated *IGF2* and *IGFBP3*/*7*; and Hofbauer cells (fetal macrophages) expressing high levels of *IGF1* and *IGFBP4*.

IGF1 and IGF2 binding to the IGF1 receptor activates the PI3K and MAPK signalling pathways to promote increased protein synthesis, cell growth and proliferation, and reduced apoptosis[200]. The IGF

binding proteins function to increase the bioavailability of IGFs and their accessibility to receptors, while also potentially synergizing with IGF to activate downstream pathways through binding to other cell surface receptors[201]. The different decidual stromal subsets and placental cell populations appear to preferentially express varying members of maternal and fetal genes in the IGF/IGFBP families, suggesting they occupy specific but complementary functional roles in modulating IGF signaling, and in turn, fetal growth.

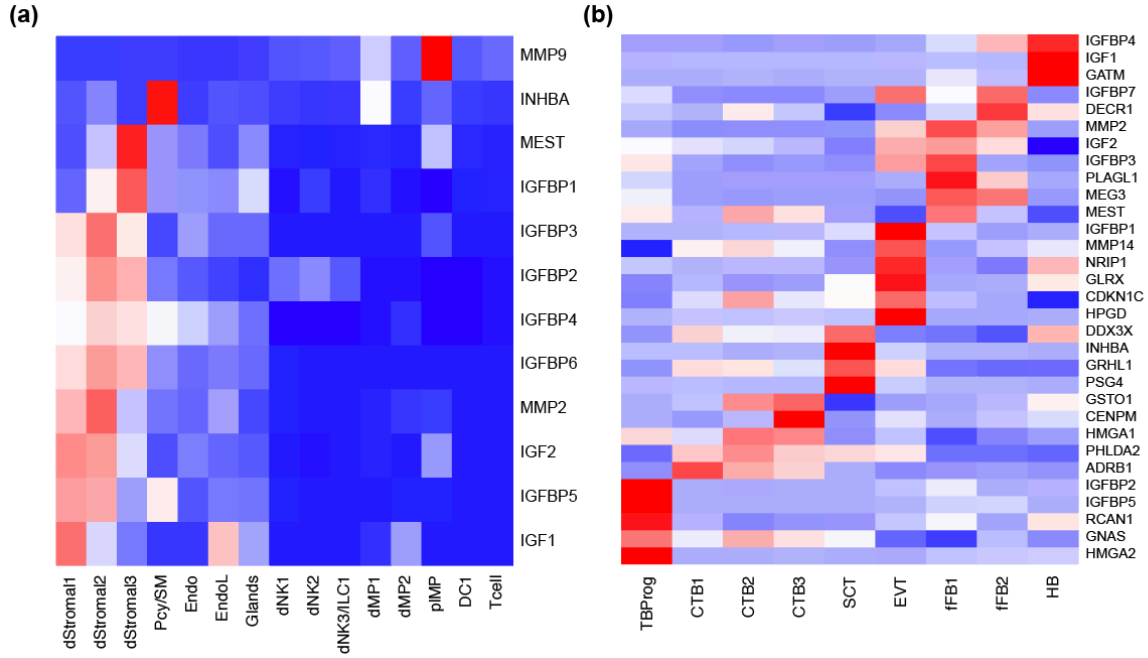

Figure 4. Genes associated with aberrant fetal growth or birth weight are preferentially expressed by maternal stromal cells and by fetal trophoblasts, fibroblasts, and Hofbauer cells. (a) Heatmap plotting fetal growth-associated genes that are known to be maternally expressed and that are significantly upregulated in specific maternal cell populations. The decidual stromal cell subsets (dStromal1-3) upregulate a number of insulin-like growth factors (IGFs) and IGF-binding proteins (IGFBPs) which comprise the IGF signaling axis. **(b)** Heatmap plotting genes linked to fetal growth that are known to be fetally expressed and that are significantly upregulated in specific fetal cell populations. Trophoblast, fibroblast, and Hofbauer cells collectively upregulate genes associated with the IGF axis.

5.4 Discussion

In this chapter I presented our analyses intersecting existing data on genes associated with pregnancy complications or fertility-related conditions with decidual and placental scRNA-seq data. We sought to explore how the cell type-specific resolution of gene expression afforded by scRNA-seq enables better understanding of which cell types are potentially driving the pathology of diseases or the development of these conditions.

Among the insights we derived from these analyses are that trophoblast subsets exhibit enriched expression of many of the fetally expressed genes implicated in preeclampsia (**Figure 3a**). This is consistent with existing knowledge that trophoblast growth and differentiation are tightly linked to the success of placentation and to the likelihood of developing preeclampsia. Collectively, the trophoblast-upregulated genes include *HSD17B1*, which regulates estradiol signaling, and *CGA*, a component of glycoprotein hormones, underscoring the notion that trophoblast cell functions are hormonally regulated and that imbalances in hormones themselves or their signaling could contribute to deficient placentation. Other enriched genes include *SASH1*, *TNFSF10* (*TRAIL*), *HTRA1*, *INHBA/INHA*, and *SOD1*, which collectively modulate the balance between cell growth, proliferation, and apoptosis, suggesting the key role of proper trophoblast development and differentiation in placentation. Trophoblast upregulation of genes such as *HTRA4*[202] and *EZR* also point to the importance of properly timed and regulated trophoblast cell adhesion, migration, and invasion at the maternal-fetal interface. Finally, the overexpression of vascular endothelial and insulin-like growth factor-involved genes such as *FLT1*, *PAPPA2*, and *PRG2* suggests that trophoblast roles in tissue and vascular remodeling are also of consequence. Overall, the intersection of fetal preeclampsia-associated genes with the placental cell types at the maternal-fetal interface enabled us to pinpoint the trophoblasts as the cell populations in which a number of these genes are most highly expressed, and in which their likely functional consequences are most apparent. At the same time, this analysis also reinforces the myriad factors underlying trophoblast cell dynamics and the importance of their coordinated regulation for proper trophoblast function, and in turn, the various means by which trophoblast cells may contribute to the pathogenesis of preeclampsia.

Meanwhile, vascular smooth muscle and endothelial cells exhibit upregulation of many of the maternally expressed genes associated with preeclampsia (**Figure 3b**), underscoring the roles of proper maternal vascular function and adaptation in ensuring successful placentation and influencing the risk of pregnancy complications linked to these processes. Smooth muscle cells express high levels of collagen IV genes *COL4A1* and *COL4A2* as well as *PXDN*, a peroxidase involved in crosslinking collagen IV chains and organizing the ECM[203,204], suggesting their consequential roles in mediating the tissue remodeling functions which are critical for regulation of EVT invasion and maternal arterial transformation. Other highly expressed genes include *WWTR1* (*TAZ*), a transcriptional coactivator in the Hippo pathway which modulates endothelial cell proliferation, metabolism, and vascular

remodeling[205]; *NOS3* (endothelial nitric oxide synthase), which synthesizes nitric oxide, a vasodilator and regulator of smooth muscle relaxation and leukocyte adhesion[206]; *IL-6*, a cytokine linked to vascular inflammation and endothelial dysfunction[207]; and *Flt-1/sFlt-1*, which bind VEGF/PIGF to either promote or inhibit angiogenesis, respectively. Collectively, these genes suggest that that fine-tuned regulation of local vascular tone, vascular growth and maintenance, and levels of pro-angiogenic and anti-angiogenic factors, along with the limitation of damaging inflammatory responses, all play important roles in controlling vascular smooth muscle and endothelial cell dynamics, and consequently, the various potential routes by which vascular dysfunction can occur and predispose the onset of preeclampsia. Taking the maternal and fetal preeclampsia-linked genes and the cell populations expressing them in aggregate highlights the complementary functional roles assumed by maternal and fetal cells and the intricate regulation of their functions that is likely necessary for facilitating proper placentation. Involved in this coordination are likely an array of interactions and mechanisms that upon dysregulation, can contribute to the complex pathogenesis of preeclampsia.

Additionally, in our examination of maternally expressed genes associated with abnormal fetal growth and birth weight, our analysis highlights the roles of decidual stromal cells as the main producers of components of the IGF axis (**Figure 4a**). We also show that trophoblasts, fibroblasts, and Hofbauer cell populations collectively express fetal IGFs and IGFBPs (**Figure 4b**). In the pregnancy context, IGFs, their binding proteins, and their receptors have been established to be pivotal to fetal development and growth. The IGF axis has been suggested to mediate nutrient availability and allocation to the fetoplacental unit, through regulation of maternal metabolism as well as various aspects of placentation[208]. IGF levels and signaling have been linked to stimulus of trophoblast growth and invasion[209] and to the regulation of placental substrate transport and hormone secretion[210,211]. Previously, only IGFBP1 was a well-documented stromal cell secretory product of relevance to IGF signaling[10,212], but our results suggest that stromal cells may in fact play a major role in mediating this important mechanism of fetal growth at the maternal-fetal interface. The elevated expression of IGFs and IGFBPs by both decidual and placental cells reinforces that IGFs potentially exert their effects through both autocrine and paracrine signaling or via both maternal and fetal circulation, highlighting the potential complexity of IGF regulation and how its modulation by multiple cell types indicates its ability to influence fetal growth through multiple modes of action.

Collectively, our results demonstrate the utility of leveraging scRNA-seq data to map disease or phenotype-associated genes identified through studies such as GWAS or gene expression profiling to specific cell types. They highlight the potential cellular functions and mechanisms of these genes, while clarifying in turn the consequential functions and processes of their associated cell types. One caveat of our approach, however, is that it is limited by the scope of gene curation and by the robustness of included studies. In the case of evaluating GWAS results, many implicated loci or risk variants fall within non-coding regions that cannot be conclusively mapped to candidate genes; thus, it may be difficult to further prioritize or otherwise study such variants based on the scRNA-seq data. Finally, in this current form of the analysis, we have not directly taken into account the fact that many gene and cellular functions are mediated through cell-cell interactions. This is particularly relevant, as our analyses strongly suggest that different cell types at the maternal-fetal interface collectively play overlapping and complementary roles in driving disease pathology or the development of specific phenotypes. A method for inferring cell-cell interactions from scRNA-seq data via the examination of ligand-receptor pairs expressed by cell populations has been recently developed (www.CellPhoneDB.org) and has been applied to further profile specific cell populations and predict communication among cell types in the decidua and placenta (Vento-Tormo R, Efremova E et al., unpublished). Intersection of the genes linked to pregnancy-related diseases or phenotypes with the ligand-receptor interactions predicted by CellPhoneDB would introduce a new layer of understanding for how cellular crosstalk at the maternal-fetal interface, rather than isolated cell types, ultimately contributes to disease processes.

Overall, this analysis facilitated an increased understanding of the development of pregnancy- and fertility-related conditions at the highly informative resolution of specific cell populations or cell states rather than merely at the tissue level. It also enabled the preliminary correlation of gene functions to the cellular functions differentiating individual cell populations, and in turn, the mapping of cell types to specific conditions. Ultimately, such analyses could aid in the development of more targeted, mechanistically-informed therapies and improved strategies for managing infertility or complications of pregnancy. These paired analyses of disease-associated genes and scRNA-seq data could be similarly applied to studying other tissues and their associated pathologies.

Chapter 6 - Conclusions and Future Directions

6.1 Conclusions

In this thesis, I presented results from our single cell-resolution characterization of the human maternal-fetal interface during early pregnancy. Single-cell transcriptomes derived from droplet-based and plate-based scRNA-seq of maternal decidua and fetal placenta were analyzed in conjunction with whole genome sequencing of maternal and fetal genomic DNA, bulk RNA-sequencing of decidual tissues, FACS index sorting and CyTOF datasets, established macrophage gene signatures and public gene expression datasets, and curated gene sets associated with complications of pregnancy and fertility.

I first demonstrated that while determination of the maternal or fetal genetic identities of decidual and placental cells requires further optimization before it can be achieved through scRNA-seq-based variant detection alone, we can successfully perform maternal/fetal assignments for these cells in cases where maternal and fetal genotypes are known, using the recently developed demuxlet algorithm. This unbiased determination of maternal/fetal origin enabled us to independently evaluate the relative presence of maternal and fetal cells in the placenta and decidua. At the same time, it also improved our annotation of cell types at the maternal-fetal interface by clarifying the genetic origins of specific cell populations of interest, including mononuclear phagocytes localized to the placenta found to be of maternal origin, and an unknown cell population found in both decidua and placenta determined to be of fetal origin.

I then showed that analyzing scRNA-seq data in conjunction with matched bulk RNA-seq data generated on the same samples represents a potential strategy by which to identify genes susceptible to single-cell dissociation protocol-induced perturbations in expression. We found that *HSPA1B*, a gene highly upregulated in a decidual T cell subpopulation identified by plate-based scRNA-seq, was not significantly expressed in bulk RNA-seq of the same decidual tissues. This suggests that *HSPA1B* and the T cell subpopulation characterized by its expression are potential scRNA-seq-associated artifacts, and we therefore excluded these cells from subsequent functional annotation and analysis.

Next, I showed how superimposition of gating identities from FACS index sorting onto scRNA-seq data enabled us to validate the transcriptome-based annotations of decidual immune cells sequenced by the plate-based SmartSeq2 protocol. In particular, FACS gating enabled us to confirm the existence of two distinct decidual mononuclear phagocyte subsets distinguished by surface expression of HLADR and

CD14 and by high and low expression of the *CD11C* gene. Using high-dimensional CyTOF, we were able to further distinguish these myeloid cell populations based on CD11C protein expression, as well as independently validate and further describe the novel dNK and distinct T cell populations that were previously annotated in the scRNA-seq data.

To further characterize the maternal mononuclear phagocyte populations at the maternal-fetal interface, we performed GO and Reactome term enrichment analysis on the upregulated genes in this population and paired single-cell transcriptomic data from these subsets with M1/M2 macrophage signatures and placenta- and endometrium-enriched genes identified from datasets deposited in the Human Protein Atlas. These analyses enabled us to determine that the mononuclear phagocytes collectively upregulate genes involved in tissue remodeling, modulation of local inflammatory responses, regulation of ROS production and detoxification, and lipid sensing and metabolism. Overall, we show that maternal decidual and placental mononuclear phagocytes do not exhibit classical M1/M2 macrophage polarization and, along with several other decidual resident immune subsets, are characterized by their elevated expression of a number of genes enriched in the placenta and endometrium, suggesting their adaptation of tissue-specific functions that heavily tailor them to the unique demands and microenvironment of the maternal-fetal interface.

Finally, the curation of genes associated with complications of pregnancy and conditions influencing fertility and the intersection of these gene sets with our decidual and placental scRNA-seq data enabled us to better understand how specific cell types at the maternal-fetal interface potentially contribute to driving these diseases or conditions. In particular, we show that fetal trophoblasts express a large proportion of the fetal genes previously associated with preeclampsia, while maternal smooth muscle and endothelial cells preferentially express a number of the maternal preeclampsia-linked genes, reinforcing the complementary roles and potential interplay between different cell populations in regulating trophoblast cell differentiation and invasion and maternal vascular adaptation, and in turn, their respective contributions to the complex pathogenesis of preeclampsia and similar disorders associated with defective placentation. Meanwhile, we show that among the genes influencing fetal growth and birth weight, maternal expression of IGFs and their binding proteins is concentrated among the decidual stromal cell subsets, while fetal expression of IGF axis genes is distributed among trophoblast cell, fibroblast, and Hofbauer cell populations, suggesting that IGF regulation of fetal growth is potentially mediated in an autocrine and paracrine fashion between the decidua and placenta and

involves similarly complex mechanisms of cross-regulation and coordination among a number of cell types at the maternal-fetal interface.

Taken as a whole, this series of analyses integrating single-cell transcriptomics with additional experimental approaches and datasets have enabled us to validate or to uncover novel findings and interesting biological aspects of the maternal-fetal interface that may not have been achievable through analyses of scRNA-seq data in isolation.

6.2 Future directions

6.2.1 Further improvements and applications of single-cell genotyping

While we were able to successfully infer the maternal or fetal identities of single cells from droplet-based scRNA-seq data through the use of demuxlet and maternal and fetal WGS, it would ultimately be desirable to develop a method to robustly genotype single cells via scRNA-seq read data alone. This would eliminate the need to generate additional genotype data from all genetically distinct individuals associated with a given sample, a practical benefit that would scale particularly as the number and variety of tissues and samples to be explored by scRNA-seq increases. There are many conceivable scenarios in which the number or identity of distinct individuals potentially contributing cells to a sample is unknown *a priori*, making it impossible to obtain the genomic DNA or genotypes needed for single-cell genotyping by demuxlet. Samples involving organisms lacking well-annotated DNA reference genomes, or more generally, any sequencing experiment in which there are potential sources of contaminating cells, present particular challenges. A method which would be able to robustly infer genetic distinctness among all cells in a sample in an unbiased manner would likely significantly advance efforts to dissect such systems.

Meanwhile, single-cell genotyping could be leveraged to further investigate certain questions of specific relevance to the maternal-fetal interface. Genomic imprinting has been observed in several genes expressed in the placenta and found to play various roles in regulating processes at the maternal-fetal interface[213]. In fact, placenta-derived *IGF2*, linked to fetal growth, has been shown to be maternally imprinted (with only the paternally inherited copy expressed)[214], and similarly, other genes involved in fetal growth and enriched in the placenta, including *MEST, MEG3,* and *PHLDA2*, have also shown to be expressed in an imprinted manner. An endeavor to identify all imprinted genes at the maternal-fetal interface would prove useful in understanding the functional and phenotypic consequences of imprinting

at specific genes, and perhaps more broadly, the evolutionary basis for imprinting to persist as a gene regulatory mechanism at the maternal-fetal interface. Single-cell genotyping could be adapted to comprehensively identify imprinted genes by determining which genes expressed in decidual and placental cells exhibit allelic imbalance, and furthermore, help clarify whether the imprinting of a gene of interest occurs exclusively in specific cell types or cell states or during specific stages of pregnancy. Single-cell genotyping could also be applied to studying microchimerism, another interesting extension of maternal-fetal biology. In cases of fetal microchimerism, cells of fetal origin pass through the placenta to the maternal circulation and establish lineages in maternal tissues, while in maternal microchimerism, maternally derived cells are passed to the child and shown to persist into adulthood[215]. Although constituting a small minority of cells in their host (e.g. in maternal T cells, up to 2.7 per 100,000 cells[216]), microchimeric cells have been observed in the immune cell populations of 39% of women after birth[216], as well as in women with history of induced or spontaneous abortion[217]. Both maternal and fetal microchimerism have been observed in hematopoietic cell lineages, as well as in cardiac myocytes, hepatocytes, and differentiated cells in other tissues[218], and have been variously associated with autoimmune conditions such as rheumatoid arthritis[219], neonatal lupus[220], complications of pregnancy[218], and cancer[221]. The ability to incorporate unbiased single-cell genotyping into the study of additional tissue samples, which are already being actively studied at single-cell resolution through initiatives such as the Human Cell Atlas (HCA) and Developmental Cell Atlas, may provide new insights into determining the extent of microchimerism events and investigating their potential functional impacts on disease.

6.2.2 Further characterization of identified cell types at maternal-fetal interface

In this study, a number of cell populations, including novel cell types or states, were described in the decidua and placenta, with identification of their distinct gene and surface protein markers, functions, and relevance to disease. Critical to robustly validating these cell populations and their proposed functions would be to further observe their predicted gene and protein expression patterns and cell-cell interactions *in vitro* or *in vivo*. Anatomical and cellular differences in animal models of pregnancy, in combination with the limitations of many *in vitro* models, remain challenges to be addressed. However, the recent development of endometrial organoids, which are capable of functionally recapitulating early pregnancy[222], may prove useful for further functional studies of cells in the decidua, such as the distinct

stromal cell populations and their respective secretory characteristics identified in this study. Meanwhile, intact decidual and placental samples can be further analyzed using RNAScope[223], a novel *in situ* hybridization assay which facilitates the examination of selected RNA biomarkers within cells in fresh frozen or formalin-fixed, paraffin-embedded tissue sections at single-cell resolution. RNAScope represents a valuable means of validating gene signatures and predicted cell-cell interactions in cell populations, while also preserving the spatial architecture of the tissue being studied, thus enabling it to control for dissociation protocol-associated perturbations in gene expression while also providing a new layer of information about the spatial organization of the cells of interest, which will be relevant to further contextualizing their functions and proposed interactions.

At the same time, additional analyses at the single-cell transcriptome level will be useful in further annotating the cell populations featured in this study. For example, in order to define relationships between the different identified trophoblast subsets, pseudotime algorithms such as Monocle[224] were employed to infer a developmental trajectory among the trophoblast cells, defining their differentiation from progenitor cells and cytotrophoblast cells into the SCT and EVT that facilitate placentation, and in turn, identifying the transcriptional changes that potentially underlie this process which were previously not well understood (Vento-Tormo R, Efremova E, et al., under submission). In this thesis, we further described the three maternal mononuclear phagocyte subsets identified in the decidua and placenta, determining that dMP1 and plMP exhibit a monocyte-derived origin and that dMP2 exhibits a markedly tissue-resident phenotype. We could employ similar approaches for trajectory inference to dissect the nature of the monocyte to tissue-resident macrophage transition that characterizes these subsets and thus better define their potential interrelationships.

Finally, extending our single-cell analyses from early pregnancy towards the study of nonpregnant endometrium, as well as near-term or term decidua and placenta, would enable the construction of a comprehensive atlas of the cell states, biology, and immunology of the maternal-fetal interface over the various time points of pregnancy, and would also enable comparative analysis and inference of how these states change over time. In particular, a longstanding question in the characterization of maternal immune cell subsets in pregnancy is whether these cells reside in the endometrium or decidua prior to pregnancy, or alternatively, at what stages before or during early pregnancy they are recruited to the maternal-fetal interface[2]. Single cell-level mapping of various states of the nonpregnant endometrium (proliferative and secretory phases) in comparison with the early pregnancy decidua could prove pivotal

in addressing this gap in our knowledge. More broadly, a single cell-resolution understanding of the successive stages of pregnancy would undoubtedly facilitate the identification of novel cell states and cell functions in addition to the refinement of known ones.

References

1. Red-Horse, K. *et al.* Trophoblast differentiation during embryo implantation and formation of the maternal-fetal interface. *J. Clin. Invest.* **114,** 744–754 (2004).
2. Erlebacher, A. Immunology of the maternal-fetal interface. *Annu. Rev. Immunol.* **31,** 387–411 (2013).
3. Henriet, P., Gaide Chevronnay, H. P. & Marbaix, E. The endocrine and paracrine control of menstruation. *Mol. Cell. Endocrinol.* **358,** 197–207 (2012).
4. Wetendorf, M. & DeMayo, F. J. The progesterone receptor regulates implantation, decidualization, and glandular development via a complex paracrine signaling network. *Mol. Cell. Endocrinol.* **357,** 108–118 (2012).
5. Gellersen, B. & Brosens, J. Cyclic AMP and progesterone receptor cross-talk in human endometrium: a decidualizing affair. *J. Endocrinol.* **178,** 357–372 (2003).
6. Kajihara, T., Brosens, J. J. & Ishihara, O. The role of FOXO1 in the decidual transformation of the endometrium and early pregnancy. *Med. Mol. Morphol.* **46,** 61–68 (2013).
7. Huyen, D. V. & Bany, B. M. Evidence for a conserved function of heart and neural crest derivatives expressed transcript 2 in mouse and human decidualization. *Reproduction* **142,** 353–368 (2011).
8. Brosens, J. J., Hayashi, N. & White, J. O. Progesterone receptor regulates decidual prolactin expression in differentiating human endometrial stromal cells. *Endocrinology* **140,** 4809–4820 (1999).
9. Kitaya, K. *et al.* IL-15 expression at human endometrium and decidua. *Biol. Reprod.* **63,** 683–687 (2000).
10. Fowler, D. J., Nicolaides, K. H. & Miell, J. P. Insulin-like growth factor binding protein-1 (IGFBP-1): a multifunctional role in the human female reproductive tract. *Hum. Reprod. Update* **6,** 495–504 (2000).
11. Shiokawa, S. *et al.* Expression of beta 1 integrins in human endometrial stromal and decidual cells. *J. Clin. Endocrinol. Metab.* **81,** 1533–1540 (1996).
12. Sugino, N., Kashida, S., Karube-Harada, A., Takiguchi, S. & Kato, H. Expression of vascular endothelial growth factor (VEGF) and its receptors in human endometrium throughout the menstrual cycle and in early pregnancy. *Reproduction* **123,** 379–387 (2002).

13. Hempstock, J., Cindrova-Davies, T., Jauniaux, E. & Burton, G. J. Endometrial glands as a source of nutrients, growth factors and cytokines during the first trimester of human pregnancy: a morphological and immunohistochemical study. *Reprod. Biol. Endocrinol.* **2,** 58 (2004).
14. King, A. Uterine leukocytes and decidualization. *Hum. Reprod. Update* **6,** 28–36 (2000).
15. Faas, M. M. & de Vos, P. Uterine NK cells and macrophages in pregnancy. *Placenta* **56,** 44–52 (2017).
16. Large, M. J. & DeMayo, F. J. The regulation of embryo implantation and endometrial decidualization by progesterone receptor signaling. *Mol. Cell. Endocrinol.* **358,** 155–165 (2012).
17. Craven, C. M., Morgan, T. & Ward, K. Decidual spiral artery remodelling begins before cellular interaction with cytotrophoblasts. *Placenta* **19,** 241–252 (1998).
18. Okada, H., Tsuzuki, T. & Murata, H. Decidualization of the human endometrium. *Reprod. Med. Biol.* **358,** 197 (2018).
19. Gellersen, B., Reimann, K., Samalecos, A., Aupers, S. & Bamberger, A.-M. Invasiveness of human endometrial stromal cells is promoted by decidualization and by trophoblast-derived signals. *Hum. Reprod.* **25,** 862–873 (2010).
20. Norwitz, E. R., Schust, D. J. & Fisher, S. J. Implantation and the survival of early pregnancy. *N. Engl. J. Med.* **345,** 1400–1408 (2001).
21. Gude, N. M., Roberts, C. T., Kalionis, B. & King, R. G. Growth and function of the normal human placenta. *Thromb. Res.* **114,** 397–407 (2004).
22. Lunghi, L., Ferretti, M. E., Medici, S., Biondi, C. & Vesce, F. Control of human trophoblast function. *Reprod. Biol. Endocrinol.* **5,** 6 (2007).
23. Mor, G., Aldo, P. & Alvero, A. B. The unique immunological and microbial aspects of pregnancy. *Nat. Rev. Immunol.* **17,** 469–482 (2017).
24. Sharma, S., Godbole, G. & Modi, D. Decidual Control of Trophoblast Invasion. *Am. J. Reprod. Immunol.* **75,** 341–350 (2016).
25. Genbacev, O., Joslin, R., Damsky, C. H., Polliotti, B. M. & Fisher, S. J. Hypoxia alters early gestation human cytotrophoblast differentiation/invasion in vitro and models the placental defects that occur in preeclampsia. *J. Clin. Invest.* **97,** 540–550 (1996).
26. Zhou, Y. *et al.* Human cytotrophoblasts adopt a vascular phenotype as they differentiate. A strategy for successful endovascular invasion? *J. Clin. Invest.* **99,** 2139–2151 (1997).

27. Fukushima, K. *et al.* Tumor necrosis factor and vascular endothelial growth factor induce endothelial integrin repertories, regulating endovascular differentiation and apoptosis in a human extravillous trophoblast cell line. *Biol. Reprod.* **73,** 172–179 (2005).
28. Lyall, F. *et al.* Human trophoblast invasion and spiral artery transformation: the role of PECAM-1 in normal pregnancy, preeclampsia, and fetal growth restriction. *Am. J. Pathol.* **158,** 1713–1721 (2001).
29. Damsky, C. H. & Fisher, S. J. Trophoblast pseudo-vasculogenesis: faking it with endothelial adhesion receptors. *Curr. Opin. Cell Biol.* **10,** 660–666 (1998).
30. Griffiths, S. K. & Campbell, J. P. Placental structure, function and drug transfer. *Contin Educ Anaesth Crit Care Pain* **15,** 84–89 (2015).
31. Wallace, A. E., Host, A. J., Whitley, G. S. & Cartwright, J. E. Decidual natural killer cell interactions with trophoblasts are impaired in pregnancies at increased risk of preeclampsia. *Am. J. Pathol.* **183,** 1853–1861 (2013).
32. te Velde, E. A., Exalto, N., Hesseling, P. & van der Linden, H. C. First trimester development of human chorionic villous vascularization studied with CD34 immunohistochemistry. *Hum. Reprod.* **12,** 1577–1581 (1997).
33. Garratt, M., Gaillard, J.-M., Brooks, R. C. & Lemaître, J.-F. Diversification of the eutherian placenta is associated with changes in the pace of life. *Proc. Natl. Acad. Sci. U. S. A.* **110,** 7760–7765 (2013).
34. King, A. *et al.* Surface expression of HLA-C antigen by human extravillous trophoblast. *Placenta* **21,** 376–387 (2000).
35. King, A. *et al.* HLA-E is expressed on trophoblast and interacts with CD94/NKG2 receptors on decidual NK cells. *Eur. J. Immunol.* **30,** 1623–1631 (2000).
36. King, A., Balendran, N., Wooding, P., Carter, N. P. & Loke, Y. W. CD3- Leukocytes Present in the Human Uterus During Early Placentation: Phenotypic and Morphologic Characterization of the CD56. *Journal of Immunology Research* **1,** 169–190 (1991).
37. Koopman, L. A. *et al.* Human decidual natural killer cells are a unique NK cell subset with immunomodulatory potential. *J. Exp. Med.* **198,** 1201–1212 (2003).
38. Cerdeira, A. S. *et al.* Conversion of peripheral blood NK cells to a decidual NK-like phenotype by a cocktail of defined factors. *J. Immunol.* **190,** 3939–3948 (2013).

39. Hanna, J. *et al.* Decidual NK cells regulate key developmental processes at the human fetal-maternal interface. *Nat. Med.* **12,** 1065–1074 (2006).
40. Höglund, P. & Brodin, P. Current perspectives of natural killer cell education by MHC class I molecules. *Nat. Rev. Immunol.* **10,** 724–734 (2010).
41. Hsu, K. C., Chida, S., Geraghty, D. E. & Dupont, B. The killer cell immunoglobulin-like receptor (KIR) genomic region: gene-order, haplotypes and allelic polymorphism. *Immunol. Rev.* **190,** 40–52 (2002).
42. Gonen-Gross, T. *et al.* Inhibitory NK receptor recognition of HLA-G: regulation by contact residues and by cell specific expression at the fetal-maternal interface. *PLoS One* **5,** e8941 (2010).
43. Braud, V. M. *et al.* HLA-E binds to natural killer cell receptors CD94/NKG2A, B and C. *Nature* **391,** 795–799 (1998).
44. Hiby, S. E. *et al.* Combinations of maternal KIR and fetal HLA-C genes influence the risk of preeclampsia and reproductive success. *J. Exp. Med.* **200,** 957–965 (2004).
45. Robinson, J. *et al.* The IPD and IMGT/HLA database: allele variant databases. *Nucleic Acids Res.* **43,** D423–31 (2015).
46. Colucci, F. & Kieckbusch, J. Maternal uterine natural killer cells nurture fetal growth: in medio stat virtus. *Trends Mol. Med.* **21,** 60–67 (2015).
47. Kieckbusch, J., Gaynor, L. M., Moffett, A. & Colucci, F. MHC-dependent inhibition of uterine NK cells impedes fetal growth and decidual vascular remodelling. *Nat. Commun.* **5,** 3359 (2014).
48. Hiby, S. E. *et al.* Maternal KIR in combination with paternal HLA-C2 regulate human birth weight. *J. Immunol.* **192,** 5069–5073 (2014).
49. Nagamatsu, T. & Schust, D. J. The contribution of macrophages to normal and pathological pregnancies. *Am. J. Reprod. Immunol.* **63,** 460–471 (2010).
50. Heikkinen, J., Möttönen, M., Komi, J., Alanen, A. & Lassila, O. Phenotypic characterization of human decidual macrophages. *Clin. Exp. Immunol.* **131,** 498–505 (2003).
51. Sayama, S. *et al.* Human decidual macrophages suppress IFN-γ production by T cells through costimulatory B7-H1:PD-1 signaling in early pregnancy. *J. Reprod. Immunol.* **100,** 109–117 (2013).
52. Hsu, P. *et al.* Altered decidual DC-SIGN+ antigen-presenting cells and impaired regulatory T-cell

induction in preeclampsia. *Am. J. Pathol.* **181,** 2149–2160 (2012).

53. Co, E. C. *et al.* Maternal decidual macrophages inhibit NK cell killing of invasive cytotrophoblasts during human pregnancy. *Biol. Reprod.* **88,** 155 (2013).
54. Gustafsson, C. *et al.* Gene expression profiling of human decidual macrophages: evidence for immunosuppressive phenotype. *PLoS One* **3,** e2078 (2008).
55. Li, M. *et al.* Modulation of Decidual Macrophage Polarization by Macrophage Colony-Stimulating Factor Derived from First-Trimester Decidual Cells: Implication in Preeclampsia. *Am. J. Pathol.* **186,** 1258–1266 (2016).
56. Engert, S. *et al.* Profiling chemokines, cytokines and growth factors in human early pregnancy decidua by protein array. *Am. J. Reprod. Immunol.* **58,** 129–137 (2007).
57. Svensson-Arvelund, J. *et al.* The human fetal placenta promotes tolerance against the semiallogeneic fetus by inducing regulatory T cells and homeostatic M2 macrophages. *J. Immunol.* **194,** 1534–1544 (2015).
58. Smith, S. D., Dunk, C. E., Aplin, J. D., Harris, L. K. & Jones, R. L. Evidence for immune cell involvement in decidual spiral arteriole remodeling in early human pregnancy. *Am. J. Pathol.* **174,** 1959–1971 (2009).
59. Schonkeren, D. *et al.* Differential distribution and phenotype of decidual macrophages in preeclamptic versus control pregnancies. *Am. J. Pathol.* **178,** 709–717 (2011).
60. McCutcheon, J. C. *et al.* Regulation of macrophage phagocytosis of apoptotic neutrophils by adhesion to fibronectin. *J. Leukoc. Biol.* **64,** 600–607 (1998).
61. Galvan, M. D., Greenlee-Wacker, M. C. & Bohlson, S. S. C1q and phagocytosis: the perfect complement to a good meal. *J. Leukoc. Biol.* **92,** 489–497 (2012).
62. Fock, V. *et al.* Macrophage-derived IL-33 is a critical factor for placental growth. *J. Immunol.* **191,** 3734–3743 (2013).
63. Hatayama, H. *et al.* Progesterone enhances macrophage colony-stimulating factor production in human endometrial stromal cells in vitro. *Endocrinology* **135,** 1921–1927 (1994).
64. Mills, C. D., Kincaid, K., Alt, J. M., Heilman, M. J. & Hill, A. M. M-1/M-2 macrophages and the Th1/Th2 paradigm. *J. Immunol.* **164,** 6166–6173 (2000).
65. Martinez, F. O., Sica, A., Mantovani, A. & Locati, M. Macrophage activation and polarization. *Front. Biosci.* **13,** 453–461 (2008).

66. Mosser, D. M. The many faces of macrophage activation. *J. Leukoc. Biol.* **73,** 209–212 (2003).
67. Gordon, S. Alternative activation of macrophages. *Nat. Rev. Immunol.* **3,** 23–35 (2003).
68. Martinez, F. O., Helming, L. & Gordon, S. Alternative activation of macrophages: an immunologic functional perspective. *Annu. Rev. Immunol.* **27,** 451–483 (2009).
69. Mantovani, A. *et al.* The chemokine system in diverse forms of macrophage activation and polarization. *Trends Immunol.* **25,** 677–686 (2004).
70. Houser, B. L., Tilburgs, T., Hill, J., Nicotra, M. L. & Strominger, J. L. Two unique human decidual macrophage populations. *J. Immunol.* **186,** 2633–2642 (2011).
71. Houser, B. L. Decidual macrophages and their roles at the maternal-fetal interface. *Yale J. Biol. Med.* **85,** 105–118 (2012).
72. Martinez, F. O. & Gordon, S. The M1 and M2 paradigm of macrophage activation: time for reassessment. *F1000Prime Rep.* **6,** 13 (2014).
73. Davies, L. C., Jenkins, S. J., Allen, J. E. & Taylor, P. R. Tissue-resident macrophages. *Nat. Immunol.* **14,** 986–995 (2013).
74. Okabe, Y. & Medzhitov, R. Tissue biology perspective on macrophages. *Nat. Immunol.* **17,** 9–17 (2016).
75. Ganz, T. Macrophages and systemic iron homeostasis. *J. Innate Immun.* **4,** 446–453 (2012).
76. Kohyama, M. *et al.* Role for Spi-C in the development of red pulp macrophages and splenic iron homeostasis. *Nature* **457,** 318–321 (2009).
77. Boyle, W. J., Simonet, W. S. & Lacey, D. L. Osteoclast differentiation and activation. *Nature* **423,** 337–342 (2003).
78. Gardner, L. & Moffett, A. Dendritic cells in the human decidua. *Biol. Reprod.* **69,** 1438–1446 (2003).
79. Kämmerer, U. *et al.* Human decidua contains potent immunostimulatory CD83(+) dendritic cells. *Am. J. Pathol.* **157,** 159–169 (2000).
80. Ban, Y.-L., Kong, B.-H., Qu, X., Yang, Q.-F. & Ma, Y.-Y. BDCA-1+, BDCA-2+ and BDCA-3+ dendritic cells in early human pregnancy decidua. *Clin. Exp. Immunol.* **151,** 399–406 (2008).
81. Allenspach, E. J., Lemos, M. P., Porrett, P. M., Turka, L. A. & Laufer, T. M. Migratory and Lymphoid-Resident Dendritic Cells Cooperate to Efficiently Prime Naive CD4 T cells. *Immunity* **29,** 795–806 (2008).

82. Tagliani, E. & Erlebacher, A. Dendritic cell function at the maternal-fetal interface. *Expert Rev. Clin. Immunol.* **7,** 593–602 (2011).
83. Croxatto, D. *et al.* Stromal cells from human decidua exert a strong inhibitory effect on NK cell function and dendritic cell differentiation. *PLoS One* **9,** e89006 (2014).
84. Collins, M. K., Tay, C.-S. & Erlebacher, A. Dendritic cell entrapment within the pregnant uterus inhibits immune surveillance of the maternal/fetal interface in mice. *J. Clin. Invest.* **119,** 2062–2073 (2009).
85. MartIn-Fontecha, A. *et al.* Regulation of dendritic cell migration to the draining lymph node: impact on T lymphocyte traffic and priming. *J. Exp. Med.* **198,** 615–621 (2003).
86. Croy, B. A. *et al.* Update on pathways regulating the activation of uterine Natural Killer cells, their interactions with decidual spiral arteries and homing of their precursors to the uterus. *J. Reprod. Immunol.* **59,** 175–191 (2003).
87. Karsten, C. M. *et al.* DC within the pregnant mouse uterus influence growth and functional properties of uterine NK cells. *Eur. J. Immunol.* **39,** 2203–2214 (2009).
88. Krey, G. *et al.* In vivo dendritic cell depletion reduces breeding efficiency, affecting implantation and early placental development in mice. *J. Mol. Med.* **86,** 999–1011 (2008).
89. Miyazaki, S., Tsuda, H., Sakai, M. & Hori, S. Predominance of Th2-promoting dendritic cells in early human pregnancy decidua. *J. Leukoc. Biol.* (2003).
90. Nancy, P. & Erlebacher, A. T cell behavior at the maternal-fetal interface. *Int. J. Dev. Biol.* **58,** 189–198 (2014).
91. Mincheva-Nilsson, L. Pregnancy and gamma/delta T cells: taking on the hard questions. *Reprod. Biol. Endocrinol.* **1,** 120 (2003).
92. Mjösberg, J., Berg, G., Jenmalm, M. C. & Ernerudh, J. FOXP3+ regulatory T cells and T helper 1, T helper 2, and T helper 17 cells in human early pregnancy decidua. *Biol. Reprod.* **82,** 698–705 (2010).
93. Tilburgs, T. *et al.* Human decidual tissue contains differentiated CD8+ effector-memory T cells with unique properties. *J. Immunol.* **185,** 4470–4477 (2010).
94. Kim, C. J., Romero, R., Chaemsaithong, P. & Kim, J.-S. Chronic inflammation of the placenta: definition, classification, pathogenesis, and clinical significance. *Am. J. Obstet. Gynecol.* **213,** S53–69 (2015).

95. Tamblyn, J. A., Lissauer, D. M., Powell, R., Cox, P. & Kilby, M. D. The immunological basis of villitis of unknown etiology - review. *Placenta* **34,** 846–855 (2013).
96. Lee, J. *et al.* A signature of maternal anti-fetal rejection in spontaneous preterm birth: chronic chorioamnionitis, anti-human leukocyte antigen antibodies, and C4d. *PLoS One* **6,** e16806 (2011).
97. Nancy, P. *et al.* Chemokine gene silencing in decidual stromal cells limits T cell access to the maternal-fetal interface. *Science* **336,** 1317–1321 (2012).
98. Robertson, S. A., Prins, J. R., Sharkey, D. J. & Moldenhauer, L. M. Seminal fluid and the generation of regulatory T cells for embryo implantation. *Am. J. Reprod. Immunol.* **69,** 315–330 (2013).
99. Moffett, A. & Loke, C. Immunology of placentation in eutherian mammals. *Nat. Rev. Immunol.* **6,** 584–594 (2006).
100. MEDAWAR & PB. Some immunological and endocrinological problems raised by the evolution of viviparity in vertebrates. *Symp. Soc. Exp. Biol.* **7,** 320–337 (1953).
101. Wegmann, T. G., Lin, H., Guilbert, L. & Mosmann, T. R. Bidirectional cytokine interactions in the maternal-fetal relationship: is successful pregnancy a TH2 phenomenon? *Immunol. Today* **14,** 353–356 (1993).
102. Laskarin, G. *et al.* Antigen-Presenting Cells and Materno-Fetal Tolerance: An Emerging Role for Dendritic Cells. *Am. J. Reprod. Immunol.* **58,** 255–267 (2007).
103. Mor, G. & Cardenas, I. The Immune System in Pregnancy: A Unique Complexity: IMMUNE SYSTEM IN PREGNANCY. *Am. J. Reprod. Immunol.* **63,** 425–433 (2010).
104. Gluckman, P. D., Hanson, M. A., Cooper, C. & Thornburg, K. L. Effect of in utero and early-life conditions on adult health and disease. *N. Engl. J. Med.* **359,** 61–73 (2008).
105. Tang, F. *et al.* mRNA-Seq whole-transcriptome analysis of a single cell. *Nat. Methods* **6,** 377–382 (2009).
106. Svensson, V., Vento-Tormo, R. & Teichmann, S. A. Exponential scaling of single-cell RNA-seq in the past decade. *Nat. Protoc.* **13,** 599–604 (2018).
107. Stegle, O., Teichmann, S. A. & Marioni, J. C. Computational and analytical challenges in single-cell transcriptomics. *Nat. Rev. Genet.* **16,** 133–145 (2015).
108. Kolodziejczyk, A. A., Kim, J. K., Svensson, V., Marioni, J. C. & Teichmann, S. A. The technology

and biology of single-cell RNA sequencing. *Mol. Cell* **58,** 610–620 (2015).

109. van den Brink, S. C. *et al.* Single-cell sequencing reveals dissociation-induced gene expression in tissue subpopulations. *Nat. Methods* **14,** 935–936 (2017).

110. Zheng, G. X. Y. *et al.* Massively parallel digital transcriptional profiling of single cells. *Nat. Commun.* **8,** 14049 (2017).

111. Picelli, S. *et al.* Full-length RNA-seq from single cells using Smart-seq2. *Nat. Protoc.* **9,** 171–181 (2014).

112. Kim, D., Langmead, B. & Salzberg, S. L. HISAT: a fast spliced aligner with low memory requirements. *Nat. Methods* **12,** 357–360 (2015).

113. Anders, S., Pyl, P. T. & Huber, W. HTSeq—a Python framework to work with high-throughput sequencing data. *Bioinformatics* **31,** 166–169 (2015).

114. Maaten, L. van der & Hinton, G. Visualizing Data using t-SNE. *J. Mach. Learn. Res.* **9,** 2579–2605 (2008).

115. Satija, R., Farrell, J. A., Gennert, D., Schier, A. F. & Regev, A. Spatial reconstruction of single-cell gene expression data. *Nat. Biotechnol.* **33,** 495–502 (2015).

116. van den Brink, S. C. *et al.* Single-cell sequencing reveals dissociation-induced gene expression in tissue subpopulations. *Nat. Methods* **14,** 935 (2017).

117. Li, H. Aligning sequence reads, clone sequences and assembly contigs with BWA-MEM. *arXiv [q-bio.GN]* (2013).

118. Li, H. *et al.* The Sequence Alignment/Map format and SAMtools. *Bioinformatics* **25,** 2078–2079 (2009).

119. Mills, R. E. *et al.* Natural genetic variation caused by small insertions and deletions in the human genome. *Genome Res.* **21,** 830–839 (2011).

120. 1000 Genomes Project Consortium *et al.* A map of human genome variation from population-scale sequencing. *Nature* **467,** 1061–1073 (2010).

121. Van der Auwera, G. A. *et al.* From FastQ data to high confidence variant calls: the Genome Analysis Toolkit best practices pipeline. *Curr. Protoc. Bioinformatics* **43,** 11.10.1–33 (2013).

122. Picard Tools - By Broad Institute. Available at: http://broadinstitute.github.io/picard/. (Accessed: 6th April 2018)

123. Li, H. A statistical framework for SNP calling, mutation discovery, association mapping and

population genetical parameter estimation from sequencing data. *Bioinformatics* **27,** 2987–2993 (2011).

124. Sherry, S. T. *et al.* dbSNP: the NCBI database of genetic variation. *Nucleic Acids Res.* **29,** 308–311 (2001).

125. Kang, H. M. *et al.* Multiplexed droplet single-cell RNA-sequencing using natural genetic variation. *Nat. Biotechnol.* **36,** 89–94 (2018).

126. Dobin, A. *et al.* STAR: ultrafast universal RNA-seq aligner. *Bioinformatics* **29,** 15–21 (2013).

127. Uhlen, M. *et al.* Towards a knowledge-based Human Protein Atlas. *Nat. Biotechnol.* **28,** 1248–1250 (2010).

128. Uhlén, M. *et al.* Proteomics. Tissue-based map of the human proteome. *Science* **347,** 1260419 (2015).

129. Knaus, B. J. & Grünwald, N. J. vcfr: a package to manipulate and visualize variant call format data in R. *Mol. Ecol. Resour.* **17,** 44–53 (2017).

130. Stacklies, W., Redestig, H., Scholz, M., Walther, D. & Selbig, J. pcaMethods--a bioconductor package providing PCA methods for incomplete data. *Bioinformatics* **23,** 1164–1167 (2007).

131. Patro, R., Duggal, G., Love, M. I., Irizarry, R. A. & Kingsford, C. Salmon provides fast and bias-aware quantification of transcript expression. *Nat. Methods* **14,** 417–419 (2017).

132. Soneson, C., Love, M. I. & Robinson, M. D. Differential analyses for RNA-seq: transcript-level estimates improve gene-level inferences. *F1000Res.* **4,** 1521 (2015).

133. Durinck, S., Spellman, P. T., Birney, E. & Huber, W. Mapping identifiers for the integration of genomic datasets with the R/Bioconductor package biomaRt. *Nat. Protoc.* **4,** 1184–1191 (2009).

134. Hahne, F. *et al.* flowCore: a Bioconductor package for high throughput flow cytometry. *BMC Bioinformatics* **10,** 106 (2009).

135. Chen, H. *et al.* Cytofkit: A Bioconductor Package for an Integrated Mass Cytometry Data Analysis Pipeline. *PLoS Comput. Biol.* **12,** e1005112 (2016).

136. Harris, M. A. *et al.* The Gene Ontology (GO) database and informatics resource. *Nucleic Acids Res.* **32,** D258–61 (2004).

137. Croft, D. *et al.* The Reactome pathway knowledgebase. *Nucleic Acids Res.* **42,** D472–7 (2014).

138. Reimand, J. *et al.* g:Profiler-a web server for functional interpretation of gene lists (2016 update). *Nucleic Acids Res.* **44,** W83–9 (2016).

139. Martinez, F. O., Gordon, S., Locati, M. & Mantovani, A. Transcriptional profiling of the human monocyte-to-macrophage differentiation and polarization: new molecules and patterns of gene expression. *J. Immunol.* **177,** 7303–7311 (2006).

140. Yanai, I. *et al.* Genome-wide midrange transcription profiles reveal expression level relationships in human tissue specification. *Bioinformatics* **21,** 650–659 (2005).

141. Kryuchkova-Mostacci, N. & Robinson-Rechavi, M. A benchmark of gene expression tissue-specificity metrics. *Brief. Bioinform.* **18,** 205–214 (2017).

142. Yu, X., Lin, J., Zack, D. J. & Qian, J. Computational analysis of tissue-specific combinatorial gene regulation: predicting interaction between transcription factors in human tissues. *Nucleic Acids Res.* **34,** 4925–4936 (2006).

143. Schug, J. *et al.* Promoter features related to tissue specificity as measured by Shannon entropy. *Genome Biol.* **6,** R33 (2005).

144. Julien, P. *et al.* Mechanisms and evolutionary patterns of mammalian and avian dosage compensation. *PLoS Biol.* **10,** e1001328 (2012).

145. Vandenbon, A. & Nakai, K. Modeling tissue-specific structural patterns in human and mouse promoters. *Nucleic Acids Res.* **38,** 17–25 (2010).

146. MacArthur, J. *et al.* The new NHGRI-EBI Catalog of published genome-wide association studies (GWAS Catalog). *Nucleic Acids Res.* **45,** D896–D901 (2017).

147. Hamosh, A., Scott, A. F., Amberger, J. S., Bocchini, C. A. & McKusick, V. A. Online Mendelian Inheritance in Man (OMIM), a knowledgebase of human genes and genetic disorders. *Nucleic Acids Res.* **33,** D514–7 (2005).

148. Lun, A. T. L., Bach, K. & Marioni, J. C. Pooling across cells to normalize single-cell RNA sequencing data with many zero counts. *Genome Biol.* **17,** 75 (2016).

149. Kharchenko, P. V., Silberstein, L. & Scadden, D. T. Bayesian approach to single-cell differential expression analysis. *Nat. Methods* **11,** 740–742 (2014).

150. Moffett, A. & Colucci, F. Uterine NK cells: active regulators at the maternal-fetal interface. *J. Clin. Invest.* **124,** 1872–1879 (2014).

151. Burton, G. J. & Watson, A. L. The Structure of the Human Placenta: Implications for Initiating and Defending Against Virus Infections. *Rev. Med. Virol.* **7,** 219–228 (1997).

152. Kampinga, H. H. *et al.* Guidelines for the nomenclature of the human heat shock proteins. *Cell*

Stress Chaperones **14,** 105–111 (2009).

153. Piskol, R., Ramaswami, G. & Li, J. B. Reliable identification of genomic variants from RNA-seq data. *Am. J. Hum. Genet.* **93,** 641–651 (2013).

154. Seval, Y., Korgun, E. T. & Demir, R. Hofbauer cells in early human placenta: possible implications in vasculogenesis and angiogenesis. *Placenta* **28,** 841–845 (2007).

155. Wetzka, B., Clark, D. E., Charnock-Jones, D. S., Zahradnik, H. P. & Smith, S. K. Isolation of macrophages (Hofbauer cells) from human term placenta and their prostaglandin E2 and thromboxane production. *Hum. Reprod.* **12,** 847–852 (1997).

156. Garcia-Lloret, M. I., Winkler-Lowen, B. & Guilbert, L. J. Monocytes adhering by LFA-1 to placental syncytiotrophoblasts induce local apoptosis via release of TNF-alpha. A model for hematogenous initiation of placental inflammations. *J. Leukoc. Biol.* **68,** 903–908 (2000).

157. Xiao, J. *et al.* ICAM-1-mediated adhesion of peripheral blood monocytes to the maternal surface of placental syncytiotrophoblasts: implications for placental villitis. *Am. J. Pathol.* **150,** 1845–1860 (1997).

158. Schelker, M. *et al.* Estimation of immune cell content in tumour tissue using single-cell RNA-seq data. *Nat. Commun.* **8,** 2032 (2017).

159. Basu, S., Binder, R. J., Ramalingam, T. & Srivastava, P. K. CD91 is a common receptor for heat shock proteins gp96, hsp90, hsp70, and calreticulin. *Immunity* **14,** 303–313 (2001).

160. van Eden, W., van der Zee, R. & Prakken, B. Heat-shock proteins induce T-cell regulation of chronic inflammation. *Nat. Rev. Immunol.* **5,** 318–330 (2005).

161. Newman, A. M. *et al.* Robust enumeration of cell subsets from tissue expression profiles. *Nat. Methods* **12,** 453–457 (2015).

162. Li, B. *et al.* Comprehensive analyses of tumor immunity: implications for cancer immunotherapy. *Genome Biol.* **17,** 174 (2016).

163. Becht, E. *et al.* Estimating the population abundance of tissue-infiltrating immune and stromal cell populations using gene expression. *Genome Biol.* **17,** 218 (2016).

164. Baron, M. *et al.* A Single-Cell Transcriptomic Map of the Human and Mouse Pancreas Reveals Inter- and Intra-cell Population Structure. *Cell Syst* **3,** 346–360.e4 (2016).

165. Gong, T. & Szustakowski, J. D. DeconRNASeq: a statistical framework for deconvolution of heterogeneous tissue samples based on mRNA-Seq data. *Bioinformatics* **29,** 1083–1085 (2013).

166. Aran, D., Hu, Z. & Butte, A. J. xCell: digitally portraying the tissue cellular heterogeneity landscape. *Genome Biol.* **18,** 220 (2017).

167. Ornatsky, O. *et al.* Highly multiparametric analysis by mass cytometry. *J. Immunol. Methods* **361,** 1–20 (2010).

168. Harly, C., Cam, M., Kaye, J. & Bhandoola, A. Development and differentiation of early innate lymphoid progenitors. *J. Exp. Med.* **215,** 249–262 (2018).

169. Carrette, F. & Surh, C. D. IL-7 signaling and CD127 receptor regulation in the control of T cell homeostasis. *Semin. Immunol.* **24,** 209–217 (2012).

170. Saito, S. *et al.* A study of CD45RO, CD45RA and CD29 antigen expression on human decidual T cells in an early stage of pregnancy. *Immunol. Lett.* **40,** 193–197 (1994).

171. Rochman, Y. *et al.* Thymic stromal lymphopoietin-mediated STAT5 phosphorylation via kinases JAK1 and JAK2 reveals a key difference from IL-7-induced signaling. *Proc. Natl. Acad. Sci. U. S. A.* **107,** 19455–19460 (2010).

172. Michalek, R. D. & Rathmell, J. C. The metabolic life and times of a T-cell. *Immunol. Rev.* **236,** 190–202 (2010).

173. Bosschaerts, T. *et al.* Alternatively activated myeloid cells limit pathogenicity associated with African trypanosomiasis through the IL-10 inducible gene selenoprotein P. *J. Immunol.* **180,** 6168–6175 (2008).

174. Leavey, K., Bainbridge, S. A. & Cox, B. J. Large scale aggregate microarray analysis reveals three distinct molecular subclasses of human preeclampsia. *PLoS One* **10,** e0116508 (2015).

175. Needleman, P., Truk, J., Jakschik, B. A., Morrison, A. R. & Lefkowith, J. B. Arachidonic Acid Metabolism. *Annu. Rev. Biochem.* **55,** 69–102 (1986).

176. Brown, G. P., Monick, M. M. & Hunninghake, G. W. Human alveolar macrophage arachidonic acid metabolism. *Am. J. Physiol.* **254,** C809–15 (1988).

177. Humes, J. L. *et al.* Evidence for two sources of arachidonic acid for oxidative metabolism by mouse peritoneal macrophages. *J. Biol. Chem.* **257,** 1591–1594 (1982).

178. Rouzer, C. A. *et al.* Secretion of leukotriene C and other arachidonic acid metabolites by macrophages challenged with immunoglobulin E immune complexes. *J. Exp. Med.* **156,** 1077–1086 (1982).

179. Remmerie, A. & Scott, C. L. Macrophages and lipid metabolism. *Cell. Immunol.* (2018).

doi:10.1016/j.cellimm.2018.01.020

180. Scott, C. L. *et al.* Bone marrow-derived monocytes give rise to self-renewing and fully differentiated Kupffer cells. *Nat. Commun.* **7,** 10321 (2016).

181. Gautier, E. L. *et al.* Systemic analysis of PPARγ in mouse macrophage populations reveals marked diversity in expression with critical roles in resolution of inflammation and airway immunity. *J. Immunol.* **189,** 2614–2624 (2012).

182. Joseph, S. B., Castrillo, A., Laffitte, B. A., Mangelsdorf, D. J. & Tontonoz, P. Reciprocal regulation of inflammation and lipid metabolism by liver X receptors. *Nat. Med.* **9,** 213–219 (2003).

183. Baker, A. D., Malur, A., Barna, B. P. & Ghosh, S. Targeted PPARγ deficiency in alveolar macrophages disrupts surfactant catabolism. *J. Lipids* (2010).

184. Moore, K. J., Sheedy, F. J. & Fisher, E. A. Macrophages in atherosclerosis: a dynamic balance. *Nat. Rev. Immunol.* **13,** 709–721 (2013).

185. McLaren, J. E., Michael, D. R., Ashlin, T. G. & Ramji, D. P. Cytokines, macrophage lipid metabolism and foam cells: implications for cardiovascular disease therapy. *Prog. Lipid Res.* **50,** 331–347 (2011).

186. Ramsay, J. E. *et al.* Maternal obesity is associated with dysregulation of metabolic, vascular, and inflammatory pathways. *J. Clin. Endocrinol. Metab.* **87,** 4231–4237 (2002).

187. Saben, J. *et al.* Maternal obesity is associated with a lipotoxic placental environment. *Placenta* **35,** 171–177 (2014).

188. Challier, J. C. *et al.* Obesity in pregnancy stimulates macrophage accumulation and inflammation in the placenta. *Placenta* **29,** 274–281 (2008).

189. Becroft, D. M., Thompson, J. M. & Mitchell, E. A. Placental villitis of unknown origin: epidemiologic associations. *Am. J. Obstet. Gynecol.* **192,** 264–271 (2005).

190. West, A. P. *et al.* TLR signalling augments macrophage bactericidal activity through mitochondrial ROS. *Nature* **472,** 476–480 (2011).

191. Zhang, Y. *et al.* ROS play a critical role in the differentiation of alternatively activated macrophages and the occurrence of tumor-associated macrophages. *Cell Res.* **23,** 898–914 (2013).

192. Al-Gubory, K. H., Fowler, P. A. & Garrel, C. The roles of cellular reactive oxygen species,

oxidative stress and antioxidants in pregnancy outcomes. *Int. J. Biochem. Cell Biol.* **42,** 1634–1650 (2010).

193. Wu, F., Tian, F.-J. & Lin, Y. Oxidative Stress in Placenta: Health and Diseases. *Biomed Res. Int.* **2015,** 293271 (2015).

194. Frendo, J. L. *et al.* Overexpression of copper zinc superoxide dismutase impairs human trophoblast cell fusion and differentiation. *Endocrinology* **142,** 3638–3648 (2001).

195. Chen, B., Longtine, M. S. & Nelson, D. M. Hypoxia induces autophagy in primary human trophoblasts. *Endocrinology* **153,** 4946–4954 (2012).

196. Forsythe, J. A. *et al.* Activation of vascular endothelial growth factor gene transcription by hypoxia-inducible factor 1. *Mol. Cell. Biol.* **16,** 4604–4613 (1996).

197. Pereira, R. D. *et al.* Angiogenesis in the placenta: the role of reactive oxygen species signaling. *Biomed Res. Int.* **2015,** 814543 (2015).

198. Bochkov, V. N. *et al.* Oxidized phospholipids stimulate angiogenesis via autocrine mechanisms, implicating a novel role for lipid oxidation in the evolution of atherosclerotic lesions. *Circ. Res.* **99,** 900–908 (2006).

199. Roberts, J. M. *et al.* Preeclampsia: an endothelial cell disorder. *Am. J. Obstet. Gynecol.* **161,** 1200–1204 (1989).

200. Hiden, U., Glitzner, E., Hartmann, M. & Desoye, G. Insulin and the IGF system in the human placenta of normal and diabetic pregnancies. *J. Anat.* **215,** 60–68 (2009).

201. Clemmons, D. R. Role of IGF Binding Proteins in Regulating Metabolism. *Trends Endocrinol. Metab.* **27,** 375–391 (2016).

202. Wang, L.-J., Cheong, M.-L., Lee, Y.-S., Lee, M.-T. & Chen, H. High-temperature requirement protein A4 (HtrA4) suppresses the fusogenic activity of syncytin-1 and promotes trophoblast invasion. *Mol. Cell. Biol.* **32,** 3707–3717 (2012).

203. Lázár, E. *et al.* Structure-function analysis of peroxidasin provides insight into the mechanism of collagen IV crosslinking. *Free Radic. Biol. Med.* **83,** 273–282 (2015).

204. Péterfi, Z. *et al.* Peroxidasin is secreted and incorporated into the extracellular matrix of myofibroblasts and fibrotic kidney. *Am. J. Pathol.* **175,** 725–735 (2009).

205. Kim, J. *et al.* YAP/TAZ regulates sprouting angiogenesis and vascular barrier maturation. *J. Clin. Invest.* **127,** 3441–3461 (2017).

206. Williams, D. J., Vallance, P. J., Neild, G. H., Spencer, J. A. & Imms, F. J. Nitric oxide-mediated vasodilation in human pregnancy. *Am. J. Physiol.* **272,** H748–52 (1997).

207. Harmon, A. C. *et al.* The role of inflammation in the pathology of preeclampsia. *Clin. Sci.* **130,** 409–419 (2016).

208. Sferruzzi-Perri, A. N., Owens, J. A., Pringle, K. G. & Roberts, C. T. The neglected role of insulin-like growth factors in the maternal circulation regulating fetal growth. *J. Physiol.* **589,** 7–20 (2011).

209. Forbes, K., Westwood, M., Baker, P. N. & Aplin, J. D. Insulin-like growth factor I and II regulate the life cycle of trophoblast in the developing human placenta. *Am. J. Physiol. Cell Physiol.* **294,** C1313–22 (2008).

210. Roos, S., Lagerlöf, O., Wennergren, M., Powell, T. L. & Jansson, T. Regulation of amino acid transporters by glucose and growth factors in cultured primary human trophoblast cells is mediated by mTOR signaling. *Am. J. Physiol. Cell Physiol.* **297,** C723–31 (2009).

211. Maruo, T., Murata, K., Matsuo, H., Samoto, T. & Mochizuki, M. Insulin-like growth factor-I as a local regulator of proliferation and differentiated function of the human trophoblast in early pregnancy. *Early Pregnancy* **1,** 54–61 (1995).

212. Matsumoto, H., Sakai, K. & Iwashita, M. Insulin-like growth factor binding protein-1 induces decidualization of human endometrial stromal cells via alpha5beta1 integrin. *Mol. Hum. Reprod.* **14,** 485–489 (2008).

213. Miozzo, M. & Simoni, G. The role of imprinted genes in fetal growth. *Biol. Neonate* **81,** 217–228 (2002).

214. Giannoukakis, N., Deal, C., Paquette, J., Goodyer, C. G. & Polychronakos, C. Parental genomic imprinting of the human IGF2 gene. *Nat. Genet.* **4,** 98–101 (1993).

215. Maloney, S. *et al.* Microchimerism of maternal origin persists into adult life. *J. Clin. Invest.* **104,** 41–47 (1999).

216. Loubière, L. S. *et al.* Maternal microchimerism in healthy adults in lymphocytes, monocyte/macrophages and NK cells. *Lab. Invest.* **86,** 1185–1192 (2006).

217. Yan, Z. *et al.* Male microchimerism in women without sons: quantitative assessment and correlation with pregnancy history. *Am. J. Med.* **118,** 899–906 (2005).

218. Nelson, J. L. The otherness of self: microchimerism in health and disease. *Trends Immunol.* **33,**

421–427 (2012).

219. Rak, J. M. *et al.* Transfer of the shared epitope through microchimerism in women with rheumatoid arthritis. *Arthritis Rheum.* **60,** 73–80 (2009).

220. Stevens, A. M., Hermes, H. M., Rutledge, J. C., Buyon, J. P. & Nelson, J. L. Myocardial-tissue-specific phenotype of maternal microchimerism in neonatal lupus congenital heart block. *Lancet* **362,** 1617–1623 (2003).

221. Gadi, V. K. & Nelson, J. L. Fetal microchimerism in women with breast cancer. *Cancer Res.* **67,** 9035–9038 (2007).

222. Turco, M. Y. *et al.* Long-term, hormone-responsive organoid cultures of human endometrium in a chemically defined medium. *Nat. Cell Biol.* **19,** 568–577 (2017).

223. Wang, F. *et al.* RNAscope: a novel in situ RNA analysis platform for formalin-fixed, paraffin-embedded tissues. *J. Mol. Diagn.* **14,** 22–29 (2012).

224. Trapnell, C. *et al.* The dynamics and regulators of cell fate decisions are revealed by pseudotemporal ordering of single cells. *Nat. Biotechnol.* **32,** 381–386 (2014).

Appendices

Appendix 1 - Supplementary Materials and Methods:

(Adapted from Vento-Tormo R, Efremova M, et al., under submission)

Decidual, placental, and peripheral blood samples

All tissue samples used in this study were obtained with written informed consent from participants in accordance with the guidelines in The Declaration of Helsinki. Human placental and decidual samples were obtained from the MRC/Wellcome-Trust-funded Human Developmental Biology Resource (HDBR[112], http://www.hdbr.org) with appropriate maternal written consent and approval from the Newcastle and North Tyneside NHS Health Authority Joint Ethics Committee (08/H0906/21+5). Peripheral blood from women undergoing elective terminations were obtained with maternal written consent and with approvals from the Newcastle Academic Health Partners (reference NAHPB-093) and HRA NHS Research Ethics committee North-East-Newcastle North Tyneside 1 (Rec reference 12/NE/0395).

Calculation of fetal development

Embryos of up to 8 post-conceptional weeks (PCW) were staged using the Carnegie staging method[113]. After 8 PCW, fetal age was estimated from measurements of foot length and heel to knee length. These were compared with a standard growth chart[114].

Single-cell isolation from decidua, placenta, and peripheral blood

Decidual and placental tissue were washed in HAMS F12 medium, macroscopically separated, and washed for at least 10 mins in RPMI or HAMS F12 medium, respectively, before processing. Decidual tissues were chopped using scalpels into approximately 0.2 mm^3 cubes and enzymatically digested in 15ml 0.4mg/mL collagenase V solution in RPMI 1640 medium/10% FCS at 37°C for 45 min. The supernatant was diluted with medium and passed through 100um cell sieve and then 40um cell sieve. The flow-through was centrifuged and resuspended in 5ml of red blood cell lysis buffer for 10min.

First trimester placenta were placed in petri dishes and placental villi were scraped from the chorionic membrane. The stripped membrane was discarded and the villous tissue was enzymatically digested in 70 ml 0.2% trypsin 250/0.02% EDTA in PBS with stirring at 37°C for 9 min. The disaggregated cell suspension was passed through sterile muslin gauze and washed with HAMS F12 medium containing 20% FBS. Cells were pelleted from the filtrate by centrifugation and re-suspended in HAMS F12. The undigested, gelatinous tissue remnant was retrieved from the gauze and further digested with 10-15 ml collagenase V at 1.0mg/ml in HAMS F12 medium/10% FBS with gentle shaking at 37°C for 10 min. The disaggregated cell suspension from collagenase digestion was passed through sterile muslin gauze and the cells pelleted from the filtrate as before. Cells obtained from both enzyme digests were pooled together and passed through 100um cell sieve and washed in HAMS F12. The flow-through was centrifuged and resuspended in 5ml of red blood cell lysis buffer for 10min.

Blood samples were layered onto a Ficoll-Paque gradient and centrifuged at 2,000 rpm for 30 min. Peripheral blood mononuclear cells from the interface between the plasma and the Ficoll-Paque gradient, were collected and washed in ice-cold PBS, followed by centrifugation at 2,000 rpm for 5 min. The pellet was resuspended in 5ml of red blood cell lysis buffer for 10min.

Flow cytometry, plate-based SmartSeq2 scRNA-seq, and droplet-based scRNA-seq

Decidual and blood cells were incubated at 4°C with 2.5ul of antibodies in 1% FBS in DPBS without Calcium and Magnesium. DAPI was used for live/dead discrimination. We used an antibody panel (Appendix 3) designed to enrich for certain populations for single-cell sorting and scRNA-seq. Cells were sorted using a Becton Dickinson (BD) FACS Aria Fusion with 5 excitation lasers (355nm, 405nm, 488nm, 561nm and 635nm Red), and 18 fluorescent detectors plus forward and side scatter. The sorter was controlled using BD FACS DIVA software (v7).

For scRNA-seq using the plate-based SmartSeq2 protocol, we created overlapping gates to comprehensively and evenly sample all immune cell populations in the decidua (gating strategy in Appendix 4). B cells ($CD19^+/CD20^+$) were excluded from analysis due to their absence in decidua[115]. Single cells were sorted into 96-well full-skirted Eppendorf plates chilled to 4°C, prepared with lysis buffer consisting of 10 ul of TCL buffer supplemented with 1% b-mercaptoethanol. Single-cell lysates were sealed, vortexed, spun down at 300g at 4°C for 1 min, immediately placed on dry ice, and transferred for storage at -80°C. The SmartSeq2 protocol was performed on single cells as described

previously[116,117], with some modifications[118]. Libraries were sequenced aiming at an average depth of 1 million reads/cell, on an Illumina HiSeq 2000 with v4 chemistry (paired-end 75-bp reads).

For droplet-based scRNA-seq, blood and decidual cells were sorted into immune ($CD45^+$) and non-immune ($CD45^-$) fractions. Only viable cells were considered, and B cells ($CD19^+/CD20^+$) were excluded. Placental cells were stained for DAPI and only viable cells were sorted. Cells were sorted into an Eppendorf tube containing PBS with 0.04% BSA. Cells were immediately counted using a Neubauer hemocytometer and loaded in the 10x Genomics Chromium. 10x Genomics v2 libraries were prepared per manufacturer's instructions. Libraries were sequenced (paired-end) aiming at a minimum coverage 50,000 raw reads per cell on an Illumina HiSeq 4000.

Bulk DNA/RNA extraction, whole genome sequencing, bulk RNA-sequencing
Tissue DNA and RNA were extracted from fresh frozen samples using the AllPrep DNA/RNA/miRNA kit following manufacturer's instructions. Libraries for whole-genome sequencing were constructed according to Illumina library protocols, and 100-bp paired-end sequencing was performed on Illumina HiSeq X genome analyzers to an average of 30× coverage. Libraries for bulk RNA-sequencing were constructed according to Illumina library protocols, and 100-bp paired-end sequencing was performed on Illumina HiSeq 2500 v4.

CyTOF staining and acquisition
Cells were resuspended to 10 million/ml and stained for 5min at room temperature (RT) with 5uM Cell-ID Cisplatin for live/dead discrimination. Cells were then stained for surface markers in two stages. First, cells were incubated with fluorescent-labeled antibodies for 30min at RT. Following washes, cells were then incubated with metal-tagged antibodies for 1 hour at RT (antibodies used are listed in Appendix 3). Cells were then fixed with 1.6% formaldehyde for 1 hour at RT. Cells were permeabilized with 0.1% Triton X-100 for 5 minutes at RT. Intracellular staining was then performed with metal-tagged antibodies at 4°C for 12 hours. Finally, cells were incubated with 125nM Cell-ID Intercalator-Iridium for 1 hour at RT.

Stained samples were washed in MilliQ water, counted, and adjusted to an optimal cell density of 0.5 million/ml before being spiked with EQ calibration beads for signal normalization. Samples were then run on a fully calibrated 3rd generation Fluidigm Helios CyTOF system. EQ bead data normalization was performed using the Helios acquisition software and FCS files were created with a half Gaussian normalization (negatives only) for analysis in FlowJo (FlowJo 5.4+).

Appendix 2 - Canonical marker genes used to annotate decidual and placental cell populations:

(Adapted from Vento-Tormo R, Efremova M, et al., under submission)

Gene	Cell Type
CD3G	T cells
CD14	Myeloid cells
PTPRC (CD45)	Immune cells
PECAM1	Endothelial cells
CLEC9A	DC1
CD1C	DC2
LYVE1	Hofbauer cells, Endothelial lymphatic cells
MKI67	Cycling
NCAM1 (CD56)	NK cells
CD11C	Myeloid cells
DKK1	Decidual stromal cells
COL4A2	Fibroblasts
RGS5	Pericytes
REN	Pericytes
PAGE4	Villous cytotrophoblasts (+++)
HLA-G	Extravillous trophoblasts
ERVFRD-1	Syncytiotrophoblast
PDGFRB	Fibroblasts, smooth muscle cells/pericytes
DLK1	Fibroblasts (fetal)
HAPLN	Fibroblasts (fetal)
PITX2	Fibroblasts (fetal)
EPCAM	Epithelial cells
CD34	Endothelial cells

Appendix 3 - Antibody panels used for FACS index sorting and CyTOF:

(Adapted from Vento-Tormo R, Efremova M, et al., under submission)

Antibody	Clone	Company	Assay	Isotope (CyTOF)	Element (CyTOF)
CD45-BUV395	Clone HI30 (RUO)	BD Bioscience	FACS		
CD94-BV421	HP-3D9 (RUO)	BD Bioscience	FACS		
CD16-BV500	3GH	BD Bioscience	FACS		
CD3-BV605	SK7	Biolegend	FACS		
CD4-BV711	RPA-T4	Biolegend	FACS		
HLA-DR BV786	L243	Biolegend	FACS		
HLA-G FITC	MEM-G/9	BioRad	FACS		
CD56-PE	REA196	Miltenyi	FACS		
CD14-PECF594	PE-CF594	BD Bioscience	FACS		
CD9-APC	M-L13	BD Bioscience	FACS		
CD8-AF700	HIT8a	Biolegend	FACS		
CD19-APCCy7	HIB19	BIoLegend	FACS		
CD20-APCCy7	2H7	BIoLegend	FACS		
CD45	HI30	Fluidigm	CyTOF (1:400)	89	Y
CD56	HCD56	Biolegend	CyTOF (1:25)	113	In
CD49d	9F10	Fluidigm	CyTOF (1:800)	141	Pr
CD19	HIB19	Fluidigm	CyTOF (1:200)	142	Nd
TCRgd	B1	Biolegend	CyTOF (1:25)	143	Nd
CD3	UCHT	Biolegend	CyTOF (1:400)	144	Nd
CD4	RPA-T4	Fluidigm	CyTOF (1:200)	145	Nd
IgD	IA6-2	Fluidigm	CyTOF (1:200)	146	Nd
CD7	CD7-6B7	Fluidigm	CyTOF (1:800)	147	Sm
CD294	BM16	Biolegend	CyTOF (1:25)	148	Nd
CD34	581	Fluidigm	CyTOF (1:400)	149	Sm
KIR2DL1-PE	REA284	Miltenyi	CyTOF (1:10)	150	Nd
anti-PE	PE001	Biolegend	CYTOF (1:150)		
CD123	6H6	Fluidigm	CyTOF (1:400)	151	Eu
FcERI	SA6.E9	Biolegend	CyTOF (1:400)	152	Sm
CD303	201A	Fluidigm	CyTOF (1:100)	153	Eu
GranzymeB	REA226	Miltenyi	CyTOF (1:200)	154	Sm
CD27	L128	Fluidigm	CyTOF (1:800)	155	Gd
SIGLEC6-FITC	REA-852	Miltenyi	CyTOF (1:50)		
anti-FITC	FIT-22	Biolegend	CyTOF (1:400)	156	Gd
AXL	MM0098-2N33	Abcam	CyTOF (1:25)	157	Gd
KIR2DL3-APC	REA147	Miltenyi	CyTOF (1:20)		
anti-APC	APC0003	Biolegend	CyTOF (1:800)	158	Gd
CD11c	Bu15	Fluidigm	CyTOF (1:400)	159	Tb
CD103	Ber-ACT8	Biolegend	CyTOF (1:100)	160	Gd
CD66	B1.1	BD	CyTOF (1:100)	161	Dy
Foxp3 intra	PCH101	Fluidigm	CyTOF (1:200)	162	Dy
CD20	2H7	Biolegend	CyTOF (1:400)	163	Dy
CD161	HP-3G10	Fluidigm	CyTOF (1:200)	164	Dy
CD127	A019D5	Fluidigm	CyTOF (1:200)	165	Ho
CLEC9A (CD370)	AER-37/8F9	Biolegend	CyTOF (1:25)	166	Er
CD45RO	UCHL1	Biolegend	CyTOF (1:100)	167	Er
CD8	SK1	Fluidigm	CyTOF (1:800)	168	Er
CD25	2A3	Fluidigm	CyTOF (1:200)	169	Tm
CD45RA	HI100	Fluidigm	CyTOF (1:800)	170	Er
CD1c	L161	Biolegend	CyTOF (1:400)	171	Yb
CD14	M5E2	Biolegend	CyTOF (1:200)	172	Yb
CD117 (C-kit)	104D2	Biolegend	CyTOF (1:25)	173	Yb
HLADR	L243	Biolegend	CyTOF (1:200)	174	Yb
BCL6	K112-91	BD	CyTOF (1:200)	175	Lu
S100A9	CF-557	Thermofisher	CyTOF (1:50)	176	Yb
CD16	3G8	Fluidigm	CyTOF (1:400)	209	Bi

Appendix 4 - Gating strategy for FACS index sorting data:

(From Vento-Tormo R, Efremova M, et al., under submission)

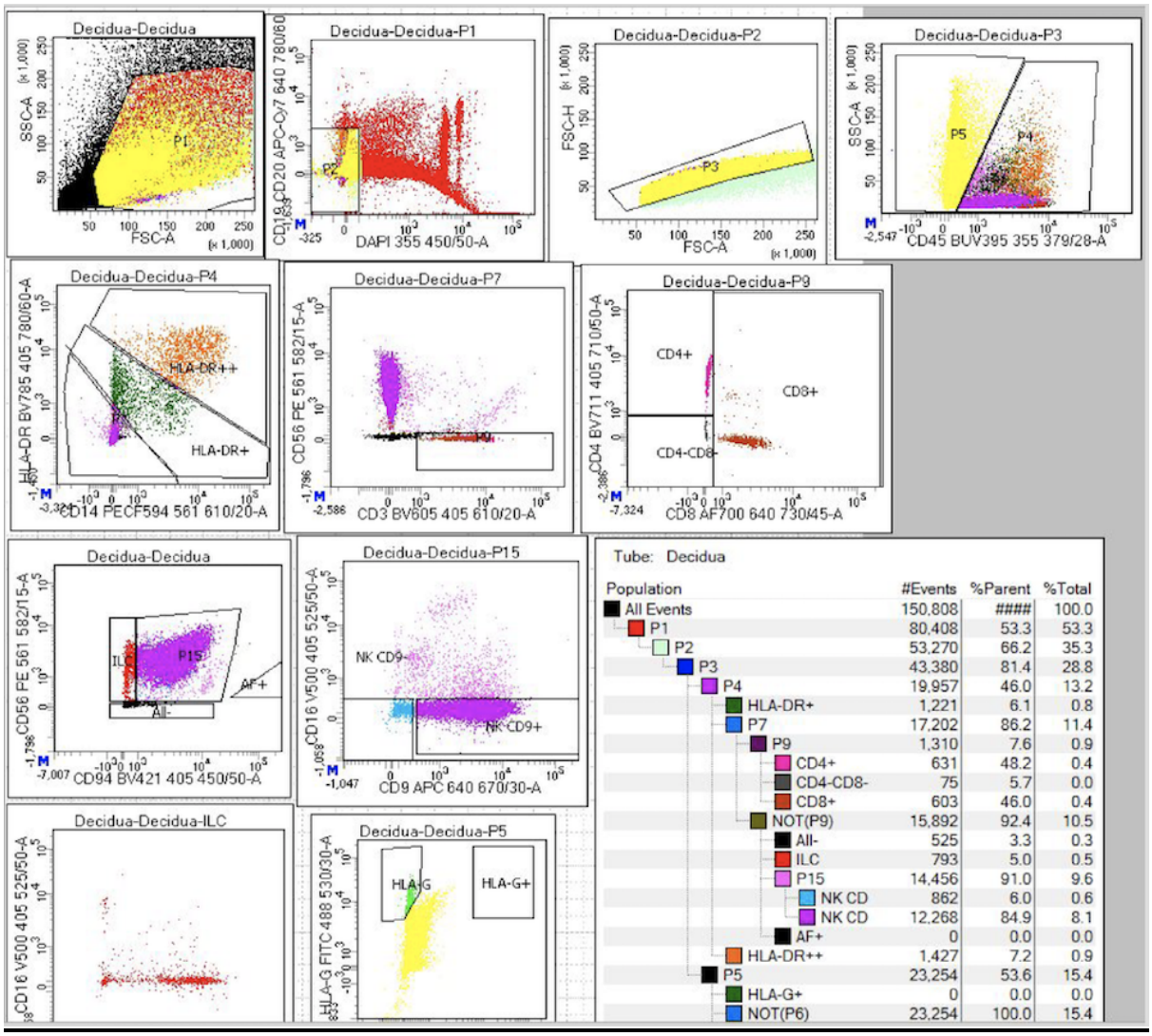

Appendix 5 - Genes determined to be enriched in placenta and endometrium (Tau ≥ 0.8) based on tissue-level expression data from the Human Protein Atlas:

Ensembl gene ID	Gene symbol	Highest-expressing tissue	Tissue gene expression (tpm)	Tau
ENSG00000002726	AOC1	placenta	711.7	0.9632
ENSG00000003436	TFPI	placenta	340.4	0.8741
ENSG00000006659	LGALS14	placenta	69	0.9959
ENSG00000006747	SCIN	placenta	116.3	0.9327
ENSG00000006788	MYH13	placenta	0.7	0.9246
ENSG00000019991	HGF	placenta	435.4	0.9829
ENSG00000029993	HMGB3	placenta	195.7	0.8588
ENSG00000038295	TLL1	placenta	10.4	0.8790
ENSG00000042304	C2orf83	placenta	2.9	0.9406
ENSG00000043591	ADRB1	placenta	45.2	0.9656
ENSG00000049192	ADAMTS6	placenta	2.7	0.8436
ENSG00000050344	NFE2L3	placenta	51.1	0.9046
ENSG00000050555	LAMC3	placenta	88.2	0.9558
ENSG00000054277	OPN3	placenta	26.8	0.8471
ENSG00000060718	COL11A1	placenta	27.9	0.9810
ENSG00000061455	PRDM6	placenta	5.9	0.8644
ENSG00000062524	LTK	placenta	15.1	0.8168
ENSG00000066056	TIE1	placenta	70.1	0.8539
ENSG00000066827	ZFAT	placenta	44	0.9422
ENSG00000070404	FSTL3	placenta	259.7	0.9233
ENSG00000070748	CHAT	placenta	7.1	0.9910
ENSG00000072694	FCGR2B	placenta	571.2	0.9808
ENSG00000076770	MBNL3	placenta	240.2	0.9470
ENSG00000080573	COL5A3	placenta	47.4	0.8538
ENSG00000081985	IL12RB2	placenta	11.7	0.9088
ENSG00000083782	EPYC	placenta	8.8	0.9886
ENSG00000085382	HACE1	placenta	43.6	0.8970
ENSG00000086696	HSD17B2	placenta	548	0.9420
ENSG00000087303	NID2	placenta	87.4	0.8800
ENSG00000091136	LAMB1	placenta	261.4	0.8247
ENSG00000100234	TIMP3	placenta	1428.9	0.8517
ENSG00000100311	PDGFB	placenta	59.5	0.8444
ENSG00000100593	ISM2	placenta	272.7	0.9989
ENSG00000100979	PLTP	placenta	630.8	0.8465
ENSG00000101197	BIRC7	placenta	9.1	0.9686
ENSG00000101846	STS	placenta	36.3	0.8318
ENSG00000101951	PAGE4	placenta	2026.4	0.9726
ENSG00000102195	GPR50	placenta	0.6	0.9676
ENSG00000102243	VGLL1	placenta	255.8	0.9948
ENSG00000102755	FLT1	placenta	617.5	0.9730
ENSG00000103310	ZP2	placenta	0.7	0.9008
ENSG00000104827	CGB	placenta	14.9	0.9953
ENSG00000105173	CCNE1	placenta	44.3	0.9169
ENSG00000105198	LGALS13	placenta	16.5	0.9988
ENSG00000105246	EBI3	placenta	208.2	0.9805
ENSG00000105492	SIGLEC6	placenta	147.1	0.9899
ENSG00000105825	TFPI2	placenta	1205.5	0.9902
ENSG00000105989	WNT2	placenta	92.5	0.9802
ENSG00000106302	HYAL4	placenta	5.9	0.8983
ENSG00000106366	SERPINE1	placenta	595.2	0.9053
ENSG00000106484	MEST	placenta	1079.4	0.9755
ENSG00000106511	MEOX2	placenta	57.2	0.9263
ENSG00000107984	DKK1	placenta	71.5	0.9508
ENSG00000108786	HSD17B1	placenta	98.3	0.9695
ENSG00000108813	DLX4	placenta	5.3	0.9686
ENSG00000109321	AREG	placenta	461	0.9623
ENSG00000110079	MS4A4A	placenta	101.4	0.8356
ENSG00000111452	ADGRD1	placenta	44.3	0.8316
ENSG00000111879	FAM184A	placenta	45.6	0.8603
ENSG00000112175	BMP5	placenta	101.7	0.9705
ENSG00000112297	AIM1	placenta	106.9	0.8354
ENSG00000112394	SLC16A10	placenta	38.2	0.8793
ENSG00000112414	ADGRG6	placenta	66.6	0.8851
ENSG00000112419	PHACTR2	placenta	119.1	0.9064
ENSG00000113140	SPARC	placenta	3224.6	0.8240
ENSG00000113494	PRLR	placenta	70.3	0.8927
ENSG00000113555	PCDH12	placenta	38.5	0.8918
ENSG00000115380	EFEMP1	placenta	485.9	0.8078

ENSG00000115414	FN1	placenta	4245.7	0.9544
ENSG00000115596	WNT6	placenta	2.9	0.9157
ENSG00000115602	IL1RL1	placenta	286.6	0.9852
ENSG00000116016	EPAS1	placenta	636.7	0.8559
ENSG00000116017	ARID3A	placenta	33.3	0.9253
ENSG00000116183	PAPPA2	placenta	82.1	0.9896
ENSG00000116194	ANGPTL1	placenta	188.3	0.8594
ENSG00000116962	NID1	placenta	323.7	0.8909
ENSG00000117385	P3H1	placenta	53.1	0.8419
ENSG00000117394	SLC2A1	placenta	133.9	0.9694
ENSG00000118495	PLAGL1	placenta	362.2	0.9421
ENSG00000118526	TCF21	placenta	62.1	0.8822
ENSG00000118785	SPP1	placenta	4016.3	0.9446
ENSG00000119630	PGF	placenta	70.9	0.8893
ENSG00000119699	TGFB3	placenta	84.3	0.8008
ENSG00000120149	MSX2	placenta	47.5	0.9438
ENSG00000120156	TEK	placenta	65.3	0.8486
ENSG00000120211	INSL4	placenta	22.2	0.9950
ENSG00000120708	TGFBI	placenta	606	0.8663
ENSG00000123243	ITIH5	placenta	122.7	0.8172
ENSG00000124019	FAM124B	placenta	12.4	0.8663
ENSG00000124208	TMEM189-UBE2V1	placenta	5.5	0.8202
ENSG00000124260	MAGEA10	placenta	13.5	0.9796
ENSG00000124440	HIF3A	placenta	39.5	0.8790
ENSG00000124467	PSG8	placenta	9.1	0.9976
ENSG00000124491	F13A1	placenta	664.9	0.9382
ENSG00000124615	MOCS1	placenta	59.8	0.8017
ENSG00000124749	COL21A1	placenta	38.7	0.8796
ENSG00000125810	CD93	placenta	195.4	0.8789
ENSG00000126709	IFI6	placenta	412.1	0.8828
ENSG00000127920	GNG11	placenta	122.3	0.8626
ENSG00000127928	GNGT1	placenta	3.9	0.9815
ENSG00000128052	KDR	placenta	118.2	0.8682
ENSG00000128917	DLL4	placenta	28.4	0.8417
ENSG00000129467	ADCY4	placenta	20.9	0.8405
ENSG00000129757	CDKN1C	placenta	202	0.9423
ENSG00000129965	INS-IGF2	placenta	4.6	0.9771
ENSG00000130513	GDF15	placenta	121.8	0.9094
ENSG00000130829	DUSP9	placenta	102.9	0.9902
ENSG00000131055	COX4I2	placenta	156.1	0.9621
ENSG00000131097	HIGD1B	placenta	152.3	0.9533
ENSG00000131203	IDO1	placenta	148	0.9380
ENSG00000131386	GALNT15	placenta	42.6	0.8620
ENSG00000132000	PODNL1	placenta	12.3	0.8579
ENSG00000132297	HHLA1	placenta	0.1	1.0000
ENSG00000133131	MORC4	placenta	113.4	0.8620
ENSG00000133800	LYVE1	placenta	211.4	0.8792
ENSG00000134323	MYCN	placenta	9.6	0.8909
ENSG00000134640	MTNR1B	placenta	1.4	0.9663
ENSG00000134871	COL4A2	placenta	827.3	0.9113
ENSG00000135047	CTSL	placenta	744	0.8647
ENSG00000135048	TMEM2	placenta	93.9	0.8310
ENSG00000135312	HTR1B	placenta	13.7	0.9550
ENSG00000135346	CGA	placenta	652.2	0.9976
ENSG00000135838	NPL	placenta	63.2	0.8089
ENSG00000135862	LAMC1	placenta	330.2	0.8758
ENSG00000135919	SERPINE2	placenta	1612.5	0.9719
ENSG00000136160	EDNRB	placenta	178.8	0.8797
ENSG00000136231	IGF2BP3	placenta	40.3	0.9795
ENSG00000136487	GH2	placenta	189	0.9997
ENSG00000136488	CSH1	placenta	13476	0.9997
ENSG00000136960	ENPP2	placenta	372.6	0.8499
ENSG00000137270	GCM1	placenta	29	0.9919
ENSG00000137507	LRRC32	placenta	75.9	0.8107
ENSG00000137672	TRPC6	placenta	29.8	0.8895
ENSG00000137869	CYP19A1	placenta	173.9	0.9928
ENSG00000137872	SEMA6D	placenta	64.3	0.8528
ENSG00000138031	ADCY3	placenta	121.3	0.8018
ENSG00000138316	ADAMTS14	placenta	11	0.8778
ENSG00000138829	FBN2	placenta	117.6	0.9893
ENSG00000139292	LGR5	placenta	26.7	0.9043
ENSG00000139567	ACVRL1	placenta	125.5	0.8551
ENSG00000140105	WARS	placenta	468.8	0.8174
ENSG00000140873	ADAMTS18	placenta	28.9	0.9888
ENSG00000142910	TINAGL1	placenta	267.7	0.9028

ENSG00000143226	FCGR2A	placenta	159.2	0.8337
ENSG00000143382	ADAMTSL4	placenta	89.1	0.9051
ENSG00000144476	ACKR3	placenta	175.2	0.8478
ENSG00000144648	ACKR2	placenta	22.8	0.9271
ENSG00000144891	AGTR1	placenta	212	0.9579
ENSG00000145604	SKP2	placenta	83.9	0.9012
ENSG00000145681	HAPLN1	placenta	102.5	0.9817
ENSG00000145715	RASA1	placenta	136.1	0.8372
ENSG00000145911	N4BP3	placenta	11.8	0.8505
ENSG00000146648	EGFR	placenta	97.3	0.8412
ENSG00000146674	IGFBP3	placenta	2649.6	0.9528
ENSG00000147113	CXorf36	placenta	58	0.8470
ENSG00000147257	GPC3	placenta	838.1	0.9762
ENSG00000147571	CRH	placenta	8	0.9844
ENSG00000147655	RSPO2	placenta	25.6	0.8850
ENSG00000148848	ADAM12	placenta	236.1	0.9839
ENSG00000148926	ADM	placenta	157.8	0.8566
ENSG00000149257	SERPINH1	placenta	327	0.8225
ENSG00000149564	ESAM	placenta	156.5	0.8627
ENSG00000149972	CNTN5	placenta	3.4	0.9199
ENSG00000150048	CLEC1A	placenta	70.5	0.9383
ENSG00000150636	CCDC102B	placenta	40.6	0.8855
ENSG00000150938	CRIM1	placenta	238.1	0.8478
ENSG00000152207	CYSLTR2	placenta	36.4	0.9139
ENSG00000152402	GUCY1A2	placenta	25.4	0.8491
ENSG00000153071	DAB2	placenta	319.5	0.8618
ENSG00000153162	BMP6	placenta	33.1	0.8839
ENSG00000154342	WNT3A	placenta	23	0.9903
ENSG00000154721	JAM2	placenta	92.1	0.8687
ENSG00000154736	ADAMTS5	placenta	42	0.8921
ENSG00000154914	USP43	placenta	11.6	0.8190
ENSG00000154930	ACSS1	placenta	165.1	0.8504
ENSG00000155622	XAGE2	placenta	292.4	0.9990
ENSG00000155966	AFF2	placenta	20.9	0.9099
ENSG00000156009	MAGEA8	placenta	18.8	0.9967
ENSG00000156466	GDF6	placenta	15	0.9672
ENSG00000158270	COLEC12	placenta	28.2	0.8726
ENSG00000162493	PDPN	placenta	192.4	0.8948
ENSG00000162624	LHX8	placenta	1.8	0.9012
ENSG00000163106	HPGDS	placenta	28	0.8862
ENSG00000163283	ALPP	placenta	45.5	0.9808
ENSG00000163638	ADAMTS9	placenta	45	0.8494
ENSG00000164093	PITX2	placenta	71.9	0.9730
ENSG00000164318	EGFLAM	placenta	72.7	0.8583
ENSG00000164451	FAM26D	placenta	33.6	0.9985
ENSG00000164488	DACT2	placenta	18.7	0.9376
ENSG00000164619	BMPER	placenta	9.4	0.8159
ENSG00000164707	SLC13A4	placenta	76.2	0.9954
ENSG00000165124	SVEP1	placenta	86.6	0.9348
ENSG00000165457	FOLR2	placenta	233.7	0.8473
ENSG00000165905	GYLTL1B	placenta	52.5	0.9171
ENSG00000166086	JAM3	placenta	143.3	0.8281
ENSG00000166147	FBN1	placenta	106.6	0.8566
ENSG00000166510	CCDC68	placenta	45.8	0.8492
ENSG00000166863	TAC3	placenta	610.5	0.9973
ENSG00000167244	IGF2	placenta	3974.6	0.9896
ENSG00000167612	ANKRD33	placenta	0.5	1.0000
ENSG00000167703	SLC43A2	placenta	31.6	0.8612
ENSG00000168065	SLC22A11	placenta	44.5	0.9770
ENSG00000168140	VASN	placenta	16	0.8120
ENSG00000168487	BMP1	placenta	21	0.8536
ENSG00000168621	GDNF	placenta	6.9	0.8072
ENSG00000168875	SOX14	placenta	2.4	0.9861
ENSG00000168952	STXBP6	placenta	60.7	0.8135
ENSG00000169495	HTRA4	placenta	94.4	0.9875
ENSG00000169635	HIC2	placenta	8.4	0.8237
ENSG00000169860	P2RY1	placenta	33.7	0.8745
ENSG00000170498	KISS1	placenta	328	0.9985
ENSG00000170542	SERPINB9	placenta	74.3	0.8426
ENSG00000170545	SMAGP	placenta	144.1	0.8824
ENSG00000170848	PSG6	placenta	70.1	0.9993
ENSG00000170891	CYTL1	placenta	64.3	0.9311
ENSG00000170965	PLAC1	placenta	37.6	0.9978
ENSG00000171056	SOX7	placenta	49.2	0.8984
ENSG00000171388	APLN	placenta	79.3	0.9677

ENSG00000171402	XAGE3	placenta	571.7	0.9996
ENSG00000172179	PRL	placenta	27.1	0.9829
ENSG00000172889	EGFL7	placenta	262.5	0.9043
ENSG00000172901	LVRN	placenta	31.2	0.9842
ENSG00000173110	HSPA6	placenta	27.7	0.8734
ENSG00000173157	ADAMTS20	placenta	0.8	0.9688
ENSG00000173391	OLR1	placenta	159.6	0.9432
ENSG00000174059	CD34	placenta	313.8	0.8602
ENSG00000174792	C4orf26	placenta	5.8	0.9808
ENSG00000174944	P2RY14	placenta	45.4	0.8653
ENSG00000175318	GRAMD2	placenta	69.4	0.9401
ENSG00000177058	SLC38A9	placenta	79.8	0.8768
ENSG00000178033	FAM26E	placenta	6.4	0.8077
ENSG00000178860	MSC	placenta	22.6	0.8010
ENSG00000179046	TRIML2	placenta	5.9	0.9831
ENSG00000179097	HTR1F	placenta	2.7	0.8940
ENSG00000179111	HES7	placenta	1.1	0.8662
ENSG00000179304	FAM156B	placenta	46.3	0.8635
ENSG00000179776	CDH5	placenta	332.2	0.9364
ENSG00000180190	TDRP	placenta	46.5	0.8133
ENSG00000180475	OR10Q1	placenta	0.1	1.0000
ENSG00000180785	OR51E1	placenta	9.5	0.9044
ENSG00000181649	PHLDA2	placenta	54.3	0.9756
ENSG00000181652	ATG9B	placenta	2	0.9375
ENSG00000182118	FAM89A	placenta	97.9	0.9112
ENSG00000182752	PAPPA	placenta	103.9	0.9785
ENSG00000182963	GJC1	placenta	50.9	0.8553
ENSG00000183632	TP53TG3	placenta	0.4	0.9583
ENSG00000183668	PSG9	placenta	146.9	0.9993
ENSG00000183671	GPR1	placenta	11.2	0.8814
ENSG00000183691	NOG	placenta	15.8	0.9655
ENSG00000183734	ASCL2	placenta	6.4	0.8255
ENSG00000183807	FAM162B	placenta	93.2	0.9411
ENSG00000184029	DSCR4	placenta	2	0.9806
ENSG00000184481	FOXO4	placenta	171.9	0.9107
ENSG00000185269	NOTUM	placenta	191.3	0.9963
ENSG00000185559	DLK1	placenta	2319	0.9782
ENSG00000186652	PRG2	placenta	3847.6	0.9990
ENSG00000187123	LYPD6	placenta	22.4	0.9004
ENSG00000187498	COL4A1	placenta	1227.8	0.9421
ENSG00000187513	GJA4	placenta	88.6	0.8709
ENSG00000187714	SLC18A3	placenta	0.6	0.9583
ENSG00000187772	LIN28B	placenta	67.2	0.9978
ENSG00000188676	IDO2	placenta	5.8	0.9746
ENSG00000188984	AADACL3	placenta	1.3	0.9744
ENSG00000189052	CGB5	placenta	31.7	0.9982
ENSG00000189120	SP6	placenta	32.3	0.9499
ENSG00000189253	TRIM64B	placenta	3	0.9944
ENSG00000196266	OR10J3	placenta	0.6	1.0000
ENSG00000196565	HBG2	placenta	20295.9	0.9996
ENSG00000196569	LAMA2	placenta	148.7	0.9275
ENSG00000197594	ENPP1	placenta	62.4	0.8937
ENSG00000197683	KRTAP26-1	placenta	1.9	0.9985
ENSG00000197769	MAP1LC3C	placenta	16	0.9002
ENSG00000197977	ELOVL2	placenta	49.8	0.9179
ENSG00000198223	CSF2RA	placenta	93.5	0.9015
ENSG00000198759	EGFL6	placenta	913.7	0.9977
ENSG00000203857	HSD3B1	placenta	110.1	0.9952
ENSG00000204262	COL5A2	placenta	152.7	0.8126
ENSG00000204291	COL15A1	placenta	309.7	0.9025
ENSG00000204414	CSHL1	placenta	216.4	0.9997
ENSG00000204450	TRIM64	placenta	1.1	1.0000
ENSG00000204595	DPRX	placenta	1.9	0.9722
ENSG00000204632	HLA-G	placenta	14.8	0.9955
ENSG00000204941	PSG5	placenta	157.4	0.9990
ENSG00000205864	KRTAP5-6	placenta	0.6	0.9815
ENSG00000206538	VGLL3	placenta	57.4	0.9072
ENSG00000213030	CGB8	placenta	29.2	0.9993
ENSG00000213218	CSH2	placenta	3928.4	0.9997
ENSG00000213934	HBG1	placenta	253.1	0.9996
ENSG00000214336	FOXI3	placenta	7.3	0.9958
ENSG00000214376	VSTM5	placenta	6.5	0.9175
ENSG00000215183	MSMP	placenta	1.8	0.9753
ENSG00000215595	C20orf202	placenta	4.8	0.9161
ENSG00000218336	TENM3	placenta	18.7	0.8372

ENSG00000221826	PSG3	placenta	188.4	0.9995
ENSG00000221878	PSG7	placenta	7.1	0.9887
ENSG00000231924	PSG1	placenta	362.6	0.9997
ENSG00000235750	KIAA0040	placenta	142.4	0.8784
ENSG00000240563	L1TD1	placenta	16.5	0.9449
ENSG00000242221	PSG2	placenta	342.1	0.9997
ENSG00000242265	PEG10	placenta	659.4	0.9733
ENSG00000242950	ERVW-1	placenta	77.1	0.9868
ENSG00000243130	PSG11	placenta	73.9	0.9996
ENSG00000244476	ERVFRD-1	placenta	51.4	0.9778
ENSG00000249861	LGALS16	placenta	7.6	0.9996
ENSG00000254535	PABPC4L	placenta	14.5	0.8776
ENSG00000254656	RTL1	placenta	4.8	0.9821
ENSG00000254979	RP11-872D17.8	placenta	10.5	0.9111
ENSG00000259384	GH1	placenta	1.2	0.9352
ENSG00000261371	PECAM1	placenta	654.4	0.9077
ENSG00000265107	GJA5	placenta	122.1	0.9403
ENSG00000266265	KLF14	placenta	1.1	0.9242
ENSG00000267534	S1PR2	placenta	26.9	0.8274
ENSG00000268964	ERVV-2	placenta	13.5	0.9994
ENSG00000269526	ERVV-1	placenta	21.9	0.9991
ENSG00000272602	ZNF595	placenta	87.4	0.9007
ENSG00000273820	USP27X	placenta	19.6	0.8268
ENSG00000275034	TP53TG3E	placenta	0.2	0.9861
ENSG00000279346	AC104389.1	placenta	11.1	0.9987
ENSG00000279824	AC104389.2	placenta	2.6	0.9979
ENSG00000003096	KLHL13	endometrium	52.2	0.8496
ENSG00000005073	HOXA11	endometrium	96	0.9525
ENSG00000026559	KCNG1	endometrium	23.4	0.8922
ENSG00000050628	PTGER3	endometrium	114.7	0.9060
ENSG00000066583	ISOC1	endometrium	174.3	0.8408
ENSG00000070047	PHRF1	endometrium	4.5	0.8068
ENSG00000072952	MRVI1	endometrium	98.6	0.8001
ENSG00000077157	PPP1R12B	endometrium	363.9	0.8188
ENSG00000078098	FAP	endometrium	50.4	0.8659
ENSG00000082175	PGR	endometrium	171.3	0.9446
ENSG00000091831	ESR1	endometrium	179.7	0.9322
ENSG00000099953	MMP11	endometrium	122.3	0.9750
ENSG00000102174	PHEX	endometrium	3.5	0.8246
ENSG00000103888	CEMIP	endometrium	54.5	0.9194
ENSG00000105419	MEIS3	endometrium	82.2	0.8597
ENSG00000105880	DLX5	endometrium	20.1	0.9116
ENSG00000111087	GLI1	endometrium	15.1	0.8352
ENSG00000113212	PCDHB7	endometrium	6.6	0.8388
ENSG00000114251	WNT5A	endometrium	46.3	0.8635
ENSG00000122133	PAEP	endometrium	437.4	0.9912
ENSG00000122420	PTGFR	endometrium	30.3	0.8604
ENSG00000122691	TWIST1	endometrium	30.7	0.8902
ENSG00000124391	IL17C	endometrium	3.5	0.9881
ENSG00000124766	SOX4	endometrium	80.4	0.8380
ENSG00000125498	KIR2DL1	endometrium	0.4	1.0000
ENSG00000127578	WFIKKN1	endometrium	0.1	0.9167
ENSG00000128709	HOXD9	endometrium	45.3	0.9054
ENSG00000128710	HOXD10	endometrium	48	0.9510
ENSG00000128713	HOXD11	endometrium	5.9	0.9605
ENSG00000128918	ALDH1A2	endometrium	117.2	0.8485
ENSG00000129009	ISLR	endometrium	198.5	0.8093
ENSG00000129116	PALLD	endometrium	441.6	0.8121
ENSG00000132329	RAMP1	endometrium	233.7	0.8680
ENSG00000133105	RXFP2	endometrium	0.8	0.9236
ENSG00000133107	TRPC4	endometrium	18.5	0.8979
ENSG00000133466	C1QTNF6	endometrium	52.2	0.9030
ENSG00000134198	TSPAN2	endometrium	71.2	0.8461
ENSG00000134200	TSHB	endometrium	1.7	0.8824
ENSG00000134533	RERG	endometrium	140.7	0.8222
ENSG00000135502	SLC26A10	endometrium	0.5	0.9222
ENSG00000136378	ADAMTS7	endometrium	7.2	0.8291
ENSG00000139926	FRMD6	endometrium	125.3	0.8012
ENSG00000140945	CDH13	endometrium	82.5	0.8273
ENSG00000143768	LEFTY2	endometrium	270.5	0.9849
ENSG00000145808	ADAMTS19	endometrium	16.4	0.9407
ENSG00000146374	RSPO3	endometrium	102.8	0.8545
ENSG00000149090	PAMR1	endometrium	91.9	0.8438
ENSG00000149451	ADAM33	endometrium	102.9	0.8146
ENSG00000149968	MMP3	endometrium	58.7	0.9703

ENSG00000152527	PLEKHH2	endometrium	31.8	0.8038
ENSG00000159674	SPON2	endometrium	105.3	0.8396
ENSG00000163501	IHH	endometrium	31.4	0.9001
ENSG00000163792	TCF23	endometrium	33.7	0.9257
ENSG00000164107	HAND2	endometrium	83.7	0.8298
ENSG00000164484	TMEM200A	endometrium	64.8	0.8870
ENSG00000164736	SOX17	endometrium	32.1	0.8677
ENSG00000164920	OSR2	endometrium	204.6	0.8896
ENSG00000166670	MMP10	endometrium	443.1	0.9984
ENSG00000167346	MMP26	endometrium	23.8	0.9993
ENSG00000169218	RSPO1	endometrium	43.3	0.9200
ENSG00000170049	KCNAB3	endometrium	14.5	0.9169
ENSG00000170166	HOXD4	endometrium	23.5	0.8552
ENSG00000170370	EMX2	endometrium	114.7	0.8866
ENSG00000177363	LRRN4CL	endometrium	16.8	0.8006
ENSG00000177519	RPRM	endometrium	21.9	0.8617
ENSG00000178031	ADAMTSL1	endometrium	20.7	0.8600
ENSG00000179300	ZCCHC5	endometrium	0.7	0.9206
ENSG00000180269	GPR139	endometrium	0.3	0.9907
ENSG00000180447	GAS1	endometrium	110.4	0.8679
ENSG00000183578	TNFAIP8L3	endometrium	118.6	0.9171
ENSG00000185630	PBX1	endometrium	246.5	0.8259
ENSG00000186860	KRTAP17-1	endometrium	0.1	1.0000
ENSG00000188133	TMEM215	endometrium	4.8	0.9554
ENSG00000197361	FBXL22	endometrium	45.1	0.8729
ENSG00000197410	DCHS2	endometrium	4	0.8181
ENSG00000198535	C2CD4A	endometrium	2.3	0.8309
ENSG00000204335	SP5	endometrium	3.9	0.8661
ENSG00000204969	PCDHA2	endometrium	1	0.8611
ENSG00000232237	ASCL5	endometrium	0.6	0.8657
ENSG00000249992	TMEM158	endometrium	32.5	0.8475
ENSG00000251184	RP11-101E3.5	endometrium	0.6	0.8380
ENSG00000253293	HOXA10	endometrium	116.3	0.9204
ENSG00000253304	TMEM200B	endometrium	68	0.8496
ENSG00000254726	MEX3A	endometrium	5.9	0.8663
ENSG00000257184	HOXA10-HOXA9	endometrium	1	0.9556
ENSG00000259752	AC066615.1	endometrium	2.1	0.8690
ENSG00000278845	MRPL45	endometrium	10.2	0.8145
ENSG00000279068	CH17-140K24.5	endometrium	1.6	0.8281
ENSG00000279261	AL360294.1	endometrium	0.1	0.8056
ENSG00000280178	AP000349.2	endometrium	4	0.9340
ENSG00000281137	AC074033.1	endometrium	2	0.9875

Appendix 6 - Literature sources and maternal/fetal expression information for genes associated with complications of pregnancy or fertility-related conditions:

Gene symbol/Ensembl ID	Alternate gene name(s)	Associated literature (Pubmed ID) and/or database entries	Maternal/fetal expression; other notes	Associated diseases or conditions
ABRAXAS1_ENSG00000163322	FAM175A	PMID: 22267201	maternal	menopause_menstrual_onset
ACVR1_ENSG00000115170	ACVR1	PMID: 24331737	mrna expression correlated with pe/pe onset/maternal	preeclampsia
ADGRL2_ENSG00000117114	LPHN2	PMID: 25599974 (EBI)	maternal	preterm_birth
ADRA1D_ENSG00000171873	ADRA1D	PMID: 23551011 (EBI)	maternal	preeclampsia
ADRB1_ENSG00000043591	ADRB1	PMID: 23202124 (EBI); PMID: 27680694	fetal	birth_weight
ADRB2_ENSG00000169252	ADRB2	PMID: 26715857	maternal/candidate gene approach	preterm_birth
AGTR2_ENSG00000180772	AGTR2	PMID: 28877031	maternal/assoc. with gestational duration and preterm birth	preterm_birth
AGT_ENSG00000135744	AGT	PMID: 21429808 (EBI); PMID: 26010865	candidate gene approach/maternal; regulator/target of susceptibility gene ided in 2014 paper/maternal	preeclampsia
ALCAM_ENSG00000170017	ALCAM	PMID: 28333195 (EBI)	maternal/ovarian disease with few adhesions	endometriosis_ovarian
ANXA5_ENSG00000164111	RPRGL3; ENX2	{Pregnancy loss, recurrent, susceptibility to, 1} - OMIM; "{Pregnancy loss, recurrent, susceptibility to, 3} - OMIM"	maternal	miscarriage
APOE_ENSG00000130203	APOE	PMID: 21429808 (EBI)	candidate gene approach/maternal	preeclampsia
AQP1_ENSG00000240583	AQP1	PMID: 23874842	meta-analysis/fetal	preeclampsia
ARHGEF7_ENSG00000102606	ARHGEF7	PMID: 19448619 (EBI)	maternal	menopause_menstrual_onset
AR_ENSG00000169083	AR	PMID: 26715857	fetal/linkage study	preterm_birth
ASH2L_ENSG00000129691	ASH2L	PMID: 22267201 (EBI); PMID: 23307926 (EBI)	maternal	menopause_menstrual_onset
BAMBI_ENSG00000095739	BAMBI	PMID: 23551011 (EBI)	maternal	preeclampsia
BANP_ENSG00000172530	BANP	PMID: 19448619 (EBI)	maternal	menopause_menstrual_onset
BCL6_ENSG00000113916	BCL6	PMID: 23874842	meta-analysis/fetal	preeclampsia
BHLHE40_ENSG00000134107	BHLHE40	PMID: 23874842	meta-analysis/fetal	preeclampsia
BRSK1_ENSG00000160469	BRSK1	PMID: 19448621 (EBI); PMID: 22269211	maternal	menopause_menstrual_onset
BUB3_ENSG00000154473	BUB3	PMID: 24045676 (EBI)	maternal	menopause_menstrual_onset
C18orf21_ENSG00000141428	C18orf21	PMID: 27506219 (EBI)	maternal/endometriosis	endometriosis_ovarian
C21orf91_ENSG00000154642	C21orf91	PMID: 28693416	fetal/placental gene network	fetal_growth_restriction
C7orf50_ENSG00000146540	C7orf50	PMID: 27506219 (EBI)	maternal/endometriosis	endometriosis_ovarian
CACNA2D1_ENSG00000153956	CACNA2D1	PMID: 25599974 (EBI); PMID: 28598419 (EBI)	maternal	preterm_birth
CALCR_ENSG00000004948	CALCR	PMID: 23202124 (EBI)	fetal	birth_weight
CAMK2B_ENSG00000058404	CAMK2B	PMID: 24046805	maternal	placental_abruption
CAPN14_ENSG00000214711	CAPN14	PMID: 28333195 (EBI)	maternal/endometriosis	endometriosis_ovarian
CCDC170_ENSG00000120262	CCDC170	PMID: 28537267 (EBI)	maternal/endometriosis	endometriosis_ovarian
CCL28_ENSG00000151882	CCL28	PMID: 27330572	fetal, methylation	fetal_growth_restriction
CCNL1_ENSG00000163660	CCNL1	PMID: 23202124 (EBI); PMID: 20372150 (EBI)	fetal	birth_weight
CDC42_ENSG00000070831	CDC42	PMID: 28171565; PMID: 23472165 (EBI)	maternal/expression regulated by risk alleles; maternal/endometriosis	endometriosis_ovarian
CDC73_ENSG00000134371	CDC73	PMID: 28333195 (EBI)	maternal/ovarian disease with few adhesions	endometriosis_ovarian
CDH20_ENSG00000101542	CDH20	PMID: 28333195 (EBI)	maternal/deep ovarian and/or rectovaginal disease with dense	endometriosis_ovarian

			adhesions	
CDKAL1_ENSG00000145996	CDKAL1	PMID: 23202124 (EBI)	fetal	birth_weight
CDKN1C_ENSG00000129757	CDKN1C	PMID: 25057881; PMID: 16125225	mrna expression/fetal/paternally imprinted; fetal	fetal_growth_restriction
CDKN2A_ENSG00000147889	CDKN2A; ARF	PMID: 21151130 (EBI)	maternal/endometriosis	endometriosis_ovarian
CDKN2B-AS1_ENSG00000240498	CDKN2BAS; CDKN2B-AS1	PMID: 21151130; PMID: 28537267 (EBI); PMID: 24676469	maternal; maternal/endometriosis	endometriosis_ovarian
CDKN2B_ENSG00000147883	CDKN2B	PMID: 21151130	maternal/endometriosis	endometriosis_ovarian
CENPM_ENSG00000100162	CENPM	PMID: 23202124 (EBI)	fetal	birth_weight
CGA_ENSG00000135346	CGA	PMID: 23874842	meta-analysis/fetal	preeclampsia
CGB3_ENSG00000104827	CGB	PMID: 23874842	meta-analysis/fetal	preeclampsia
CGB5_ENSG00000189052	CGB	PMID: 23874842	meta-analysis/fetal	preeclampsia
CKAP2L_ENSG00000169607	CKAP2L	PMID: 20844546 (EBI)	maternal/endometriosis	endometriosis_ovarian
COL24A1_ENSG00000171502	COL24A1	PMID: 28598419 (EBI)	maternal	preterm_birth
COL4A1_ENSG00000187498	COL4A1	PMID: 24331737 ; PMID: 26715857	mrna expression correlated with pe/pe onset/maternal; maternal/candidate gene approach	preeclampsia; preterm_birth
COL4A2_ENSG00000134871	COL4A2	PMID: 24331737	mrna expression correlated with pe/pe onset/maternal	preeclampsia
COL4A3_ENSG00000169031	COL4A3	PMID: 26715857	maternal/candidate gene approach	preterm_birth
CORIN_ENSG00000145244	CORIN; TMPRSS10; ATC2	Preeclampsia/eclampsia 5 - OMIM	maternal	preeclampsia
COX10_ENSG00000006695	COX10	PMID: 25549360	fetal	placental_abruption
COX5A_ENSG00000178741	COX5A	PMID: 24046805	maternal	placental_abruption
CREB3_ENSG00000107175	CREB3	PMID: 28693416	fetal/placental gene network	fetal_growth_restriction
CRH_ENSG00000147571	CRH	PMID: 16125225; PMID: 23874842	mrna expression/fetal; meta-analysis/fetal	fetal_growth_restriction; preeclampsia
CRNKL1_ENSG00000101343	CRN	Preeclampsia/eclampsia 5 - OMIM	maternal	preeclampsia
CSMD1_ENSG00000183117	CSMD1	PMID: 23472165 (EBI)	maternal/endometriosis	endometriosis_ovarian
CTNNA2_ENSG00000066032	CTNNA2	PMID: 25549360	fetal	placental_abruption
CXCL12_ENSG00000107562	CXCL12	PMID: 23472165 (EBI)	maternal/endometriosis	endometriosis_ovarian
CXXC1_ENSG00000154832	SPP1	PMID: 23874842	meta-analysis/fetal	preeclampsia
CYP11A1_ENSG00000140459	CYP11A1	PMID: 23874842	meta-analysis/fetal	preeclampsia
DAB2_ENSG00000153071	DAB2	PMID: 9696034	fetal	gtd_hydatidiform-mole
DCP1A_ENSG00000272886	DCP1A	PMID: 25599974 (EBI)	maternal	preterm_birth
DDX3X_ENSG00000215301	DDX3X	PMID: 28693416	fetal/placental gene network	fetal_growth_restriction
DECR1_ENSG00000104325	DECR1	PMID: 27330572	fetal, methylation	fetal_growth_restriction
DEFA1_ENSG00000206047	DEFA1	PMID: 21151130 (EBI); PMID: 28333195 (EBI)	maternal/endometriosis	endometriosis_ovarian
DGKB_ENSG00000136267	DGKB	PMID: 23205182	maternal	placental_abruption
DMRTA1_ENSG00000176399	DMRTA1	PMID: 28537267 (EBI); PMID: 28333195 (EBI)	maternal/ovarian disease with few adhesions; maternal/endometriosis	endometriosis_ovarian
DNAJA4_ENSG00000140403	DNAJA4	PMID: 27330572	fetal, methylation	fetal_growth_restriction
DNAJC14_ENSG00000135392	DNAJC14	PMID: 28693416	fetal/placental gene network	fetal_growth_restriction
DOC2A_ENSG00000149927	DOC2A	PMID: 9696034	fetal	gtd_hydatidiform-mole
DOCK10_ENSG00000135905	DOCK10	PMID: 23307926 (EBI)	maternal	menopause_menstrual_onset
DPH6_ENSG00000134146	ATPBD4	PMID: 24045676 (EBI)	maternal	menopause_menstrual_onset
DUSP4_ENSG00000120875	DUSP4	PMID: 28598419 (EBI)	maternal	preterm_birth
DYNC1H1_ENSG00000197102	DYNC1H1	PMID: 19448619 (EBI)	maternal	menopause_menstrual_onset
EBF1_ENSG00000164330	EBF1	PMID: 28877031	maternal/assoc. with gestational duration and preterm birth	preterm_birth
EBI3_ENSG00000105246	EBI3	PMID: 23874842	meta-analysis/fetal	preeclampsia
EEFSEC_ENSG00000132394	EEFSEC	PMID: 28877031	maternal/assoc. with gestational duration and preterm birth	preterm_birth

EMX2_ENSG00000170370	EMX2	PMID: 28333195 (EBI)	maternal/ovarian disease with few adhesions	endometriosis_ovarian
ENG_ENSG00000106991	ENG	PMID: 16751767; PMID: 23874842	seng elevated in pe patients/fetal; meta-analysis/fetal	preeclampsia
EPHX1_ENSG00000143819	EPHX	PMID: 21429808 (EBI)	candidate gene approach/maternal	preeclampsia
ERAP1_ENSG00000164307	ERAP1	PMID: 24331737	mrna expression correlated with pe/pe onset/maternal	preeclampsia
ERAP2_ENSG00000164308	ERAP2	PMID: 24331737	mrna expression correlated with pe/pe onset/maternal	preeclampsia
ERP44_ENSG00000023318	ERP44	PMID: 23551011 (EBI)	maternal	preeclampsia
ESR1_ENSG00000091831	ESR1	PMID: 28537267 (EBI); PMID: 22248077	maternal/endometriosis; maternal	endometriosis_ovarian; menopause_menstrual_onset
ESR2_ENSG00000140009	ESR2	PMID: 25264875	maternal/assoc with pprom, integrated snp/gene expression analysis	preterm_birth
ETAA1_ENSG00000143971	ETAA1	PMID: 28537267 (EBI)	maternal/endometriosis	endometriosis_ovarian
EXO1_ENSG00000174371	EXO1	PMID: 22267201 (EBI)	maternal	menopause_menstrual_onset
EZR_ENSG00000092820	EZR	PMID: 23874842	meta-analysis/fetal	preeclampsia
F2_ENSG00000180210	THPH1; F2; RPRGL2 ; F2	PMID: 27842992; "{Pregnancy loss, recurrent, susceptibility to, 2} - OMIM"; PMID: 18277167; PMID: 21429808 (EBI); PMID: 23132613; PMID: 26715857	maternal; maternal/metaanalysis; meta-analysis of genetic association studies/maternal; candidate gene approach/maternal; maternal/candidate gene approach	miscarriage; placental_abruption; preeclampsia; preterm_birth
F5_ENSG00000198734	THPH2; F5	{Pregnancy loss, recurrent, susceptibility to, 1} - OMIM; PMID: 27842992; PMID: 18277167 ; PMID: 21429808 (EBI); PMID: 23132613; PMID: 23874842	maternal; maternal/metaanalysis; meta-analysis of genetic association studies/maternal; candidate gene approach/maternal; meta-analysis/fetal	miscarriage; placental_abruption; preeclampsia
FANCI_ENSG00000140525	FANCI	PMID: 22267201	maternal	menopause_menstrual_onset
FERMT1_ENSG00000101311	FERMT1	PMID: 19448619 (EBI)	maternal	menopause_menstrual_onset
FGF14_ENSG00000102466	FGF14	PMID: 23551011 (EBI)	maternal	preeclampsia
FGF1_ENSG00000113578	FGF1	PMID: 26715857	maternal/candidate gene approach	preterm_birth
FLT1_ENSG00000102755	VEGFR1; FLT1	PMID: 21429808 (EBI); PMID: 28628106; PMID: 23874842	candidate gene approach/maternal; meta-analysis/fetal; fetal	preeclampsia
FN1_ENSG00000115414	FN1	PMID: 28333195 (EBI)	maternal/deep ovarian and/or rectovaginal disease with dense adhesions	endometriosis_ovarian
FNDC4_ENSG00000115226	FNDC4	PMID: 22267201 (EBI)	maternal	menopause_menstrual_onset
FOXP2_ENSG00000128573	FOXP2	PMID: 28333195 (EBI)	maternal/deep ovarian and/or rectovaginal disease with dense adhesions	endometriosis_ovarian
FSHB_ENSG00000131808	FSHB	PMID: 28537267 (EBI); PMID: 26732621(EBI)	maternal/impairs fertility but protective against endometriosis; maternal/endometriosis; maternal/age at menarche	endometriosis_ovarian; menopause_menstrual_onset
FSTL3_ENSG00000070404	FSTL3	PMID: 23874842	meta-analysis/fetal	preeclampsia
FTO_ENSG00000140718	FTO	PMID: 25845303	maternal	miscarriage
GALNT13_ENSG00000144278	GALNT13	PMID: 17903295 (EBI)	maternal	menopause_menstrual_onset
GATM_ENSG00000171766	GATM	PMID: 16125225	mrna	fetal_growth_restriction

			expression/fetal/imprinted	
GCM2_ENSG00000124827	GCM2	PMID: 19448621 (EBI)	maternal	menopause_menstrual_onset
GLIS3_ENSG00000107249	GLIS3	PMID: 25599974 (EBI)	maternal	preterm_birth
GLRX_ENSG00000173221	GLRX	PMID: 16125225	mrna expression/fetal	fetal_growth_restriction
GNAS_ENSG00000087460	GNAS	PMID: 16125225	mrna expression/fetal/imprinted	fetal_growth_restriction
GNE_ENSG00000159921	GNE	PMID: 27330572	fetal, methylation	fetal_growth_restriction
GNG4_ENSG00000168243	GNG4	PMID: 17903295 (EBI)	maternal	menopause_menstrual_onset
GREB1_ENSG00000196208	GREB1	PMID: 28537267 (EBI); PMID: 24676469; PMID: 21151130 (EBI)	maternal; maternal/endometriosis	endometriosis_ovarian
GRHL1_ENSG00000134317	GRHL1	PMID: 28693416	fetal/placental gene network	fetal_growth_restriction
GSPT1_ENSG00000103342	GSPT1	PMID: 22267201 (EBI); PMID: 23307926 (EBI)	maternal	menopause_menstrual_onset
GSTK1_ENSG00000197448	GST	PMID: 21429808 (EBI)	candidate gene approach/maternal	preeclampsia
GSTO1_ENSG00000148834	GSTO1	PMID: 27330572	fetal, methylation	fetal_growth_restriction
H19_ENSG00000130600	H19	PMID: 25549360	maternal/fetal	placental_abruption
HELQ_ENSG00000163312	HELQ	PMID: 22267201 (EBI); PMID: 22267201	maternal	menopause_menstrual_onset
HEXB_ENSG00000049860	HEXB	PMID: 23874842	meta-analysis/fetal	preeclampsia
HGF_ENSG00000019991	HGF	PMID: 28598419 (EBI)	maternal	preterm_birth
HK3_ENSG00000160883	HK3	PMID: 19448621; PMID: 22248077	maternal	menopause_menstrual_onset
HMGA1_ENSG00000137309	HMGA1	PMID: 27680694	fetal	birth_weight
HMGA2_ENSG00000149948	HMGA2	PMID: 23202124 (EBI)	fetal	birth_weight
HPGD_ENSG00000164120	HPGD	PMID: 16125225	mrna expression/fetal	fetal_growth_restriction
HSD17B1_ENSG00000108786	HSD17B1	PMID: 23874842	meta-analysis/fetal	preeclampsia
HSPA1A_ENSG00000204389	HSPA1A	PMID: 27330572	fetal, methylation	fetal_growth_restriction
HSPA1L_ENSG00000204390	HSPA1L	PMID: 27330572	fetal, methylation	fetal_growth_restriction
HTRA1_ENSG00000166033	HTRA1	PMID: 23874842	meta-analysis/fetal	preeclampsia
HTRA4_ENSG00000169495	HTRA4	PMID: 23874842	meta-analysis/fetal	preeclampsia
ID4_ENSG00000172201	ID4	PMID: 28333195 (EBI); PMID: 28537267 (EBI); PMID: 24676469; PMID: 23472165 (EBI)	maternal/deep ovarian and/or rectovaginal disease with dense adhesions; maternal; maternal/endometriosis	endometriosis_ovarian
IDO1_ENSG00000131203	INDO	PMID: 16125225	mrna expression/fetal	fetal_growth_restriction
IFNG_ENSG00000111537	IFNG	PMID: 27842992 ; PMID: 26010865 ; PMID: 26715857	maternal/metaanalysis; regulator/target of susceptibility gene ided in 2014 paper/maternal; maternal/candidate gene approach	miscarriage; preeclampsia; preterm_birth
IGF1R_ENSG00000140443	IGF1R	PMID: 27506219 (EBI) ; PMID: 20817666; PMID: 14657428	maternal/endometriosis; maternal; fetal	endometriosis_ovarian; fetal_growth_restriction
IGF1_ENSG00000017427	IGF1	PMID: 16125225; PMID: 26823688; PMID: 20817666; PMID: 14657428 ; PMID: 23298525	fetal/mrna/methylation; mrna expression/fetal; maternal; fetal; maternal/integrated snp/gene pathway analysis	fetal_growth_restriction; preterm_birth
IGF2R_ENSG00000197081	IGF2R	PMID: 20817666	fetal/maternal	fetal_growth_restriction
IGF2_ENSG00000167244	IGF2	PMID: 12087403; PMID: 20817666; PMID: 16125225; PMID: 25549360 ; PMID: 26715857	fetal/maternal; mrna expression/fetal/maternally imprinted; fetal; maternal/fetal; maternal/candidate gene approach	fetal_growth_restriction; placental_abruption; preterm_birth
IGFBP1_ENSG00000146678	IGFBP1	PMID: 18219215; PMID: 26823688; PMID: 23874842	fetal/mrna/methylation; maternal; meta-analysis/fetal	fetal_growth_restriction; preeclampsia
IGFBP2_ENSG00000115457	IGFBP2	PMID: 26823688 ; PMID: 18219215	fetal/mrna/methylation; maternal	fetal_growth_restriction
IGFBP3_ENSG00000146674	IGFBP3	PMID: 26823688 ; PMID: 18219215	fetal/mrna/methylation; fetal/maternal	fetal_growth_restriction
IGFBP4_ENSG00000141753	IGFBP4	PMID: 18219215; PMID:	fetal/mrna/methylation;	fetal_growth_restriction

		26823688	fetal/maternal	
IGFBP5_ENSG00000115461	IGFBP5	PMID: 18219215	fetal/maternal	fetal_growth_restriction
IGFBP6_ENSG00000167779	IGFBP6	PMID: 18219215	maternal	fetal_growth_restriction
IGFBP7_ENSG00000163453	IGFBP7	PMID: 26823688	fetal/mrna/methylation	fetal_growth_restriction
IL10_ENSG00000136634	IL10	PMID: 27842992; PMID: 21429808 (EBI)	maternal/metaanalysis; candidate gene approach/maternal	miscarriage; preeclampsia
IL11_ENSG00000095752	IL11	PMID: 22267201	maternal	menopause_menstrual_onset
IL1A_ENSG00000115008	IL1A	PMID: 25336714; PMID: 28537267 (EBI); PMID: 20844546 (EBI)	maternal; maternal/endometriosis	endometriosis_ovarian
IL1B_ENSG00000125538	IL1B	PMID: 28537267 (EBI)	maternal/endometriosis	endometriosis_ovarian
IL1RN_ENSG00000136689	IL1RN	PMID: 26715857	maternal/candidate gene approach	preterm_birth
IL2RG_ENSG00000147168	IL2RG	PMID: 26715857	fetal/linkage study	preterm_birth
IL2_ENSG00000109471	IL2	PMID: 26715857	maternal/candidate gene approach	preterm_birth
IL33_ENSG00000137033	IL33	PMID: 23472165 (EBI)	maternal/endometriosis	endometriosis_ovarian
IL6R_ENSG00000160712	IL6R	PMID: 26715857	maternal/candidate gene approach; fetal	preterm_birth
IL6_ENSG00000136244	IL6	PMID: 26010865	regulator/target of susceptibility gene ided in 2014 paper/maternal	preeclampsia
INHA_ENSG00000123999	INHA	PMID: 24331737; PMID: 23874842	meta-analysis/fetal; mrna expression correlated with pe/pe onset/maternal	preeclampsia
INHBA_ENSG00000122641	INHBA	PMID: 16125225 ; PMID: 26010865; PMID: 23874842	mrna expression/fetal; meta-analysis/fetal; regulator/target of susceptibility gene ided in 2014 paper/maternal	fetal_growth_restriction; preeclampsia
INHBB_ENSG00000163083	INHBB	PMID: 24331737; PMID: 22432041	maternal; mrna expression correlated with pe/pe onset/maternal	preeclampsia
INVS_ENSG00000119509	INVS	PMID: 23551011 (EBI)	maternal	preeclampsia
IRF3_ENSG00000126456	IRF3	PMID: 25264875	maternal/integrated snp/gene expression analysis	preterm_birth
ITPK1_ENSG00000100605	ITPK1	PMID: 23472165 (EBI)	maternal/endometriosis	endometriosis_ovarian
KDR_ENSG00000128052	VEGFR2; KDR ; VEGFR2	PMID: 27453397 ; PMID: 28537267 (EBI); PMID: 27453397 ; PMID: 16310040	maternal; maternal/endometriosis; fetal	endometriosis_ovarian; placenta_accreta
KHDC3L_ENSG00000203908	KHDC3L; ECAT1	Hydatidiform mole, recurrent, 2 - OMIM	omim/maternal	gtd_hydatidiform-mole
KIR3DL1_ENSG00000167633	KIR	PMID: 27842992	maternal/metaanalysis	miscarriage
KMT5C_ENSG00000133247	SUV420H2	PMID: 19448619 (EBI)	maternal	menopause_menstrual_onset
KPNA3_ENSG00000102753	KPNA3	PMID: 22267201 (EBI)	maternal	menopause_menstrual_onset
KRT19_ENSG00000171345	KRT19	PMID: 23874842	meta-analysis/fetal	preeclampsia
KSR2_ENSG00000171435	KSR2	PMID: 23472165 (EBI)	maternal/endometriosis	endometriosis_ovarian
LAMC3_ENSG00000050555	LAMC3	PMID: 28333195 (EBI)	maternal/deep ovarian and/or rectovaginal disease with dense adhesions; maternal/endometriosis	endometriosis_ovarian
LCORL_ENSG00000178177	LCORL	PMID: 23202124 (EBI)	fetal	birth_weight
LEKR1_ENSG00000197980	LEKR1	PMID: 23202124 (EBI); PMID: 20372150 (EBI)	fetal	birth_weight
LEPR_ENSG00000116678	LEPR	PMID: 27330572	fetal, methylation	fetal_growth_restriction
LEP_ENSG00000174697	LEP	PMID: 16125225; PMID: 23874842	mrna expression/fetal; meta-analysis/fetal	fetal_growth_restriction; preeclampsia
LHB_ENSG00000104826	LHB	PMID: 23874842	meta-analysis/fetal	preeclampsia
LHFPL6_ENSG00000183722	LHFP	PMID: 23551011 (EBI)	maternal	preeclampsia
LIN28B_ENSG00000187772	LIN28B	PMID: 19448621	maternal	menopause_menstrual_onset
LINC00339_ENSG00000218510	LINC00339	PMID: 28171565	maternal/expression regulated by risk alleles	endometriosis_ovarian
LNPEP_ENSG00000113441	LNPEP	PMID: 24331737	mrna expression	preeclampsia

			correlated with pe/pe onset/maternal	
LOC100506403_ENSG00000159216	RUNX1	PMID: 23551011 (EBI)	maternal	preeclampsia
LRRC28_ENSG00000168904	LRRC28	PMID: 28598419 (EBI)	maternal	preterm_birth
LRRN4_ENSG00000125872	LRRN4	PMID: 19448619 (EBI)	maternal	menopause_menstrual_onset
LTF_ENSG00000012223	LTF	PMID: 26715857	maternal/candidate gene approach	preterm_birth
LZTS1_ENSG00000061337	LZTS1	PMID: 23551011 (EBI)	maternal	preeclampsia
MAN1A1_ENSG00000111885	MAN1A1	PMID: 25599974 (EBI)	maternal	preterm_birth
MAP3K4_ENSG00000085511	MAP3K4	PMID: 28333195 (EBI)	maternal/ovarian disease with few adhesions	endometriosis_ovarian
MBL2_ENSG00000165471	MBL	PMID: 27842992	maternal/metaanalysis	miscarriage
MCM8_ENSG00000125885	MCM8	PMID: 19448619 (EBI); PMID: 23307926 (EBI); PMID: 19448621 (EBI); PMID: 19448621; PMID: 22267201 (EBI); PMID: 20952801 ; PMID: 23551011 (EBI)	maternal	menopause_menstrual_onset; preeclampsia
MEF2A_ENSG00000068305	MEF2A	PMID: 28598419 (EBI)	maternal	preterm_birth
MEF2C_ENSG00000081189	MEF2C	PMID: 27664809	na	preterm_birth
MEG3_ENSG00000214548	MEG3	PMID: 16125225	mrna expression/fetal/paternally imprinted	fetal_growth_restriction
MEIS1_ENSG00000143995	MEIS1	PMID: 27506219 (EBI)	maternal/endometriosis	endometriosis_ovarian
MEST_ENSG00000106484	MEST	PMID: 16125225	mrna expression/fetal/maternally imprinted	fetal_growth_restriction
MIR17HG_ENSG00000215417	MIR17HG	PMID: 23205182	maternal	placental_abruption
MMP14_ENSG00000157227	MMP14	PMID: 23470162	fetal/mrna expression	fetal_growth_restriction
MMP1_ENSG00000196611	MMP1	PMID: 22406112	maternal	miscarriage
MMP2_ENSG00000087245	MMP2	PMID: 17367869; PMID: 22406112 ; PMID: 23316964	fetal; maternal	fetal_growth_restriction; miscarriage; preeclampsia
MMP3_ENSG00000149968	MMP3	PMID: 22406112	maternal	miscarriage
MMP9_ENSG00000100985	MMP9	PMID: 17367869; PMID: 22406112 ; PMID: 23316964	fetal; maternal	fetal_growth_restriction; miscarriage; preeclampsia
MOAP1_ENSG00000165943	MOAP1	PMID: 23472165 (EBI)	maternal/endometriosis	endometriosis_ovarian
MTHFD1_ENSG00000100714	MTHFD1	PMID: 18277167	maternal	placental_abruption
MTHFR_ENSG00000177000	MTHFR	PMID: 27842992 ; PMID: 18277167 ; PMID: 21429808 (EBI)	maternal/metaanalysis; maternal; candidate gene approach/maternal	miscarriage; placental_abruption; preeclampsia
MUC21_ENSG00000204544	MUC21	PMID: 23551011 (EBI)	maternal	preeclampsia
MUC22_ENSG00000261272	MUC22	PMID: 23551011 (EBI)	maternal	preeclampsia
MYCBP2_ENSG00000005810	MYCBP2	PMID: 23551011 (EBI)	maternal	preeclampsia
NAALADL2_ENSG00000177694	NAALADL2	PMID: 28333195 (EBI)	maternal/deep ovarian and/or rectovaginal disease with dense adhesions	endometriosis_ovarian
NANOS3_ENSG00000187556	NOS3	PMID: 21429808 (EBI); "{Hypertension, pregnancy-induced} - OMIM"	candidate gene approach/maternal; maternal	preeclampsia
NDUFB6_ENSG00000165264	NDUFB6	PMID: 24046805	maternal	placental_abruption
NECTIN4_ENSG00000143217	PVRL4	PMID: 23874842	meta-analysis/fetal	preeclampsia
NFE2L3_ENSG00000050344	NFE2L3	PMID: 28333195 (EBI)	maternal/deep ovarian and/or rectovaginal disease with dense adhesions; maternal/endometriosis	endometriosis_ovarian
NFKB1_ENSG00000109320	NFKB1	PMID: 25264875	maternal/integrated snp/gene expression analysis	preterm_birth
NLRP11_ENSG00000179873	NLRP11	PMID: 22267201 (EBI); PMID: 22267201; PMID: 23307926 (EBI)	maternal	menopause_menstrual_onset
NLRP7_ENSG00000167634	PYPAF3; NLRP7; NOD12;	Hydatidiform mole, recurrent, 1 - OMIM; https://academic.oup.com/	omim/maternal; maternal	gtd_hydatidiform-mole

	NALP7	hmg/article/18/5/888/615820		
NOS3_ENSG00000164867	NOS3	PMID: 27842992; {Placental abruption} - OMIM; PMID: 18277167 ; PMID: 21429808 (EBI); "{Hypertension, pregnancy-induced} - OMIM"	maternal/metaanalysis; maternal; candidate gene approach/maternal	miscarriage; placental_abruption; preeclampsia
NOTCH1_ENSG00000148400	NOTCH1	PMID: 26732621(EBI)	maternal/age at menarche	menopause_menstrual_onset
NPVF_ENSG00000105954	NPVF	PMID: 23551011 (EBI)	maternal	preeclampsia
NR1H3_ENSG00000025434	NR1H3	PMID: 24046805	maternal	placental_abruption
NR3C1_ENSG00000113580	NR3C1	PMID: 25264875	maternal/integrated snp/gene expression analysis	preterm_birth
NRIP1_ENSG00000180530	NRIP1	PMID: 27680694	fetal	birth_weight
NTRK2_ENSG00000148053	NTRK2	PMID: 24950379 (EBI)	fetal	birth_weight
NYAP2_ENSG00000144460	NYAP2	PMID: 23307926 (EBI)	maternal	menopause_menstrual_onset
OPCML_ENSG00000183715	OPCML	PMID: 19448619 (EBI)	maternal	menopause_menstrual_onset
OR1D2_ENSG00000184166	OR1D2	PMID: 23472165 (EBI)	maternal/endometriosis	endometriosis_ovarian
OR1G1_ENSG00000183024	OR1G1	PMID: 23472165 (EBI)	maternal/endometriosis	endometriosis_ovarian
PAEP_ENSG00000122133	PAEP	PMID: 21880722	fetal	gtd_hydatidiform-mole
PAPPA2_ENSG00000116183	PAPPA2	PMID: 23874842	meta-analysis/fetal	preeclampsia
PAPPA_ENSG00000182752	PAPPA	PMID: 14973274	fetal	fetal_growth_restriction; preeclampsia
PDE1C_ENSG00000154678	PDE1C	PMID: 23472165 (EBI)	maternal/endometriosis	endometriosis_ovarian
PGF_ENSG00000119630	PGF	PMID: 23874842	meta-analysis/fetal	preeclampsia
PHLDA2_ENSG00000181649	PHLDA2	PMID: 16125225	mrna expression/fetal/paternally imprinted	fetal_growth_restriction
PHYHIP_ENSG00000168490	PHYHIP	PMID: 23874842	meta-analysis/fetal	preeclampsia
PIK3CG_ENSG00000105851	PIK3CG	PMID: 19448619 (EBI)	maternal	menopause_menstrual_onset
PLAGL1_ENSG00000118495	PLAGL1	PMID: 16125225	mrna expression/fetal/imprinted	fetal_growth_restriction
PLEC_ENSG00000178209	PLEC	PMID: 23874842	meta-analysis/fetal	preeclampsia
PLPPR3_ENSG00000129951	PRG2	PMID: 21865357	circulating protein levels/maternal/fetal	preeclampsia
POLG_ENSG00000140521	POLG	PMID: 22267201 (EBI)	maternal	menopause_menstrual_onset
PPARG_ENSG00000132170	PPARG	PMID: 24046805; PMID: 25549360 ; PMID: 25264875	maternal; maternal/fetal; maternal/integrated snp/gene expression analysis	placental_abruption; preterm_birth
PRG2_ENSG00000186652	PRG2	PMID: 21865357	circulating protein levels/maternal/fetal	preeclampsia
PRIM1_ENSG00000198056	PRIM1	PMID: 22267201 (EBI)	maternal	menopause_menstrual_onset
PRKCA_ENSG00000154229	PRKCA	PMID: 24046805	maternal	placental_abruption
PROZ_ENSG00000126231	PROZ	PMID: 27842992	maternal/metaanalysis	miscarriage
PRRC2A_ENSG00000204469	PRRC2A	PMID: 22267201 (EBI); PMID: 23307926 (EBI)	maternal	menopause_menstrual_onset
PSG11_ENSG00000243130	PSG11	PMID: 22748001	maternal	preeclampsia
PSG4_ENSG00000243137	PSG4	PMID: 16125225	mrna expression/fetal	fetal_growth_restriction
PSG9_ENSG00000183668	PSG11	PMID: 22748001	maternal	preeclampsia
PTCH1_ENSG00000185920	PTCH1	PMID: 27680694	fetal	birth_weight
PTGDR_ENSG00000168229	AS1	PMID: 24045676 (EBI)	maternal	menopause_menstrual_onset
PXDN_ENSG00000130508	PRG2	PMID: 21865357	circulating protein levels/maternal/fetal	preeclampsia
RAP2C_ENSG00000123728	RAP2C	PMID: 28877031	maternal/assoc. with gestational duration	preterm_birth
RBM43_ENSG00000184898	RBM43	PMID: 23472165 (EBI)	maternal/endometriosis	endometriosis_ovarian
RCAN1_ENSG00000159200	DSCR1	PMID: 16125225	mrna expression/fetal	fetal_growth_restriction
RDH13_ENSG00000160439	RDH13	PMID: 23874842	meta-analysis/fetal	preeclampsia
RHBDL2_ENSG00000158315	RHBDL2	PMID: 22267201 (EBI)	maternal	menopause_menstrual_onset
RHOU_ENSG00000116574	RHOU	PMID: 20844546 (EBI)	maternal/endometriosis	endometriosis_ovarian
RNASET2_ENSG00000026297	RNASET2	PMID: 25599974 (EBI)	maternal	preterm_birth

RND3_ENSG00000115963	RND3	PMID: 23472165 (EBI)	maternal/endometriosis	endometriosis_ovarian
RNF144B_ENSG00000137393	RNF144B	PMID: 23472165 (EBI)	maternal/endometriosis	endometriosis_ovarian
RNF44_ENSG00000146083	RNF44	PMID: 22267201 (EBI)	maternal	menopause_menstrual_onset
RTN4RL1_ENSG00000185924	RTN4RL1	PMID: 27453397	maternal	endometriosis_ovarian
SASH1_ENSG00000111961	SASH1	PMID: 23874842	meta-analysis/fetal	preeclampsia
SCN2B_ENSG00000149575	SCN2B	PMID: 23551011 (EBI)	maternal	preeclampsia
SCN4B_ENSG00000177098	SCN4B	PMID: 23551011 (EBI)	maternal	preeclampsia
SEMA4C_ENSG00000168758	SEMA4C	PMID: 23874842	meta-analysis/fetal	preeclampsia
SERPINE1_ENSG00000106366	SERPINE1	PMID: 27842992; PMID: 21429808 (EBI); PMID: 26010865	maternal/metaanalysis; candidate gene approach/maternal; regulator/target of susceptibility gene ided in 2014 paper/maternal	miscarriage; preeclampsia
SFR1_ENSG00000156384	SFR1	PMID: 23551011 (EBI)	maternal	preeclampsia
SGIP1_ENSG00000118473	SGIP1	PMID: 23307926 (EBI)	maternal	menopause_menstrual_onset
SIGLEC6_ENSG00000105492	SIGLEC6	PMID: 23089140; PMID: 23874842	fetal; meta-analysis/fetal	gtd_hydatidiform-mole; preeclampsia
SLC2A4_ENSG00000181856	SLC2A4	PMID: 23202124 (EBI)	fetal	birth_weight
SLC44A4_ENSG00000204385	SLC44A4	PMID: 19448619 (EBI)	maternal	menopause_menstrual_onset
SLCO2A1_ENSG00000174640	SLCO2A1	PMID: 23874842	meta-analysis/fetal	preeclampsia
SMAD2_ENSG00000175387	SMAD2	PMID: 23205182	maternal	placental_abruption
SMAD9_ENSG00000120693	SMAD9	PMID: 25599974 (EBI)	maternal	preterm_birth
SOD1_ENSG00000142168	SOD1	PMID: 23874842	meta-analysis/fetal	preeclampsia
SORCS1_ENSG00000108018	SORCS1	PMID: 23472165 (EBI)	maternal/endometriosis	endometriosis_ovarian
SORL1_ENSG00000137642	SORL1	PMID: 25599974 (EBI)	maternal	preterm_birth
SPAG4_ENSG00000061656	SPAG4	PMID: 23874842	meta-analysis/fetal	preeclampsia
SPP1_ENSG00000118785	SPP1	PMID: 23874842	meta-analysis/fetal	preeclampsia
STAT1_ENSG00000115415	STAT1	PMID: 25264875	maternal/assoc with pprom, integrated snp/gene expression analysis	preterm_birth
STC2_ENSG00000113739	STC2	PMID: 25533459	fetal	fetal_growth_restriction
STOX1_ENSG00000165730	STOX1	Preeclampsia/eclampsia 4 - OMIM	maternal	preeclampsia
SYCP2L_ENSG00000153157	SYCP2L	PMID: 19448621 (EBI); PMID: 22267201 (EBI)	maternal	menopause_menstrual_onset
SYCP3_ENSG00000139351	RPRGL4; SPGF4; COR1; SYCP3; SCP3	Pregnancy loss, recurrent, 4 - OMIM	maternal	miscarriage
SYNE1_ENSG00000131018	SYNE1	PMID: 28537267 (EBI)	maternal/endometriosis	endometriosis_ovarian
TDRD3_ENSG00000083544	TDRD3	PMID: 22267201 (EBI)	maternal	menopause_menstrual_onset
TEK_ENSG00000120156	TIE2	PMID: 16458662	fetal	placenta_accreta
TENM3_ENSG00000218336	TENM3	PMID: 23551011 (EBI)	maternal	preeclampsia
TGFB1_ENSG00000105329	TGFB1	PMID: 26010865	regulator/target of susceptibility gene ided in 2014 paper/maternal	preeclampsia
TGFBRAP1_ENSG00000135966	TGFBRAP1	PMID: 23551011 (EBI)	maternal	preeclampsia
THRB_ENSG00000151090	THRB	PMID: 24046805; PMID: 25549360	maternal; fetal	placental_abruption
TIMP2_ENSG00000035862	TIMP2	PMID: 26715857	maternal/candidate gene approach	preterm_birth
TIMP3_ENSG00000100234	TIMP3	PMID: 20442742; PMID: 23172037	hypomethylation/fetal	preeclampsia
TLE4_ENSG00000106829	TLE4	PMID: 19448619 (EBI)	maternal	menopause_menstrual_onset
TLK1_ENSG00000198586	TLK1	PMID: 22267201 (EBI)	maternal	menopause_menstrual_onset
TMEM150B_ENSG00000180061	TMEM150B; TMEM224	PMID: 22267201 (EBI); PMID: 19448619 (EBI); PMID: 23307926 (EBI)	maternal	menopause_menstrual_onset
TNFRSF1A_ENSG00000067182	TNFRSF1A	PMID: 25549360	fetal	placental_abruption
TNFSF10_ENSG00000121858	TNFSF10	PMID: 23874842	meta-analysis/fetal	preeclampsia
TNF_ENSG00000232810	TNF	PMID: 27842992; PMID: 21429808 (EBI); PMID: 23316964	maternal/metaanalysis; candidate gene approach/maternal; fetal	miscarriage; preeclampsia
TREM1_ENSG00000124731	TREM1	PMID: 23874842	meta-analysis/fetal	preeclampsia

TRMT6_ENSG00000089195	TRMT6	PMID: 19448621 (EBI)	maternal	menopause_menstrual_onset
TTC39B_ENSG00000155158	TTC39B	PMID: 27453397	maternal	endometriosis_ovarian
TUNAR_ENSG00000250366	TUNAR	PMID: 28333195 (EBI)	maternal/deep ovarian and/or rectovaginal disease with dense adhesions	endometriosis_ovarian
UIMC1_ENSG00000087206	UIMC1	PMID: 19448621 (EBI); PMID: 22267201 (EBI)	maternal/age at menarche; maternal	menopause_menstrual_onset
VEGFA_ENSG00000112715	VEGFA ; VEGF ; VEGFA	PMID: 27842992; PMID: 16310040 ; PMID: 21429808 (EBI); PMID: 26010865; PMID: 23874842	maternal/metaanalysis; fetal; candidate gene approach/maternal; meta-analysis/fetal; regulator/target of susceptibility gene ided in 2014 paper/maternal	miscarriage; placenta_accreta; preeclampsia
VEZT_ENSG00000028203	VEZT	PMID: 23104006 (EBI); PMID: 28537267 (EBI); PMID: 23472165 (EBI) ; PMID: 24676469	maternal; maternal/endometriosis	endometriosis_ovarian
VIM_ENSG00000026025	VIM	PMID: 23874842	meta-analysis/fetal	preeclampsia
WNT4_ENSG00000162552	WNT4	PMID: 23472166 (EBI); PMID: 21151130 (EBI); PMID: 28333195 (EBI); PMID: 28537267 (EBI); PMID: 24676469; PMID: 23472165 (EBI) ; PMID: 28877031	maternal/deep ovarian and/or rectovaginal disease with dense adhesions; maternal; maternal/endometriosis; maternal/assoc. with gestational duration	endometriosis_ovarian; preterm_birth
WWTR1_ENSG00000018408	WWTR1	PMID: 23551011 (EBI)	maternal	preeclampsia
YKT6_ENSG00000106636	YKT6	PMID: 27680694	fetal	birth_weight
ZBTB40_ENSG00000184677	ZBTB40	PMID: 23472165 (EBI)	maternal/endometriosis	endometriosis_ovarian
ZBTB7A_ENSG00000178951	FBI1	PMID: 26093985	fetal/mrna expression	gtd_hydatidiform-mole
ZBTB7B_ENSG00000160685	ZBTB7B	PMID: 27680694	fetal	birth_weight
ZNF295-AS1_ENSG00000237232	ZNF295-AS1	PMID: 23551011 (EBI)	maternal	preeclampsia
ZNF300_ENSG00000145908	ZNF300	PMID: 27330572	fetal, methylation	fetal_growth_restriction
ZNRF3_ENSG00000183579	ZNRF3	PMID: 25549360	fetal	placental_abruption

Appendix 7 - CyTOF validation of decidual NK and T cell subsets in maternal decidua from Donors 2 and 10:

(a) t-SNE plots show protein expression of dNK and ILC markers on live cells gated on $CD45^{+}CD56^{+}CD14^{-}HLA\text{-}DR^{-}CD3^{-}$ events from maternal decidua (Donors 2 and 10). **(b)** t-SNE plots showing protein expression of T cell markers on live cells gated on $CD45^{+}CD3^{+}CD14^{-}HLA\text{-}DR^{-}CD56^{-}$ events from Donor 3 maternal decidua (Donors 2 and 10).

Appendix 8 - Genes upregulated in maternal mononuclear phagocyte subsets relative to all other cell types at the maternal-fetal interface (log_2(fold-change) ≥ 0.5, adjusted *p* < 0.05):

Gene ID/Ensembl ID	p value	log2(fold change)	pct.1	pct.2	adjusted p value	cluster
APOC1_ENSG00000130208	0	3.474628312	0.984	0.396	0	pIMP
SPP1_ENSG00000118785	2.12E-212	2.939855199	0.954	0.404	5.32E-208	pIMP
APOE_ENSG00000130203	1.34E-210	2.565089336	0.961	0.618	3.37E-206	pIMP
FTL_ENSG00000087086	6.48E-256	2.403379017	1	0.994	1.63E-251	pIMP
FABP5_ENSG00000164687	2.89E-274	2.31287541	0.977	0.381	7.24E-270	pIMP
CTSD_ENSG00000117984	6.44E-246	1.982533089	0.995	0.789	1.61E-241	pIMP
CD68_ENSG00000129226	0	1.917236032	1	0.335	0	pIMP
TREM2_ENSG00000095970	0	1.883612334	0.961	0.108	0	pIMP
GCHFR_ENSG00000137880	0	1.844221269	0.88	0.166	0	pIMP
CSTB_ENSG00000160213	1.88E-231	1.807923324	0.998	0.76	4.72E-227	pIMP
GPNMB_ENSG00000136235	0	1.801323615	0.963	0.27	0	pIMP
CD9_ENSG00000010278	0	1.712729073	0.988	0.32	0	pIMP
GPX1_ENSG00000233276	1.51E-247	1.667258038	1	0.735	3.80E-243	pIMP
CTSB_ENSG00000164733	8.76E-232	1.648652025	0.993	0.687	2.20E-227	pIMP
PSAP_ENSG00000197746	4.53E-243	1.618523523	1	0.839	1.14E-238	pIMP
GRN_ENSG00000030582	8.92E-240	1.617299643	0.995	0.617	2.24E-235	pIMP
HLA-DRA_ENSG00000204287	5.39E-264	1.597306072	1	0.365	1.35E-259	pIMP
LYZ_ENSG00000090382	0	1.580091579	0.949	0.156	0	pIMP
SDS_ENSG00000135094	0	1.569110072	0.831	0.035	0	pIMP
LIPA_ENSG00000107798	2.09E-298	1.53167195	0.961	0.325	5.24E-294	pIMP
HLA-DPB1_ENSG00000223865	3.42E-276	1.484424551	0.998	0.324	8.58E-272	pIMP
ACP5_ENSG00000102575	4.35E-272	1.474577238	0.905	0.264	1.09E-267	pIMP
CD74_ENSG00000019582	7.12E-221	1.452318047	1	0.5	1.78E-216	pIMP
HLA-DPA1_ENSG00000231389	2.31E-288	1.421232223	0.995	0.3	5.81E-284	pIMP
HLA-DRB1_ENSG00000196126	0	1.42054236	0.995	0.244	0	pIMP
NPC2_ENSG00000119655	3.68E-229	1.388666837	1	0.761	9.24E-225	pIMP
HLA-DQB1_ENSG00000179344	0	1.372421009	0.963	0.165	0	pIMP
CYBA_ENSG00000051523	3.71E-221	1.372395588	1	0.651	9.32E-217	pIMP
CTSS_ENSG00000163131	1.95E-276	1.36278302	0.963	0.292	4.88E-272	pIMP
CHI3L1_ENSG00000133048	0	1.347135645	0.389	0.029	0	pIMP
IL1RN_ENSG00000136689	2.11E-241	1.3323977	0.465	0.063	5.28E-237	pIMP
CTSZ_ENSG00000101160	2.67E-289	1.328343999	0.963	0.311	6.70E-285	pIMP
S100A8_ENSG00000143546	0	1.323439766	0.766	0.07	0	pIMP
HLA-DMA_ENSG00000204257	0	1.311537574	0.933	0.18	0	pIMP
SPI1_ENSG00000066336	0	1.279694948	0.965	0.12	0	pIMP
PLAUR_ENSG00000011422	4.95E-248	1.272093049	0.94	0.321	1.24E-243	pIMP
C15orf48_ENSG00000166920	2.44E-285	1.259864305	0.894	0.209	6.13E-281	pIMP
HLA-DRB5_ENSG00000198502	0	1.255916102	0.998	0.19	0	pIMP
TYMP_ENSG00000025708	1.87E-227	1.255349313	0.977	0.445	4.70E-223	pIMP
LAPTM5_ENSG00000162511	9.35E-238	1.23825525	0.998	0.427	2.34E-233	pIMP
CAPG_ENSG00000042493	5.49E-206	1.228204723	0.995	0.474	1.38E-201	pIMP
ATP6V1F_ENSG00000128524	7.70E-226	1.225944363	0.998	0.7	1.93E-221	pIMP
S100A11_ENSG00000163191	8.02E-211	1.225921077	1	0.91	2.01E-206	pIMP
TSPO_ENSG00000100300	8.48E-227	1.211278564	0.993	0.589	2.13E-222	pIMP
FTH1_ENSG00000167996	7.55E-213	1.211201938	1	0.999	1.89E-208	pIMP
FBP1_ENSG00000165140	0	1.203672919	0.794	0.044	0	pIMP
HLA-DMB_ENSG00000242574	0	1.1890504	0.836	0.139	0	pIMP
HAMP_ENSG00000105697	0	1.185889254	0.653	0.044	0	pIMP
CD36_ENSG00000135218	0	1.167271163	0.829	0.089	0	pIMP
BRI3_ENSG00000164713	1.66E-237	1.156980145	0.984	0.451	4.17E-233	pIMP
ASAH1_ENSG00000104763	1.33E-206	1.144976798	0.988	0.52	3.34E-202	pIMP
LGMN_ENSG00000100600	1.15E-186	1.143711506	0.887	0.316	2.88E-182	pIMP

LTA4H_ENSG00000111144	2.49E-277	1.143042825	0.843	0.224	6.24E-273	pIMP
HLA-DQA1_ENSG00000196735	0	1.127538223	0.891	0.128	0	pIMP
OLR1_ENSG00000173391	0	1.11730615	0.926	0.149	0	pIMP
ITGB2_ENSG00000160255	9.01E-253	1.111725	0.979	0.294	2.26E-248	pIMP
LINC01272_ENSG00000224397	0	1.098740184	0.766	0.03	0	pIMP
CYP27A1_ENSG00000135929	0	1.087753219	0.734	0.048	0	pIMP
IFI30_ENSG00000216490	0	1.078619593	0.87	0.072	0	pIMP
VIM_ENSG00000026025	1.33E-142	1.055035923	1	0.821	3.34E-138	pIMP
HMOX1_ENSG00000100292	0	1.052134008	0.926	0.184	0	pIMP
SGK1_ENSG00000118515	6.11E-267	1.049580569	0.921	0.244	1.53E-262	pIMP
GSTO1_ENSG00000148834	4.23E-191	1.047374942	0.975	0.562	1.06E-186	pIMP
TYROBP_ENSG00000011600	2.88E-172	1.043126007	1	0.501	7.23E-168	pIMP
S100A10_ENSG00000197747	6.65E-162	1.032044056	1	0.517	1.67E-157	pIMP
LGALS3_ENSG00000131981	2.62E-132	1.028114848	0.984	0.61	6.56E-128	pIMP
PLD3_ENSG00000105223	1.52E-114	1.026271203	0.896	0.539	3.81E-110	pIMP
MS4A7_ENSG00000166927	0	1.026230796	0.928	0.111	0	pIMP
AIF1_ENSG00000204472	2.69E-303	1.018541371	0.986	0.229	6.75E-299	pIMP
S100A9_ENSG00000163220	0	1.010621421	0.88	0.2	0	pIMP
NCF2_ENSG00000116701	0	0.99913223	0.796	0.044	0	pIMP
LPL_ENSG00000175445	0	0.998594886	0.641	0.022	0	pIMP
ATP6V0B_ENSG00000117410	5.40E-182	0.994190143	0.984	0.634	1.36E-177	pIMP
CXCL16_ENSG00000161921	0	0.993395831	0.873	0.124	0	pIMP
HLA-DQA2_ENSG00000237541	0	0.984065959	0.843	0.097	0	pIMP
MSR1_ENSG00000038945	0	0.96032345	0.748	0.073	0	pIMP
SERPINA1_ENSG00000197249	0	0.952198443	0.831	0.076	0	pIMP
DBI_ENSG00000155368	6.11E-167	0.934957247	0.986	0.743	1.53E-162	pIMP
SLC7A7_ENSG00000155465	0	0.930056105	0.824	0.074	0	pIMP
PLA2G7_ENSG00000146070	2.42E-183	0.926454483	0.669	0.17	6.06E-179	pIMP
SH3BGRL3_ENSG00000142669	6.15E-126	0.917158193	1	0.905	1.54E-121	pIMP
LILRB4_ENSG00000186818	0	0.902156865	0.787	0.053	0	pIMP
SLC11A1_ENSG00000018280	0	0.902010684	0.766	0.062	0	pIMP
PRDX1_ENSG00000117450	2.85E-149	0.894965201	0.991	0.642	7.16E-145	pIMP
C1orf162_ENSG00000143110	2.89E-284	0.887552703	0.905	0.191	7.24E-280	pIMP
ATP6V0D1_ENSG00000159720	8.07E-162	0.884479615	0.912	0.437	2.02E-157	pIMP
MNDA_ENSG00000163563	0	0.87684512	0.794	0.073	0	pIMP
PDXK_ENSG00000160209	5.33E-279	0.874387038	0.81	0.185	1.34E-274	pIMP
LY96_ENSG00000154589	0	0.865143976	0.907	0.151	0	pIMP
MMP9_ENSG00000100985	0	0.856529741	0.292	0.019	0	pIMP
LST1_ENSG00000204482	0	0.851932896	0.914	0.147	0	pIMP
MAFB_ENSG00000204103	0	0.846339285	0.896	0.173	0	pIMP
CTSH_ENSG00000103811	6.25E-179	0.83996661	0.91	0.328	1.57E-174	pIMP
C5AR1_ENSG00000197405	0	0.838940696	0.794	0.076	0	pIMP
PPT1_ENSG00000131238	7.04E-172	0.838383906	0.903	0.367	1.77E-167	pIMP
ALOX5AP_ENSG00000132965	1.17E-138	0.832886959	0.78	0.248	2.93E-134	pIMP
LAIR1_ENSG00000167613	0	0.817988356	0.845	0.098	0	pIMP
GLUL_ENSG00000135821	5.49E-133	0.816288599	0.984	0.644	1.38E-128	pIMP
LY86_ENSG00000112799	0	0.808852694	0.796	0.088	0	pIMP
CSTA_ENSG00000121552	0	0.808774673	0.766	0.11	0	pIMP
DNASE2_ENSG00000105612	6.16E-164	0.796724422	0.812	0.283	1.55E-159	pIMP
FCGRT_ENSG00000104870	1.75E-158	0.795943565	0.975	0.498	4.38E-154	pIMP
H2AFY_ENSG00000113648	5.18E-148	0.794733463	0.951	0.535	1.30E-143	pIMP
VAMP8_ENSG00000118640	1.35E-140	0.788005618	0.988	0.546	3.39E-136	pIMP
SYNGR2_ENSG00000108639	7.63E-184	0.786549682	0.924	0.324	1.91E-179	pIMP
AP2S1_ENSG00000042753	3.00E-141	0.781619189	0.979	0.657	7.53E-137	pIMP
ALDH2_ENSG00000111275	1.80E-165	0.774030651	0.725	0.218	4.51E-161	pIMP
FCGR3A_ENSG00000203747	0	0.771741109	0.824	0.112	0	pIMP
CCL2_ENSG00000108691	1.06E-14	0.76718962	0.299	0.163	2.66E-10	pIMP
IL4I1_ENSG00000104951	0	0.761747886	0.593	0.034	0	pIMP
ARPC1B_ENSG00000130429	1.97E-137	0.759918922	0.991	0.745	4.95E-133	pIMP
BLVRB_ENSG00000090013	3.05E-170	0.756715535	0.933	0.403	7.65E-166	pIMP

LSP1_ENSG00000130592	2.14E-120	0.750117631	0.981	0.513	5.38E-116	pIMP
ANXA2_ENSG00000182718	4.11E-110	0.747528151	0.998	0.81	1.03E-105	pIMP
CPM_ENSG00000135678	0	0.744760299	0.664	0.095	0	pIMP
PYCARD_ENSG00000103490	2.54E-161	0.743057271	0.889	0.308	6.36E-157	pIMP
UCP2_ENSG00000175567	1.72E-190	0.742283313	0.877	0.242	4.32E-186	pIMP
MS4A6A_ENSG00000110077	5.72E-212	0.739019454	0.694	0.14	1.44E-207	pIMP
PLXDC2_ENSG00000120594	0	0.736168944	0.773	0.088	0	pIMP
OAZ1_ENSG00000104904	3.76E-185	0.73561062	1	0.958	9.43E-181	pIMP
SMCO4_ENSG00000166002	0	0.73410519	0.757	0.103	0	pIMP
RNF130_ENSG00000113269	7.30E-156	0.733048997	0.921	0.377	1.83E-151	pIMP
CREG1_ENSG00000143162	2.76E-192	0.731282877	0.866	0.274	6.92E-188	pIMP
ATP6V1B2_ENSG00000147416	2.94E-175	0.729455165	0.794	0.257	7.38E-171	pIMP
NOP10_ENSG00000182117	6.57E-121	0.727320533	0.984	0.721	1.65E-116	pIMP
PLIN2_ENSG00000147872	3.32E-105	0.720558476	0.912	0.484	8.32E-101	pIMP
CHCHD10_ENSG00000250479	1.23E-113	0.720390944	0.919	0.497	3.08E-109	pIMP
RETN_ENSG00000104918	0	0.719237022	0.37	0.026	0	pIMP
RNASET2_ENSG00000026297	1.59E-166	0.717280917	0.928	0.334	3.98E-162	pIMP
SAT1_ENSG00000130066	1.49E-106	0.711347248	1	0.85	3.73E-102	pIMP
NPL_ENSG00000135838	0	0.708675357	0.799	0.126	0	pIMP
RP11-1143G9.4_ENSG00000257764	0	0.707840228	0.53	0.055	0	pIMP
MARCO_ENSG00000019169	0	0.703958701	0.539	0.019	0	pIMP
FN1_ENSG00000115414	1.57E-127	0.703632729	0.861	0.365	3.94E-123	pIMP
TGFBI_ENSG00000120708	8.82E-155	0.700749958	0.852	0.291	2.21E-150	pIMP
BCL2A1_ENSG00000140379	0	0.700008122	0.66	0.095	0	pIMP
SDSL_ENSG00000139410	0	0.695424634	0.708	0.103	0	pIMP
LIMS1_ENSG00000169756	5.40E-125	0.693831734	0.868	0.386	1.35E-120	pIMP
SQRDL_ENSG00000137767	4.36E-266	0.691716526	0.789	0.166	1.09E-261	pIMP
LGALS9_ENSG00000168961	5.53E-177	0.6867502	0.898	0.291	1.39E-172	pIMP
CCL18_ENSG00000275385	0	0.679249888	0.257	0.007	0	pIMP
YBX1_ENSG00000065978	5.02E-120	0.677861199	1	0.908	1.26E-115	pIMP
FAM195A_ENSG00000172366	8.18E-222	0.666987108	0.764	0.184	2.05E-217	pIMP
FUOM_ENSG00000148803	0	0.666220708	0.734	0.096	0	pIMP
ATOX1_ENSG00000177556	1.01E-109	0.665648586	0.942	0.569	2.53E-105	pIMP
MFSD1_ENSG00000118855	5.48E-191	0.663584794	0.838	0.251	1.38E-186	pIMP
CPVL_ENSG00000106066	1.90E-188	0.661502258	0.743	0.183	4.76E-184	pIMP
MMP7_ENSG00000137673	1.96E-265	0.659295463	0.176	0.008	4.91E-261	pIMP
FCGR1A_ENSG00000150337	0	0.655209102	0.63	0.065	0	pIMP
CCDC88A_ENSG00000115355	0	0.650865834	0.715	0.121	0	pIMP
HEXB_ENSG00000049860	4.07E-134	0.648908959	0.931	0.428	1.02E-129	pIMP
PKM_ENSG00000067225	6.94E-92	0.647726875	0.968	0.688	1.74E-87	pIMP
AKR1A1_ENSG00000117448	1.33E-120	0.647113102	0.868	0.426	3.34E-116	pIMP
CD52_ENSG00000169442	1.19E-97	0.643645036	0.903	0.386	2.99E-93	pIMP
CTSL_ENSG00000135047	1.47E-93	0.641274183	0.961	0.563	3.69E-89	pIMP
GPX4_ENSG00000167468	1.68E-117	0.640113125	1	0.808	4.22E-113	pIMP
HMGA1_ENSG00000137309	9.56E-158	0.636357612	0.854	0.26	2.40E-153	pIMP
FABP4_ENSG00000170323	7.74E-192	0.632838531	0.204	0.015	1.94E-187	pIMP
IGSF6_ENSG00000140749	0	0.630600046	0.588	0.073	0	pIMP
SAMHD1_ENSG00000101347	7.36E-237	0.629483526	0.81	0.175	1.85E-232	pIMP
SCARB2_ENSG00000138760	4.55E-137	0.627015377	0.764	0.276	1.14E-132	pIMP
ALCAM_ENSG00000170017	0	0.625966933	0.609	0.05	0	pIMP
MS4A4A_ENSG00000110079	0	0.62540035	0.75	0.093	0	pIMP
LACTB_ENSG00000103642	9.92E-256	0.625286011	0.729	0.151	2.49E-251	pIMP
RMDN3_ENSG00000137824	7.65E-146	0.624688555	0.637	0.187	1.92E-141	pIMP
RGS10_ENSG00000148908	9.23E-139	0.620102937	0.887	0.344	2.32E-134	pIMP
ARRB2_ENSG00000141480	2.88E-223	0.615539453	0.831	0.19	7.23E-219	pIMP
MPP1_ENSG00000130830	1.84E-197	0.612624874	0.806	0.205	4.62E-193	pIMP
RNASE6_ENSG00000169413	2.10E-272	0.609210663	0.692	0.111	5.27E-268	pIMP
SNX10_ENSG00000086300	1.06E-112	0.606464559	0.785	0.315	2.67E-108	pIMP
APOC2_ENSG00000234906	1.00E-149	0.603627611	0.273	0.035	2.52E-145	pIMP
ARPC3_ENSG00000111229	2.14E-125	0.592200846	0.995	0.874	5.37E-121	pIMP

ADAP2_ENSG00000184060	0	0.589555015	0.734	0.097	0	pIMP
YWHAH_ENSG00000128245	1.90E-95	0.587725648	0.919	0.515	4.76E-91	pIMP
CECR1_ENSG00000093072	0	0.584657904	0.639	0.087	0	pIMP
RENBP_ENSG00000102032	0	0.578296373	0.66	0.059	0	pIMP
HN1_ENSG00000189159	3.87E-93	0.577760774	0.894	0.46	9.70E-89	pIMP
CLEC7A_ENSG00000172243	0	0.577137875	0.669	0.088	0	pIMP
GRB2_ENSG00000177885	3.94E-117	0.572195322	0.873	0.382	9.88E-113	pIMP
SLC16A3_ENSG00000141526	2.03E-125	0.570760248	0.907	0.365	5.08E-121	pIMP
TNFSF13B_ENSG00000102524	0	0.567061445	0.66	0.072	0	pIMP
TM4SF19_ENSG00000145107	0	0.562945196	0.324	0.002	0	pIMP
EMP3_ENSG00000142227	2.34E-46	0.561293743	0.949	0.664	5.87E-42	pIMP
FCER1G_ENSG00000158869	7.71E-71	0.560220414	0.995	0.484	1.93E-66	pIMP
ST14_ENSG00000149418	0	0.558284987	0.625	0.062	0	pIMP
FPR3_ENSG00000187474	0	0.557333095	0.616	0.049	0	pIMP
PLEK_ENSG00000115956	7.36E-203	0.551065352	0.773	0.165	1.85E-198	pIMP
S100A4_ENSG00000196154	4.78E-53	0.548376759	0.995	0.835	1.20E-48	pIMP
SLC25A5_ENSG00000005022	5.54E-83	0.544908603	0.961	0.695	1.39E-78	pIMP
HM13_ENSG00000101294	5.44E-71	0.542144484	0.85	0.504	1.36E-66	pIMP
FERMT3_ENSG00000149781	3.77E-164	0.540564859	0.769	0.205	9.46E-160	pIMP
GM2A_ENSG00000196743	9.64E-202	0.539444417	0.623	0.126	2.42E-197	pIMP
CD84_ENSG00000066294	0	0.534237836	0.625	0.045	0	pIMP
DNPH1_ENSG00000112667	8.74E-93	0.533456155	0.766	0.348	2.19E-88	pIMP
TWF2_ENSG00000247596	5.49E-117	0.5317722	0.812	0.326	1.38E-112	pIMP
CD81_ENSG00000110651	9.15E-92	0.52863427	0.852	0.403	2.29E-87	pIMP
EFHD2_ENSG00000142634	1.94E-127	0.528603887	0.789	0.272	4.87E-123	pIMP
MGLL_ENSG00000074416	6.33E-98	0.526829372	0.593	0.2	1.59E-93	pIMP
FAM96A_ENSG00000166797	6.09E-110	0.52364128	0.831	0.353	1.53E-105	pIMP
M6PR_ENSG00000003056	1.27E-101	0.519737428	0.815	0.36	3.19E-97	pIMP
SDCBP_ENSG00000137575	2.21E-63	0.519150865	0.988	0.726	5.55E-59	pIMP
SLC15A3_ENSG00000110446	0	0.517781822	0.62	0.062	0	pIMP
OTOA_ENSG00000155719	0	0.512771923	0.475	0.025	0	pIMP
ME2_ENSG00000082212	1.71E-169	0.511348929	0.65	0.159	4.28E-165	pIMP
NUP214_ENSG00000126883	2.19E-194	0.511287301	0.549	0.104	5.49E-190	pIMP
ATF5_ENSG00000169136	2.35E-179	0.509709794	0.583	0.123	5.89E-175	pIMP
HNMT_ENSG00000150540	2.29E-116	0.509051201	0.826	0.33	5.74E-112	pIMP
USF2_ENSG00000105698	1.59E-161	0.508879795	0.741	0.21	3.98E-157	pIMP
RGS2_ENSG00000116741	3.96E-65	0.506986741	0.762	0.363	9.92E-61	pIMP
MARCKS_ENSG00000277443	4.36E-85	0.505558929	0.859	0.402	1.09E-80	pIMP
CD63_ENSG00000135404	2.28E-78	0.504503952	1	0.959	5.71E-74	pIMP
IL18_ENSG00000150782	0	0.504234032	0.6	0.078	0	pIMP
C3AR1_ENSG00000171860	0	0.503990903	0.632	0.073	0	pIMP
CST6_ENSG00000175315	3.30E-247	0.503627039	0.41	0.047	8.27E-243	pIMP
CORO1C_ENSG00000110880	1.49E-117	0.501988536	0.743	0.274	3.75E-113	pIMP
GNB4_ENSG00000114450	5.43E-242	0.501841489	0.664	0.124	1.36E-237	pIMP
BLOC1S1_ENSG00000135441	5.92E-80	0.501035537	0.938	0.622	1.48E-75	pIMP
C1QA_ENSG00000173372	0	3.24151265	0.999	0.227	0	dMP2
C1QC_ENSG00000159189	0	3.16302791	1	0.157	0	dMP2
C1QB_ENSG00000173369	0	3.15122934	1	0.198	0	dMP2
RNASE1_ENSG00000129538	0	3.024758896	0.982	0.29	0	dMP2
CD74_ENSG00000019582	0	2.774901599	1	0.478	0	dMP2
CD14_ENSG00000170458	0	2.639914304	0.976	0.168	0	dMP2
HLA-DRB5_ENSG00000198502	0	2.478885991	0.973	0.155	0	dMP2
HLA-DRA_ENSG00000204287	0	2.462895081	0.997	0.337	0	dMP2
AIF1_ENSG00000204472	0	2.461597705	0.995	0.195	0	dMP2
FOLR2_ENSG00000165457	0	2.313737909	0.927	0.084	0	dMP2
HLA-DPA1_ENSG00000231389	0	2.245462909	0.981	0.27	0	dMP2
MS4A6A_ENSG00000110077	0	2.239257868	0.94	0.101	0	dMP2
SEPP1_ENSG00000250722	0	2.175239076	0.943	0.551	0	dMP2
HLA-DRB1_ENSG00000196126	0	2.151967145	0.977	0.212	0	dMP2
HLA-DPB1_ENSG00000223865	0	2.08620883	0.979	0.295	0	dMP2

HSPA1A_ENSG00000204389	0	2.026854323	0.937	0.405	0	dMP2
MS4A7_ENSG00000166927	0	1.868642506	0.815	0.081	0	dMP2
STAB1_ENSG00000010327	0	1.864780156	0.789	0.086	0	dMP2
CCL4L2_ENSG00000276070	0	1.814583551	0.778	0.231	0	dMP2
CCL3L3_ENSG00000276085	0	1.802098806	0.818	0.175	0	dMP2
CYBA_ENSG00000051523	0	1.727117843	0.992	0.635	0	dMP2
HSPA1B_ENSG00000204388	0	1.708641748	0.884	0.374	0	dMP2
HLA-DMA_ENSG00000204257	0	1.701953421	0.821	0.153	0	dMP2
HLA-DQB1_ENSG00000179344	0	1.687763028	0.82	0.137	0	dMP2
CCL2_ENSG00000108691	0	1.684438364	0.497	0.145	0	dMP2
MS4A4A_ENSG00000110079	0	1.662923116	0.721	0.065	0	dMP2
HLA-DQA1_ENSG00000196735	0	1.659157951	0.779	0.1	0	dMP2
CSF1R_ENSG00000182578	0	1.647267235	0.759	0.1	0	dMP2
TREM2_ENSG00000095970	0	1.631193757	0.733	0.083	0	dMP2
FCGRT_ENSG00000104870	0	1.61069762	0.933	0.479	0	dMP2
TMEM176B_ENSG00000106565	0	1.609488848	0.735	0.148	0	dMP2
HLA-DQA2_ENSG00000237541	0	1.596957663	0.708	0.072	0	dMP2
GPR34_ENSG00000171659	0	1.592747648	0.688	0.068	0	dMP2
VSIG4_ENSG00000155659	0	1.585974556	0.676	0.064	0	dMP2
CYBB_ENSG00000165168	0	1.567105889	0.683	0.062	0	dMP2
MAFB_ENSG00000204103	0	1.556650205	0.672	0.153	0	dMP2
NPC2_ENSG00000119655	0	1.554515798	0.992	0.75	0	dMP2
MAF_ENSG00000178573	0	1.534114627	0.74	0.215	0	dMP2
RNASE6_ENSG00000169413	0	1.52733585	0.71	0.084	0	dMP2
FCGR2A_ENSG00000143226	0	1.506355817	0.69	0.082	0	dMP2
RGS10_ENSG00000148908	0	1.503666495	0.815	0.324	0	dMP2
F13A1_ENSG00000124491	0	1.502400748	0.627	0.045	0	dMP2
LY96_ENSG00000154589	0	1.471365902	0.726	0.128	0	dMP2
FCGR3A_ENSG00000203747	0	1.456955285	0.678	0.088	0	dMP2
HLA-DMB_ENSG00000242574	0	1.455485848	0.69	0.117	0	dMP2
LPAR6_ENSG00000139679	0	1.450111931	0.652	0.136	0	dMP2
FTL_ENSG00000087086	0	1.444380814	1	0.993	0	dMP2
CD68_ENSG00000129226	0	1.433221481	0.875	0.312	0	dMP2
SPI1_ENSG00000066336	0	1.402776339	0.711	0.097	0	dMP2
CTSZ_ENSG00000101160	0	1.379740803	0.755	0.293	0	dMP2
GPX1_ENSG00000233276	0	1.370685891	0.987	0.724	0	dMP2
SLCO2B1_ENSG00000137491	0	1.366055173	0.596	0.046	0	dMP2
HAMP_ENSG00000105697	0	1.360471319	0.369	0.033	0	dMP2
LGMN_ENSG00000100600	0	1.356240915	0.71	0.301	0	dMP2
LST1_ENSG00000204482	0	1.341760985	0.718	0.124	0	dMP2
IGSF6_ENSG00000140749	0	1.33835922	0.559	0.052	0	dMP2
PSAP_ENSG00000197746	0	1.329246709	0.992	0.832	0	dMP2
MARCKS_ENSG00000277443	0	1.308048006	0.831	0.383	0	dMP2
A2M_ENSG00000175899	0	1.261791599	0.727	0.229	0	dMP2
KLF2_ENSG00000127528	0	1.257693101	0.602	0.164	0	dMP2
RB1_ENSG00000139687	0	1.256292178	0.586	0.131	0	dMP2
SLC40A1_ENSG00000138449	0	1.247907878	0.769	0.332	0	dMP2
DAB2_ENSG00000153071	0	1.245095046	0.757	0.337	0	dMP2
RNASET2_ENSG00000026297	0	1.235965292	0.75	0.318	0	dMP2
TYROBP_ENSG00000011600	0	1.228587651	0.998	0.478	0	dMP2
PLTP_ENSG00000100979	0	1.220549775	0.578	0.275	0	dMP2
KLF6_ENSG00000067082	0	1.193046758	0.954	0.797	0	dMP2
ADAP2_ENSG00000184060	0	1.187896229	0.535	0.08	0	dMP2
CCL3_ENSG00000277632	0	1.185471226	0.972	0.437	0	dMP2
KCTD12_ENSG00000178695	0	1.182279528	0.588	0.156	0	dMP2
IER5_ENSG00000162783	0	1.177337246	0.584	0.255	0	dMP2
FCGR1A_ENSG00000150337	0	1.160483507	0.5	0.047	0	dMP2
MSR1_ENSG00000038945	0	1.157266276	0.507	0.056	0	dMP2
C3_ENSG00000125730	0	1.155237335	0.611	0.261	0	dMP2
MEF2C_ENSG00000081189	0	1.151767001	0.579	0.128	0	dMP2

LY86_ENSG00000112799	0	1.150726095	0.527	0.072	0	dMP2
CST3_ENSG00000101439	0	1.148610099	1	0.825	0	dMP2
CD163_ENSG00000177575	0	1.139050802	0.504	0.054	0	dMP2
HPGDS_ENSG00000163106	0	1.133056661	0.491	0.035	0	dMP2
SGK1_ENSG00000118515	0	1.125083022	0.609	0.231	0	dMP2
NINJ1_ENSG00000131669	0	1.103647438	0.649	0.319	0	dMP2
MRC1_ENSG00000260314	0	1.082199082	0.446	0.039	0	dMP2
OTUD1_ENSG00000165312	0	1.068607659	0.444	0.121	0	dMP2
ALOX5AP_ENSG00000132965	0	1.059342743	0.668	0.231	0	dMP2
RUNX1_ENSG00000159216	0	1.057344415	0.498	0.126	0	dMP2
DUSP6_ENSG00000139318	0	1.047258488	0.47	0.163	0	dMP2
CD4_ENSG00000010610	0	1.039312676	0.486	0.079	0	dMP2
FCER1G_ENSG00000158869	0	1.026398258	0.993	0.462	0	dMP2
LTC4S_ENSG00000213316	0	1.016681163	0.45	0.083	0	dMP2
CTSS_ENSG00000163131	0	1.015752761	0.703	0.277	0	dMP2
ZFP36L1_ENSG00000185650	0	1.014858663	0.924	0.712	0	dMP2
TMEM176A_ENSG00000002933	0	1.008580114	0.472	0.112	0	dMP2
CD81_ENSG00000110651	0	1.004484594	0.653	0.394	0	dMP2
HMOX1_ENSG00000100292	0	1.003708633	0.528	0.174	0	dMP2
PYCARD_ENSG00000103490	0	0.999991265	0.647	0.295	0	dMP2
FCGBP_ENSG00000275395	0	0.999512877	0.265	0.023	0	dMP2
GRN_ENSG00000030582	0	0.992205505	0.857	0.608	0	dMP2
MNDA_ENSG00000163563	0	0.99166856	0.45	0.06	0	dMP2
YWHAH_ENSG00000128245	5.25E-288	0.98716314	0.697	0.51	1.32E-283	dMP2
C3AR1_ENSG00000171860	0	0.984153447	0.43	0.06	0	dMP2
LAPTM5_ENSG00000162511	0	0.980401364	0.888	0.408	0	dMP2
TTYH3_ENSG00000136295	0	0.960785577	0.417	0.088	0	dMP2
GAL3ST4_ENSG00000197093	0	0.957893008	0.378	0.034	0	dMP2
MPEG1_ENSG00000197629	0	0.956547891	0.405	0.041	0	dMP2
SAT1_ENSG00000130066	0	0.955920327	0.986	0.844	0	dMP2
MFSD1_ENSG00000118855	0	0.949551206	0.536	0.242	0	dMP2
CTSB_ENSG00000164733	0	0.948535424	0.907	0.678	0	dMP2
CD93_ENSG00000125810	0	0.935398686	0.391	0.058	0	dMP2
AP1B1_ENSG00000100280	0	0.928367467	0.465	0.153	0	dMP2
IER3_ENSG00000137331	0	0.914921396	0.761	0.433	0	dMP2
GADD45B_ENSG00000099860	0	0.912732719	0.872	0.704	0	dMP2
GPR183_ENSG00000169508	0	0.908626629	0.577	0.154	0	dMP2
RHOB_ENSG00000143878	2.27E-297	0.902680734	0.819	0.665	5.70E-293	dMP2
CLEC7A_ENSG00000172243	0	0.897493185	0.412	0.077	0	dMP2
TBXAS1_ENSG00000059377	0	0.878922367	0.399	0.057	0	dMP2
FAM26F_ENSG00000188820	0	0.872282539	0.382	0.082	0	dMP2
NEAT1_ENSG00000245532	0	0.866730208	0.953	0.857	0	dMP2
CX3CR1_ENSG00000168329	0	0.860116566	0.297	0.007	0	dMP2
HSPA6_ENSG00000173110	5.29E-288	0.85878606	0.241	0.049	1.33E-283	dMP2
PLAU_ENSG00000122861	1.52E-171	0.854270722	0.402	0.2	3.81E-167	dMP2
BIN1_ENSG00000136717	1.16E-173	0.85234764	0.492	0.301	2.90E-169	dMP2
BMP2K_ENSG00000138756	0	0.848054395	0.381	0.077	0	dMP2
NCF4_ENSG00000100365	0	0.841491973	0.385	0.069	0	dMP2
VMP1_ENSG00000062716	4.84E-156	0.838477022	0.612	0.511	1.21E-151	dMP2
MGAT4A_ENSG00000071073	0	0.837753561	0.446	0.154	0	dMP2
VAMP8_ENSG00000118640	0	0.837473865	0.88	0.532	0	dMP2
HNMT_ENSG00000150540	1.91E-199	0.834998024	0.526	0.325	4.80E-195	dMP2
C6orf62_ENSG00000112308	1.11E-171	0.830661381	0.556	0.398	2.78E-167	dMP2
P2RY13_ENSG00000181631	0	0.828286875	0.278	0.01	0	dMP2
TYMP_ENSG00000025708	3.07E-232	0.825040907	0.646	0.44	7.71E-228	dMP2
PLXDC2_ENSG00000120594	0	0.821551031	0.37	0.08	0	dMP2
LAIR1_ENSG00000167613	0	0.8206194	0.401	0.089	0	dMP2
GAS6_ENSG00000183087	5.42E-198	0.816383293	0.475	0.255	1.36E-193	dMP2
CD83_ENSG00000112149	0	0.812460456	0.479	0.175	0	dMP2
MARCH1_ENSG00000145416	0	0.810977328	0.341	0.036	0	dMP2

RASSF4_ENSG00000107551	0	0.799724155	0.374	0.086	0	dMP2
FPR3_ENSG00000187474	0	0.798209543	0.344	0.039	0	dMP2
CXCL16_ENSG00000161921	0	0.793763487	0.407	0.117	0	dMP2
RGS2_ENSG00000116741	2.79E-164	0.78909855	0.56	0.357	7.00E-160	dMP2
C1orf54_ENSG00000118292	6.51E-275	0.788451684	0.404	0.147	1.63E-270	dMP2
CTSD_ENSG00000117984	0	0.785839995	0.903	0.785	0	dMP2
LILRB4_ENSG00000186818	0	0.784299388	0.352	0.045	0	dMP2
GATM_ENSG00000171766	0	0.781990352	0.325	0.034	0	dMP2
ATP6V0B_ENSG00000117410	7.57E-268	0.777074491	0.745	0.632	1.90E-263	dMP2
SIGLEC1_ENSG00000088827	0	0.768198109	0.304	0.037	0	dMP2
SPRED1_ENSG00000166068	0	0.764179708	0.315	0.058	0	dMP2
C5AR1_ENSG00000197405	0	0.763414895	0.368	0.068	0	dMP2
RAP2B_ENSG00000181467	2.62E-189	0.754346066	0.393	0.18	6.58E-185	dMP2
OLFML3_ENSG00000116774	1.01E-165	0.753971913	0.522	0.315	2.53E-161	dMP2
NAIP_ENSG00000249437	0	0.751599518	0.317	0.049	0	dMP2
FCGR1B_ENSG00000198019	0	0.749934807	0.294	0.019	0	dMP2
CTSH_ENSG00000103811	2.27E-182	0.749051993	0.525	0.324	5.69E-178	dMP2
ARRB2_ENSG00000141480	2.47E-277	0.746516821	0.46	0.182	6.19E-273	dMP2
TRA2B_ENSG00000136527	1.94E-169	0.741036991	0.697	0.645	4.85E-165	dMP2
CD302_ENSG00000241399	1.58E-161	0.729547347	0.356	0.166	3.96E-157	dMP2
OGFRL1_ENSG00000119900	9.51E-297	0.726063241	0.34	0.099	2.38E-292	dMP2
CD86_ENSG00000114013	0	0.724698189	0.331	0.055	0	dMP2
RP11-386I14.4_ENSG00000273338	3.13E-188	0.723423005	0.399	0.173	7.85E-184	dMP2
KLF4_ENSG00000136826	2.33E-179	0.722976299	0.663	0.459	5.83E-175	dMP2
ASAH1_ENSG00000104763	1.56E-146	0.72218963	0.624	0.52	3.90E-142	dMP2
HSPH1_ENSG00000120694	2.69E-79	0.718710281	0.372	0.251	6.75E-75	dMP2
CREG1_ENSG00000143162	1.34E-139	0.717318742	0.448	0.271	3.37E-135	dMP2
HCK_ENSG00000101336	0	0.716943623	0.32	0.048	0	dMP2
RGS1_ENSG00000090104	0	0.715795005	0.891	0.399	0	dMP2
BST2_ENSG00000130303	1.72E-277	0.715190497	0.79	0.508	4.32E-273	dMP2
ARHGAP18_ENSG00000146376	2.56E-205	0.715081329	0.406	0.179	6.42E-201	dMP2
DNAJB1_ENSG00000132002	2.63E-128	0.713487407	0.623	0.53	6.60E-124	dMP2
GYPC_ENSG00000136732	2.53E-152	0.713389585	0.627	0.498	6.34E-148	dMP2
FGL2_ENSG00000127951	0	0.712821403	0.353	0.077	0	dMP2
GMFG_ENSG00000130755	2.05E-273	0.710391817	0.68	0.363	5.14E-269	dMP2
CAPZB_ENSG00000077549	2.95E-280	0.709356164	0.807	0.758	7.39E-276	dMP2
GNAI2_ENSG00000114353	9.93E-160	0.705834138	0.591	0.447	2.49E-155	dMP2
CXCL8_ENSG00000169429	0	0.704690927	0.657	0.295	0	dMP2
PHACTR1_ENSG00000112137	0	0.704597009	0.299	0.069	0	dMP2
ITM2B_ENSG00000136156	0	0.702753237	0.992	0.964	0	dMP2
CH17-373J23.1_ENSG00000276216	2.75E-190	0.701110904	0.317	0.114	6.89E-186	dMP2
CNPY3_ENSG00000137161	3.04E-131	0.70054867	0.508	0.371	7.62E-127	dMP2
C4orf48_ENSG00000243449	2.04E-156	0.700458344	0.566	0.409	5.12E-152	dMP2
CLECL1_ENSG00000184293	0	0.691824927	0.274	0.023	0	dMP2
RP11-480C22.1_ENSG00000273409	0	0.690891638	0.227	0.003	0	dMP2
ITGB2_ENSG00000160255	1.08E-291	0.68905848	0.637	0.283	2.70E-287	dMP2
GIMAP4_ENSG00000133574	6.85E-245	0.684972273	0.39	0.138	1.72E-240	dMP2
PLEK_ENSG00000115956	2.10E-240	0.683245654	0.419	0.158	5.27E-236	dMP2
MGST2_ENSG00000085871	5.96E-173	0.68105625	0.487	0.278	1.49E-168	dMP2
LGALS9_ENSG00000168961	6.95E-171	0.676769563	0.496	0.286	1.74E-166	dMP2
TNFSF13B_ENSG00000102524	0	0.675811204	0.326	0.065	0	dMP2
IFI30_ENSG00000216490	2.83E-303	0.665606858	0.294	0.069	7.10E-299	dMP2
C2_ENSG00000166278	1.07E-115	0.661353302	0.348	0.188	2.67E-111	dMP2
MTSS1_ENSG00000170873	3.17E-275	0.659441282	0.265	0.064	7.94E-271	dMP2
PPT1_ENSG00000131238	1.71E-92	0.659422233	0.468	0.368	4.29E-88	dMP2
FRMD4B_ENSG00000114541	1.54E-204	0.658444057	0.351	0.134	3.86E-200	dMP2
BRI3_ENSG00000164713	7.66E-138	0.658388996	0.578	0.45	1.92E-133	dMP2
CYTH4_ENSG00000100055	1.23E-230	0.657047456	0.391	0.145	3.08E-226	dMP2
NRP1_ENSG00000099250	5.04E-89	0.647001647	0.386	0.255	1.26E-84	dMP2
SYNGR2_ENSG00000108639	2.47E-137	0.64199751	0.497	0.321	6.20E-133	dMP2

QKI_ENSG00000112531	3.16E-93	0.64161907	0.383	0.25	7.92E-89	dMP2
CYFIP1_ENSG00000273749	1.33E-95	0.639560502	0.319	0.18	3.34E-91	dMP2
ZEB2_ENSG00000169554	7.26E-139	0.638107879	0.444	0.253	1.82E-134	dMP2
SAMHD1_ENSG00000101347	3.04E-159	0.633404568	0.372	0.172	7.62E-155	dMP2
CSF2RA_ENSG00000198223	1.28E-183	0.631553282	0.393	0.168	3.20E-179	dMP2
NCKAP1L_ENSG00000123338	5.69E-241	0.618829289	0.338	0.109	1.43E-236	dMP2
SPATS2L_ENSG00000196141	2.19E-70	0.615804213	0.412	0.314	5.48E-66	dMP2
MEF2A_ENSG00000068305	1.71E-97	0.61318911	0.347	0.201	4.29E-93	dMP2
FAM105A_ENSG00000145569	3.98E-161	0.609076901	0.313	0.127	9.99E-157	dMP2
GABARAP_ENSG00000170296	6.95E-76	0.607885307	0.397	0.291	1.74E-71	dMP2
RHOG_ENSG00000177105	8.03E-92	0.603532163	0.511	0.433	2.01E-87	dMP2
NPL_ENSG00000135838	3.42E-170	0.599779843	0.318	0.124	8.59E-166	dMP2
BLVRB_ENSG00000090013	9.43E-112	0.596496391	0.522	0.403	2.36E-107	dMP2
ARHGAP4_ENSG00000089820	4.25E-169	0.593729611	0.333	0.133	1.07E-164	dMP2
TIMP2_ENSG00000035862	2.60E-80	0.592680396	0.453	0.342	6.52E-76	dMP2
SPP1_ENSG00000118785	9.84E-160	0.591263499	0.595	0.4	2.47E-155	dMP2
CD84_ENSG00000066294	0	0.590443784	0.257	0.04	0	dMP2
ARPC3_ENSG00000111229	8.89E-267	0.587979296	0.876	0.876	2.23E-262	dMP2
JUN_ENSG00000177606	3.65E-256	0.585583093	0.975	0.828	9.15E-252	dMP2
RPPH1_ENSG00000259001	3.84E-193	0.584755214	0.191	0.045	9.63E-189	dMP2
UCP2_ENSG00000175567	4.90E-137	0.583781359	0.441	0.239	1.23E-132	dMP2
ADORA3_ENSG00000282608	0	0.580480945	0.215	0.011	0	dMP2
CTSC_ENSG00000109861	9.01E-144	0.577978086	0.749	0.703	2.26E-139	dMP2
CPVL_ENSG00000106066	1.31E-147	0.57731577	0.376	0.179	3.29E-143	dMP2
TUBA1B_ENSG00000123416	7.11E-184	0.573983429	0.845	0.785	1.78E-179	dMP2
USF2_ENSG00000105698	3.57E-75	0.571908621	0.332	0.209	8.97E-71	dMP2
GNB4_ENSG00000114450	6.86E-113	0.570923243	0.271	0.122	1.72E-108	dMP2
ETV5_ENSG00000244405	1.84E-205	0.566811651	0.237	0.065	4.61E-201	dMP2
HIF1A_ENSG00000100644	2.60E-58	0.564941042	0.478	0.425	6.52E-54	dMP2
TPP1_ENSG00000166340	2.32E-60	0.564723883	0.405	0.322	5.81E-56	dMP2
RENBP_ENSG00000102032	1.14E-295	0.564426954	0.257	0.055	2.86E-291	dMP2
MERTK_ENSG00000153208	0	0.564283009	0.215	0.033	0	dMP2
ITGAM_ENSG00000169896	5.19E-198	0.56207737	0.261	0.078	1.30E-193	dMP2
MKNK1_ENSG00000079277	1.79E-90	0.56108636	0.305	0.166	4.49E-86	dMP2
TMEM51_ENSG00000171729	2.23E-275	0.556228505	0.221	0.045	5.60E-271	dMP2
SLC15A3_ENSG00000110446	2.21E-234	0.550843094	0.239	0.059	5.55E-230	dMP2
HSP90AA1_ENSG00000080824	1.84E-203	0.550823014	0.906	0.891	4.61E-199	dMP2
EGR2_ENSG00000122877	2.06E-154	0.547309422	0.188	0.051	5.18E-150	dMP2
FUOM_ENSG00000148803	1.43E-151	0.546402153	0.26	0.094	3.58E-147	dMP2
CASP1_ENSG00000137752	6.46E-120	0.545900426	0.34	0.168	1.62E-115	dMP2
ITPR2_ENSG00000123104	1.10E-134	0.54560503	0.254	0.097	2.77E-130	dMP2
PLD3_ENSG00000105223	1.43E-53	0.545190908	0.541	0.543	3.59E-49	dMP2
UNC93B1_ENSG00000110057	2.42E-112	0.543659413	0.321	0.159	6.08E-108	dMP2
JUND_ENSG00000130522	9.50E-91	0.543628846	0.693	0.704	2.38E-86	dMP2
ARL4C_ENSG00000188042	3.00E-75	0.540345779	0.306	0.17	7.52E-71	dMP2
TNFSF12_ENSG00000239697	2.56E-129	0.536413375	0.267	0.109	6.43E-125	dMP2
B4GALT1_ENSG00000086062	5.14E-35	0.53561315	0.367	0.302	1.29E-30	dMP2
SLC7A7_ENSG00000155465	1.01E-197	0.535358159	0.251	0.073	2.53E-193	dMP2
PLXND1_ENSG00000004399	5.20E-81	0.53396618	0.269	0.142	1.30E-76	dMP2
TMSB10_ENSG00000034510	0	0.533323537	1	0.998	0	dMP2
ACTR2_ENSG00000138071	2.15E-65	0.531146088	0.54	0.511	5.40E-61	dMP2
HEXA_ENSG00000213614	5.75E-47	0.529863397	0.485	0.481	1.44E-42	dMP2
LAP3_ENSG00000002549	6.71E-52	0.529641126	0.403	0.332	1.68E-47	dMP2
CCND1_ENSG00000110092	2.22E-134	0.526958921	0.219	0.074	5.56E-130	dMP2
PTAFR_ENSG00000169403	0	0.525916212	0.216	0.03	0	dMP2
CPEB4_ENSG00000113742	3.95E-97	0.525485179	0.235	0.102	9.92E-93	dMP2
SIRPA_ENSG00000198053	8.34E-186	0.52536877	0.242	0.072	2.09E-181	dMP2
CLTC_ENSG00000141367	1.23E-36	0.524840821	0.346	0.286	3.09E-32	dMP2
DRAM2_ENSG00000156171	5.74E-43	0.524754328	0.385	0.327	1.44E-38	dMP2
EHBP1L1_ENSG00000173442	1.93E-138	0.522924752	0.232	0.081	4.85E-134	dMP2

RNF130_ENSG00000113269	7.36E-72	0.521988916	0.476	0.378	1.85E-67	dMP2
NDUFB1_ENSG00000183648	5.13E-81	0.521628386	0.65	0.677	1.29E-76	dMP2
NAMPT_ENSG00000105835	9.16E-59	0.520696504	0.455	0.377	2.30E-54	dMP2
IFNGR2_ENSG00000159128	7.03E-46	0.520461114	0.415	0.363	1.76E-41	dMP2
EFHD2_ENSG00000142634	6.04E-61	0.518703802	0.379	0.272	1.52E-56	dMP2
LYN_ENSG00000254087	4.79E-56	0.5180456	0.338	0.24	1.20E-51	dMP2
LILRB5_ENSG00000105609	0	0.51615337	0.168	0.013	0	dMP2
TM6SF1_ENSG00000136404	4.88E-269	0.515615891	0.234	0.05	1.22E-264	dMP2
C1orf162_ENSG00000143110	3.23E-123	0.511831459	0.388	0.189	8.11E-119	dMP2
TNFRSF1B_ENSG00000028137	7.77E-101	0.50859673	0.305	0.151	1.95E-96	dMP2
ATP5E_ENSG00000124172	0	0.507748342	0.987	0.97	0	dMP2
CADM1_ENSG00000182985	8.23E-129	0.506872122	0.225	0.079	2.07E-124	dMP2
SLC4A7_ENSG00000033867	2.03E-74	0.506406031	0.247	0.127	5.08E-70	dMP2
PTPN6_ENSG00000111679	9.78E-101	0.505756168	0.401	0.229	2.45E-96	dMP2
SNX6_ENSG00000129515	2.19E-42	0.505057658	0.488	0.492	5.48E-38	dMP2
HCLS1_ENSG00000180353	3.07E-84	0.504362055	0.449	0.311	7.69E-80	dMP2
PTPRJ_ENSG00000149177	1.72E-276	0.503659871	0.202	0.037	4.32E-272	dMP2
PLD4_ENSG00000166428	0	0.50344953	0.184	0.021	0	dMP2
CAPG_ENSG00000042493	9.98E-191	0.503333801	0.752	0.464	2.50E-186	dMP2
PLEKHO1_ENSG00000023902	1.38E-46	0.501406457	0.324	0.238	3.46E-42	dMP2
ATP6V1F_ENSG00000128524	7.11E-96	0.501138037	0.669	0.705	1.78E-91	dMP2
ANKH_ENSG00000154122	3.43E-62	0.500247361	0.238	0.13	8.59E-58	dMP2
CXCL8_ENSG00000169429	0	2.988468901	0.907	0.282	0	dMP1
IL1B_ENSG00000125538	0	2.765940892	0.766	0.122	0	dMP1
CXCL2_ENSG00000081041	0	2.76462106	0.797	0.171	0	dMP1
LYZ_ENSG00000090382	0	2.688285557	0.88	0.125	0	dMP1
CXCL3_ENSG00000163734	0	2.617866892	0.648	0.089	0	dMP1
S100A8_ENSG00000143546	0	2.580463197	0.452	0.057	0	dMP1
S100A9_ENSG00000163220	0	2.514195459	0.71	0.18	0	dMP1
G0S2_ENSG00000123689	0	2.35072647	0.51	0.093	0	dMP1
CCL3L3_ENSG00000276085	0	2.246262185	0.762	0.179	0	dMP1
GPR183_ENSG00000169508	0	2.142837468	0.852	0.139	0	dMP1
IER3_ENSG00000137331	0	2.116372547	0.934	0.424	0	dMP1
HLA-DRB1_ENSG00000196126	0	2.024891042	0.96	0.214	0	dMP1
BCL2A1_ENSG00000140379	0	2.021036525	0.728	0.067	0	dMP1
FTL_ENSG00000087086	0	1.973744266	1	0.993	0	dMP1
PLAUR_ENSG00000011422	0	1.968932404	0.906	0.296	0	dMP1
EREG_ENSG00000124882	0	1.967570436	0.495	0.022	0	dMP1
HLA-DRA_ENSG00000204287	0	1.957729002	0.988	0.339	0	dMP1
SPP1_ENSG00000118785	4.61E-275	1.769734594	0.678	0.396	1.16E-270	dMP1
HLA-DPA1_ENSG00000231389	0	1.760316229	0.929	0.274	0	dMP1
CCL20_ENSG00000115009	0	1.741397017	0.276	0.029	0	dMP1
NAMPT_ENSG00000105835	0	1.734622447	0.92	0.352	0	dMP1
CCL3_ENSG00000277632	0	1.733793461	0.965	0.438	0	dMP1
HLA-DPB1_ENSG00000223865	0	1.720478968	0.921	0.299	0	dMP1
IL1RN_ENSG00000136689	0	1.710425512	0.568	0.04	0	dMP1
HLA-DQB1_ENSG00000179344	0	1.68026167	0.862	0.136	0	dMP1
FTH1_ENSG00000167996	0	1.66562492	1	0.999	0	dMP1
HLA-DQA1_ENSG00000196735	0	1.650247975	0.766	0.102	0	dMP1
SGK1_ENSG00000118515	0	1.608557904	0.808	0.221	0	dMP1
HLA-DRB5_ENSG00000198502	0	1.605099686	0.912	0.16	0	dMP1
FCN1_ENSG00000085265	0	1.600065995	0.375	0.014	0	dMP1
CD74_ENSG00000019582	0	1.576897019	0.994	0.479	0	dMP1
CTSS_ENSG00000163131	0	1.572813418	0.888	0.268	0	dMP1
RP11-1143G9.4_ENSG00000257764	0	1.539975552	0.462	0.038	0	dMP1
C15orf48_ENSG00000166920	0	1.536792566	0.637	0.193	0	dMP1
AIF1_ENSG00000204472	0	1.526231744	0.944	0.199	0	dMP1
LST1_ENSG00000204482	0	1.506213231	0.804	0.121	0	dMP1
CD83_ENSG00000112149	0	1.499898548	0.835	0.156	0	dMP1
SOD2_ENSG00000112096	0	1.492256315	0.921	0.495	0	dMP1

CTSD_ENSG00000117984	0	1.430917977	0.919	0.785	0	dMP1
CD68_ENSG00000129226	0	1.416309178	0.89	0.312	0	dMP1
GPX1_ENSG00000233276	0	1.376577262	0.983	0.725	0	dMP1
FABP5_ENSG00000164687	2.71E-209	1.35637364	0.62	0.375	6.79E-205	dMP1
CCL4L2_ENSG00000276070	0	1.349002161	0.684	0.237	0	dMP1
SAT1_ENSG00000130066	0	1.339365199	0.995	0.844	0	dMP1
TYMP_ENSG00000025708	0	1.338092326	0.894	0.426	0	dMP1
FCGR3A_ENSG00000203747	0	1.335913694	0.671	0.09	0	dMP1
C5AR1_ENSG00000197405	0	1.325817396	0.689	0.051	0	dMP1
HLA-DMA_ENSG00000204257	0	1.29662234	0.792	0.156	0	dMP1
NFKBIA_ENSG00000100906	0	1.292307518	0.982	0.868	0	dMP1
C1QB_ENSG00000173369	0	1.291031809	0.663	0.217	0	dMP1
CTSB_ENSG00000164733	0	1.26150458	0.922	0.677	0	dMP1
C1QC_ENSG00000159189	0	1.256497384	0.641	0.178	0	dMP1
HLA-DQA2_ENSG00000237541	0	1.252946264	0.666	0.075	0	dMP1
APOC1_ENSG00000130208	2.83E-95	1.243776153	0.523	0.396	7.10E-91	dMP1
CYBA_ENSG00000051523	0	1.228749532	0.971	0.637	0	dMP1
RNASE1_ENSG00000129538	0	1.218462739	0.732	0.305	0	dMP1
SPI1_ENSG00000066336	0	1.212183727	0.79	0.093	0	dMP1
NEAT1_ENSG00000245532	0	1.210493461	0.982	0.856	0	dMP1
MS4A6A_ENSG00000110077	0	1.210012925	0.751	0.113	0	dMP1
C1QA_ENSG00000173372	0	1.209677597	0.7	0.245	0	dMP1
LINC00936_ENSG00000271614	0	1.195369904	0.636	0.114	0	dMP1
LAPTM5_ENSG00000162511	0	1.180556331	0.966	0.404	0	dMP1
TNF_ENSG00000232810	0	1.177564342	0.511	0.094	0	dMP1
GPNMB_ENSG00000136235	0	1.173423543	0.6	0.26	0	dMP1
CD14_ENSG00000170458	0	1.170741313	0.839	0.177	0	dMP1
TYROBP_ENSG00000011600	0	1.165786056	0.997	0.479	0	dMP1
NLRP3_ENSG00000162711	0	1.16520169	0.482	0.02	0	dMP1
FCGR2A_ENSG00000143226	0	1.147089172	0.68	0.083	0	dMP1
OLR1_ENSG00000173391	0	1.129122374	0.597	0.134	0	dMP1
PTGS2_ENSG00000073756	0	1.129085257	0.386	0.021	0	dMP1
MSR1_ENSG00000038945	0	1.12155835	0.519	0.056	0	dMP1
CSTA_ENSG00000121552	0	1.115165276	0.572	0.093	0	dMP1
IFI30_ENSG00000216490	0	1.114724379	0.608	0.052	0	dMP1
PSAP_ENSG00000197746	0	1.109517153	0.99	0.832	0	dMP1
CXCL16_ENSG00000161921	0	1.108416044	0.68	0.102	0	dMP1
CTSZ_ENSG00000101160	0	1.097229678	0.755	0.294	0	dMP1
CLEC7A_ENSG00000172243	0	1.093181347	0.656	0.064	0	dMP1
SRGN_ENSG00000122862	0	1.077358327	0.996	0.53	0	dMP1
LY96_ENSG00000154589	0	1.076976234	0.733	0.128	0	dMP1
SERPINA1_ENSG00000197249	0	1.057221388	0.556	0.059	0	dMP1
MS4A7_ENSG00000166927	0	1.055900628	0.702	0.089	0	dMP1
RNASE6_ENSG00000169413	0	1.0334729	0.678	0.087	0	dMP1
S100A12_ENSG00000163221	0	1.028342969	0.175	0.003	0	dMP1
MNDA_ENSG00000163563	0	1.024386263	0.539	0.056	0	dMP1
HLA-DMB_ENSG00000242574	0	1.016927921	0.645	0.12	0	dMP1
RNASET2_ENSG00000026297	0	1.015749834	0.823	0.314	0	dMP1
MAFB_ENSG00000204103	0	1.013206119	0.612	0.157	0	dMP1
PLEK_ENSG00000115956	0	1.012619955	0.677	0.145	0	dMP1
TREM2_ENSG00000095970	0	1.008844713	0.545	0.094	0	dMP1
PHACTR1_ENSG00000112137	0	0.98753671	0.534	0.056	0	dMP1
SDS_ENSG00000135094	0	0.973934409	0.391	0.026	0	dMP1
GRN_ENSG00000030582	0	0.966234818	0.913	0.605	0	dMP1
HMOX1_ENSG00000100292	0	0.963240393	0.525	0.174	0	dMP1
RGS2_ENSG00000116741	0	0.956324467	0.715	0.348	0	dMP1
S100A10_ENSG00000197747	0	0.946589977	0.927	0.501	0	dMP1
GLUL_ENSG00000135821	0	0.941962648	0.887	0.634	0	dMP1
C1orf162_ENSG00000143110	0	0.928212402	0.702	0.172	0	dMP1
SLC11A1_ENSG00000018280	0	0.925857956	0.514	0.046	0	dMP1

NPC2_ENSG00000119655	0	0.92009947	0.967	0.752	0	dMP1
TNFSF13B_ENSG00000102524	0	0.916355499	0.57	0.052	0	dMP1
TREM1_ENSG00000124731	0	0.915893922	0.452	0.038	0	dMP1
LGMN_ENSG00000100600	5.46E-210	0.913976391	0.575	0.309	1.37E-205	dMP1
HBEGF_ENSG00000113070	0	0.906532068	0.485	0.046	0	dMP1
ITGB2_ENSG00000160255	0	0.90360556	0.829	0.273	0	dMP1
CSTB_ENSG00000160213	1.26E-256	0.897821622	0.878	0.756	3.15E-252	dMP1
OSM_ENSG00000099985	0	0.876807619	0.398	0.075	0	dMP1
CD9_ENSG00000010278	0	0.871926214	0.677	0.308	0	dMP1
ZEB2_ENSG00000169554	0	0.864626806	0.689	0.24	0	dMP1
CHMP1B_ENSG00000255112	3.72E-215	0.85374567	0.727	0.536	9.34E-211	dMP1
IL10_ENSG00000136634	0	0.844533592	0.328	0.017	0	dMP1
PLIN2_ENSG00000147872	2.67E-231	0.842772595	0.725	0.476	6.70E-227	dMP1
FGL2_ENSG00000127951	0	0.839205791	0.489	0.07	0	dMP1
CDKN1A_ENSG00000124762	0	0.838550563	0.652	0.268	0	dMP1
TNFAIP3_ENSG00000118503	0	0.8358732	0.761	0.407	0	dMP1
LY86_ENSG00000112799	0	0.831680014	0.599	0.068	0	dMP1
APOBEC3A_ENSG00000128383	0	0.830387389	0.228	0.006	0	dMP1
CD44_ENSG00000026508	0	0.815342399	0.87	0.552	0	dMP1
CYBB_ENSG00000165168	0	0.811374904	0.545	0.071	0	dMP1
HIF1A_ENSG00000100644	0	0.809823459	0.735	0.411	0	dMP1
VMO1_ENSG00000182853	0	0.808183926	0.296	0.025	0	dMP1
FPR3_ENSG00000187474	0	0.803372331	0.449	0.034	0	dMP1
VEGFA_ENSG00000112715	0	0.798471351	0.425	0.088	0	dMP1
CD163_ENSG00000177575	0	0.794877871	0.438	0.058	0	dMP1
CD86_ENSG00000114013	0	0.790261044	0.512	0.045	0	dMP1
MXD1_ENSG00000059728	0	0.788702589	0.475	0.083	0	dMP1
CH17-373J23.1_ENSG00000276216	0	0.787956358	0.426	0.108	0	dMP1
RP11-670E13.6_ENSG00000274213	3.31E-276	0.785366912	0.386	0.128	8.30E-272	dMP1
FCGRT_ENSG00000104870	0	0.782165841	0.842	0.485	0	dMP1
PHLDA1_ENSG00000139289	4.18E-123	0.771780239	0.551	0.345	1.05E-118	dMP1
OTUD1_ENSG00000165312	0	0.760436238	0.478	0.12	0	dMP1
PLD3_ENSG00000105223	2.54E-90	0.757792442	0.624	0.538	6.38E-86	dMP1
PPIF_ENSG00000108179	1.66E-251	0.753979549	0.453	0.186	4.17E-247	dMP1
EMP3_ENSG00000142227	3.84E-299	0.751465887	0.877	0.656	9.62E-295	dMP1
ASAH1_ENSG00000104763	0	0.751365769	0.775	0.512	0	dMP1
ICAM1_ENSG00000090339	0	0.742601492	0.512	0.136	0	dMP1
PNRC1_ENSG00000146278	3.12E-237	0.73969912	0.928	0.824	7.82E-233	dMP1
NFKBIZ_ENSG00000144802	2.22E-301	0.739322372	0.754	0.43	5.58E-297	dMP1
KLF6_ENSG00000067082	1.17E-303	0.738740354	0.941	0.798	2.94E-299	dMP1
HSPA1A_ENSG00000204389	1.10E-62	0.735094133	0.549	0.427	2.75E-58	dMP1
IGSF6_ENSG00000140749	0	0.735079297	0.469	0.057	0	dMP1
EVI2B_ENSG00000185862	0	0.733132315	0.605	0.162	0	dMP1
CEBPB_ENSG00000172216	7.85E-275	0.732191814	0.885	0.62	1.97E-270	dMP1
NINJ1_ENSG00000131669	0	0.731888111	0.66	0.319	0	dMP1
FCER1G_ENSG00000158869	0	0.729185732	0.989	0.463	0	dMP1
TSPO_ENSG00000100300	0	0.724397522	0.84	0.58	0	dMP1
LINC01272_ENSG00000224397	0	0.715719092	0.349	0.022	0	dMP1
FPR1_ENSG00000171051	0	0.714684931	0.41	0.029	0	dMP1
TGFBI_ENSG00000120708	0	0.714218	0.668	0.277	0	dMP1
CSF1R_ENSG00000182578	0	0.710379827	0.568	0.111	0	dMP1
TNFRSF1B_ENSG00000028137	0	0.709809848	0.543	0.138	0	dMP1
FAM26F_ENSG00000188820	0	0.709014319	0.448	0.078	0	dMP1
ARRB2_ENSG00000141480	0	0.705774437	0.616	0.174	0	dMP1
AP1S2_ENSG00000182287	4.35E-221	0.704798102	0.611	0.34	1.09E-216	dMP1
AQP9_ENSG00000103569	0	0.700724907	0.288	0.012	0	dMP1
NCF2_ENSG00000116701	0	0.698575376	0.445	0.031	0	dMP1
RNF130_ENSG00000113269	0	0.693339537	0.712	0.365	0	dMP1
RGS10_ENSG00000148908	0	0.692334011	0.681	0.332	0	dMP1
LILRB4_ENSG00000186818	0	0.690045797	0.447	0.04	0	dMP1

RILPL2_ENSG00000150977	0	0.687309156	0.506	0.172	0	dMP1
STX11_ENSG00000135604	0	0.683152241	0.451	0.077	0	dMP1
CD4_ENSG00000010610	0	0.681423152	0.484	0.08	0	dMP1
RASGEF1B_ENSG00000138670	0	0.67911445	0.455	0.117	0	dMP1
LIPA_ENSG00000107798	1.50E-79	0.677431399	0.457	0.326	3.75E-75	dMP1
RGS1_ENSG00000090104	0	0.673644842	0.877	0.4	0	dMP1
S100A4_ENSG00000196154	1.35E-233	0.672599973	0.95	0.83	3.39E-229	dMP1
CTSH_ENSG00000103811	1.30E-273	0.67205713	0.631	0.319	3.26E-269	dMP1
MS4A4A_ENSG00000110079	0	0.670913055	0.452	0.081	0	dMP1
INSIG1_ENSG00000186480	3.59E-159	0.668699661	0.416	0.198	9.01E-155	dMP1
STXBP2_ENSG00000076944	2.66E-196	0.658190518	0.531	0.256	6.66E-192	dMP1
GADD45B_ENSG00000099860	7.12E-241	0.656845202	0.879	0.704	1.78E-236	dMP1
ATP6V1F_ENSG00000128524	4.84E-274	0.656591925	0.845	0.695	1.21E-269	dMP1
S100A11_ENSG00000163191	0	0.655280913	0.987	0.907	0	dMP1
ARL4C_ENSG00000188042	2.40E-303	0.653924954	0.479	0.161	6.03E-299	dMP1
KDM6B_ENSG00000132510	4.43E-300	0.651237327	0.539	0.216	1.11E-295	dMP1
PYCARD_ENSG00000103490	0	0.650371963	0.685	0.294	0	dMP1
RP11-386I14.4_ENSG00000273338	8.30E-275	0.648895243	0.474	0.17	2.08E-270	dMP1
PFKFB3_ENSG00000170525	0	0.646374202	0.382	0.079	0	dMP1
DSE_ENSG00000111817	0	0.642938079	0.422	0.082	0	dMP1
ACP5_ENSG00000102575	4.98E-142	0.629147053	0.488	0.259	1.25E-137	dMP1
BRI3_ENSG00000164713	9.65E-251	0.622911637	0.72	0.443	2.42E-246	dMP1
ISG15_ENSG00000187608	1.96E-142	0.621166721	0.791	0.613	4.92E-138	dMP1
MARCKS_ENSG00000277443	6.16E-239	0.620505304	0.7	0.391	1.55E-234	dMP1
PLSCR1_ENSG00000188313	9.21E-244	0.619123819	0.657	0.376	2.31E-239	dMP1
CST3_ENSG00000101439	3.55E-295	0.617856793	0.985	0.826	8.90E-291	dMP1
C3AR1_ENSG00000171860	0	0.617651191	0.428	0.06	0	dMP1
LRRFIP1_ENSG00000124831	2.99E-211	0.615921193	0.72	0.463	7.50E-207	dMP1
LIMS1_ENSG00000169756	1.10E-195	0.615495179	0.619	0.379	2.75E-191	dMP1
CREG1_ENSG00000143162	4.74E-220	0.612880842	0.536	0.266	1.19E-215	dMP1
GMFG_ENSG00000130755	0	0.611475505	0.781	0.358	0	dMP1
NR4A3_ENSG00000119508	0	0.609593506	0.376	0.071	0	dMP1
MFSD1_ENSG00000118855	3.58E-258	0.60708479	0.537	0.243	8.97E-254	dMP1
PPT1_ENSG00000131238	5.89E-224	0.603234162	0.616	0.36	1.48E-219	dMP1
ABL2_ENSG00000143322	1.68E-205	0.599384083	0.302	0.097	4.20E-201	dMP1
PILRA_ENSG00000085514	0	0.598786838	0.528	0.179	0	dMP1
CD300E_ENSG00000186407	0	0.594997879	0.261	0.004	0	dMP1
SLC7A7_ENSG00000155465	0	0.59372285	0.417	0.064	0	dMP1
PPP1R15A_ENSG00000087074	1.34E-215	0.592108254	0.91	0.781	3.36E-211	dMP1
STAB1_ENSG00000010327	0	0.5905682	0.414	0.108	0	dMP1
CPVL_ENSG00000106066	0	0.590339001	0.506	0.173	0	dMP1
IER5_ENSG00000162783	9.24E-205	0.584285049	0.536	0.258	2.32E-200	dMP1
CLEC10A_ENSG00000132514	0	0.584092825	0.198	0.008	0	dMP1
OAZ1_ENSG00000104904	0	0.582960468	0.984	0.957	0	dMP1
TTYH3_ENSG00000136295	0	0.58245745	0.353	0.092	0	dMP1
CECR1_ENSG00000093072	0	0.581612051	0.416	0.076	0	dMP1
LAIR1_ENSG00000167613	0	0.579358746	0.441	0.088	0	dMP1
H2AFY_ENSG00000113648	4.76E-202	0.579192036	0.724	0.529	1.19E-197	dMP1
CD93_ENSG00000125810	0	0.576723133	0.392	0.059	0	dMP1
EIF4E_ENSG00000151247	2.26E-69	0.57609097	0.558	0.453	5.67E-65	dMP1
HCK_ENSG00000101336	0	0.575206074	0.409	0.043	0	dMP1
KB-1507C5.4_ENSG00000254281	0	0.574470129	0.255	0.007	0	dMP1
FCGR1A_ENSG00000150337	0	0.56767869	0.393	0.053	0	dMP1
VIM_ENSG00000026025	2.10E-236	0.562243211	0.985	0.815	5.26E-232	dMP1
PDE4B_ENSG00000184588	0	0.55986202	0.428	0.121	0	dMP1
BNIP3L_ENSG00000104765	3.02E-124	0.552971073	0.627	0.455	7.58E-120	dMP1
MPEG1_ENSG00000197629	0	0.551943279	0.396	0.042	0	dMP1
ETS2_ENSG00000157557	1.10E-147	0.549679293	0.494	0.28	2.76E-143	dMP1
TPP1_ENSG00000166340	1.29E-197	0.546641905	0.567	0.313	3.25E-193	dMP1
JUND_ENSG00000130522	7.29E-163	0.546449418	0.839	0.696	1.83E-158	dMP1

MAP3K8_ENSG00000107968	1.68E-165	0.544729714	0.687	0.446	4.22E-161	dMP1
MGAT1_ENSG00000131446	3.34E-156	0.544043938	0.627	0.422	8.37E-152	dMP1
JAML_ENSG00000160593	0	0.538614651	0.294	0.031	0	dMP1
MCL1_ENSG00000143384	2.80E-267	0.534128161	0.949	0.811	7.01E-263	dMP1
CD36_ENSG00000135218	0	0.533477331	0.363	0.083	0	dMP1
GNA13_ENSG00000120063	3.25E-294	0.53341129	0.449	0.152	8.14E-290	dMP1
VSIG4_ENSG00000155659	0	0.530688413	0.372	0.082	0	dMP1
ALOX5AP_ENSG00000132965	5.78E-198	0.529345019	0.552	0.238	1.45E-193	dMP1
GSTO1_ENSG00000148834	1.76E-159	0.528212086	0.726	0.558	4.41E-155	dMP1
CARD16_ENSG00000204397	1.03E-183	0.527939246	0.598	0.32	2.59E-179	dMP1
CD37_ENSG00000104894	7.79E-297	0.527870739	0.737	0.307	1.95E-292	dMP1
UPP1_ENSG00000183696	1.47E-188	0.526746897	0.536	0.259	3.70E-184	dMP1
ATF5_ENSG00000169136	1.55E-211	0.526190995	0.34	0.117	3.89E-207	dMP1
THBD_ENSG00000178726	9.69E-215	0.526181833	0.266	0.073	2.43E-210	dMP1
METRNL_ENSG00000176845	3.21E-242	0.525167742	0.443	0.162	8.04E-238	dMP1
SIRPA_ENSG00000198053	0	0.524058127	0.367	0.065	0	dMP1
CFP_ENSG00000126759	0	0.523022917	0.198	0.008	0	dMP1
KLF4_ENSG00000136826	2.88E-165	0.521838639	0.723	0.456	7.23E-161	dMP1
GK_ENSG00000198814	0	0.520977797	0.287	0.034	0	dMP1
LGALS9_ENSG00000168961	1.14E-230	0.520781708	0.592	0.281	2.86E-226	dMP1
SAMHD1_ENSG00000101347	0	0.518803778	0.504	0.165	0	dMP1
MARCO_ENSG00000019169	0	0.518190565	0.192	0.016	0	dMP1
ODF3B_ENSG00000177989	2.14E-289	0.518113705	0.407	0.13	5.36E-285	dMP1
ATP6V0B_ENSG00000117410	4.63E-207	0.517667803	0.797	0.629	1.16E-202	dMP1
SH3BGRL3_ENSG00000142669	4.58E-263	0.516356958	0.978	0.903	1.15E-258	dMP1
RUNX1_ENSG00000159216	2.07E-304	0.514900891	0.428	0.131	5.18E-300	dMP1
CXCL1_ENSG00000163739	2.55E-186	0.514503899	0.134	0.023	6.39E-182	dMP1
CCRL2_ENSG00000121797	0	0.512240353	0.3	0.042	0	dMP1
THAP2_ENSG00000173451	3.01E-173	0.509124642	0.301	0.108	7.55E-169	dMP1
PTPRE_ENSG00000132334	1.41E-205	0.509057949	0.47	0.205	3.55E-201	dMP1
ZNF385A_ENSG00000161642	2.96E-251	0.508470318	0.377	0.128	7.42E-247	dMP1
GNAI2_ENSG00000114353	9.34E-192	0.506947891	0.686	0.441	2.34E-187	dMP1
NPL_ENSG00000135838	3.58E-287	0.506855896	0.396	0.12	8.98E-283	dMP1
MT-ND3_ENSG00000198840	1.50E-181	0.506470206	0.983	0.952	3.77E-177	dMP1
RHOG_ENSG00000177105	8.98E-164	0.504239943	0.634	0.427	2.25E-159	dMP1
RP11-160E2.6_ENSG00000262202	8.82E-157	0.502549584	0.388	0.171	2.21E-152	dMP1
THEMIS2_ENSG00000130775	0	0.500139096	0.38	0.058	0	dMP1

Appendix 9 - Genes differentially expressed between maternal mononuclear phagocytes ($|\log_2(\text{fold-change})| \geq 1.0$, adjusted $p < 0.05$):

Gene ID/Ensembl ID	p value	log2(fold change)	pct.1	pct.2	adjusted p value	cluster
APOC1_ENSG00000130208	1.63E-215	2.357334076	0.984	0.492	4.10E-211	pIMP
APOE_ENSG00000130203	3.76E-162	2.029333108	0.961	0.619	9.42E-158	pIMP
CGA_ENSG00000135346	0.00E+00	1.886344068	0.928	0.026	0.00E+00	pIMP
PAGE4_ENSG00000101951	0	1.722991913	0.796	0.012	0	pIMP
GCHFR_ENSG00000137880	8.17E-272	1.637063863	0.88	0.184	2.05E-267	pIMP
SPP1_ENSG00000118785	2.09E-63	1.592918289	0.954	0.636	5.24E-59	pIMP
FABP5_ENSG00000164687	2.55E-178	1.553425842	0.977	0.376	6.39E-174	pIMP
CHI3L1_ENSG00000133048	0.00E+00	1.407906861	0.389	0.003	0.00E+00	pIMP
LGALS3_ENSG00000131981	6.41E-156	1.241710591	0.984	0.556	1.61E-151	pIMP
CSTB_ENSG00000160213	4.00E-139	1.179349318	0.998	0.795	1.00E-134	pIMP
CD9_ENSG00000010278	3.03E-150	1.172126361	0.988	0.512	7.61E-146	pIMP
ACP5_ENSG00000102575	9.50E-158	1.15799954	0.905	0.315	2.38E-153	pIMP
ANXA2_ENSG00000182718	4.91E-155	1.07820269	0.998	0.716	1.23E-150	pIMP
VIM_ENSG00000026025	1.91E-124	1.028287648	1	0.783	4.80E-120	pIMP
KRT8_ENSG00000170421	0.00E+00	1.027293567	0.843	0.032	0.00E+00	pIMP
LIPA_ENSG00000107798	1.20E-151	1.023098163	0.961	0.378	3.00E-147	pIMP
FN1_ENSG00000115414	2.09E-222	1.021857998	0.861	0.163	5.24E-218	pIMP
KRT18_ENSG00000111057	0.00E+00	1.005458258	0.794	0.025	0.00E+00	pIMP
GPNMB_ENSG00000136235	7.16E-131	1.005241646	0.963	0.432	1.80E-126	pIMP
PNRC1_ENSG00000146278	5.20E-59	-1.00617427	0.773	0.794	1.30E-54	pIMP
FCGR2A_ENSG00000143226	2.11E-62	-1.049019156	0.463	0.685	5.30E-58	pIMP
KLF2_ENSG00000127528	1.71E-39	-1.059375232	0.218	0.484	4.30E-35	pIMP
NAMPT_ENSG00000105835	7.94E-44	-1.073553012	0.62	0.684	1.99E-39	pIMP
IFITM2_ENSG00000185201	2.54E-72	-1.084092124	0.532	0.723	6.38E-68	pIMP
GADD45B_ENSG00000099860	7.03E-89	-1.102790277	0.843	0.876	1.76E-84	pIMP
IER5_ENSG00000162783	1.63E-45	-1.103162137	0.324	0.56	4.10E-41	pIMP
TNFAIP3_ENSG00000118503	3.63E-34	-1.105763493	0.322	0.514	9.11E-30	pIMP
MAF_ENSG00000178573	2.08E-33	-1.111278399	0.373	0.53	5.21E-29	pIMP
EREG_ENSG00000124882	8.41E-07	-1.116553011	0.183	0.258	2.11E-02	pIMP
IFITM3_ENSG00000142089	9.24E-76	-1.130125951	0.789	0.827	2.32E-71	pIMP
RHOB_ENSG00000143878	6.67E-46	-1.158336745	0.627	0.702	1.67E-41	pIMP
DNAJB1_ENSG00000132002	3.01E-32	-1.17511846	0.433	0.552	7.55E-28	pIMP
IER2_ENSG00000160888	1.82E-98	-1.179960769	0.907	0.918	4.57E-94	pIMP
DUSP2_ENSG00000158050	8.87E-44	-1.202157774	0.394	0.597	2.23E-39	pIMP
F13A1_ENSG00000124491	1.97E-54	-1.224712944	0.06	0.441	4.93E-50	pIMP
FOSB_ENSG00000125740	8.89E-109	-1.241229351	0.81	0.874	2.23E-104	pIMP
CCL20_ENSG00000115009	6.07E-16	-1.26214616	0.014	0.157	1.52E-11	pIMP
GZMA_ENSG00000145649	1.84E-88	-1.263881381	0.035	0.569	4.62E-84	pIMP
KLF6_ENSG00000067082	3.12E-126	-1.277370365	0.912	0.948	7.82E-122	pIMP
SLC40A1_ENSG00000138449	2.47E-33	-1.333709594	0.301	0.501	6.19E-29	pIMP
CTSW_ENSG00000172543	4.77E-102	-1.341363138	0.06	0.637	1.20E-97	pIMP
GPR183_ENSG00000169508	1.04E-54	-1.347184726	0.56	0.712	2.62E-50	pIMP
JUN_ENSG00000177606	1.22E-83	-1.35461767	0.905	0.912	3.05E-79	pIMP
NFKBIA_ENSG00000100906	4.70E-94	-1.358789934	0.896	0.921	1.18E-89	pIMP
STAB1_ENSG00000010327	1.22E-63	-1.417779194	0.282	0.604	3.07E-59	pIMP
CD14_ENSG00000170458	3.99E-108	-1.43005694	0.729	0.909	1.00E-103	pIMP
GZMB_ENSG00000100453	2.63E-124	-1.476350079	0.046	0.708	6.59E-120	pIMP
EGR1_ENSG00000120738	5.36E-95	-1.59591603	0.319	0.718	1.34E-90	pIMP
C1QC_ENSG00000159189	6.67E-93	-1.658588054	0.6	0.823	1.67E-88	pIMP
RNASE1_ENSG00000129538	6.27E-75	-1.725105782	0.72	0.859	1.57E-70	pIMP
C1QB_ENSG00000173369	8.39E-99	-1.726598542	0.546	0.834	2.10E-94	pIMP
IER3_ENSG00000137331	1.95E-111	-1.733805299	0.646	0.846	4.90E-107	pIMP
CXCL2_ENSG00000081041	2.13E-26	-1.735894111	0.419	0.558	5.34E-22	pIMP
CXCL3_ENSG00000163734	2.27E-30	-1.776251535	0.185	0.433	5.69E-26	pIMP
NKG7_ENSG00000105374	9.31E-171	-1.816014588	0.102	0.849	2.34E-166	pIMP
CCL3_ENSG00000277632	1.90E-149	-1.844844821	0.799	0.968	4.78E-145	pIMP
C1QA_ENSG00000173372	5.69E-107	-1.865602774	0.569	0.851	1.43E-102	pIMP

FOLR2_ENSG00000165457	2.43E-95	-1.872586817	0.199	0.671	6.09E-91	pIMP
HSPA1B_ENSG00000204388	1.74E-81	-1.951539763	0.215	0.629	4.36E-77	pIMP
CCL3L3_ENSG00000276085	1.55E-103	-2.004003108	0.382	0.79	3.90E-99	pIMP
IL1B_ENSG00000125538	8.51E-49	-2.176179776	0.183	0.502	2.13E-44	pIMP
HSPA1A_ENSG00000204389	1.84E-100	-2.232529963	0.384	0.746	4.61E-96	pIMP
CXCL8_ENSG00000169429	1.29E-95	-2.299218151	0.412	0.78	3.24E-91	pIMP
CCL4L2_ENSG00000276070	1.25E-108	-2.301416181	0.19	0.732	3.12E-104	pIMP
SEPP1_ENSG00000250722	3.15E-86	-2.38568031	0.31	0.701	7.90E-82	pIMP
CCL4_ENSG00000275302	6.21E-194	-2.616398891	0.25	0.941	1.56E-189	pIMP
GNLY_ENSG00000115523	2.37E-236	-3.18759823	0.16	0.984	5.95E-232	pIMP
SEPP1_ENSG00000250722	0.00E+00	1.893575834	0.943	0.426	0.00E+00	dMP2
FOLR2_ENSG00000165457	0.00E+00	1.596688389	0.927	0.371	0.00E+00	dMP2
SLC40A1_ENSG00000138449	0.00E+00	1.592508577	0.769	0.239	0.00E+00	dMP2
C1QA_ENSG00000173372	0.00E+00	1.427869753	0.999	0.676	0.00E+00	dMP2
C1QC_ENSG00000159189	0.00E+00	1.343666208	1	0.634	0.00E+00	dMP2
RNASE1_ENSG00000129538	0.00E+00	1.321671818	0.982	0.73	0.00E+00	dMP2
C1QB_ENSG00000173369	0.00E+00	1.317559841	1	0.642	0.00E+00	dMP2
C3_ENSG00000125730	1.84E-217	1.301788333	0.611	0.221	4.62E-213	dMP2
HSPA1B_ENSG00000204388	0.00E+00	1.272026455	0.884	0.339	0.00E+00	dMP2
MAF_ENSG00000178573	1.21E-275	1.238218086	0.74	0.325	3.03E-271	dMP2
HSPA1A_ENSG00000204389	0.00E+00	1.198944617	0.937	0.519	0.00E+00	dMP2
F13A1_ENSG00000124491	1.50E-221	1.187032054	0.627	0.216	3.76E-217	dMP2
OLFML3_ENSG00000116774	8.94E-194	1.169044581	0.522	0.151	2.24E-189	dMP2
GPR34_ENSG00000171659	8.81E-234	1.166052286	0.688	0.316	2.21E-229	dMP2
STAB1_ENSG00000010327	1.27E-269	1.158687027	0.789	0.39	3.19E-265	dMP2
CD14_ENSG00000170458	0	1.150999704	0.976	0.819	0	dMP2
LPAR6_ENSG00000139679	2.84E-204	1.108745621	0.652	0.309	7.11E-200	dMP2
JUN_ENSG00000177606	0.00E+00	1.091122783	0.975	0.858	0.00E+00	dMP2
CCL2_ENSG00000108691	8.12E-83	1.070118251	0.497	0.256	2.04E-78	dMP2
TMEM176B_ENSG00000106565	1.10E-227	1.05745291	0.735	0.358	2.76E-223	dMP2
DAB2_ENSG00000153071	1.13E-200	1.046895573	0.757	0.489	2.84E-196	dMP2
RHOB_ENSG00000143878	5.82E-211	1.020229939	0.819	0.589	1.46E-206	dMP2
BIN1_ENSG00000136717	2.21E-146	1.004220589	0.492	0.189	5.53E-142	dMP2
AREG_ENSG00000109321	1.25E-96	-1.029551651	0.156	0.45	3.14E-92	dMP2
FTH1_ENSG00000167996	0.00E+00	-1.078484835	1	1	0.00E+00	dMP2
DUSP2_ENSG00000158050	1.25E-183	-1.100293034	0.362	0.758	3.13E-179	dMP2
CD44_ENSG00000026508	0	-1.114642725	0.304	0.879	0	dMP2
RP11-1143G9.4_ENSG00000257764	4.84E-126	-1.115265986	0.126	0.474	1.21E-121	dMP2
LGALS3_ENSG00000131981	2.85E-225	-1.127455806	0.35	0.807	7.16E-221	dMP2
LSP1_ENSG00000130592	0	-1.12876955	0.277	0.876	0	dMP2
CD52_ENSG00000169442	1.29E-177	-1.13928875	0.348	0.757	3.23E-173	dMP2
NFKBIA_ENSG00000100906	1.57E-200	-1.166381609	0.862	0.966	3.93E-196	dMP2
PHLDA1_ENSG00000139289	4.79E-219	-1.235264547	0.099	0.558	1.20E-214	dMP2
RGCC_ENSG00000102760	8.06E-256	-1.255856011	0.175	0.688	2.02E-251	dMP2
PLAUR_ENSG00000011422	0	-1.281807079	0.418	0.912	0	dMP2
S100A10_ENSG00000197747	0	-1.289739598	0.476	0.94	0	dMP2
PLIN2_ENSG00000147872	1.76E-277	-1.298291392	0.219	0.759	4.41E-273	dMP2
SPP1_ENSG00000118785	2.16E-37	-1.348963725	0.595	0.728	5.41E-33	dMP2
SOD2_ENSG00000112096	3.85E-267	-1.366985457	0.48	0.909	9.65E-263	dMP2
OLR1_ENSG00000173391	0	-1.367048177	0.081	0.656	0	dMP2
FN1_ENSG00000115414	1.52E-158	-1.373073627	0.046	0.388	3.81E-154	dMP2
TIMP1_ENSG00000102265	6.78E-227	-1.429458876	0.334	0.813	1.70E-222	dMP2
FCN1_ENSG00000085265	2.87E-167	-1.447908651	0.017	0.351	7.21E-163	dMP2
CXCL8_ENSG00000169429	9.22E-113	-1.463815604	0.657	0.817	2.31E-108	dMP2
S100A6_ENSG00000197956	0	-1.487052586	0.637	0.975	0	dMP2
APOC1_ENSG00000130208	1.04E-48	-1.557089526	0.462	0.607	2.60E-44	dMP2
CCL20_ENSG00000115009	1.45E-72	-1.568852622	0.041	0.228	3.63E-68	dMP2
IL1RN_ENSG00000136689	3.87E-243	-1.56894386	0.077	0.549	9.71E-239	dMP2
S100A9_ENSG00000163220	1.34E-98	-1.609065871	0.428	0.741	3.36E-94	dMP2
BCL2A1_ENSG00000140379	0.00E+00	-1.652186217	0.135	0.716	0.00E+00	dMP2
VIM_ENSG00000026025	0.00E+00	-1.712454417	0.586	0.988	0.00E+00	dMP2
C15orf48_ENSG00000166920	0.00E+00	-1.771287796	0.119	0.684	0.00E+00	dMP2

EREG_ENSG00000124882	8.93E-216	-1.773313648	0.027	0.438	2.24E-211	dMP2
CXCL3_ENSG00000163734	1.43E-141	-1.790987813	0.224	0.564	3.58E-137	dMP2
LYZ_ENSG00000090382	1.16E-291	-1.824137521	0.426	0.892	2.90E-287	dMP2
CXCL2_ENSG00000081041	3.04E-204	-1.912993795	0.327	0.728	7.62E-200	dMP2
IL1B_ENSG00000125538	1.46E-206	-2.001437266	0.246	0.66	3.67E-202	dMP2
S100A8_ENSG00000143546	1.14E-153	-2.093196617	0.137	0.509	2.86E-149	dMP2
FABP5_ENSG00000164687	2.09E-299	-2.11722936	0.139	0.685	5.24E-295	dMP2
G0S2_ENSG00000123689	1.19E-221	-2.352174009	0.054	0.487	2.98E-217	dMP2
G0S2_ENSG00000123689	4.56E-209	2.323849913	0.51	0.112	1.14E-204	dMP1
IL1B_ENSG00000125538	0.00E+00	2.269956654	0.766	0.234	0.00E+00	dMP1
CXCL2_ENSG00000081041	7.66E-299	2.129194335	0.797	0.343	1.92E-294	dMP1
CXCL3_ENSG00000163734	2.14E-228	2.027952194	0.648	0.217	5.36E-224	dMP1
EREG_ENSG00000124882	4.11E-259	1.884524355	0.495	0.055	1.03E-254	dMP1
CXCL8_ENSG00000169429	2.02E-269	1.781901101	0.907	0.614	5.07E-265	dMP1
S100A8_ENSG00000143546	6.17E-57	1.763423795	0.452	0.248	1.55E-52	dMP1
CCL20_ENSG00000115009	3.43E-116	1.745151483	0.276	0.037	8.61E-112	dMP1
BCL2A1_ENSG00000140379	6.85E-288	1.599638309	0.728	0.228	1.72E-283	dMP1
S100A9_ENSG00000163220	1.78E-50	1.576430209	0.71	0.508	4.47E-46	dMP1
LYZ_ENSG00000090382	5.00E-225	1.523372681	0.88	0.519	1.25E-220	dMP1
SOD2_ENSG00000112096	0.00E+00	1.500072568	0.921	0.546	0.00E+00	dMP1
FCN1_ENSG00000085265	3.91E-160	1.458258504	0.375	0.058	9.80E-156	dMP1
TIMP1_ENSG00000102265	1.53E-238	1.437338603	0.826	0.409	3.83E-234	dMP1
NFKBIA_ENSG00000100906	0.00E+00	1.403262666	0.982	0.868	0.00E+00	dMP1
DUSP2_ENSG00000158050	2.03E-304	1.318541401	0.839	0.368	5.08E-300	dMP1
C15orf48_ENSG00000166920	1.24E-162	1.229526871	0.637	0.256	3.11E-158	dMP1
AREG_ENSG00000109321	3.16E-144	1.188303254	0.511	0.16	7.92E-140	dMP1
IL1RN_ENSG00000136689	6.58E-206	1.166620815	0.568	0.146	1.65E-201	dMP1
PHLDA1_ENSG00000139289	4.11E-164	1.148256159	0.551	0.185	1.03E-159	dMP1
TNFAIP3_ENSG00000118503	1.47E-255	1.121535282	0.761	0.282	3.69E-251	dMP1
PLAUR_ENSG00000011422	1.40E-255	1.118230804	0.906	0.511	3.50E-251	dMP1
NAMPT_ENSG00000105835	2.58E-305	1.096437007	0.92	0.485	6.46E-301	dMP1
RP11-1143G9.4_ENSG00000257764	5.51E-89	1.088538764	0.462	0.198	1.38E-84	dMP1
IER3_ENSG00000137331	2.09E-228	1.084787063	0.934	0.74	5.24E-224	dMP1
GPR183_ENSG00000169508	6.98E-182	1.077153859	0.852	0.574	1.75E-177	dMP1
S100A12_ENSG00000163221	6.21E-85	1.022557225	0.175	0.011	1.56E-80	dMP1
CD44_ENSG00000026508	2.18E-274	1.02175185	0.87	0.413	5.47E-270	dMP1
RGCC_ENSG00000102760	2.86E-191	1.014011577	0.687	0.267	7.17E-187	dMP1
PTGS2_ENSG00000073756	4.08E-162	1.010919604	0.386	0.057	1.02E-157	dMP1
BTG1_ENSG00000133639	1.12E-239	1.005625189	0.958	0.753	2.81E-235	dMP1
SRGN_ENSG00000122862	0.00E+00	1.005442319	0.996	0.962	0.00E+00	dMP1
GPR34_ENSG00000171659	8.96E-175	-1.016302696	0.283	0.648	2.25E-170	dMP1
C1QB_ENSG00000173369	7.87E-257	-1.029139921	0.663	0.919	1.97E-252	dMP1
RNASE1_ENSG00000129538	2.81E-179	-1.033658013	0.732	0.936	7.04E-175	dMP1
MAF_ENSG00000178573	1.16E-176	-1.033965598	0.314	0.675	2.91E-172	dMP1
C1QC_ENSG00000159189	1.22E-283	-1.064561222	0.641	0.929	3.06E-279	dMP1
CCL2_ENSG00000108691	1.37E-63	-1.072853781	0.247	0.462	3.44E-59	dMP1
OLFML3_ENSG00000116774	1.53E-176	-1.091326187	0.108	0.49	3.84E-172	dMP1
C1QA_ENSG00000173372	1.81E-292	-1.131453679	0.7	0.923	4.53E-288	dMP1
C3_ENSG00000125730	1.85E-188	-1.198601433	0.177	0.577	4.64E-184	dMP1
FOLR2_ENSG00000165457	5.22E-261	-1.31045158	0.409	0.798	1.31E-256	dMP1
SLC40A1_ENSG00000138449	1.39E-244	-1.386420162	0.226	0.686	3.50E-240	dMP1
SEPP1_ENSG00000250722	1.60E-257	-1.577564412	0.452	0.831	4.01E-253	dMP1

Appendix 10 - Significantly overexpressed M1/M2 macrophage genes in the three maternal mononuclear phagocyte subsets (adjusted p < 0.05):

M1 gene ID/Ensembl ID	p value	log2(fold change)	pct.1	pct.2	adjusted p value	cluster
BCL2A1_ENSG00000140379	0	2.021036525	0.728	0.067	0	dMP1
CCL20_ENSG00000115009	0	1.741397017	0.276	0.029	0	dMP1
TNF_ENSG00000232810	0	1.177564342	0.511	0.094	0	dMP1
PFKFB3_ENSG00000170525	0	0.646374202	0.382	0.079	0	dMP1
BIRC3_ENSG00000023445	4.69E-98	0.308435396	0.265	0.107	1.18E-93	dMP1
SLC31A2_ENSG00000136867	1.09E-87	0.289786722	0.288	0.137	2.73E-83	dMP1
ATF3_ENSG00000162772	1.30E-73	0.374360434	0.624	0.458	3.25E-69	dMP1
IL2RA_ENSG00000134460	7.92E-284	0.382212434	0.141	0.017	1.99E-279	dMP2
TNF_ENSG00000232810	2.21E-116	0.467607038	0.269	0.107	5.54E-112	dMP2
SLC31A2_ENSG00000136867	3.35E-07	0.260884247	0.169	0.144	0.008396776	dMP2
BCL2A1_ENSG00000140379	0	0.700008122	0.66	0.095	0	pIMP
SLC31A2_ENSG00000136867	1.24E-138	0.351945611	0.581	0.14	3.11E-134	pIMP

M2 gene ID/Ensembl ID	p value	log2(fold change)	pct.1	pct.2	adjusted p value	cluster
MS4A6A_ENSG00000110077	0	1.210012925	0.751	0.113	0	dMP1
MSR1_ENSG00000038945	0	1.12155835	0.519	0.056	0	dMP1
IL10_ENSG00000136634	0	0.844533592	0.328	0.017	0	dMP1
FGL2_ENSG00000127951	0	0.839205791	0.489	0.07	0	dMP1
MS4A4A_ENSG00000110079	0	0.670913055	0.452	0.081	0	dMP1
CD36_ENSG00000135218	0	0.533477331	0.363	0.083	0	dMP1
CXCR4_ENSG00000121966	0	0.416607417	0.759	0.246	0	dMP1
MRC1_ENSG00000260314	0	0.397008774	0.262	0.05	0	dMP1
EGR2_ENSG00000122877	2.93E-99	0.292030188	0.167	0.053	7.34E-95	dMP1
HEXB_ENSG00000049860	7.87E-89	0.316822005	0.59	0.425	1.97E-84	dMP1
LIPA_ENSG00000107798	1.50E-79	0.677431399	0.457	0.326	3.75E-75	dMP1
HNMT_ENSG00000150540	1.62E-79	0.351649267	0.48	0.328	4.07E-75	dMP1
LTA4H_ENSG00000111144	1.70E-42	0.345529694	0.327	0.226	4.26E-38	dMP1
MS4A6A_ENSG00000110077	0	2.239257868	0.94	0.101	0	dMP2
MS4A4A_ENSG00000110079	0	1.662923116	0.721	0.065	0	dMP2
MAF_ENSG00000178573	0	1.534114627	0.74	0.215	0	dMP2
MSR1_ENSG00000038945	0	1.157266276	0.507	0.056	0	dMP2
MRC1_ENSG00000260314	0	1.082199082	0.446	0.039	0	dMP2
FGL2_ENSG00000127951	0	0.712821403	0.353	0.077	0	dMP2
HNMT_ENSG00000150540	1.91E-199	0.834998024	0.526	0.325	4.80E-195	dMP2
EGR2_ENSG00000122877	2.06E-154	0.547309422	0.188	0.051	5.18E-150	dMP2
CTSC_ENSG00000109861	9.01E-144	0.577978086	0.749	0.703	2.26E-139	dMP2
SLC4A7_ENSG00000033867	2.03E-74	0.506406031	0.247	0.127	5.08E-70	dMP2
SLC38A6_ENSG00000139974	4.27E-31	0.307314869	0.135	0.072	1.07E-26	dMP2
IGF1_ENSG00000017427	1.20E-20	0.252426476	0.28	0.212	3.01E-16	dMP2
TGFBR2_ENSG00000163513	3.67E-15	0.320785075	0.192	0.146	9.20E-11	dMP2
CD36_ENSG00000135218	0	1.167271163	0.829	0.089	0	pIMP
MSR1_ENSG00000038945	0	0.96032345	0.748	0.073	0	pIMP
CCL18_ENSG00000275385	0	0.679249888	0.257	0.007	0	pIMP
MS4A4A_ENSG00000110079	0	0.62540035	0.75	0.093	0	pIMP
SLC38A6_ENSG00000139974	0	0.476221342	0.583	0.07	0	pIMP
LIPA_ENSG00000107798	2.09E-298	1.53167195	0.961	0.325	5.24E-294	pIMP
LTA4H_ENSG00000111144	2.49E-277	1.143042825	0.843	0.224	6.24E-273	pIMP
HS3ST1_ENSG00000002587	2.37E-259	0.320799147	0.359	0.035	5.96E-255	pIMP
MS4A6A_ENSG00000110077	5.72E-212	0.739019454	0.694	0.14	1.44E-207	pIMP
HEXB_ENSG00000049860	4.07E-134	0.648908959	0.931	0.428	1.02E-129	pIMP
FN1_ENSG00000115414	1.57E-127	0.703632729	0.861	0.365	3.94E-123	pIMP
HNMT_ENSG00000150540	2.29E-116	0.509051201	0.826	0.33	5.74E-112	pIMP

Appendix 11 - Heatmaps of cell type-specific expression pattern of genes associated with additional pregnancy complications and fertility-related conditions:

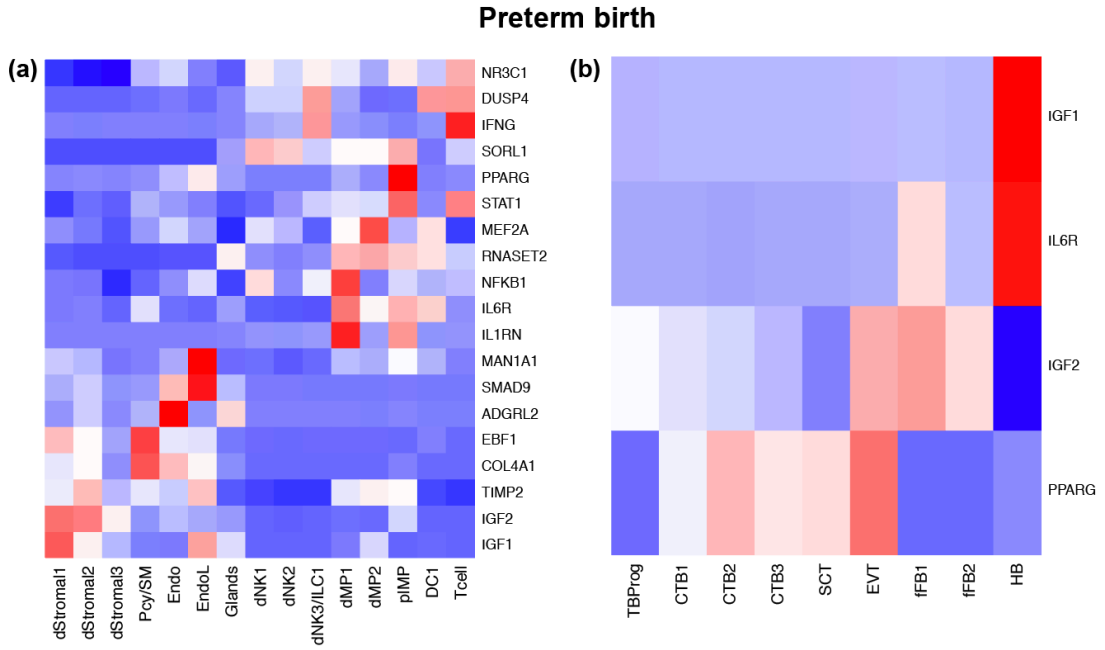

(a) Maternally and **(b)** fetally expressed genes associated with preterm birth are upregulated in maternal smooth muscle and endothelial cells and maternal mononuclear phagocytes and in fetal trophoblasts, fibroblasts, and Hofbauer cells.

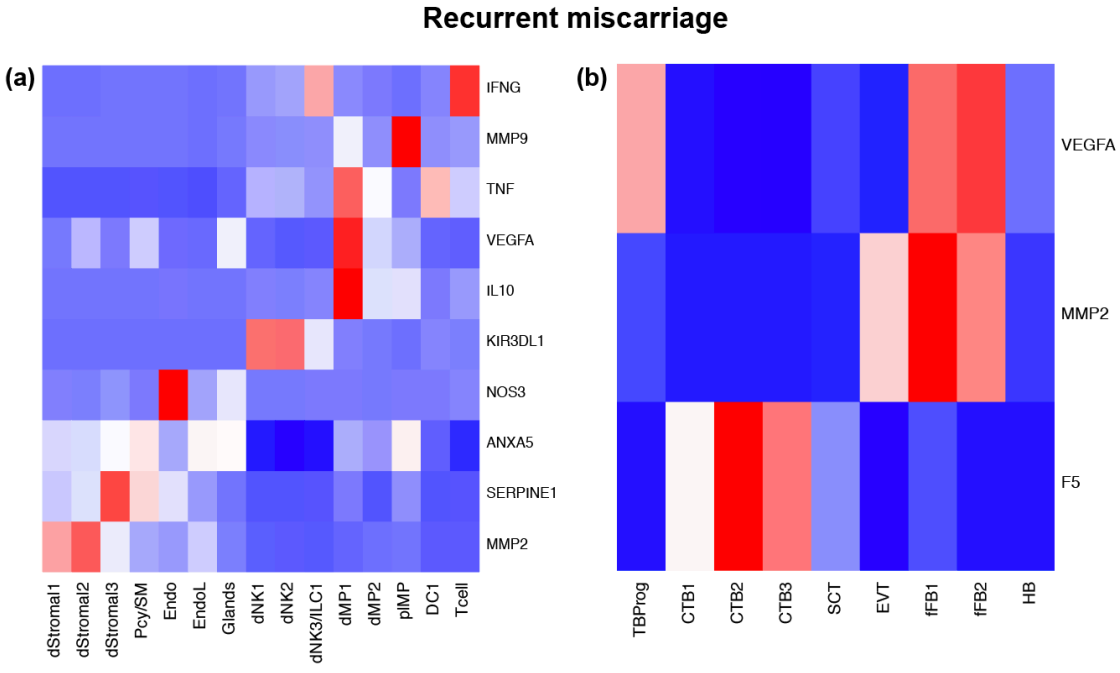

(a) Maternally and **(b)** fetally expressed genes associated with recurrent miscarriage are upregulated in maternal stromal, dNK, and mononuclear phagocyte cells and in fetal trophoblasts and fibroblasts.

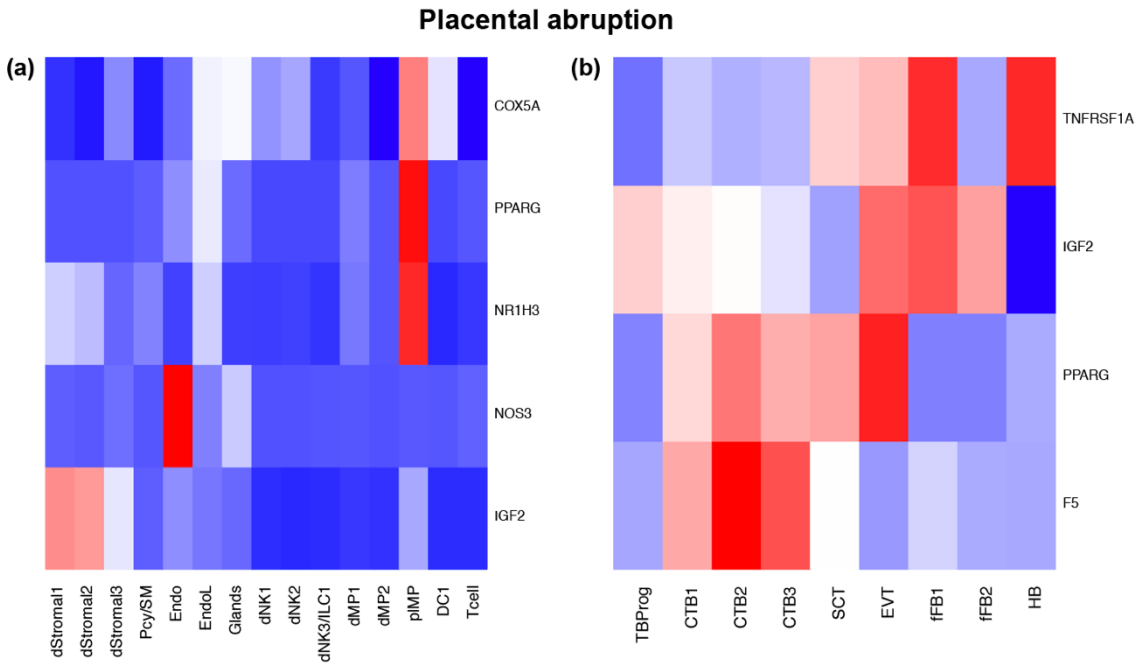

(a) Maternally and **(b)** fetally expressed genes associated with placental abruption are upregulated in maternal stromal cell, endothelial cell, and placental mononuclear phagocyte populations and in fetal trophoblasts, fibroblasts, and Hofbauer cells.

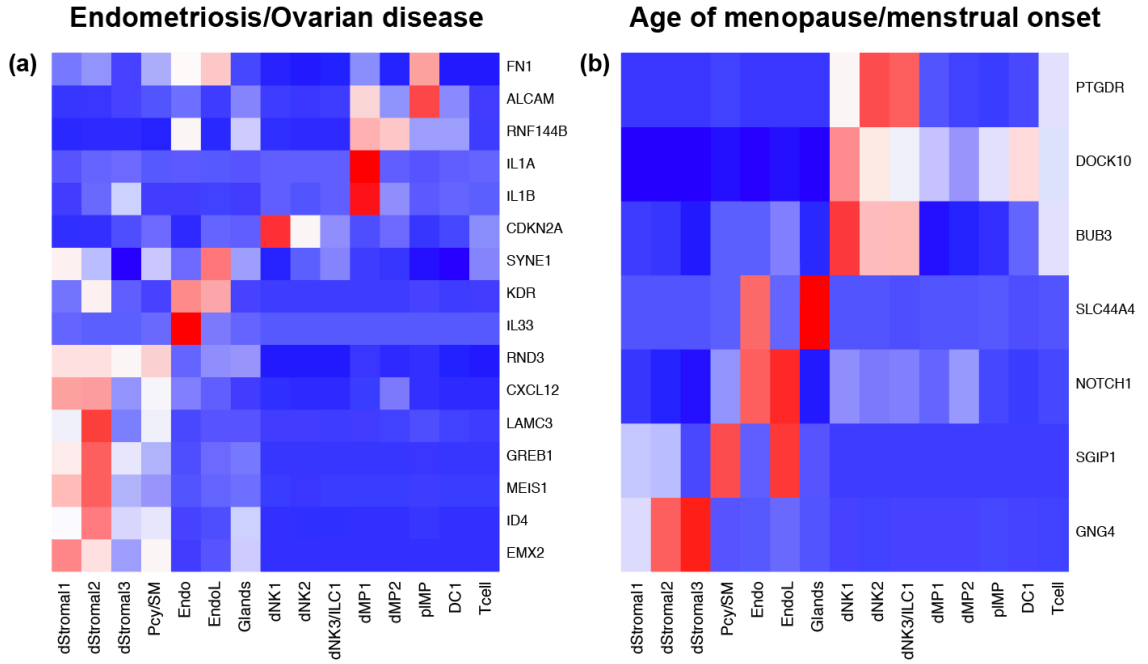

(a) Maternally expressed genes associated with endometriosis or ovarian disease are upregulated in maternal stromal cell, endothelial cell, and mononuclear phagocyte populations. **(b)** Maternally expressed genes associated with menopause and menstrual onset are upregulated in maternal stromal cell, endothelial cell, and dNK populations.